University of Thessaly

School of Engineering

Department of Mechanical Engineering

Diploma Thesis

CRYSTAL PLASTICITY

A rate–independent constitutive model. The effect of Hydrogen concentration

by

NIKOLAOS VASIOS

Approved by the Following Members of the Advisory Committee:

First Member (Supervisor)
_____

Nikolaos Aravas
Professor of Computational Mechanics,
Department of Mechanical Engineering, University of Thessaly

Second Member
_____

Gregory Haidemenopoulos
Professor of Physical Metallurgy,
Department of Mechanical Engineering, University of Thessaly

Third Member
_____

Alexis Kermanidis
Assistant Professor of Mechanical Behavior of Materials,
Department of Mechanical Engineering, University of Thessaly

Abstract

Crystal Plasticity

Nikolaos Vasios

Supervisor: Professor N.Aravas

This work is concerned with the formulation of a rate–independent constitutive model for single crystal plasticity and it's computational implementation. The development of the constitutive model is based on multiplicative decomposition of the deformation gradient as well as on the physics of dislocation motion. Motivated by the theoretical predictions and experimental observations on hydrogen–charged metal single crystals, we introduce a comprehensive methodology to implement the effects of hydrogen concentration to the constitutive model. Computationally, we emphasise on the formulation of a heuristic and two optimization based stress–update algorithms that are able to incrementally determine the set of active slip systems. The constitutive model is implemented in the Abaqus general purpose finite element software, in the form of a User MATerial subroutine and is rigorously tested in a series of uniaxial tension simulations. Through the FEM simulations we investigate three different specimen designs for uniaxial tension and also determine the crystal's tensile behavior for various orientations. Finally, we perform a comparative study on stress–update algorithms and also examine the proposed plasticity model accounting for hydrogen concentration.

Keywords: Crystal Plasticity; Stress–Update Algorithms; Orientation Sensitivity;
Hydrogen Concentration;

Acknowledgements

This thesis was carried out at the Laboratory of Mechanics & Strength of Materials in partial fulfilment of the requirements for the Diploma in Mechanical Engineering at the Department of Mechanical Engineering of University of Thessaly.

First and foremost I would like to express my sincere gratitude to my diploma thesis advisor, Professor Nikolaos Aravas for introducing me to solid and computational mechanics, for instilling me with his knowledge, for the all the valuable advice and continuous guidance throughout my studies but more importantly for trusting me on this subject. His expertise and personality will always be a form of inspiration for me.

Secondly, I am deeply thankful to the members of the advisory committee Professor Gregory Haidemenopoulos and Assistant Professor Alexis Kermanidis for all the valuable time they devoted in reviewing this thesis but also for their numerous insightful comments during my undergraduate studies.

I would also like to thank Professor Costas Papadimitiou and Professor Spyros Karamanos for broadening my engineering knowledge field and influencing my way of thinking. I am grateful to Researcher Dr.Leonidas Spyrou (CE.R.T.H.), Ph.D. candidate Ioanna Papadioti and Mr.George Tsantidis for the abundant advices on the Abaqus Finite Element Software and the LaTeX 2_ε typesetting system.

I especially need to thank Anastasia for the undivided moral support, and for always being by my side all these years. Without her, I would not be able to endure all the difficulties, nor achieve so much.

Finally and more importantly, I express my deepest gratitude to my parents Dimitris and Maria and to my younger sister Marianna for all their love and support, without whom I would not be able to complete my studies.

Contents

List of Tables

List of Figures

Introduction

Single crystals, are monocrystalline solids whose structure consists of a single, continuous and unbroken grain. They are characterized by their extraordinary mechanical properties, which are mainly attributed to the absence of structural defects associated with grain boundaries. These properties and especially the inherent creep resistance of metal single crystals is the main reason for their widespread implementation in turbines and the energy industry. However, research on the mechanical behavior of single crystals is not entirely motivated by the continuous need for innovative industrial applications.

From a mechanics point of view, mesoscale approaches to the multi–scale modelling of granular materials are fundamentally based on the development of crystal plasticity theories (Taylor 1934 [49], Mandel 1965 [39], Hill 1966 [28], Asaro 1983 [9]). A universal characteristic of these theories is the explicit modelling of slip systems within the crystal lattice to constitute a model that naturally accounts for plastic slip, dislocation motion and their interactions. Even though the widespread implementation of a crystal–based multiscale plasticity model is for the most part quite limited due to the unavailability of computational resources, crystal plasticity theories provide a robust theoretical framework that leads to the development of better phenomenological plasticity models.

This thesis is concerned with the formulation of a rate–independent crystal plasticity model accounting for finite elastoplastic deformations. The first Chapter serves as a concise introduction to the fundamental principles of Continuum mechanics, presented in the books by Aravas [8], Asaro & Lubarda [10], Bigoni [14], Bonet & Wood [17], Gurtin & Anand [26], Hjelmstad [30] and Malvern [38] and intends to establish a theoretical background. The principles presented and the quantities defined are considered prerequisites to the study and constitutive description of crystal plasticity. Subsequently, in an effort to approach single crystals from a material's science point of view, Chapter 2 presents the basic elements of crystallography defining elementary concepts such as slip systems, planes and directions

within a crystal lattice. We also introduce the method of stereographic projection, whose applications, although not limited to crystallography are extremely useful to the development of our constitutive model. The third chapter presents the constitutive model itself giving particular emphasis on the multiplicative decomposition of the deformation gradient, the hardening model, as well as on the numerical integration of elastoplastic equations. In Chapter 4, based on the experimental observations of Delafosse [23] and Yagodzinskyy [52, 53] and the finite element simulations of Schebler [48] we are concerned with introducing a modified formulation to the crystal plasticity model, to incorporate the effect of Hydrogen concentration. The next two chapters present the computational issues encountered in the context of the crystal plasticity model. In particular, Chapter 5 addresses the issue of determining the set of active systems, which is a prerequisite to integrate the elastoplastic equations. We present a heuristic and two optimization based stress–update algorithms and also exhibit the special treatment required in the case of hydrogen charged crystals. In Chapter 6, we introduce the finite element approximation of the boundary value problem for finite deformations. We derive an approximate expression for the 'local stiffness matrix' and discuss the role of User MATerial subroutines. Finally, Chapter 7 presents the results of the finite element simulations performed in the context of this work. Particular emphasis is given on the interpretation of the FEA results as well as on their qualitative and quantitative comparison with the existing experimental observations.

Standard notation is assumed throughout. Fraktur symbols like $\mathfrak{B}$, denote body configurations whereas Ralph Smith's Formal script symbols like $\mathscr{A}$ denote sets. Boldface symbols denote tensors the orders of which are indicated by the context[1]. All tensor components are written with respect to a fixed Cartesian coordinate system with base vectors $\mathbf{e}_i$ $(i = 1, 2, 3)$, and the summation convention is used for repeated Latin indices, unless otherwise indicated. The prefix det indicates the determinant, a superscript T the transpose, a superposed dot the material time derivative, and the subscripts s and a the symmetric and anti-symmetric parts of a second order tensor. Let $\mathbf{a}$, $\mathbf{b}$ be vectors, $\mathbf{A}$, $\mathbf{B}$ second-order tensors, and $\boldsymbol{\mathcal{C}}$ a fourth-order tensor; the following products are used in the text $\mathbf{a} \cdot \mathbf{b} = a_i\, b_i$, $(\mathbf{a}\, \mathbf{b})_{ij} = a_i\, b_j$, $(\mathbf{a}\, \mathbf{b}\, \mathbf{c}\, \mathbf{d})_{ijkl} = a_i\, b_j\, c_k\, d_l$, $(\mathbf{A} \cdot \mathbf{a})_i = A_{ik}\, a_k$, $(\mathbf{a} \cdot \mathbf{A})_i = a_k\, A_{ki}$, $\mathbf{A} : \mathbf{B} = A_{ij}\, B_{ij}$, $(\mathbf{A} \cdot \mathbf{B})_{ij} = A_{ik}\, B_{kj}$, $(\mathbf{A}\, \mathbf{B})_{ijkl} = A_{ij}\, B_{kl}$, $\mathbf{a} \cdot \mathbf{A} \cdot \mathbf{b} = a_i\, A_{ij}\, b_j = (\mathbf{a}\mathbf{b}) : \mathbf{A}$, $(\boldsymbol{\mathcal{C}} : \mathbf{A})_{ij} = \mathcal{C}_{ijkl}\, A_{kl}$, $(\mathbf{A} : \boldsymbol{\mathcal{C}})_{ij} = A_{kl}\, \mathcal{C}_{klij}$, $\mathbf{A} : \boldsymbol{\mathcal{C}} : \mathbf{B} = A_{ij}\, \mathcal{C}_{ijkl}\, B_{kl}$ and $(\mathcal{C} : \boldsymbol{\mathcal{D}})_{ijkl} = \mathcal{C}_{ijpq}\, \mathcal{D}_{pqkl}$. The inverse $\boldsymbol{\mathcal{C}}^{-1}$ of a fourth-order tensor $\boldsymbol{\mathcal{C}}$ that has the 'minor' symmetries $\mathcal{C}_{ijkl} = \mathcal{C}_{jikl} = \mathcal{C}_{ijlk}$ is defined so that $\boldsymbol{\mathcal{C}} : \boldsymbol{\mathcal{C}}^{-1} = \boldsymbol{\mathcal{C}}^{-1} : \boldsymbol{\mathcal{C}} = \boldsymbol{\mathcal{I}}$, where $\boldsymbol{\mathcal{I}}$ is the symmetric fourth-order identity tensor with Cartesian components $\mathcal{I}_{ijkl} = (\delta_{ik}\, \delta_{jl} + \delta_{il}\, \delta_{jk})/2$, δ_{ij} being the Kronecker delta.

---

[1]In an effort to be as consistent as possible, capital boldface symbols are used for 2nd order tensors whereas lowercase boldface symbols are used to represent vectors. Cauchy and Kirchhoff stress measures are the only exceptions, which although they represent 2nd order tensors, are denoted as $\boldsymbol{\sigma}$ and $\boldsymbol{\tau}$ respectively

Chapter 1

Theory

1.1 Deformation Map

Let us consider a continuum body made up of an infinite collection of material points. In order to provide a precise description of changes in shape, size and orientation of that continuum body, we have to define an initial configuration at time $t_0 = 0$ which we call **reference configuration** and denote as $\mathfrak{B}_0$. We also define the **deformed configuration** $\mathfrak{B}_t$, as any other configuration of the continuum body at subsequent times t. The concept of **deformation** is introduced as any geometry related deviation between the reference and deformed configuration. We next postulate that the motion of the continuum body can be described by introducing a smooth and differentiable mapping function $\mathbf{x}(\mathbf{X}, t)$ so that any material point $\hat{\mathbf{X}} \in \mathfrak{B}_0$ maps to a single point $\hat{\mathbf{x}} \in \mathfrak{B}_t$ at time t. In general:

$$\mathbf{x} = \mathbf{x}(\mathbf{X}, t) : \mathfrak{B}_0 \rightarrow \mathfrak{B}_t \tag{1.1}$$

Now assume that existing material points cannot be destroyed and new material points cannot be added to the infinite collection. In this case, the mapping is reversible and also bijective in the sense that a single material point in the undeformed shape, corresponds to a single point in the deformed shape and vice versa. In math form:

$$\mathbf{x} = \mathbf{x}(\mathbf{X}, t) \Rightarrow \mathbf{X} = \mathbf{X}(\mathbf{x}, t)$$

However, it is rather difficult to derive a physical interpretation of the mapping function if the variation in both $\mathbf{X}$ and t is maintained. We can obtain two different interpretations assuming a variation in one of those variables at a time, while the other is assumed to remain constant. Deciding to follow a given material point we set on (1.1) $\mathbf{X} = \hat{\mathbf{X}} = \text{ct}$ to get:
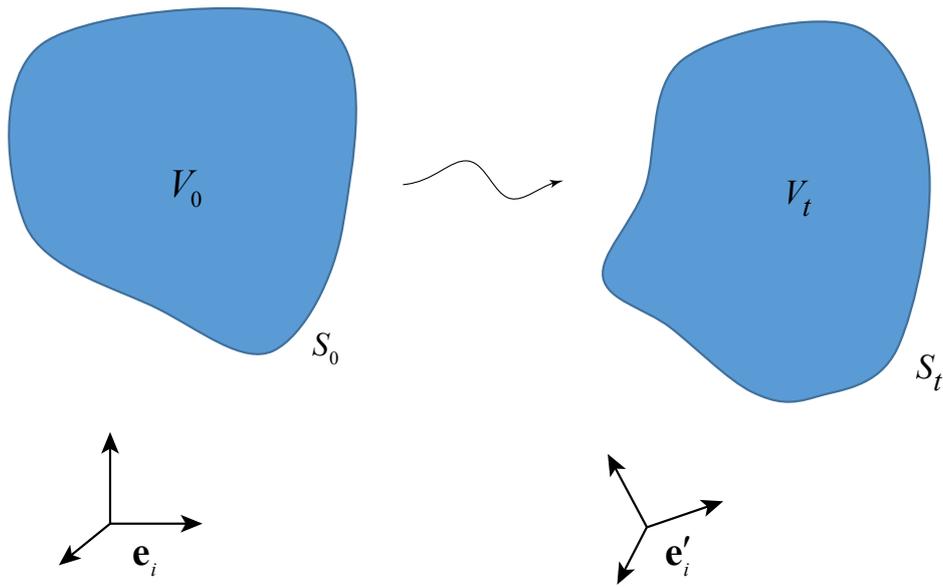
Figure 1.1: Reference state vs Deformed state

$$\mathbf{x} = \mathbf{x}(\mathbf{X} = \hat{\mathbf{X}}, t) \Rightarrow \mathbf{x} = \hat{\mathbf{x}}(t)$$

which essentially defines the motion equation for material point $\hat{\mathbf{X}}$. Now assuming that the mapping function is twice–differentiable in time, we can define the velocity $\hat{\boldsymbol{v}}(t)$ and acceleration $\hat{\mathbf{a}}(t)$ of material point $\hat{\mathbf{X}}$ as:

$$\hat{\boldsymbol{v}}(t) = \frac{d\hat{\mathbf{x}}(t)}{dt} \qquad \hat{\mathbf{a}}(t) = \frac{d^2\hat{\mathbf{x}}(t)}{dt^2}$$

Such expressions may be of great importance when we are interested in studying the dynamics of a desired material point, but they do not facilitate the description of the kinematics of deformation of the continuum body.

1.2 The Deformation Gradient

Now if we choose to evaluate the mapping function at a given time instance $t = \hat{t}$, we get:

$$\mathbf{x} = \mathbf{x}(\mathbf{X}, t = \hat{t}) \Rightarrow \mathbf{x}_{\hat{t}} = \mathbf{x}(\mathbf{X}) \tag{1.2}$$

This expression essentially maps every material point from the reference state $\boldsymbol{\mathfrak{B}}_0$ at time t_0 to a single point in the current (deformed) state $\boldsymbol{\mathfrak{B}}_t$ at $\hat{t}$. Now imagine an arbitrary infinitesimal material fiber $d\mathbf{X}$ originating from the point $\mathbf{X}$ in $\boldsymbol{\mathfrak{B}}_0$. If we are able to determine this infinitesimal material fiber in the current configuration $d\mathbf{x}$, we will get an immediate sense of deformation infinitesimally close to the point $\mathbf{X}$. Hence, by differentiating (1.2) with respect to $\mathbf{X}$ and dropping the subscript $\hat{t}$ we obtain:

$$\mathbf{x} = \mathbf{x}(\mathbf{X}) \Rightarrow d\mathbf{x} = \frac{\partial \mathbf{x}(\mathbf{X})}{\partial \mathbf{X}} \cdot d\mathbf{X}$$

The quantity $\partial\mathbf{x}(\mathbf{X})/\partial\mathbf{X}$ defines a second order tensor which is called the **Deformation Gradient**.

$$\mathbf{F} = \mathbf{x}\boldsymbol{\nabla}_{\mathbf{X}} = \frac{\partial\mathbf{x}(\mathbf{X})}{\partial\mathbf{X}} \quad \text{or:} \quad F_{ij} = \frac{\partial x_i}{\partial X_j} \tag{1.3}$$
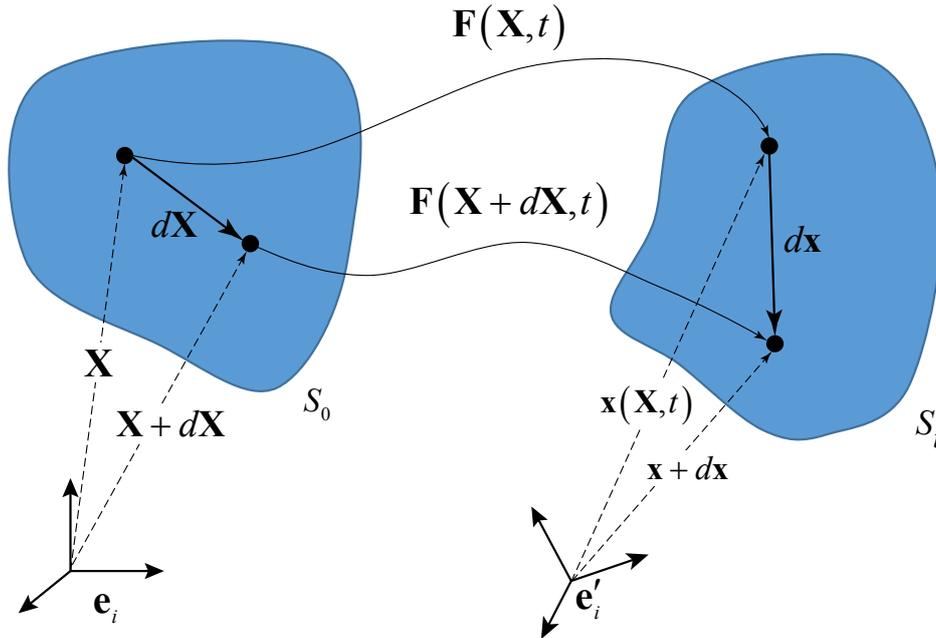
Figure 1.2: The deformation gradient maps every point in the continuum from the reference to the deformed state

The Deformation Gradient is one of the most important quantities defined in Continuum mechanics. The fact that it maps infinitesimal material fibers from the reference to the current configuration, suggests that $\mathbf{F}$ contains all deformation related information infinitesimally close to the point that the fiber originates. Alternatively, the definition (1.3) can also be written in the form:

$$d\mathbf{x} = \mathbf{F} \cdot d\mathbf{X} \tag{1.4}$$

The Deformation Gradient is from definition the Jacobian matrix of the transformation from $\mathfrak{B}_0$ to $\mathfrak{B}_t$ and therefore assigns 'quantities' from the reference to the current state. It is reasonable then to assume that changes of shape, size and orientation have to be expressed in terms of $\mathbf{F}$. In fact, with tensor analysis it can be shown that changes in length and relative orientation of infinitesimal material fibers as well as surface and volume changes within the continuum body are all given by expressions that involve the deformation gradient $\mathbf{F}$. Next we summarize these expressions without proving[1] them as it is beyond the scope of this discussion.

---

[1] The detailed proofs of the following expressions can be found in the book *Mechanics of Materials* (Aravas 2014 [8])
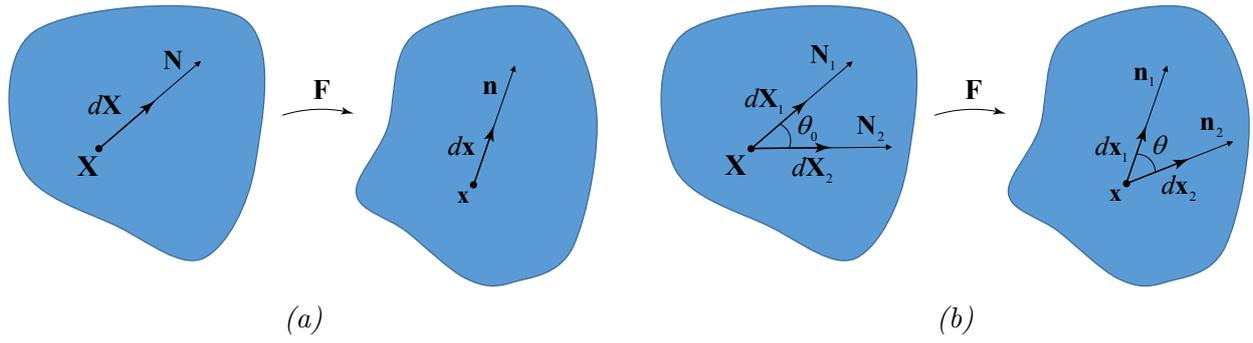
Figure 1.3: Stretch of an infinitesimal material fiber (a) and change of the relative orientation between two infinitesimal material fibers (b)

Let us consider an arbitrary infinitesimal material fiber $d\mathbf{X} = ds_0\,\mathbf{N}$ in the reference configuration, that is transformed to $d\mathbf{x} = ds\,\mathbf{n}$ in the deformed configuration. The infinitesimal lengths ds_0 and ds can be expressed in terms of $d\mathbf{X}$ and $d\mathbf{x}$ respectively as:

$$ds_0^2 = d\mathbf{X} \cdot d\mathbf{X} \tag{1.5}$$

$$ds^2 = d\mathbf{x} \cdot d\mathbf{x} \tag{1.6}$$

It can be proven that the stretch ratio λ of the material fiber defined as $\lambda = ds/ds_0$ is given by:

$$\lambda = \sqrt{\mathbf{N} \cdot \mathbf{F}^T \cdot \mathbf{F} \cdot \mathbf{N}} \quad \text{where:} \quad \mathbf{N} = \frac{d\mathbf{X}}{ds_0} \tag{1.7}$$

The quantity $\mathbf{F}^T \cdot \mathbf{F}$ appears quite often in deformation analysis of continuum mediums and defines the **Right Cauchy–Green** tensor as:

$$\boxed{\mathbf{C} = \mathbf{F}^T \cdot \mathbf{F}} \tag{1.8}$$

The **Left Cauchy–Green** tensor $\mathbf{B}$ can also be defined as:

$$\boxed{\mathbf{B} = \mathbf{F} \cdot \mathbf{F}^T} \tag{1.9}$$

The angle in the deformed state, between two infinitesimal material fibers $(d\mathbf{X}_1, \mathbf{N}_1)$ and $(d\mathbf{X}_2, \mathbf{N}_2)$ (Figure 1.3b) is essentially the angle between the new unit vectors $\mathbf{n}_1, \mathbf{n}_2$. The cosine is given by:

$$\cos(\hat{\mathbf{n}}_1, \hat{\mathbf{n}}_2) = \frac{\mathbf{N}_1 \cdot \mathbf{C} \cdot \mathbf{N}_2}{\lambda_1\,\lambda_2} \tag{1.10}$$

where λ_1 and λ_2 are the stretch ratios corresponding to $d\mathbf{X}_1$ and $d\mathbf{X}_2$ respectively and are defined in (1.7). An infinitesimal surface dS_0 whose normal vector in the reference state was $\hat{\mathbf{N}}$, transforms in the deformed configuration (Figure 1.4a) according to Nanson's formula as:

$$\frac{dS}{dS_0} = (\det\mathbf{F})\sqrt{\hat{\mathbf{N}} \cdot \mathbf{C}^{-1} \cdot \hat{\mathbf{N}}} \tag{1.11}$$

while the new normal vector $\hat{\mathbf{n}}$ is given by:

$$\hat{\mathbf{n}} = \frac{1}{\sqrt{\hat{\mathbf{N}} \cdot \mathbf{C}^{-1} \cdot \hat{\mathbf{N}}}} \cdot (\hat{\mathbf{N}} \cdot \mathbf{F}^{-1}) \tag{1.12}$$
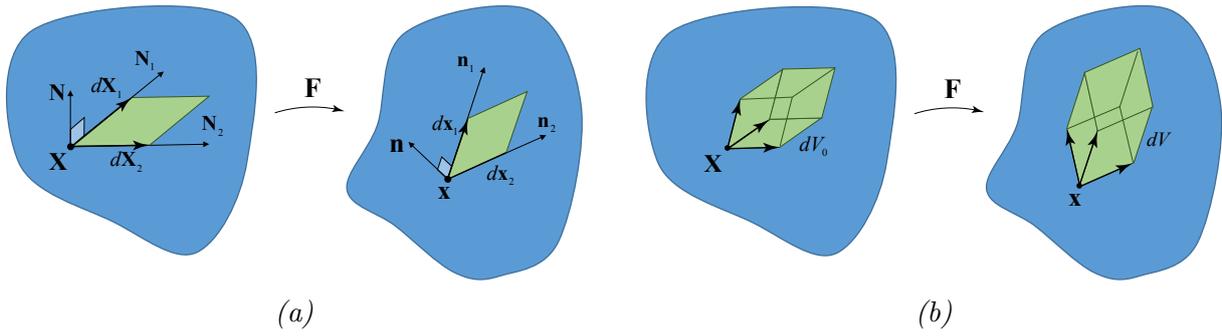
Figure 1.4: Change of infinitesimal surface (a) and infinitesimal volume (b)

At this point is should be noted that the normal vector transforming from $\hat{\mathbf{N}}$ into $\hat{\mathbf{n}}$ does not in general follow a material fiber. The transformation in (1.12) is derived by demanding that $\mathbf{n}$ remains perpendicular to the infinitesimal surface, at all times during deformation.

Finally it can be shown that an infinitesimal volume dV_0 transforms into dV (Figure 1.4b) according to:

$$\frac{dV}{dV_0} = J = \det\mathbf{F} \tag{1.13}$$

1.3 The Polar Decomposition Theorem

Any 2nd order invertible tensor can be expressed as the product of a symmetric and an orthogonal tensor. In the context of continuum mechanics, $\mathbf{F}$ can be decomposed as such, with the orthogonal tensor representing rigid rotations associated with the motion $\mathbf{F}$, whereas the symmetric tensor expresses 'pure' deformation. In math form:

$$\mathbf{F} = \mathbf{R} \cdot \mathbf{U} = \mathbf{V} \cdot \mathbf{R} \tag{1.14}$$

It can be shown [10] that tensors $\mathbf{R}$, $\mathbf{U}$, $\mathbf{V}$ are unique and expression (1.14) defines the **Polar Decomposition** of $\mathbf{F}$. Tensor $\mathbf{R}$ is orthogonal while $\mathbf{U}$,$\mathbf{V}$ are symmetric and positive definite. Tensors $\mathbf{U}$ and $\mathbf{V}$ are also commonly referred to as **right** and **left** stretch tensors respectively. Symmetry and positive–definiteness of $\mathbf{U}$ and $\mathbf{V}$ also suggest that their eigenvalues are real and positive while also their eigenvectors define an orthonormal base. Let us denote as $\mathbf{N}_i$ the eigenvectors of $\mathbf{U}$ defining a **Lagrangian** triad and as $\mathbf{n}_i$ the corresponding **Eulerian** base defined by the eigenvectors of $\mathbf{V}$. The left and right stretch tensors can now be expressed in terms of their principal directions as:

$$\mathbf{U} = \sum_{i=1}^{3} \lambda_i \, \mathbf{N}_i \, \mathbf{N}_i \tag{1.15a}$$

$$\mathbf{V} = \sum_{i=1}^{3} \lambda_i \, \mathbf{n}_i \, \mathbf{n}_i \tag{1.15b}$$
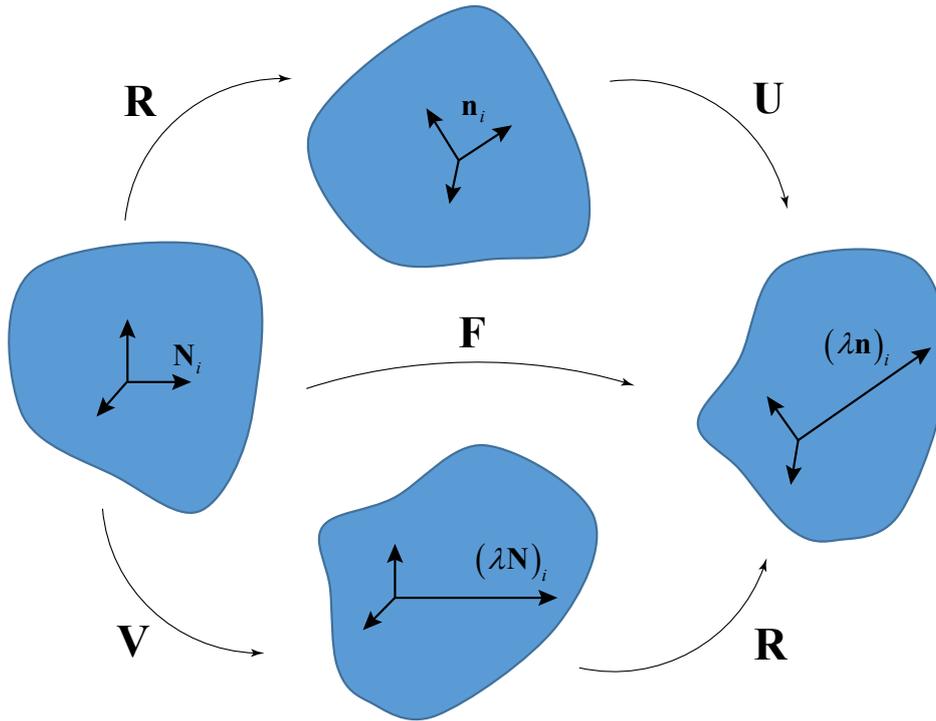
Figure 1.5: The Polar Decomposition of **F**

where λ_i represent the eigenvalues of **U** and **V**. Tensors **U** and **V** can also be expressed in terms of the right and left Cauchy–Green tensors that we defined earlier as:

$$\mathbf{U} = \sqrt{\mathbf{C}} \quad , \quad \mathbf{V} = \sqrt{\mathbf{B}}$$

It is important to note however that the square root of a second order tensor can only be evaluated as the square root of the tensor's eigenvalues once the tensor is expressed in terms of a coordinate system whose axes are aligned with the tensor's principal directions. Therefore, the process of determining the square root of an arbitrary invertible matrix **A**, always involves solving an eigenvalue problem. The expression of **U** and **V** as the square root of **C** and **B** respectively, suggests that the left and right Cauchy–Green tensors can also be expressed with respect to their principal directions as:

$$\mathbf{C} = \sum_{i=1}^{3} \lambda_i^2 \, \mathbf{N}_i \, \mathbf{N}_i$$

$$\mathbf{B} = \sum_{i=1}^{3} \lambda_i^2 \, \mathbf{n}_i \, \mathbf{n}_i$$

Finally, the orthogonal tensor **R** can be expressed in terms of the Eulerian $\mathbf{n}_i$ and Lagrangian $\mathbf{N}_i$ directors as:

$$\mathbf{R} = \mathbf{n}\mathbf{N} \qquad (1.16)$$

1.4 Strain Measures

As aforementioned, the deformation gradient $\mathbf{F}$ contains every 'information' concerning deformation for every material point within the continuum body. In addition, the polar decomposition of $\mathbf{F}$ suggests that we can eliminate rigid rotations from $\mathbf{F}$ and express 'pure–deformation' in terms of the stretch tensors $\mathbf{U}$ and $\mathbf{V}$. A quite reasonable assertion would therefore be to suggest that strain tensors must be coaxial[2] with either $\mathbf{U}$ or $\mathbf{V}$, leading to the definition of two general strain measures:

$$\mathbf{E}^{(m)} = f^{(m)}(\lambda_i)\,\mathbf{N}_i\,\mathbf{N}_i \tag{1.17a}$$

$$\mathbf{e}^{(m)} = f^{(m)}(\lambda_i)\,\mathbf{n}_i\,\mathbf{n}_i \tag{1.17b}$$

All strain measures derived from (1.17a) are referred to as Lagrangian strains, after the triad $\mathbf{N}_i$, while strain measures derived from (1.17b) are Eulerian[3] strains. Functions $f(\lambda_i)$ have to be chosen so that for small[4] strains, the strain measures being defined are consistent with the infinitesimal strain theory. Recalling that the stretch ratio λ is defined as the ratio of the current to the original length of a material fiber, the infinitesimal strain theory suggests:

$$\varepsilon = \frac{l - l_0}{l_0} = \frac{l}{l_0} - 1 = \lambda - 1 \tag{1.18}$$

Now, in the simplest possible case of uniaxial straining, we can expand $f^{(m)}(\lambda)$ around $\lambda = 1$ (small strains) to derive:

$$E(\lambda)|_{\lambda \to 1} = f^{(m)}(1) + \frac{df^{(m)}(\lambda)}{d\lambda}\bigg|_{\lambda=1}(\lambda - 1) + O((\lambda - 1)^2) \tag{1.19}$$

To ensure the aforementioned consistency, expression (1.19) must reduce to $\lambda - 1$. This demand leads to the following restrictions for the functions $f^{(m)}(\lambda_i)$:

$$f^{(m)}(1) = 0 \quad , \quad \frac{df^{(m)}(\lambda)}{d\lambda}\bigg|_{\lambda=1} = 1$$

while simultaneously $f'(\lambda) > 0 \ \forall \ \lambda > 0$. A family of strains that satisfies all of the above constraints is defined as follows:

$$f^{(m)} = \begin{cases} \frac{1}{m}(\lambda^m - 1) & , \quad m \neq 0 \\[2mm] \ln\lambda & , \quad m = 0 \end{cases} \qquad m \in \mathbb{Z} \tag{1.20}$$

The most commonly encountered strain tensors derived from the above strain family are summarized below:

[2]Two arbitrary tensors $\mathbf{A}$ and $\mathbf{B}$ are coaxial if they can be diagonalized in the same coordinate system. As a result of coaxiality, the commutative property holds in the sense: $\mathbf{A} \cdot \mathbf{B} = \mathbf{B} \cdot \mathbf{A}$

[3]Lagrangian Strains are coaxial with $\mathbf{U}$, while Eulerian strains are coaxial with $\mathbf{V}$

[4]Small strains correspond to $\lambda \cong 1$ or equivalently to $\lambda - 1 \cong 0$

Table 1.1: Strain measures commonly encountered in continuum mechanics applications

	Strain	**Definition**
$m = 0$	Logarithmic/Hencky	$\mathbf{E}^{(0)} = \ln \mathbf{U}$
		$\mathbf{e}^{(0)} = \ln \mathbf{V}$
$m = -2$	Almansi	$\mathbf{e}^A = \mathbf{e}^{(-2)} = \frac{1}{2}(\boldsymbol{\delta} - \mathbf{B}^{-1})$
$m = 2$	Green	$\mathbf{E}^G = \mathbf{E}^{(2)} = \frac{1}{2}(\mathbf{C} - \boldsymbol{\delta})$
$m = 1$	Biot	$\mathbf{E}^B = \mathbf{E}^{(1)} = \mathbf{U} - \boldsymbol{\delta}$

Selection of the 'proper' strain measure for each application strongly depends on the physics of the problem under consideration and should also be consistent with the stress measure being selected[5]. Figure 1.6 comparatively demonstrates the evolution of the strain measures defined in table 1.1 as a function of λ for a uniaxial straining experiment. As expected,
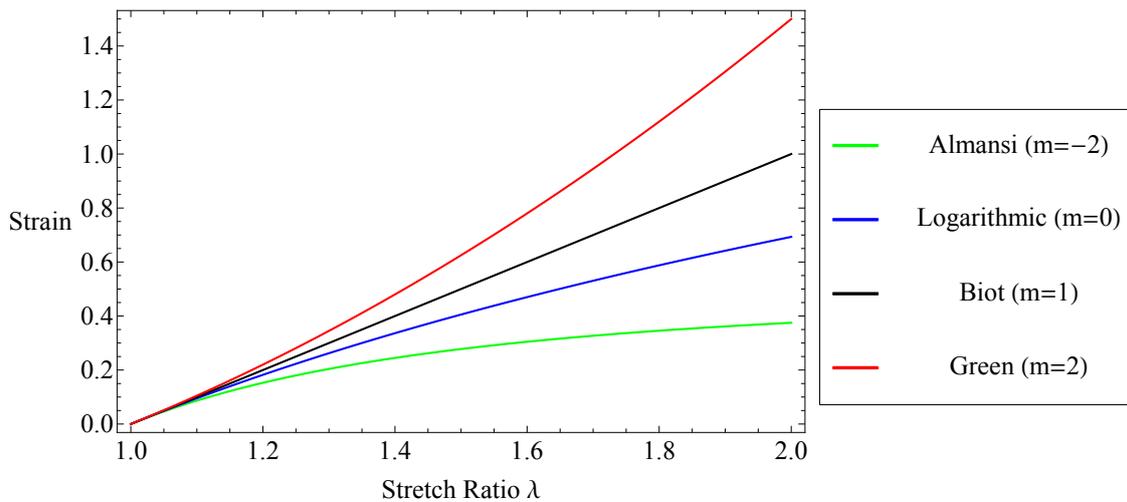
Figure 1.6: A comparative graph for Biot, Logarithmic, Almansi and Green strain measures as a funcion of λ for uniaxial straining

all strains are asymptotically equal at small strains, but diverge as the stretch ratio (and deformation) increases.

1.5 Rate of Deformation

When studying the dynamics of a moving body, apart from it's position $\mathbf{x}(t)$, we also need it's velocity $\boldsymbol{v}(t)$ in order to describe its motion. In complete resemblance, when studying the kinematics of deformation within a continuum body we are interested in determining

---

[5]It is wise to select stress and strain measures that represent work–conjugate pairs (see Section 1.6)

the rate of deformation within the body apart from the deformation $\mathbf{F}$ itself. We begin by defining the velocity field that corresponds to the motion $\mathbf{x}(\mathbf{X}, t)$:

$$\boldsymbol{v}\left(\mathbf{x}\left(\mathbf{X}\right), t\right) = \frac{\partial \mathbf{x}(\mathbf{X}, t)}{\partial t} \tag{1.21}$$

Following the same rationale with Section 1.2, we observe that for a given time instance t the velocity field $\boldsymbol{v}\left(\mathbf{x}, t\right)$ is a function of $\mathbf{x}$. We are interested in determining the variation of the velocity field $d\boldsymbol{v}$ in an infinitesimal 'neighbourhood' $d\mathbf{x}$ around the point $\mathbf{x}$ under consideration. Hence:

$$d\boldsymbol{v} = \boldsymbol{v}\left(\mathbf{x}(\mathbf{X} + d\mathbf{X}), t\right) - \boldsymbol{v}\left(\mathbf{x}(\mathbf{X}), t\right) = \frac{\partial \boldsymbol{v}(\mathbf{x}, t)}{\partial \mathbf{x}} \cdot d\mathbf{x} \tag{1.22}$$

The above relationship leads to the definition of the **Velocity Gradient** tensor as:

$$\boxed{\mathbf{L} = \boldsymbol{v}\boldsymbol{\nabla}_{\mathbf{x}} = \frac{\partial \boldsymbol{v}(\mathbf{x}, t)}{\partial \mathbf{x}}} \tag{1.23}$$

and expression (1.22) can be rewritten as:

$$d\boldsymbol{v} = \mathbf{L} \cdot d\mathbf{x} \tag{1.24}$$

Now recall that in the previous section in (1.4) we had that $d\mathbf{x} = \mathbf{F} \cdot d\mathbf{X}$. Taking into account that $d\boldsymbol{v} = d\dot{\mathbf{x}}$ and in general $\mathbf{F} = \mathbf{F}(t)$ we can write:

$$d\mathbf{x} = \mathbf{F} \cdot d\mathbf{X} \Rightarrow \frac{\partial}{\partial t}\left(d\mathbf{x}\right) = \dot{\mathbf{F}} \cdot d\mathbf{X} \Rightarrow d\boldsymbol{v} = \dot{\mathbf{F}} \cdot \mathbf{F}^{-1} \cdot d\mathbf{x}$$

with:

$$\dot{\mathbf{F}} \cdot \mathbf{F}^{-1} = \frac{\partial}{\partial t}\left[\frac{\partial \mathbf{x}(\mathbf{X}, t)}{\partial \mathbf{X}}\right] \cdot \frac{\partial \mathbf{X}}{\partial \mathbf{x}} = \frac{\partial}{\partial \mathbf{X}}\left[\frac{\partial \mathbf{x}(\mathbf{X}, t)}{\partial t}\right] \cdot \frac{\partial \mathbf{X}}{\partial \mathbf{x}} = \frac{\partial \boldsymbol{v}(\mathbf{X}, t)}{\partial \mathbf{x}} \tag{1.25}$$

Expressions (1.23) and (1.25) clearly state that the velocity gradient tensor can be alternatively expressed in terms of the deformation gradient as:

$$\boxed{\mathbf{L} = \dot{\mathbf{F}} \cdot \mathbf{F}^{-1}} \tag{1.26}$$

Recalling that any 2nd order tensor can be expressed as the sum of a symmetric and an antisymmetric tensor, we also define the next two important rates. The **Deformation Rate D** is defined as the symmetric part of $\mathbf{L}$, while its antisymmetric part $\mathbf{W}$ defines the **Spin Tensor**. In math form:

$$\mathbf{L} = \mathbf{D} + \mathbf{W} \tag{1.27}$$

$$\mathbf{D} = \text{symm}\left(\mathbf{L}\right) = \frac{1}{2}\left(\mathbf{L} + \mathbf{L}^T\right) \Rightarrow \mathbf{D} = \frac{1}{2}\left(\frac{\partial v_i}{\partial x_j} + \frac{\partial v_j}{\partial x_i}\right)\mathbf{e}_i\mathbf{e}_j \tag{1.28}$$

$$\mathbf{W} = \text{skew}\left(\mathbf{L}\right) = \frac{1}{2}\left(\mathbf{L} - \mathbf{L}^T\right) \Rightarrow \mathbf{W} = \frac{1}{2}\left(\frac{\partial v_i}{\partial x_j} - \frac{\partial v_j}{\partial x_i}\right)\mathbf{e}_i\mathbf{e}_j \tag{1.29}$$

1.5.i Physical Interpretation of D

Let us reconsider an arbitrary infinitesimal material fiber $d\mathbf{X} = ds_0 \, \mathbf{N}$ in the reference configuration, that is transformed to $d\mathbf{x} = ds \, \mathbf{n}$ in the deformed configuration and the infinitesimal lengths ds_0 and ds are given by expressions (1.5) and (1.6) respectively. We are interested in determining the rate of change of the infinitesimal length ds, so we differentiate (1.6) with respect to t to derive:

$$\frac{\partial}{\partial t}\left(ds^2\right) = \frac{\partial}{\partial t}\left(d\mathbf{x} \cdot d\mathbf{x}\right) \Rightarrow 2ds\frac{\partial}{\partial t}\left(ds\right) = \frac{\partial}{\partial t}\left(d\mathbf{x}\right) \cdot d\mathbf{x} + d\mathbf{x} \cdot \frac{\partial}{\partial t}\left(d\mathbf{x}\right) \Rightarrow$$

$$2ds\frac{\partial}{\partial t}\left(ds\right) = d\mathbf{x} \cdot \mathbf{L}^T \cdot d\mathbf{x} + d\mathbf{x} \cdot \mathbf{L} \cdot d\mathbf{x} \Rightarrow 2ds\frac{\partial}{\partial t}\left(ds\right) = d\mathbf{x} \cdot \left(\mathbf{L} + \mathbf{L}^T\right) \cdot d\mathbf{x} \Rightarrow$$

$$2ds\frac{\partial}{\partial t}\left(ds\right) = 2d\mathbf{x} \cdot \mathbf{D} \cdot d\mathbf{x} \Rightarrow \frac{ds}{ds^2}\frac{\partial}{\partial t}\left(ds\right) = \frac{d\mathbf{x}}{ds} \cdot \mathbf{D} \cdot \frac{d\mathbf{x}}{ds} \Rightarrow$$

$$\boxed{\frac{1}{ds}\frac{\partial}{\partial t}\left(ds\right) = \mathbf{n} \cdot \mathbf{D} \cdot \mathbf{n}} \tag{1.30}$$

Equation (1.30) suggests that direct components of $\mathbf{D}$, (D_{nn}), express the rate of extension per unit length of a material fiber which, in the current configuration, is momentarily aligned with the direction of $\mathbf{n}$.

Before proceeding with the physical interpretation of the shear components of $\mathbf{D}$, we first need to define the rate of change of a unit vector $\mathbf{m}$ that is attached to a material fiber $d\mathbf{x} = ds\mathbf{m}$. Hence, using equation (1.30):

$$\dot{\mathbf{m}} = \frac{\partial}{\partial t}\left(\frac{d\mathbf{x}}{ds}\right) = \frac{1}{ds}\frac{\partial}{\partial t}\left(d\mathbf{x}\right) - \frac{d\mathbf{x}}{ds^2}\frac{\partial}{\partial t}\left(ds\right) = \mathbf{L} \cdot \mathbf{m} - \left(\mathbf{m} \cdot \mathbf{D} \cdot \mathbf{m}\right) =$$

$$= \left(\mathbf{W} + \mathbf{D}\right) \cdot \mathbf{m} - \left(\mathbf{m} \cdot \mathbf{D} \cdot \mathbf{m}\right) = \mathbf{W} \cdot \mathbf{m} + \mathbf{D} \cdot \mathbf{m} - \left(\mathbf{m} \cdot \mathbf{D} \cdot \mathbf{m}\right) =$$

$$= \mathbf{W} \cdot \mathbf{m} + \mathbf{D} \cdot \mathbf{m}\underbrace{\mathbf{m} \cdot \mathbf{m}}_{1} - \left(\mathbf{m} \cdot \mathbf{D} \cdot \mathbf{m}\right) = \left(\mathbf{W} + \mathbf{D} \cdot \mathbf{m}\,\mathbf{m} - \mathbf{m}\,\mathbf{m} \cdot \mathbf{D}\right) \cdot \mathbf{m}$$

The above expression suggests that the rate $\dot{\mathbf{m}}$ of a unit vector $\mathbf{m}$ attached to a material fiber can be expressed as follows:

$$\dot{\mathbf{m}} = \mathbf{W}^{\mathbf{m}} \cdot \mathbf{m} = -\mathbf{m} \cdot \mathbf{W}^{\mathbf{m}} \tag{1.31}$$

where:

$$\mathbf{W}^{\mathbf{m}} = \mathbf{W} + \mathbf{D} \cdot \mathbf{m}\,\mathbf{m} - \mathbf{m}\,\mathbf{m} \cdot \mathbf{D} \tag{1.32}$$

Now let us consider two arbitrary unit vectors $\mathbf{n}$ and $\mathbf{m}$ that are attached to infinitesimal material fibers $d\mathbf{x}_1$ and $d\mathbf{x}_2$ which, in the current state, intersect at $\mathbf{x}$ as illustrated in Figure 1.3b. Recalling that the cosine of angle θ between $d\mathbf{X}_1$ and $d\mathbf{X}_2$ can be expressed as the dot product between $\mathbf{m}$ and $\mathbf{n}$ we write:

$$\mathbf{m} \cdot \mathbf{n} = \cos\theta \Rightarrow \dot{\theta} = -\frac{1}{\sin\theta}\frac{\partial}{\partial t}\left(\mathbf{m} \cdot \mathbf{n}\right) \tag{1.33}$$

Now let us evaluate the derivative $\partial(\mathbf{m} \cdot \mathbf{n})/\partial t$, in terms of $\mathbf{D}$ to determine the rate of change of the relative orientation between those arbitrary fibers.

$$(\mathbf{m} \cdot \mathbf{n})^{\cdot} = \dot{\mathbf{m}} \cdot \mathbf{n} + \mathbf{m} \cdot \dot{\mathbf{n}} \overset{(1.31)}{=} -\mathbf{m} \cdot \mathbf{W^m} \cdot \mathbf{n} + \mathbf{m} \cdot \mathbf{W^n} \cdot \mathbf{n} =$$

$$= \mathbf{m} \cdot (\mathbf{W^n} - \mathbf{W^m}) \cdot \mathbf{n} \overset{(1.32)}{=} \mathbf{m} \cdot (\mathbf{D} \cdot \mathbf{n}\,\mathbf{n} - \mathbf{n}\,\mathbf{n} \cdot \mathbf{D} - \mathbf{D} \cdot \mathbf{m}\,\mathbf{m} + \mathbf{m}\,\mathbf{m} \cdot \mathbf{D}) \cdot \mathbf{n} =$$

$$= \mathbf{m} \cdot \mathbf{D} \cdot \mathbf{n} - \cos\theta\,(D_{nn} + D_{mm}) + \mathbf{m} \cdot \mathbf{D} \cdot \mathbf{n} =$$

$$= 2\,\mathbf{m} \cdot \mathbf{D} \cdot \mathbf{n} - \cos\theta\,(D_{nn} + D_{mm}) \qquad (1.34)$$

and by substituting (1.34) to (1.33) we derive:

$$\boxed{\dot{\theta} = \frac{1}{\sin\theta}\Big[(D_{mm} + D_{nn})\,\cos\theta - 2\,\mathbf{m} \cdot \mathbf{D} \cdot \mathbf{n} \Big]} \qquad (1.35)$$

Expression (1.35) is rather difficult to interpret in this general form, so we take $\mathbf{m} = \mathbf{e}_1$ and $\mathbf{n} = \mathbf{e}_2$ where $\cos\theta = 0$ and $\sin\theta = 1$ to get:

$$\dot{\theta} = -2\mathbf{e}_1 \cdot \mathbf{D} \cdot \mathbf{e}_2 = -2\,D_{12} \Rightarrow D_{12} = -\frac{1}{2}\dot{\theta}$$

Now this result suggests that the shear components of $\mathbf{D}$, (D_{ij}), express the rate of decrease of the angle between a pair of material fibers which, in the current configuration, intersect at $\mathbf{x}$ and are momentarily aligned with the directions $\mathbf{e}_i$ and $\mathbf{e}_j$[6]. The latter also implies that the rate of change of the relative orientation of the material fibers which, in the current state, are momentarily aligned with the principal directions of $\mathbf{D}$, is zero.

Concluding this discussion regarding the physical interpretation of $\mathbf{D}$, it is interesting to note that even though the components of $\mathbf{D}$ can be though to express the rate of deformation infinitesimally close to the point of interest, there is no strain tensor $\mathbf{E}$ such that $\dot{\mathbf{E}} = \mathbf{D}$.

1.5.ii Physical Interpretation of W

Recall equations (1.31) and (1.32) which are used to define the rate of change of an arbitrary unit vector $\mathbf{m}$. In the special case where the unit vector $\mathbf{m}$ is along a material fiber that is momentarily aligned with one of the principal directions[7] of $\mathbf{D}$, equation (1.32) suggests that $\mathbf{W^m} = \mathbf{W}$. This implies that the spin tensor $\mathbf{W}$ could be thought as the spin of the material fibers that instantaneously coincide with the principal directions of $\mathbf{D}$. According to Aravas and Aifantis [5] however, we could also derive another interesting physical interpretation of $\mathbf{W}$ as follows. Since $\mathbf{W}$ is from definition an anti–symmetric tensor, it can be written in the form:

$$\mathbf{W} = w_3\,(-\mathbf{e}_1\,\mathbf{e}_2 + \mathbf{e}_2\,\mathbf{e}_1) + w_1\,(-\mathbf{e}_2\,\mathbf{e}_3 + \mathbf{e}_3\,\mathbf{e}_2) + w_2\,(-\mathbf{e}_3\,\mathbf{e}_1 + \mathbf{e}_1\,\mathbf{e}_3)$$

---

[6]And are therefore perpendicular to each other

[7]The principal directions of $\mathbf{D}$ are aligned with different material fibers at different times in general
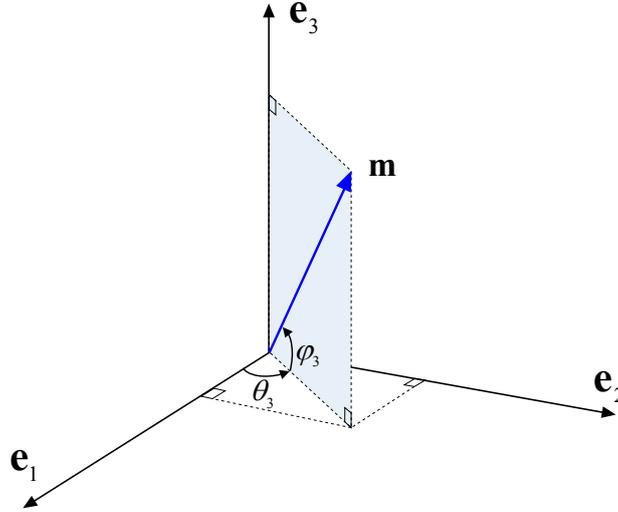
*Figure 1.7: Orientation of a unit vector **m** in the current configuration*

where $\mathbf{e}_i$ are the unit vectors along the coordinate axes. Let us also express the arbitrary unit vector **m** shown illustrated in Figure 1.7 as:

$$\mathbf{m} = \cos\theta_3 \cos\phi_3 \, \mathbf{e}_1 + \sin\theta_3 \cos\phi_3 \, \mathbf{e}_2 + \sin\phi_3 \, \mathbf{e}_3$$

The rate of change of θ_3 can be found to be:

$$\dot{\theta}_3 = w_3 + \tan\phi_3 \left(-w_2 \sin\theta_3 + w_1 \cos\theta_3\right) + \frac{1}{2}\left(D_{22} - D_{11}\right)\sin 2\theta_3 + D_{12}\cos 2\theta_3$$
$$+ \tan\phi_3 \left(-D_{13}\sin\theta_3 + D_{23}\cos\theta_3\right) \tag{1.36}$$

The local mean rate of rotation about the x_3–axis is defined as:

$$\langle\dot{\theta}_3\rangle = \frac{1}{2\pi^2} \int\limits_{-\pi/2}^{\pi/2} \int\limits_{0}^{2\pi} \dot{\theta}_3 \, d\theta_3 \, d\phi \tag{1.37}$$

which when combined with (1.36) yields:

$$\langle\dot{\theta}_3\rangle = w_3 \tag{1.38}$$

Similarly, considering the rotations about the axes x_1 and x_2, it can be shown:

$$\langle\dot{\theta}_1\rangle = w_1 \tag{1.39}$$

$$\langle\dot{\theta}_2\rangle = w_2 \tag{1.40}$$

Equations (1.38–1.40) demonstrate that the spin tensor **W** is the average spin of all directions around a material point[8].

---

[8]This physical interpretation of **W** is demonstrated in greater detail in the Appendix of [5]

1.6 Stress Measures

In the vast majority of continuum mechanics applications we mainly consider two general types of forces [10], body forces[9] and surface traction. Body forces are defined as a density of force in the sense that a body force density $\mathbf{b}$ acting on a volume element dV would result in a force $\mathbf{b}\,dV$. Surface traction on the other hand is reasonably defined as the force acting per unit area of the body and is denoted as $\mathbf{t}$. In order to completely describe the surface traction however, it is necessary to provide the unit normal $\mathbf{n}$ to the surface element that $\mathbf{t}$ acts on.

We consider the tetrahedron shown in Figure 1.8 in the current configuration, known as the Cauchy tetrahedron. Let $\mathbf{n}_i$ be the unit normals to the three faces of the tetrahedron along the directions $\mathbf{e}_i$. The tetrahedron occupies volume dV, whereas the faces with normals $\mathbf{n}_i$ have surface areas dA_i respectively. Finally, the surface area of the oblique face is dA and its corresponding unit normal is denoted as $\mathbf{n}$. Now let us express the traction forces $\mathbf{t}_i$
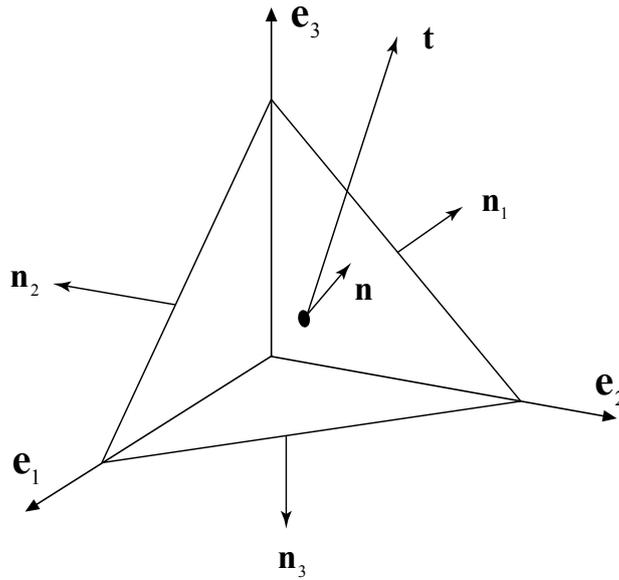
Figure 1.8: The traction vector $\mathbf{t}$ acting on an arbitrary triangular volume dV in the current configuration

acting on surfaces dA_i with respect to the coordinate system $\mathbf{e}_i$ as:

$$\mathbf{t}_i = \sigma_{i1}\,\mathbf{e}_1 + \sigma_{i2}\,\mathbf{e}_2 + \sigma_{i3}\,\mathbf{e}_3 = \sigma_{ij}\,\mathbf{e}_j \tag{1.41}$$

and try to determine $\mathbf{t}$ on dA. Applying Newton's 2nd law of motion to the tetrahedron we write:

$$\Sigma\mathbf{F} = \rho\,\mathbf{a}\,dV \Rightarrow \mathbf{t}\,dA - \mathbf{t}_i\,dA_i + \rho\,\mathbf{b}\,dV = \rho\,\mathbf{a}\,dV \Rightarrow \mathbf{t} = \mathbf{t}_i\,\underbrace{\frac{dA_i}{dA}}_{\mathbf{n}_i} + \rho(\mathbf{a}-\mathbf{b})\,\underbrace{\frac{dV}{dA}}_{\frac{1}{3}h}$$

---

[9]Indicative body force examples would be gravitational forces, electrostatic forces, magnetic forces etc.

where h is the 'height' of the tetrahedron or the shortest distance between the oblique face and the origin. In the limit case where $h \to 0$ the above equation can be restated as:

$$\mathbf{t} = \mathbf{t}_i\, \mathbf{n}_i \Rightarrow \mathbf{t} = \mathbf{n} \cdot \overbrace{\mathbf{e}_i\, \sigma_{ij}\, \mathbf{e}_j}^{\boldsymbol{\sigma}} \Rightarrow \mathbf{t} = \mathbf{n} \cdot \boldsymbol{\sigma} \tag{1.42}$$

Equation (1.42) suggests that any traction vector acting on any arbitrary infinitesimal surface of the continuum body can be expressed in terms of the quantities σ_{ij}, leading to the definition of the **Cauchy stress** as:

$$\boxed{\boldsymbol{\sigma} = \sigma_{ij}\mathbf{e}_i\mathbf{e}_j} \tag{1.43}$$

The component σ_{ij} expresses the j–th component of force per unit area in the current configuration, on a surface element of the current configuration whose normal is currently in the i direction. We also define the **Kirchhoff stress** in the current configuration from $\boldsymbol{\sigma}$ as:

$$\boldsymbol{\tau} = J\boldsymbol{\sigma} \tag{1.44}$$

The Kirchhoff stress tensor $\boldsymbol{\tau}$ is widely used in numerical algorithms for metal plasticity, since plastic deformation of common metals is isochoric. Both Cauchy and Kirchhoff stress are defined in the current state and are therefore a measure of force per unit deformed area. The unit normal $\mathbf{n}$ of a surface element in the current state however, is constantly changing with deformation making it difficult to determine. In contrary, the unit normal $\mathbf{N}$ of a surface element in the reference state is easier to determine, since the undeformed geometry is known. This resulted to the definition of the **Nominal stress** from $\boldsymbol{\sigma}$ as:

$$\mathbf{T} = J\,\mathbf{F}^{-1} \cdot \boldsymbol{\sigma} \tag{1.45}$$

where in this case the component T_{ij} expresses the j–th component of force per unit area in the reference configuration, on a surface element of the current configuration whose normal was in the i direction in the undeformed state.

The Nominal stress is derived from the Cauchy stress by expressing the unit normal $\mathbf{n}$ in terms of $\mathbf{N}$ which can be achieved recalling equations (1.11–1.12). Note however that from its definition the Nominal stress is not symmetric in general since $\mathbf{F}$ is not symmetric[10].We also define the **1st Piola–Kirchhoff stress** as the transpose of the Nominal stress as:

$$\mathbf{P} = J\,\boldsymbol{\sigma}^T \cdot \mathbf{F}^{-T} = \mathbf{T}^T \tag{1.46}$$

The **2nd Piola–Kirchhoff stress S** is defined in the reference configuration and expressed in terms of the Kirchhoff and Cauchy stress as:

$$\mathbf{S} = \mathbf{F}^{-1} \cdot \boldsymbol{\tau} \cdot \mathbf{F}^{-T} = J\,\mathbf{F}^{-1} \cdot \boldsymbol{\sigma} \cdot \mathbf{F}^{-T} \tag{1.47}$$

---

[10]Symmetry of the Cauchy stress is derived as a result of the Axiom of Balance of Angular Momentum which is discussed in the following section

In finite deformation elastoplasticity where the deformation gradient $\mathbf{F}$ is regularly decomposed into an elastic $\mathbf{F}^e$ and a plastic $\mathbf{F}^p$ component[11] we define the **Mandel stress** as follows:

$$\mathbf{\Sigma} = \mathbf{C}^e \cdot \mathbf{S}^e \tag{1.48}$$

where $\mathbf{C}^e$ is the Right Cauchy–Green tensor corresponding to $\mathbf{F}^e$ and $\mathbf{S}^e$ is the 2nd Piola Kirchhoff elastic stress.

The reason behind the definition of all these stress and strain measures (see Section 1.4) lies in the primary hypothesis that the reference and current states may, in general, be significantly different. Selecting stress and strain pairs for engineering applications however is not an arbitrary process. Stresses and strains are to be chosen in pairs that are work–conjugate, in the sense that the product of stress and strain rate must express a form of *virtual work*. Table 1.2 summarizes some work–conjugate stress–strain rate pairs that are commonly encountered in bibliography.

Table 1.2: Work Rate Conjugate Stress–Strain rate pairs

	Stress	**Strain Rate**	**Work Rate**
Rate of work per unit deformed volume	$\boldsymbol{\sigma}$	$\mathbf{D}$	$\sigma_{ij}D_{ij}$
Rate of work per unit undeformed volume	$\boldsymbol{\tau}$	$\mathbf{D}$	$\tau_{ij}D_{ij}$
	$\mathbf{T}$	$\dot{\mathbf{F}}$	$T_{ij}\dot{F}_{ij}$
	$\mathbf{P}$	$\dot{\mathbf{F}}^T$	$P_{ij}\dot{F}_{ji}$
	$\mathbf{S}$	$\dot{\mathbf{E}}^G$	$S_{ij}\dot{E}^G_{ij}$
	$\mathbf{\Sigma}$	$\dot{\mathbf{E}}^G$	$\Sigma_{ij}\dot{E}^G_{ij}$
-	$\mathbf{B}$[12]	$\dot{\mathbf{E}}^B$	$B_{ij}\dot{E}^B_{ij}$

1.7 Axioms of Continuum Mechanics

1.7.i Conservation of Mass

The total mass of any subregion dV within a deformable body must be conserved. This statement constitutes the first axiom of continuum mechanics and can be expressed in integral form as follows:

$$\dot{m} = 0 \Rightarrow \frac{d}{dt}\int_V \rho dV = 0 \quad \forall V \Rightarrow \int_V \rho dV = \int_{V_0} \rho_0 dV_0 \quad \forall V \Rightarrow \int_V \rho dV = \int_{V_0} \frac{\rho_0}{J} dV \quad \forall V \Rightarrow$$

---

[11]The multiplicative decomposition of the deformation gradient in crystal plasticity is discussed in further detail in Section 3.1.i

[12]$\mathbf{B}$ stands for the Biot or Jaumann stress defined as $\mathbf{B} = \text{symm}\left[\mathbf{R}^T \cdot \mathbf{P}\right]$ and has not a particular physical interpretation. Is is work–conjugate to the Biot strain defined in Section 1.4

$$\int\limits_V \left(\rho - \frac{\rho_0}{J}\right) dV = 0 \quad \forall V \Rightarrow \boxed{\rho\, J = \rho_0} \tag{1.49}$$

where $J = \det\mathbf{F}$. This result suggests that the mass density of the continuum body is constrained, in the sense that the product $\rho\, J$ must be constant at all times within the continuum during deformation. In addition, we can take the rate form of (1.49) to derive:

$$\frac{d}{dt}\left(\rho\, J\right) = \frac{d}{dt}\left(\rho_0\right) \Rightarrow \dot{\rho}\, J + \rho\, \dot{J} = 0 \tag{1.50}$$

But notice that

$$\dot{J} = J\, L_{kk} = J\, D_{kk} = J\, v_{k,k} = J\, \boldsymbol{\nabla} \cdot \boldsymbol{v} \tag{1.51}$$

Thus, combining (1.50) and (1.51) we end up with:

$$\boxed{\dot{\rho} + \rho\, \boldsymbol{\nabla} \cdot \boldsymbol{v} = 0} \tag{1.52}$$

which defines the **Continuity Equation**.

1.7.ii Balance of Linear Momentum

The linear momentum $\boldsymbol{l}$ of a continuum deformable body that occupies volume V is defined as:

$$\boldsymbol{l} = \int\limits_V \rho\, \boldsymbol{v} dV \tag{1.53}$$

and the rate of linear momentum, denoted as $\dot{\boldsymbol{l}}$, can be directly derived from (1.53) using Reynold's transport theorem:

$$\dot{\boldsymbol{l}} = \int\limits_V \rho\, \dot{\boldsymbol{v}} dV = \int\limits_V \rho\, \mathbf{a} dV \tag{1.54}$$

The total forces $\Sigma\mathbf{F}$ acting on an arbitrary subregion V of the continuum body is generally expressed as the sum of body forces and surface loads as:

$$\Sigma\mathbf{F} = \int\limits_V \rho\, \mathbf{b} dV + \int\limits_S \mathbf{t}\, dS \tag{1.55}$$

The Axiom of Balance of Linear Momentum demands that the total forces acting on any subregion V of the body must be equal with the rate of linear momentum of that subregion. The latter is expressed as:

$$\Sigma\mathbf{F} = \dot{\boldsymbol{l}} \quad \forall V \tag{1.56}$$

Substituting (1.54) and (1.55) to (1.56) and performing the algebraic calculations leads to the following equation:

$$\int\limits_V \left(\boldsymbol{\sigma} \cdot \boldsymbol{\nabla} + \rho\, \mathbf{b} - \rho\, \mathbf{a}\right) dV \quad \forall V \Rightarrow$$

Since the above equation must hold for any subregion V within the continuum body, we can take advantage of the localization theorem to derive:

$$\boxed{\boldsymbol{\sigma} \cdot \boldsymbol{\nabla} + \rho\, \mathbf{b} = \rho\, \mathbf{a}} \tag{1.57}$$

Expression (1.57) is referred to as the equilibrium equations which along with the kinematics and constitutive equations form the Boundary Value Problem (BVP).

1.7.iii Balance of Angular Momentum

The angular momentum $\mathbf{H}$ of a continuum deformable body that occupies volume V is defined as:

$$\mathbf{H} = \int_V \rho\, \mathbf{r} \times \boldsymbol{v}\, dV \tag{1.58}$$

where $\mathbf{r}$ stands for the position vector of the material point. Again, using Reynold's transport theorem, the rate of angular momentum is expressed as:

$$\dot{\mathbf{H}} = \int_V \rho\, (\dot{\mathbf{r}} \times \boldsymbol{v} + \mathbf{r} \times \dot{\boldsymbol{v}})\, dV = \int_V \rho\, (\boldsymbol{v} \times \boldsymbol{v} + \mathbf{r} \times \mathbf{a})\, dV = \int_V \rho\, \mathbf{r} \times \mathbf{a}\, dV \tag{1.59}$$

The sum of moments acting in an arbitrary subregion V of the continuum body is generally expressed as:

$$\Sigma\mathbf{M} = \int_V \rho\, \mathbf{r} \times \mathbf{b}\, dV + \int_S \mathbf{r} \times \mathbf{t}\, dS \tag{1.60}$$

The principle of conservation of angular momentum demands that the sum of moments in any subregion within the deformable continuum body must equal the rate of angular momentum of that subregion, which is expressed as

$$\dot{\mathbf{H}} = \Sigma\mathbf{M} \quad \forall\, V \tag{1.61}$$

Substituting (1.59) and (1.60) to (1.61) and performing the algebraic calculations[13] eventually yields:

$$e_{ijk}\, \sigma_{jk} = 0 \tag{1.62}$$

Evaluating the above expression[14] for $i = 1, 2, 3$ leads to:

$$\boxed{\boldsymbol{\sigma} = \boldsymbol{\sigma}^T} \tag{1.63}$$

suggesting that the Cauchy stress tensor $\boldsymbol{\sigma}$ is symmetric.

---

[13]The divergence theorem is also required to convert surface integrals to volume integrals

[14]Note that expression (1.62) is essentially 3 equations since i is a free index

1.7.iv **Conservation of Energy**

Postulating that the continuum body undergoes only mechanical and thermal phenomena[15], it's total energy can be expressed as the sum of it's kinetic and internal energies as follows:

$$E = K + U = \int_V \frac{1}{2}\rho\,\boldsymbol{v}\cdot\boldsymbol{v}\,dV + \int_V \rho\,u\,dV \tag{1.64}$$

where $\boldsymbol{v}$ stands for the velocity field of the continuum body and u represents the body's internal energy per unit mass. Now the supply of power to the body can be expressed as the sum of a thermal generation component, a surface heat flux component and a component due to external forces as:

$$I = R + Q + P = \int_V \rho\,r\,dV - \int_S \mathbf{q}\cdot\mathbf{n}\,dS + \int_V \rho\,\mathbf{b}\cdot\boldsymbol{v}\,dV + \int_S \mathbf{t}\cdot\boldsymbol{v}\,dS \tag{1.65}$$

where r expresses the generated heat per unit mass and $\mathbf{q}$ is the thermal power provided per unit of surface. The conservation of energy axiom demands that the supply of power to the body must equal the rate of total energy in the body, which can be expressed as:

$$I = \dot{E} \quad \forall\, V \tag{1.66}$$

Substituting $\dot{E}$[16] and I from (1.64–1.65) and performing the algebraic calculations[17] yields:

$$\boxed{\rho\,\dot{u} = \boldsymbol{\sigma} : \mathbf{D} + \rho\,r - \boldsymbol{\nabla}\cdot\mathbf{q}} \tag{1.67}$$

1.7.v **Entropy**

The entropy S of a subregion V in the continuum body is introduced as:

$$S = \int_V \rho\,s\,dV \tag{1.68}$$

where s is the entropy per unit mass. We next define the entropy input rate I_s in a subregion V, as the sum of two main components; a heat generation component and a surface heat flux component.

$$I_s = \int_V \frac{\rho\,r}{\theta}\,dV - \int_S \frac{1}{\theta}\,\mathbf{q}\cdot\mathbf{n}\,dS \tag{1.69}$$

where θ is the absolute temperature. The 2nd law of thermodynamics requires that the rate of entropy must always be greater or equal[18] to the entropy input rate in any subregion V

---

[15]This assumption can be easily relaxed by assuming other phenomena (i.e. electrostatic, magnetic etc.) as well. In this subsection we only assume mechanical and thermal phenomena in the continuum for the sake of simplicity

[16]Reynold's transport theorem is required to evaluate $\dot{E}$ from E

[17]The divergence theorem is also required to convert surface integrals to volume integrals

[18]Equality is satisfied only in reversible processes

of the continuum body. In math form:

$$\dot{S} \geq I_s \quad \forall V \tag{1.70}$$

This inequality can be restated as:

$$\boxed{\dot{s} \geq \frac{r}{\theta} - \frac{1}{\rho} \boldsymbol{\nabla} \cdot \left(\frac{\mathbf{q}}{\theta} \right)} \tag{1.71}$$

by substituting expressions (1.68) and (1.69). The above constraint is also referred to as the **Clausius–Duhem Inequality**. We can also take advantage of the energy balance in (1.67) to derive:

$$\boxed{\boldsymbol{\sigma} : \mathbf{D} - \frac{1}{\theta} \mathbf{q} \cdot \boldsymbol{\nabla}\theta - \rho \left(\dot{\psi} + s\dot{\theta} \right) \geq 0} \tag{1.72}$$

where ψ is the Helmholtz free energy defined as $\psi = u - s\,\theta$. The Clausius–Duhem inequality is of major importance in the development of a specific constitutive model, by providing restrictions to the constitutive functions being used as well as to their dependent variables.

1.8 Objectivity and Rates

Consider the motion $\mathbf{x} = \mathbf{x}(\mathbf{X}, t)$ with a deformation gradient $\mathbf{F}(\mathbf{X}, t)$ and superpose a rigid body motion so that:

$$\overline{\mathbf{x}}(\mathbf{X}, t) = \mathbf{Q}(t) \cdot \mathbf{x}(\mathbf{X}, t) + \mathbf{c}(t)$$

where $\mathbf{Q}(t)$ is a proper orthogonal tensor with $\mathbf{Q}(0) = \boldsymbol{\delta}$ and the translation $\mathbf{c}(t)$ is such that $\mathbf{c}(0) = \mathbf{0}$. The two motions $\mathbf{x}$ and $\overline{\mathbf{x}}$ are schematically illustrated in Figure 1.9. The deformation gradient $\overline{\mathbf{F}}$ corresponding to the new motion $\overline{\mathbf{x}}$ can be readily expressed by differentiating the above equation as:

$$\overline{\mathbf{F}}(\mathbf{X}, t) = \mathbf{Q}(t) \cdot \mathbf{F}(\mathbf{X}, t)$$

We introduce the concept of **Objectivity**[19] in the sense that the qualitative and quantitative characteristics of an Objective quantity are unaffected when the quantity is observed under a variety of conditions. For instance, material properties of a continuum body are invariant from the observer's motion and are therefore objective quantities.

More precisely, assuming that the two motions $\mathbf{x}$ and $\overline{\mathbf{x}}$ are recorded by two different observers we can define objective tensors in the following sense:

1. Lagrangian tensors defined in $\boldsymbol{\mathfrak{B}}_0$ are objective if only they remains unaffected by the observer's motion in the sense:

$$\overline{\mathbf{a}}(\mathbf{X}, t) = \mathbf{a}(\mathbf{X}, t)$$

---

[19]Also referred to as the concept of Frame Invariance
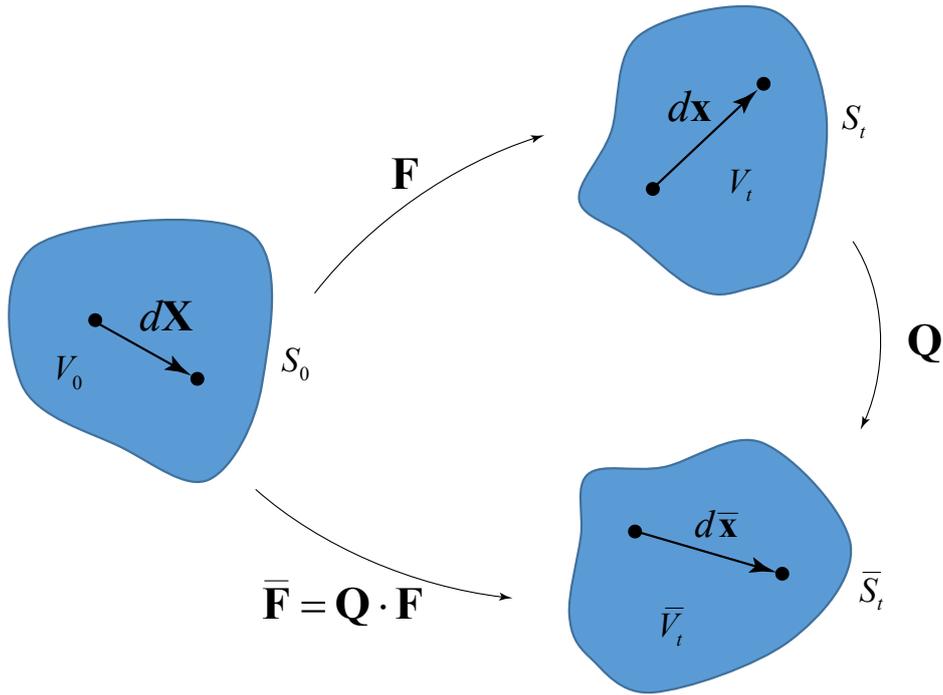
Figure 1.9: Reference state and the deformed states before and after superposing a rigid body motion

$$\overline{\mathbf{A}}(\mathbf{X}, t) = \mathbf{A}(\mathbf{X}, t)$$

2. Eulerian tensors defined in $\mathfrak{B}_t$ are objective if only they transform according to:

$$\overline{\mathbf{a}}(\overline{\mathbf{x}}, t) = \mathbf{Q}(t) \cdot \mathbf{a}(\mathbf{X}, t)$$
$$\overline{\mathbf{A}}(\overline{\mathbf{x}}, t) = \mathbf{Q}(t) \cdot \mathbf{A}(\mathbf{X}, t) \cdot \mathbf{Q}^T(t)$$

3. Two–point second order tensors are objective if only they transform according to:

$$\overline{\mathbf{A}} = \mathbf{Q}(t) \cdot \mathbf{A} \quad \text{or} \quad \overline{\mathbf{A}} = \mathbf{A} \cdot \mathbf{Q}^T(t)$$

Using these definitions it is easy to show that the deformation gradient $\mathbf{F}$ is two-point objective, Cauchy $\boldsymbol{\sigma}$ and Kirchhoff $\boldsymbol{\tau}$ stresses are both Eulerian objective, while the Deformation rate $\mathbf{D}$ is also Eulerian objective. The Nominal stress $\mathbf{T}$ is two point objective, whereas $\mathbf{S}$ and $\boldsymbol{\Sigma}$ are Lagrangian objective. Furthermore, if a 2nd order tensor $\mathbf{A}$ is Lagrangian objective then can be proved that the rate $\dot{\mathbf{A}}$ is also Lagrangian objective. In contrast, if $\mathbf{A}$ is an Eulerian objective tensor, the rate $\dot{\mathbf{A}}$ is **not** an objective tensor[20]. However, the rates of Eulerian objective tensors like the Cauchy and Kirchhoff stresses are often required in continuum mechanics, especially in the constitutive laws accounting for finite deformations and rotations. The latter resulted into the definition of the so–called **Co-rotational** Eulerian Objective rates, the most popular of which [17] are presented in Table 1.3.

---

[20]For instance, the rate of Cauchy stress $\dot{\boldsymbol{\sigma}}$ is not objective, even though the Cauchy stress itself is Eulerian objective

Table 1.3: Objective rates of an Eulerian 2nd order tensor $\mathbf{A}$

Rate	Definition
Truesdell	$\overset{\circ}{\mathbf{A}} = \dot{\mathbf{A}} - \mathbf{L} \cdot \mathbf{A} - \mathbf{A} \cdot \mathbf{L}^T + \mathrm{tr}[\mathbf{L}]\,\mathbf{A}$
Oldroyd	$\overset{\square}{\mathbf{A}} = \dot{\mathbf{A}} - \mathbf{L} \cdot \mathbf{A} - \mathbf{A} \cdot \mathbf{L}^T$
Cotter–Rivlin	$\overset{*}{\mathbf{A}} = \dot{\mathbf{A}} + \mathbf{L}^T \cdot \mathbf{A} + \mathbf{A} \cdot \mathbf{L}$
Green–Naghdi	$\overset{\triangle}{\mathbf{A}} = \dot{\mathbf{A}} - \left(\dot{\mathbf{R}} \cdot \mathbf{R}^T\right)\mathbf{A} + \mathbf{A} \cdot \left(\dot{\mathbf{R}} \cdot \mathbf{R}^T\right)$
Jaumann	$\overset{\nabla}{\mathbf{A}} = \dot{\mathbf{A}} - \mathbf{W} \cdot \mathbf{A} + \mathbf{A} \cdot \mathbf{W}$

The axiom of objectivity demands that the stress and strain rates being used in a constitutive law are such that the constitutive model is objective. Therefore, the definition of a constitutive law[21] in terms of the Cauchy stress requires the implementation of one of the objective rates defined in Table 1.3, since $\boldsymbol{\sigma}$ is Eulerian objective. The Jaumann rate is the most commonly encountered objective stress rate in the constitutive laws of solids, mainly because it is the easiest to implement in a computational model. In the context of the rate–independent constitutive model for crystal plasticity and its computational implementation, which are the main focus of this thesis, we implement the Jaumann rate of Kirchhoff stress $\overset{\nabla}{\boldsymbol{\tau}}$ in the constitutive stress rate–strain rate law in section 3.6. The Jaumann rate of Cauchy stress $\overset{\nabla}{\boldsymbol{\sigma}}$ is also implemented in the Finite Element Equations to evaluate the Elemental Stiffness matrix as presented in Section 6.2.

---

[21]It is implied that the constitutive law is introduced in rate form

Chapter 2

Crystallography

2.1 The Crystal Lattice

The vast majority of metals form crystalline solids when they solidify from the liquid state[1]. Crystalline solids, as opposed to their amorphous counterparts (i.e. glass) and fluids, exhibit a periodic arrangement of atoms in space. This periodicity enables us to consider the solid as a spatial superposition of the smallest possible repeating unit, which we call the **unit cell**. The periodical arrangement of unit cells in the three dimensional space subsequently defines the **crystal lattice** and the position vector $\mathbf{r}$ of any arbitrary point within the lattice is:

$$\mathbf{r} = u\,\mathbf{a} + v\,\mathbf{b} + w\,\mathbf{c} \tag{2.1}$$

,where $\mathbf{a}, \mathbf{b}, \mathbf{c}$ are the crystal's reference axes or **crystal axes**, whom length and orientation depends on the crystal under consideration. The consideration of all possible angle and length combinations between the crystal axes leads to the definition of the 14 **Bravais Lattices** illustrated in Figure 2.1 that follows. Every Bravais lattice is assigned with a crystal axes system to enable the description of any position vector as equation (2.1) suggests. The latter defines a total of 7 discrete crystal axes systems that form the basis for the classification of each crystal to its corresponding crystal system. The 7 crystal axes systems are presented in Table 2.1 below, along with their corresponding relationships for their axes lengths and angles.

In the context of crystallography, we often refer to crystallographic directions and planes to facilitate the study of crystals and their properties. We therefore need to find a convenient way to describe them with respect to the appropriate crystal axes system. As far as crystal

---

[1]This section is mainly based on Chapter 2 of Book [27]
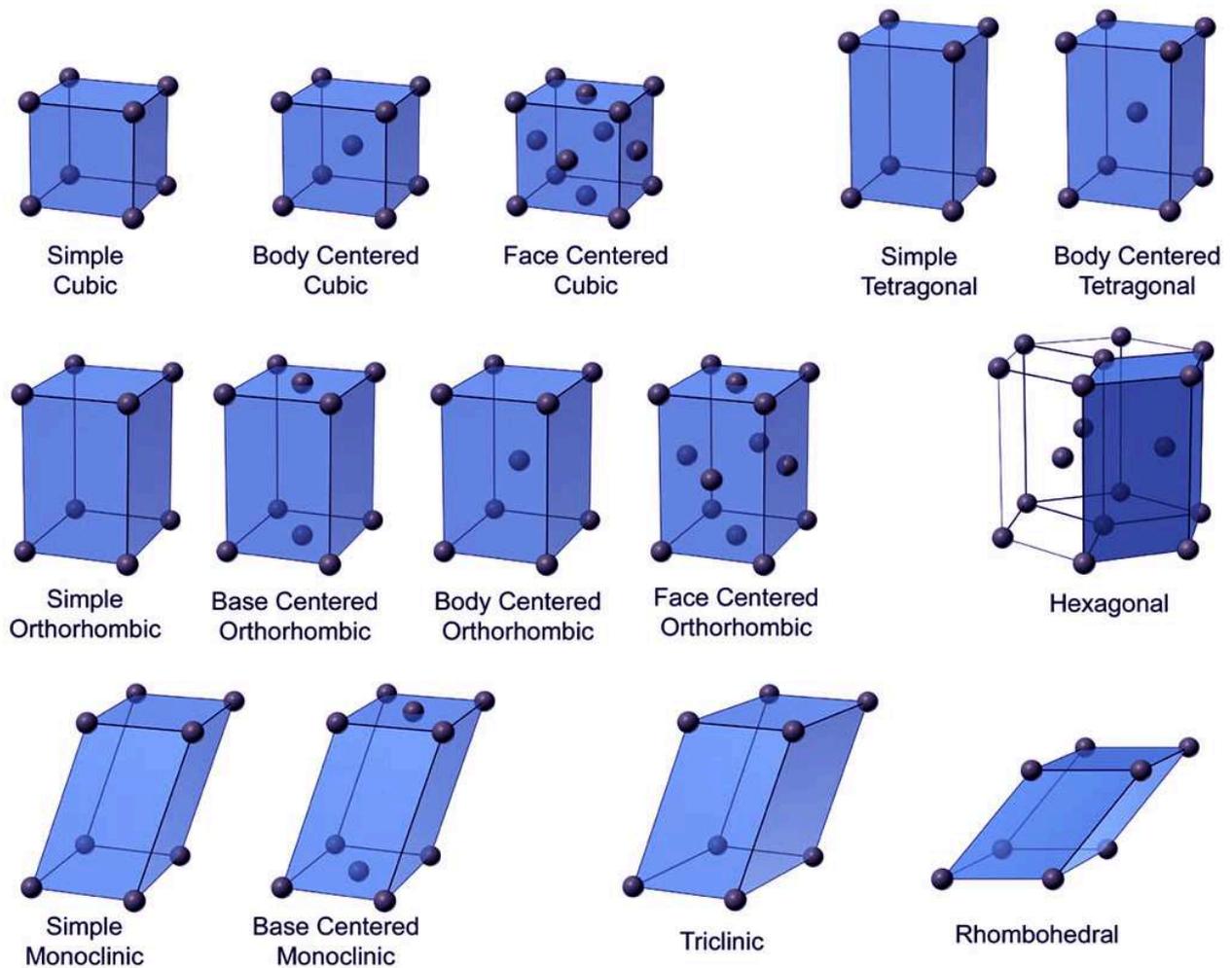
Figure 2.1: The Bravais Lattices

directions are concerned, we implement the notation $[uvw]$ to refer to the crystal direction $\mathbf{r} = u\mathbf{a}+v\mathbf{b}+w\mathbf{c}$. This notation is essentially a compact form of expression (2.1), where u, v, w are the smallest possible integers that can describe the desired direction. Negative vector components are indicated with a bar above the number[2] and crystallographic directions that belong to the same direction families are referred to as $< uvw >$ for the sake of brevity[3].

Crystallographic planes on the other hand are described using **Miller indices**. Miler indices are able to describe the orientation of a desired plane irrespectively of its distance from the point of origin. Hence, parallel planes are denoted with the same Miller indices whom in order to find we have to do the following:

- Find the points of intersection between the desired plane and the crystal axes

- Inverse these numbers

---

[2]i.e. the crystal direction $\hat{\mathbf{r}} = -\mathbf{a} + \mathbf{b} - 3\mathbf{c}$ should be denoted as $[\bar{1}1\bar{3}]$

[3]In the special case of cubic crystals, the directions aligned with the diagonals of the cube are thought to form a **direction family** which is denoted as $< 111 >$

- Reduce the triad to the smallest possible integers h, k, l

- The Miller indices are k, k, l respectively

The Miller indices h, k, l are then enclosed in parenthesis and the corresponding plane is referred to as (hkl). Note however, that the notation (hkl) representing a plane Π is not exclusive, since all planes parallel to Π are defined using the same Miller indices. Particular planes, along which the atom arrangement is identical, are assumed to be *Equivalent* and are denoted all together using curly brackets as $\{hkl\}$.

Table 2.1: The 7 Crystal Axes Systems

Crystal System	**Axes and Angles**[4]	**Examples**
Triclinic	$a \neq b \neq c$ $\hat{\alpha} \neq \hat{\beta} \neq \hat{\gamma} \neq 90$	K_2CrO_7
Monoclinic	$a \neq b \neq c$ $\hat{\alpha} = \hat{\gamma} = 90 \neq \hat{\beta}$	$\beta - S, CaSO_4$
Orthorhombic	$a \neq b \neq c$ $\hat{\alpha} = \hat{\beta} = \hat{\gamma} = 90$	$\alpha - S, Fe_3C$
Tetragonal	$a = b \neq c$ $\hat{\alpha} = \hat{\beta} = \hat{\gamma} = 90$	TiO_2
Cubic	$a = b = c$ $\hat{\alpha} = \hat{\beta} = \hat{\gamma} = 90$	Fe,Cu,Ni,Au
Hexagonal [5]	$a_1 = a_2 = a_3 \neq c$ $\hat{\alpha} = \hat{\beta} = 90, \hat{\gamma} = 120$	Zn,Mg
Rhombohedral	$a = b = c$ $\hat{\alpha} = \hat{\beta} = \hat{\gamma} \neq 90$	Sb,Bi

Now for simplicity purposes let us visualize atoms in the crystal lattice of metals, as rigid and equally sized spheres. Individual crystal structures can now be interpreted as different ways that these spheres can be arranged to fill the space. According to Goldschmidt and Laves, filling of space is subjected to 3 basic principles:

- Atoms in crystal structures are packed in such a way so as to efficiently fill the space (close packing)

- The spaces occupied by atoms are such to produce the maximum possible symmetry in the structure

---

[4] Note that a, b, c represent the crystal axes while $\hat{\alpha}, \hat{\beta}, \hat{\gamma}$ the corresponding angles between them.
[5] The Hexagonal crystal system consists of three equal axes that lie on the same plane along with a fourth axis c which is perpendicular to that plane

- Atoms are packed in such a way, so as to maximize their coordination number (CN) (i.e. maximum # of neighbours)

These principles suggest that atoms are arranged in such a way, that dense structures are formed. The vast majority of metals crystallize into one the following dense cubic crystal structures:

- Body Centered Cubic (BCC)

- Face Centered Cubic (FCC)

- Hexagonal Close Packed (HCP)

The unit cells of the BCC and FCC structures are illustrated in Figure 2.2, where the spheres represent atoms as aforementioned and the size of the spheres is proportional to the distances between them.
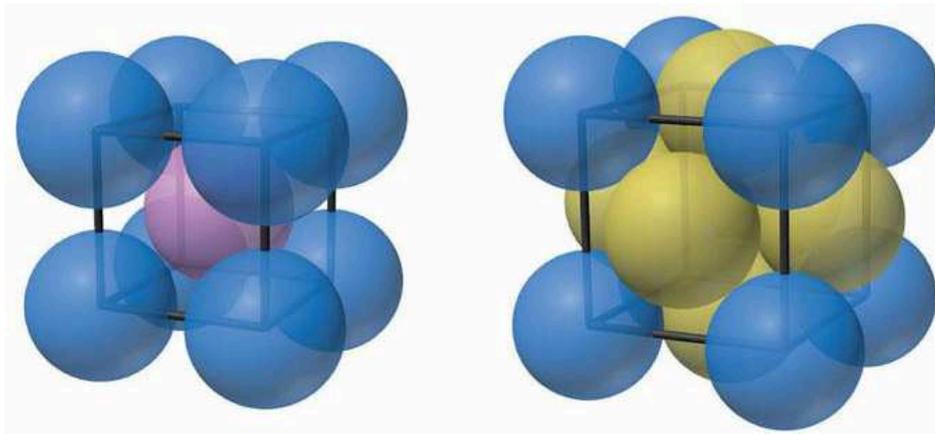
Figure 2.2: The arrangement of atoms in the two most popular crystal structures of metals, BCC (left) and FCC (right)

2.2 Slip Systems, Dense Planes and Directions

Let us define the **dense planes** of a crystal structure, as the ones at which the denser possible arrangement of atoms (spheres) is achieved. Subsequently, we also define the directions along which the atoms are sorted in the denser possible manner as **dense directions**. In most dense crystal structures, atoms osculate along dense planes and directions. It should be noted however, that dense planes and directions are typical of the specific structure since they depend on the exact atom arrangement. For instance, planes of the {111} plane family are the dense planes and crystallographic directions $< 110 >$ are the dense directions of the FCC structure. On the other hand, the dense planes of the BCC structure are the {110} whereas their dense directions are the $< 111 >$.

The combination of dense planes and directions in the sense $\{abc\} < hkl >$ defines the structure's **slip systems**. Slip systems are greatly important to the plasticity of metal single crystals, since atomic slip can only occur along dense directions located on dense planes. The latter also justifies the fact that dense directions are also commonly referred to as **slip directions**, whereas dense planes as **slip planes**. FCC metals contain 12 $\{111\} < 110 >$ slip systems whereas metals of the BCC structure only 5 systems of the family $\{110\} < 111 >$. The relative position of dense planes and directions forming the slip systems of BCC and FCC crystals are schematically illustrated in Figures 2.3a and 2.3b respectively.

(a)   (b)
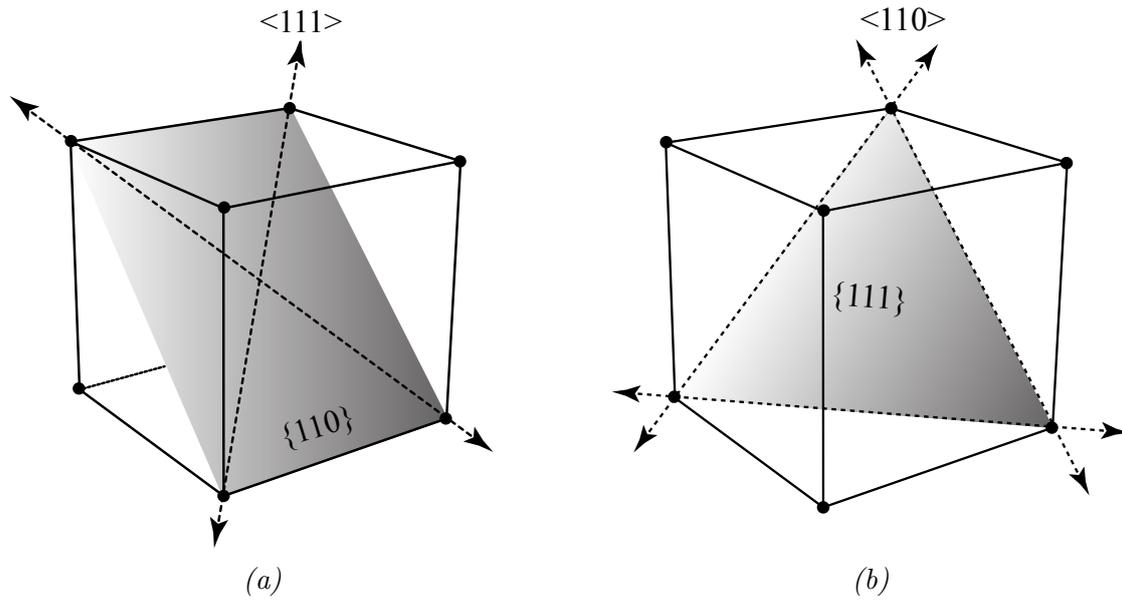
Figure 2.3: The Slip systems of a BCC (a) and a FCC (b) crystal

FCC crystals present the greatest challenge in terms of developing a constitutive model that accounts for their inelastic behavior, since they possess the greatest number of available slip systems. From this point on, we focus our attention entirely on FCC crystals. Table 2.2 presents the 12 slip systems of FCC crystals denoting the slip (dense) planes and the corresponding slip direction.

Table 2.2: The 12 Slip Systems of FCC Metals

Slip System	Slip Plane	Slip Direction
1		$[01\bar{1}]$
2	(111)	$[\bar{1}01]$
3		$[1\bar{1}0]$
4		$[0\bar{1}1]$
5	$(1\bar{1}\bar{1})$	$[\bar{1}0\bar{1}]$
6		$[110]$

Continues on next page

Table 2.2 – Continued

Slip System	Slip Plane	Slip Direction
7		$[011]$
8	$(\bar{1}1\bar{1})$	$[10\bar{1}]$
9		$[\bar{1}\bar{1}0]$
10		$[0\bar{1}\bar{1}]$
11	$(\bar{1}\bar{1}1)$	$[101]$
12		$[\bar{1}10]$

Before we conclude the present discussion on the Slip systems of crystal structures it is necessary to address the concept of optimally oriented systems and the effect of slip system orientation to the deformation of a single crystal. For this reason, let us consider the case of a uniaxial tension experiment of a single crystal where the stress tensor has the following simple form:

$$\boldsymbol{\sigma} = \sigma\, \mathbf{p}\, \mathbf{p} \tag{2.2}$$

where $\mathbf{p}$ stands for the unit vector along the loading direction. Taking into consideration that plastic deformation can only occur on a given slip system, we consider a slip plane with unit normal $\mathbf{n}$, along which lies the slip direction defined by the unit vector $\mathbf{s}$. The resolved shear stress on that system, given equation (2.2), can be readily expressed as:

$$\tau = \mathbf{s} \cdot \boldsymbol{\sigma} \cdot \mathbf{n} \Rightarrow \tau = \sigma\,(\mathbf{s} \cdot \mathbf{p})\,(\mathbf{p} \cdot \mathbf{n}) \tag{2.3}$$

We next define angle ϕ as the angle between $\mathbf{p}$ and $\mathbf{n}$ and also angle λ as the one between $\mathbf{s}$ and $\mathbf{p}$. Using these definitions and assuming that vectors $\mathbf{p}, \mathbf{s}, \mathbf{n}$ are introduced as unit vectors we write:

$$\mathbf{s} \cdot \mathbf{p} = \cos\lambda$$

$$\mathbf{p} \cdot \mathbf{n} = \cos\phi$$

And the resolved shear stress on the slip system $(\mathbf{s}, \mathbf{n})$ in (2.3) can be restated in the form:

$$\tau = \sigma\,\cos\phi\,\cos\lambda \tag{2.4}$$

Figure 2.4 constitutes a schematic illustration of the aforementioned uniaxial tension setting, indicating the directions $\mathbf{p}, \mathbf{s}, \mathbf{n}$ and angles ϕ, λ. The cosine product $\cos\phi\,\cos\lambda$ defines the Schmid factor, which is essentially a measure of optimal orientation for a given slip system. For a given loading direction, slip systems with the greatest Schmid factor, are subjected to greater τ for the same applied macroscopic σ. A system can then be declared (in terms of the Schmid factor) as **optimally oriented** for plastic slip, if the Schmid factor of that system is the greatest. In a uniaxial tension experiment at which only one system is initially optimally oriented, the crystal is said to embody an easy glide orientation. Once the first system is active, the crystal rotates until the slip direction is aligned with the loading axis and the

corresponding Schmid factor becomes zero. In reality however, crystal rotation eventually triggers the activation of a second slip system, which then changes the rotation direction. The concept of crystal rotation with plastic deformation is addressed in further detail in Section 3.2.i.
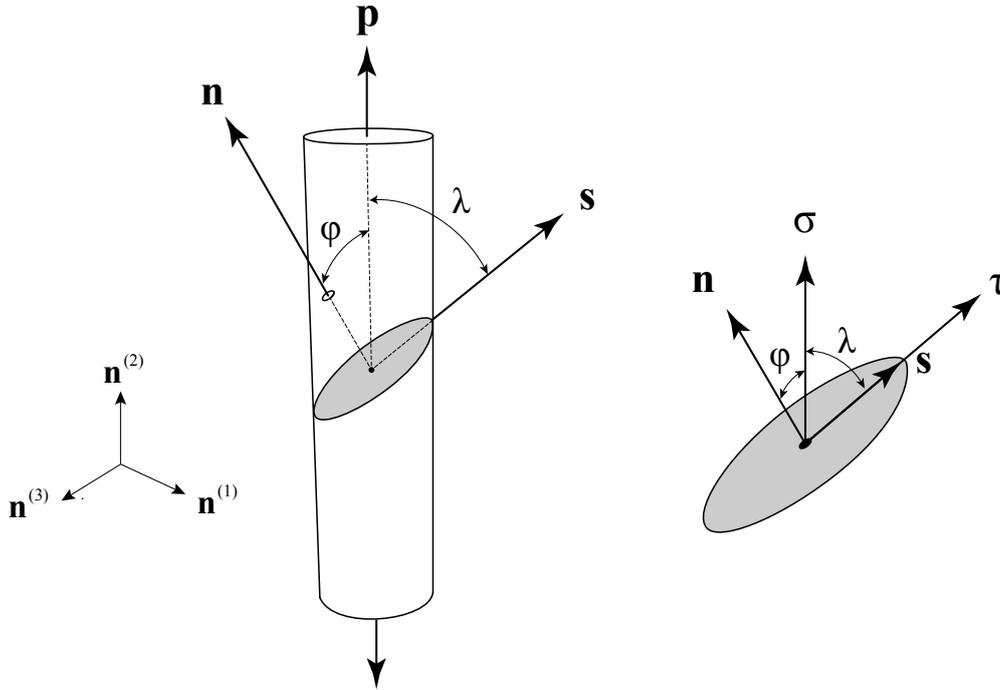
Figure 2.4: A single crystal specimen subjected to uniaxial tension, highlighting the slip and normal unit vectors of an arbitrary slip system

Evidently, description and understanding of the basic concepts of crystals (i.e. slip systems, dense planes and directions etc.) involves the process of visualizing both the crystal structure and the desired directions in the three dimensional space, which is rather difficult and not always straightforward. We therefore have to find a simple and convenient method to refer to such concepts. The method of Stereographic Projection is amongst the most popular methods used for that purpose and is presented in the following section.

2.3 Stereographic Projection

Stereographic projection is a graphical method that is used to map geometric information from the 3-dimensional space into a plane. This method can be used to project crystallographic directions into a plane, facilitating the supervision of crystal orientation. However, it should be noted that this projection is general and it's applications are not limited to crystallography.

The projection is defined on the entire sphere apart from the projection point. The

projection is also smooth, bijective and conformal in the sense that angles are preserved. Lengths and areas however are not preserved, consisting it a non–isometric projection. The stereographic projection of any crystal direction can be obtained by following the steps presented in Table 2.3 and schematically illustrated in Figure 2.5.
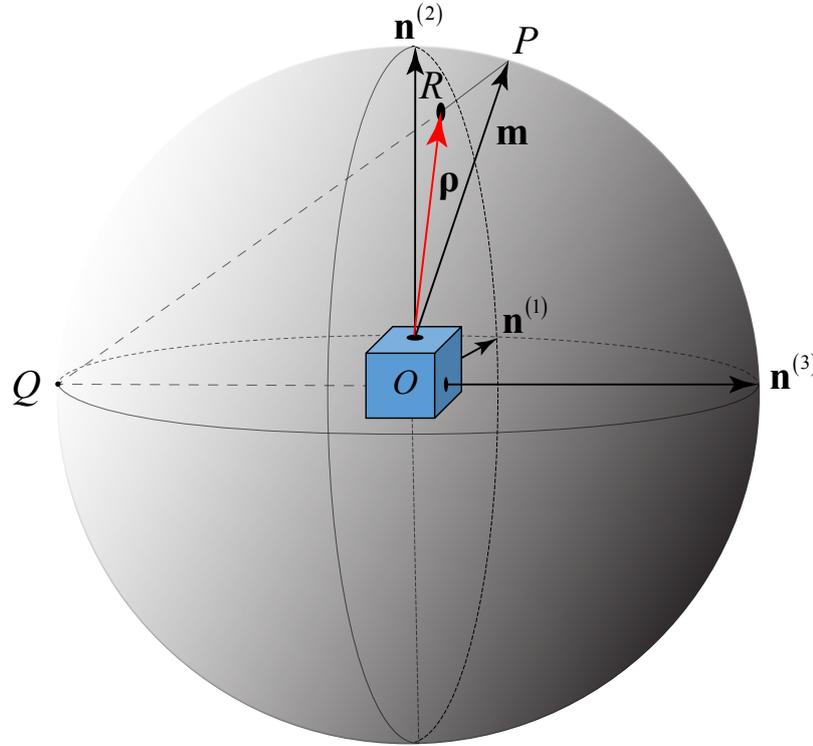
Figure 2.5: A schematic representation of stereographic projection

Table 2.3: Steps to obtain the stereographic projection $\boldsymbol{\rho}$ of an arbitrary crystal direction $\mathbf{m}$

> **1.** The cubic crystal is centered inside an imaginary sphere with radius $|r| = 1$ and center O
>
> **2.** We define a coordinate system $\mathbf{n}^{(i)}$ originating from the center of the sphere
>
> **3.** The crystal direction to be projected $\mathbf{m}$, intersects the sphere at a point P
>
> **4.** The horizontal axis also intersects the sphere at a different point Q
>
> **5.** We draw the line PQ
>
> **6.** The line PQ intersects the meridian plane at a new point R
>
> **7.** The vector $(OR) = \boldsymbol{\rho}$ is the stereographic projection of $\mathbf{m}$

From a mathematical point of view it can be proven that the transformation between a general vector $\mathbf{m}$ and its stereographic projection $\boldsymbol{\rho}$ is the following:

$$\boldsymbol{\rho} = \frac{\mathbf{m} - (\mathbf{m} \cdot \mathbf{n}^{(3)})\mathbf{n}^{(3)}}{1 + \mathbf{m} \cdot \mathbf{n}^{(3)}} \tag{2.5a}$$

$$\mathbf{m} = \frac{2\boldsymbol{\rho} + (1 - \boldsymbol{\rho} \cdot \boldsymbol{\rho})\mathbf{n}^{(3)}}{1 + \boldsymbol{\rho} \cdot \boldsymbol{\rho}} \tag{2.5b}$$

Equation (2.5a) can also be written in the following form:

$$\boldsymbol{\rho} = \rho_1 \mathbf{n}^{(1)} + \rho_2 \mathbf{n}^{(2)} = |\boldsymbol{\rho}| \left(\cos \Theta \, \mathbf{n}^{(1)} + \sin \Theta \, \mathbf{n}^{(2)} \right) \tag{2.6}$$

In crystal plasticity, we take advantage of the projection mainly to monitor the transformations[6] of crystal directions and vectors, as the crystal undergoes plastic deformation. Initially, we choose three specific crystal directions to be aligned with the crystal base $\mathbf{n}^{(i)}$ and we then calculate the stereographic projection of the directions that present the greatest interest to our study. Plotting the evolution of the calculated projections in a polar domain, defines the **inverse pole figure** diagram[7]. However, the projection can also be used to plot different crystal directions as points within a circle, defining the **pole figure** diagram. An example of a pole figure diagram is presented in Figure 2.6 displaying the projections of some commonly encountered crystal directions.
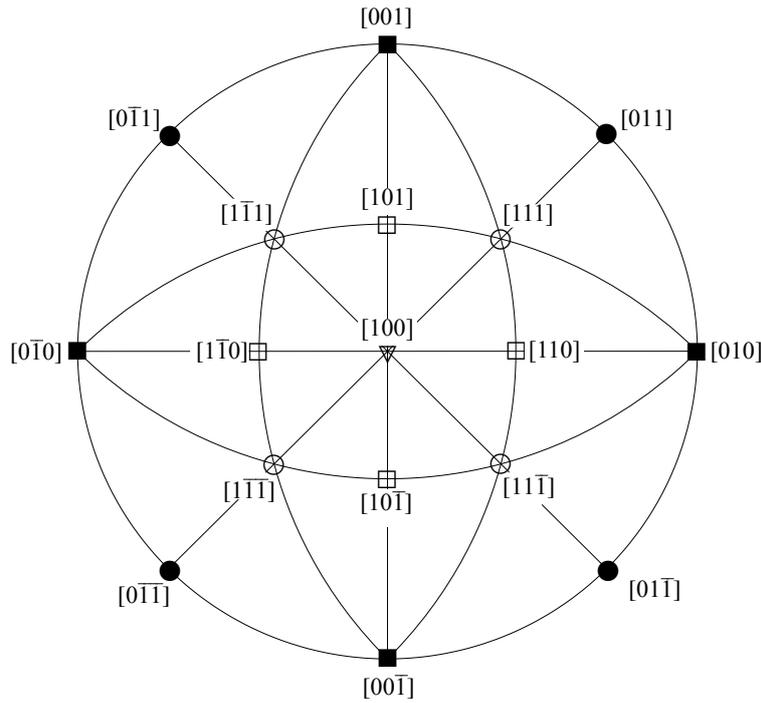
Figure 2.6: A pole figure diagram showing the stereographic projections of several crystal directions

As shown in the pole figure diagram, the total projection region is divided into several curvilinear triangles. We focus on the first quartile on which lie the projections of all crystal directions with positive indices. The first quartile consists of 6 curvilinear triangles in total, which are presented in greater detail in Figure 2.7 below. The 6 curvilinear triangles are equivalent, since they only differ in terms of the order of indices of the crystal direction being

---

[6]i.e. rotation

[7]The inverse pole figure diagram can be used to monitor the rotation of the imposed loading direction during the uniaxial tension of a single crystal
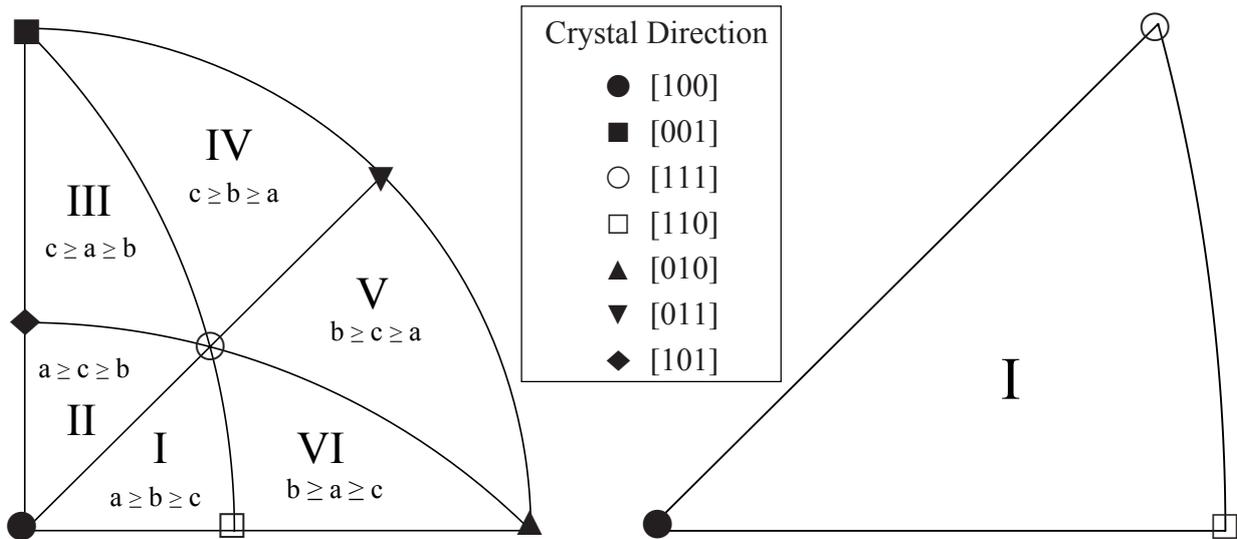
Figure 2.7: The stereographic projection region for crystal directions with positive indices [a b c] (left). The region is divided into 6 curvilinear triangles. The standard triangle on which lie the stereographic projection of all crystal directions with indices in a descending order (right)

projected. The standard triangle presented in Figure 2.7 (right), is the region of the pole figure diagram on which lie the the stereographic projections of all crystal directions with indices in a descending order. From now on, we will present the pole figure and inverse pole figure diagrams using only the standard triangle, since we can easily manipulate[8] any crystal direction so that its projection lies in the standard triangle.

2.3.i Cartesian and Spherical Coordinates

The process of determining the crystal direction that corresponds to a specific plot point in a pole figure diagram, as well as the calculation of the polar components for the projection of a given direction are just two examples that require to switch between the cartesian and spherical coordinate systems. Apart from crystallography itself, the aforementioned procedures are frequently required in the calculations within a crystal plasticity model. In this subsection, we present the relationships defining a point's spherical coordinates given their values in the cartesian system and vice–versa.

Figure 2.8 illustrates the description of a point P using the cartesian and spherical coordinate systems respectively. The relationships defining the cartesian coordinates (x_1, x_2, x_2) of a point P given (r, θ, ϕ) are [8]:

$$x_1 = r \sin \theta \cos \phi \tag{2.7a}$$

$$x_2 = r \sin \theta \sin \phi \tag{2.7b}$$

$$x_3 = r \cos \theta \tag{2.7c}$$

---

[8]Changing the order of indices. This can be achieved by multiplying the crystal direction with a properly defined matrix
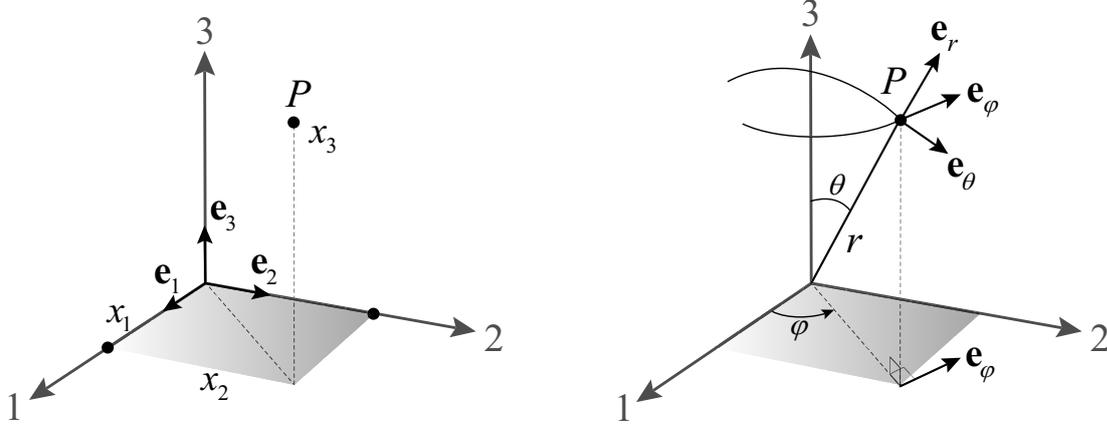
Figure 2.8: Cartesian (x_1, x_2, x_3) and spherical (r, θ, ϕ) coordinates of a point P

The relationships to define the spherical coordinates (r, θ, ϕ) given (x_1, x_2, x_2) are [8]:

$$r = \sqrt{x_1^2 + x_2^2 + x_3^2} \tag{2.8a}$$

$$\theta = \cos^{-1} \frac{x_3}{\sqrt{x_1^2 + x_2^2 + x_3^2}} \tag{2.8b}$$

$$\phi = \tan^{-1} \frac{x_2}{x_1} \tag{2.8c}$$

Finally the unit vectors of the spherical base can be expressed in terms of the cartesian base as [8]:

$$\mathbf{e}_r(\theta, \phi) = \sin\theta \, \cos\phi \, \mathbf{e}_1 + \sin\theta \, \sin\phi \, \mathbf{e}_2 + \cos\theta \, \mathbf{e}_3 \tag{2.9a}$$

$$\mathbf{e}_\theta(\theta, \phi) = \cos\theta \, \cos\phi \, \mathbf{e}_1 + \cos\theta \, \sin\phi \, \mathbf{e}_2 - \sin\theta \, \mathbf{e}_3 \tag{2.9b}$$

$$\mathbf{e}_\phi(\theta, \phi) = \mathbf{e}_r \times \mathbf{e}_\theta = -\sin\phi \, \mathbf{e}_1 + \cos\phi \, \mathbf{e}_2 \tag{2.9c}$$

Inverting the above equations leads to the corresponding expressions defining the cartesian base from the spherical as [8]:

$$\mathbf{e}_1 = \sin\theta \, \cos\phi \, \mathbf{e}_r + \cos\theta \, \cos\phi \, \mathbf{e}_\theta - \sin\phi \, \mathbf{e}_\phi \tag{2.10a}$$

$$\mathbf{e}_2 = \sin\theta \, \sin\phi \, \mathbf{e}_r + \cos\theta \, \sin\phi \, \mathbf{e}_\theta + \cos\theta \, \mathbf{e}_3 \tag{2.10b}$$

$$\mathbf{e}_3 = \cos\theta \, \mathbf{e}_r - \sin\theta \, \mathbf{e}_\theta \tag{2.10c}$$

Chapter 3

Constitutive Modelling

Constitutive laws for finite deformation isothermal elastoplasticity are generally expressed in rate form as $\overset{*}{\boldsymbol{\sigma}} = F(\mathbf{D}, \mathscr{I})$, where $\overset{*}{\boldsymbol{\sigma}}$ represents an objective[1] stress rate, $\mathbf{D}$ is the deformation rate defined in Section 1.5 and $\mathscr{I}$ is an abbreviation for the internal variables of the model under consideration. In the case of metal plasticity, a concave yield surface[2] is also introduced to distinguish elastic from plastic material response, in the sense that stress states located 'inside' the yield surface $(\Phi(\boldsymbol{\sigma}) < 0)$ indicate elastic material response whereas stress states directly on the yield surface $(\Phi(\boldsymbol{\sigma}) = 0)$ result into elastoplastic behavior. The constitutive model may also require a flow rule, defining the evolution of the yield surface as a function of the total accumulated plastic strain.

While the concept of crystal elastoplasticity is based on the same principles, the inherent deformation anisotropy of single crystals, introduces additional complexities to the constitutive model. The 'physical' description of crystal plasticity leads to the definition of a unique form for the plastic part of the velocity gradient tensor $\mathbf{L}^p$. Furthermore, in contrast to polycrystalline metal plasticity, elastic–plastic behavior of single crystals cannot be determined using a unique yield criterion. As discussed in Chapter 2, FCC crystals which are the main focus of this thesis, comprise of 12 slip systems on which plastic slip is accomplished resulting to the definition of 12 distinct yield functions to determine the behavior of the corresponding system. Finally, a flow rule must be introduced based on the 'physics' of dislocation glide and their interactions while simultaneously being in agreement with experimental observations.

---

[1] A more detailed reference on co–rotational rates can be found in Section 1.8

[2] A scalar function of the stress components σ_{ij} of the form $\Phi(\sigma_{ij})$

3.1 Kinematics of Crystal Deformation

In the vast majority of metals, plastic deformation is mainly[3] produced by dislocation glide. Dislocations are linear type defects, existing in thermodynamic equilibrium within the crystal lattices of all metals. The macroscopic non–reversible plastic deformation is attributed to the superposition of numerous dislocation movements occurring on the slip systems of each grain within the metal's microstructure. The fact that dislocations are only able to glide along preferable directions indicates that the deformation produced as result of a single plastic slip is highly anisotropic.

Isotropic plasticity is only present in metals whose microstructure consists of numerous randomly sized and oriented grains. The inherent 'variety' of grain orientations, essentially eliminates the anisotropy induced from plastic slip on each grain, and macroscopically renders an isotropic–like behavior.

A single crystal however, is a monocrystalline solid whose crystal lattice is continuous and unbroken forming a single grain and therefore a unique crystal lattice orientation. As a result, the microscopic anisotropy associated with dislocation glide, is propagated in the macroscale in the form of anisotropic plasticity. The finite number of dislocation glide possibilities[4] suggests that macroscopic plasticity must be microscopically interpreted as a superposition of discrete dislocation glides upon the available slip systems.

The plastic deformation of metal single crystals can be thought to be similar with that of a simple shear motion, since dislocations can only glide upon the slip systems of each crystal structure, and thus along **slip directions**, and on **slip planes**. More precisely, at any given time that a single crystal deforms plastically, dislocations glide on multiple (in general) slip systems simultaneously, which we call **active** systems. The physically based assumption, that crystal plasticity is the result of simultaneous simple shears[5] along the crystal's active systems allows us to express the velocity gradient associated with plastic slip as (Aravas [5]):

$$\mathbf{L}_i^p = \sum_{\alpha=1}^{Nas} \dot{\gamma}^\alpha(t) \mathbf{s}_0^\alpha \mathbf{m}_0^\alpha \tag{3.1}$$

where $\mathbf{s}_0^\alpha, \mathbf{m}_0^\alpha$ are the unit vectors along the slip and normal directions of slip system α respectively, defined in the reference configuration $\mathfrak{B}_0$. The summation in 3.1 is carried over the active systems at the time of calculation (Nas)[6]. Now recalling (eq.1.28–1.29) that the deformation rate $\mathbf{D}$ and spin tensor $\mathbf{W}$ are defined as the symmetric and skew parts of $\mathbf{L}$ respectively, we can also define:

$$\mathbf{D}_i^p = \mathrm{symm}(\mathbf{L}_i^p) = \sum_{\alpha=1}^{Nas} \dot{\gamma}^\alpha(t)\, \mathrm{symm}\left[\mathbf{s}_0^\alpha \mathbf{m}_0^\alpha\right] \Rightarrow \mathbf{D}_i^p = \sum_{\alpha=1}^{Nas} \gamma^\alpha(t)\, \mathbf{M}_0^\alpha \tag{3.2}$$

---

[3]Plasticity in metals can also be attributed to mechanisms such as twinning and martensitic transformation [27]

[4]along the crystal's dense directions

[5]A concise description of the simple shear motion can be found in Appendix A of this thesis

[6]Number of Active Systems

$$\mathbf{W}_i^p = \text{skew}(\mathbf{L}_i^p) = \sum_{\alpha=1}^{Nas} \dot{\gamma}^\alpha(t)\,\text{skew}\,[\mathbf{s}_0^\alpha \mathbf{m}_0^\alpha] \Rightarrow \mathbf{W}_i^p = \sum_{\alpha=1}^{Nas} \gamma^\alpha(t)\,\mathbf{\Omega}_0^\alpha \qquad (3.3)$$

3.1.i Decomposition of F for Single Crystal Plasticity

Metal single crystals, just like isotropic metals, interpret the total deformation resulting from the application of external forces into a purely elastic (reversible) and into a purely plastic (irreversible) part. The theory of finite inelastic deformations is fundamentally based in the assumption that at a specific length scale of observation exists an intermediate configuration $\mathfrak{B}_i$, free of internal and external forces[7]. Such a configuration, is in most cases impossible to reproduce in the real world, but it is vital from the perspective of continuum mechanics to formulate a comprehensive description of inelastic deformations. The intermediate configuration in finite deformation elastoplasticity is obtained from the deformed configuration by elastic destressing to zero stress. In this sense, $\mathfrak{B}_i$ is obtained from $\mathfrak{B}_0$ by enforcing an irreversible plastic deformation and differs from $\mathfrak{B}_t$ by a reversible elastic deformation.

The aforementioned definition however, is insufficient to determine a unique intermediate configuration, since the superposition of arbitrary rigid translations and rotations is always possible without stressing the body. In the context of crystal plasticity, the intermediate configuration is defined as the imaginary[8] state where the embodiment of plastic slip does not alter the initially defined crystal orientation with respect to a global coordinate system. In this case, the intermediate configuration is said ro be **isoclinic**.

Ignoring the inherent discrete dislocation substructure [37], we assume that plastic deformation occurs in the form of smooth shearing on slip planes and slip directions to enable the formulation of a continuum plasticity model (Hill [28]). A continuum approach combined with the proper definition of reference $\mathfrak{B}_0$, isoclinic $\mathfrak{B}_i$ and deformed $\mathfrak{B}_t$ configurations leads to the multiplicative decomposition of the deformation gradient $\mathbf{F}$ as follows:

$$\boxed{\mathbf{F} = \mathbf{F}^e \cdot \mathbf{F}^p} \qquad (3.4)$$

where:

$$\mathbf{F} : \mathfrak{B}_0 \to \mathfrak{B}_t$$

$$\mathbf{F}^p : \mathfrak{B}_0 \to \mathfrak{B}_i$$

$$\mathbf{F}^e : \mathfrak{B}_i \to \mathfrak{B}_t$$

---

[7]Such a configuration may or may not be able to exist in some length scales. Consider for instance the case of inelastic deformation of a heterogenous deformable body, which is bound to develop interfacial residual stresses. In the unloaded state, such a body will simultaneously be globally relaxed and microscopically stressed obstructing the definition of the intermediate configuration. In such cases, the body must be divided into small pieces, in order to relieve such internal stress fields, suggesting that a 'change' in length scale is necessary

[8]In most cases, the intermediate state cannot be physically achieved and thus constitutes an imaginary mathematical concept

Figure 3.1 illustrates a schematic representation of the multiplicative decomposition of the total deformation gradient, while displaying the corresponding reference $\mathfrak{B}_0$, isoclinic $\mathfrak{B}_i$ and deformed $\mathfrak{B}_t$ states.
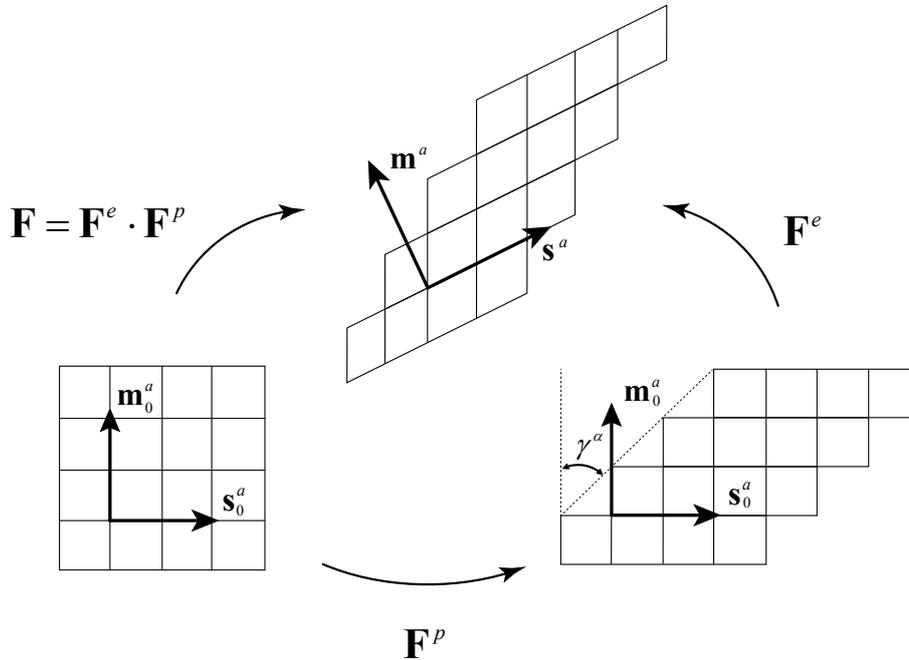
Figure 3.1: The multiplicative decomposition of the deformation gradient

The slip direction vector $\mathbf{s}_0^\alpha$ is embedded in the lattice and transforms during deformation according to $\mathbf{s}^\alpha = \mathbf{F}^e \cdot \mathbf{s}_0^\alpha$. In contrast, the unit normal to the slip plane $\mathbf{m}_0^\alpha$ transforms as $\mathbf{m}^\alpha = \mathbf{m}_0^\alpha \cdot \mathbf{F}^{e-1}$, so that it constantly remains perpendicular to the slip plane.

As aforementioned, the definition of the isoclinic configuration is fundamentally based on the existence of a 'material' coordinate system that will remain unaffected by $\mathbf{F}^p$. Apart from the defining the system itself however, it is also important to express its components with respect to a global reference system[9]. A concise methodology to define such a 'material' system, is presented in the section that follows.

3.2 Global versus Crystal Axes

A relatively easy way to define the crystal's relative orientation in the case where a unique loading direction makes sense[10] is by defining two sets of coordinate systems, namely a **crystal system** and a **global system**. Let $\mathbf{n}^{(i)}$ be the unit vectors of the crystal base and $\mathbf{e}_i$ the unit vectors of the global Cartesian coordinate system. In order to position the crystal in space we assume that two arbitrary unit vectors $\mathbf{p}$ and $\mathbf{s}$ are known with respect to

---

[9]This is extremely useful for the computational implementation of the constitutive model which we address in Chapters 5 and 6

[10]i.e. The case of a uniaxial tension experiment

both the crystal and the global axes. Two such vectors could be the loading direction $\mathbf{p}$ and the slip direction $\mathbf{s}$, although other choices are also possible since the following methodology is general. Hence:
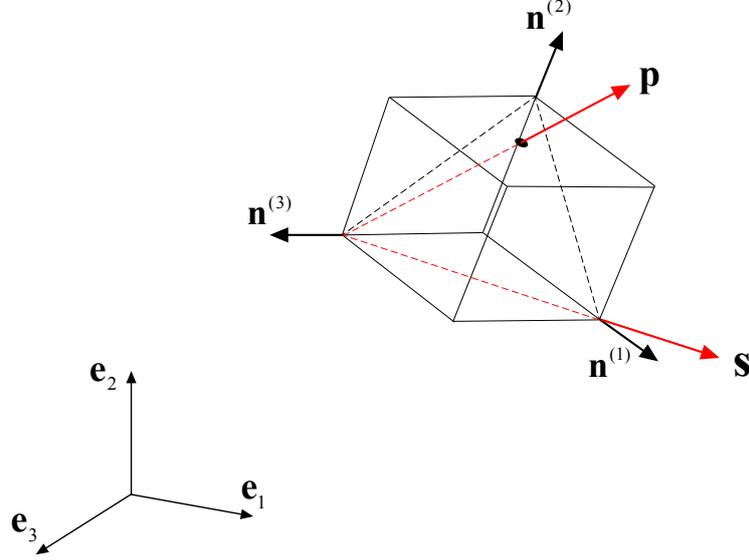
Figure 3.2: The local crystal system $\mathbf{n}^{(i)}$ and the global coordinate system $\mathbf{e}_i$

$$\mathbf{p} = p^{(1)}\mathbf{n}^{(1)} + p^{(2)}\mathbf{n}^{(2)} + p^{(3)}\mathbf{n}^{(3)} = p_1\mathbf{e}_1 + p_2\mathbf{e}_2 + p_3\mathbf{e}_3 \tag{3.5}$$

$$\mathbf{s} = s^{(1)}\mathbf{n}^{(1)} + s^{(2)}\mathbf{n}^{(2)} + s^{(3)}\mathbf{n}^{(3)} = s_1\mathbf{e}_1 + s_2\mathbf{e}_2 + s_3\mathbf{e}_3 \tag{3.6}$$

These load and slip vectors, define a plane. A third vector $\mathbf{m}$ can be introduced, normal to that plane as:

$$\mathbf{m} \equiv \mathbf{q} \times \mathbf{p} = \begin{vmatrix} \mathbf{n}^1 & \mathbf{n}^2 & \mathbf{n}^2 \\ s^{(1)} & s^{(2)} & s^{(3)} \\ p^{(1)} & p^{(2)} & p^{(3)} \end{vmatrix} = \begin{vmatrix} \mathbf{e}_1 & \mathbf{e}_2 & \mathbf{e}_3 \\ s_1 & s_2 & s_3 \\ p_1 & p_2 & p_3 \end{vmatrix} \Rightarrow$$

$$\mathbf{m} = m^{(1)}\mathbf{n}^{(1)} + m^{(2)}\mathbf{n}^{(2)} + m^{(3)}\mathbf{n}^{(3)} = m_1\mathbf{e}_1 + m_2\mathbf{e}_2 + m_3\mathbf{e}_3 \tag{3.7}$$

Since all components $p^{(i)}, p_i, s^{(i)}, s_i$ are known, we can also calculate the components $m^{(i)}, m_i$ as:

$$m^{(1)} = s^{(2)}p^{(3)} - p^{(2)}s^{(3)} \qquad\qquad m_1 = s_2p_3 - p_2s_3$$

$$m^{(2)} = -s^{(1)}p^{(3)} + p^{(1)}s^{(3)} \qquad\qquad m_2 = -s_1p_3 + p_1s_3$$

$$m^{(3)} = s^{(1)}p^{(2)} - p^{(1)}s^{(2)} \qquad\qquad m_3 = s_1p_2 - p_1s_2$$

In order to derive an analytical expression for the transformation between the crystal base vectors $\mathbf{n}^{(i)}$ defining the crystal coordinate system and the global system's base vectors $\mathbf{e}_i$,

we write equations (3.5), (3.6), and (3.7) in matrix form as:

$$
\begin{bmatrix} p^{(1)} & p^{(2)} & p^{(3)} \\ s^{(1)} & s^{(2)} & s^{(3)} \\ m^{(1)} & m^{(2)} & m^{(3)} \end{bmatrix} \cdot \begin{bmatrix} \mathbf{n}^{(1)} \\ \mathbf{n}^{(2)} \\ \mathbf{n}^{(3)} \end{bmatrix} = \begin{bmatrix} p_1 & p_2 & p_3 \\ s_1 & s_2 & s_3 \\ m_1 & m_2 & m_3 \end{bmatrix} \cdot \begin{bmatrix} \mathbf{e}_1 \\ \mathbf{e}_2 \\ \mathbf{e}_3 \end{bmatrix} \Rightarrow
$$

$$
\underbrace{\begin{bmatrix} p^{(1)} & p^{(2)} & p^{(3)} \\ s^{(1)} & s^{(2)} & s^{(3)} \\ m^{(1)} & m^{(2)} & m^{(3)} \end{bmatrix}}_{[A]} \qquad \underbrace{\begin{bmatrix} p_1 & p_2 & p_3 \\ s_1 & s_2 & s_3 \\ m_1 & m_2 & m_3 \end{bmatrix}}_{[B]}
$$

$$
\begin{bmatrix} \mathbf{n}^{(1)} \\ \mathbf{n}^{(2)} \\ \mathbf{n}^{(3)} \end{bmatrix} = \underbrace{[A]^{-1} \cdot [B]}_{[Q]} \cdot \begin{bmatrix} \mathbf{e}_1 \\ \mathbf{e}_2 \\ \mathbf{e}_3 \end{bmatrix} = [Q] \cdot \begin{bmatrix} \mathbf{e}_1 \\ \mathbf{e}_2 \\ \mathbf{e}_3 \end{bmatrix} \equiv \begin{bmatrix} n_1^{(1)} & n_2^{(1)} & n_3^{(1)} \\ n_1^{(2)} & n_2^{(2)} & n_3^{(2)} \\ n_1^{(3)} & n_2^{(3)} & n_3^{(3)} \end{bmatrix} \cdot \begin{bmatrix} \mathbf{e}_1 \\ \mathbf{e}_2 \\ \mathbf{e}_3 \end{bmatrix}
$$

and in a more compact form:

$$
\mathbf{n}^{(i)} = Q_{ij}\mathbf{e}_j = \mathbf{Q} \cdot \mathbf{e}_j \tag{3.8}
$$

where:

$$
[Q] = [A]^{-1} \cdot [B] \quad, \qquad [Q]^{-1} = [Q]^T \quad, \qquad \mathbf{Q} = Q_{ij}\mathbf{n}^{(i)}\mathbf{n}^{(j)} = Q_{ij}\mathbf{e}_i\mathbf{e}_j
$$

and matrix $[A]$ is defined as the the matrix of the 3 vector components with respect to the crystal system, whereas matrix $[B]$ contains the components of the same vectors with respect to the global system.

3.2.i Rotation of a unit vector during plastic deformation

Let us consider a unit vector $\mathbf{p}$ defined in the reference configuration $\mathfrak{B}_\mathbf{o}$ of a continuum body, that is known with respect to the crystal system and essentially represents a crystal direction[11]. Assuming that the body experiences plasticity $\mathbf{F}^p$, we need to determine the current position of the crystal direction $\mathbf{p}\prime$ in terms of $\mathbf{F}^p$. Initially, we assume that the crystal direction $\mathbf{p}$ is expressed:

$$
\mathbf{p} = p_i\,\mathbf{n}^{(i)} \tag{3.9}
$$

The deformation gradient associated with the plastic deformation is expressed in terms of the global system as:

$$
\mathbf{F}^p = F_{ij}^p\,\mathbf{e}_i\,\mathbf{e}_j \tag{3.10}
$$

Using the transformation defined in (3.8) we can also express $\mathbf{F}^p$ with respect to the crystal axes as:

$$
\mathbf{F}^p = \hat{F}_{ij}^p\,\mathbf{n}^{(i)}\,\mathbf{n}^{(j)} \tag{3.11}
$$

where

$$
[\hat{F}^p] = [Q][F^p][Q]^T \tag{3.12}
$$

---

[11]The vector $\mathbf{p}$ under consideration is not a material fiber itself. It just happens to be aligned with a specific material fiber that would be different in general, after deformation

Now recall that any vector can be 'repositioned' from the reference to the current configuration using the definition of the deformation gradient. In this case, we use $\mathbf{F}^p$ so:

$$\mathbf{p}' = \mathbf{F}^p \cdot \mathbf{p} \tag{3.13}$$

Combining equations (3.11–3.13) we derive:

$$\{p'\} = [Q][F^p][Q]^T \{p\} \tag{3.14}$$

Equation (3.14) defines the current position of the vector that was initially $\mathbf{p}$. Once we normalize $\mathbf{p}'$, we can use the stereographic projection (*see* Section 2.3) to plot the initial and current position as points in an inverse pole figure diagram.

3.3 The Elasticity Matrix

The constitutive relationship for the elastic behavior of an FCC metal single crystal is taken to be that of an linearly elastic solid with cubic symmetry. In this case the constitutive law can be parameterized with respect to 3 independent material constants and with respect to the crystal axes can be written in the form (Aravas [8]):

$$\begin{Bmatrix} \sigma_{11} \\ \sigma_{22} \\ \sigma_{33} \\ \sigma_{12} \\ \sigma_{13} \\ \sigma_{23} \end{Bmatrix} = \begin{bmatrix} C_{11} & C_{12} & C_{12} & & & \\ & C_{11} & C_{12} & & & \\ & & C_{11} & & & \\ & sym & & C_{44} & & \\ & & & & C_{44} & \\ & & & & & C_{44} \end{bmatrix} \cdot \begin{Bmatrix} \varepsilon_{11} \\ \varepsilon_{22} \\ \varepsilon_{33} \\ 2\varepsilon_{12} \\ 2\varepsilon_{13} \\ 2\varepsilon_{23} \end{Bmatrix} \Rightarrow \{\sigma\} = [\mathcal{L}^e] \cdot \{\varepsilon\} \tag{3.15}$$

where, $\mathcal{L}^e = \mathcal{L}^e_{ijkl} \mathbf{n}^{(i)} \mathbf{n}^{(j)} \mathbf{n}^{(k)} \mathbf{n}^{(l)}$ and:

$$\mathcal{L}^e_{1111} = \mathcal{L}^e_{2222} = \mathcal{L}^e_{3333} \equiv C_{11}$$

$$\mathcal{L}^e_{1122} = \mathcal{L}^e_{2211} = \mathcal{L}^e_{1133} = \mathcal{L}^e_{3311} \equiv C_{12}$$

$$\mathcal{L}^e_{1212} = \mathcal{L}^e_{2112} = \mathcal{L}^e_{1221} = \mathcal{L}^e_{2121} =$$

$$= \mathcal{L}^e_{1313} = \mathcal{L}^e_{3113} = \mathcal{L}^e_{1331} =$$

$$= \mathcal{L}^e_{2323} = \mathcal{L}^e_{3131} = \mathcal{L}^e_{3223} = \mathcal{L}^e_{2332} = \mathcal{L}^e_{3232} = C_{44}$$

The above equations suggest that we can write the elasticity matrix $\mathcal{L}^e$ with respect to the crystal axes and in terms of C_{ij} as:

$$\begin{aligned} \mathcal{L}^e =& C_{11} \left(\mathbf{n}^{(1)} \mathbf{n}^{(1)} \mathbf{n}^{(1)} \mathbf{n}^{(1)} + \mathbf{n}^{(2)} \mathbf{n}^{(2)} \mathbf{n}^{(2)} \mathbf{n}^{(2)} + \mathbf{n}^{(3)} \mathbf{n}^{(3)} \mathbf{n}^{(3)} \mathbf{n}^{(3)} \right) + \\ & C_{12} \left(\mathbf{n}^{(1)} \mathbf{n}^{(1)} \mathbf{n}^{(2)} \mathbf{n}^{(2)} + \mathbf{n}^{(2)} \mathbf{n}^{(2)} \mathbf{n}^{(1)} \mathbf{n}^{(1)} + \mathbf{n}^{(1)} \mathbf{n}^{(1)} \mathbf{n}^{(3)} \mathbf{n}^{(3)} + \mathbf{n}^{(3)} \mathbf{n}^{(3)} \mathbf{n}^{(1)} \mathbf{n}^{(1)} \right) + \end{aligned}$$

$$C_{44} \left(\mathbf{n}^{(1)} \mathbf{n}^{(2)} \mathbf{n}^{(1)} \mathbf{n}^{(2)} + \mathbf{n}^{(2)} \mathbf{n}^{(1)} \mathbf{n}^{(1)} \mathbf{n}^{(2)} + \mathbf{n}^{(1)} \mathbf{n}^{(2)} \mathbf{n}^{(2)} \mathbf{n}^{(1)} + \mathbf{n}^{(2)} \mathbf{n}^{(1)} \mathbf{n}^{(2)} \mathbf{n}^{(1)} \right) +$$

$$C_{44} \left(\mathbf{n}^{(1)} \mathbf{n}^{(3)} \mathbf{n}^{(1)} \mathbf{n}^{(3)} + \mathbf{n}^{(3)} \mathbf{n}^{(1)} \mathbf{n}^{(1)} \mathbf{n}^{(3)} + \mathbf{n}^{(1)} \mathbf{n}^{(3)} \mathbf{n}^{(3)} \mathbf{n}^{(1)} + \mathbf{n}^{(3)} \mathbf{n}^{(1)} \mathbf{n}^{(3)} \mathbf{n}^{(1)} \right) +$$

$$C_{44} \left(\mathbf{n}^{(2)} \mathbf{n}^{(3)} \mathbf{n}^{(2)} \mathbf{n}^{(3)} + \mathbf{n}^{(3)} \mathbf{n}^{(2)} \mathbf{n}^{(2)} \mathbf{n}^{(3)} + \mathbf{n}^{(2)} \mathbf{n}^{(3)} \mathbf{n}^{(3)} \mathbf{n}^{(2)} + \mathbf{n}^{(3)} \mathbf{n}^{(2)} \mathbf{n}^{(3)} \mathbf{n}^{(2)} \right) \quad (3.16)$$

However, we are interested in deriving an expression for the elastic response with respect to any global coordinate system instead of the local crystal system. Recalling that the global axes $\mathbf{e}_i$ can be expressed in terms of the crystal axes $\mathbf{n}^i$ using equation (3.8) we write:

$$\overline{\mathcal{L}^e_{ijkl}} = Q_{im} Q_{jn} Q_{kp} Q_{lq} \mathcal{L}^e_{mnpq} \quad (3.17)$$

3.4 Hardening of Single Crystals

A typical stress–strain curve of an FCC metal crystal exhibits three distinct deformation stages. Initially, in Stage I, plastic slip is attributed to the activation of only one out of the twelve possible slip systems[12] [11, 27]. The orientation of that system (α) is such that the resolved shear stress reaches the critical value τ^α_{cr} prior to all other systems and it is therefore referred to as an **optimally oriented** system. Dislocation glide in Stage I is unhindered producing weak hardening h_I, since only one system is active and dislocation interactions are not present. Hence, Stage I is also referred to as **easy glide stage**. Clearly, the optimally oriented system as well as the extent (in terms of deformation) of Stage I, both depend on the relative orientation of the crystal in regard to the loading direction. The latter only makes sense in a uniaxial tension experiment as complex stress fields would (in general) trigger the simultaneous activation of several slip systems and thus Stage I could not be manifested. Furthermore, the abundance of available slip systems in FCC crystals restricts the extent of Stage I ($\gamma^\alpha_{S_I} < 10\%$) since other slip systems quickly activate as well, signaling its conclusion.

The activation of an equivalent or a secondary system, as well as of other systems thereafter indicate the initiation of Stage II. In Stage II, dislocations glide in intersecting planes and interact with each other, obstructing further plastic slip. The main dislocation interactions occurring in Stage II are "dislocation junctions", "forest hardening" and "Lommer-Cottrel immobilization" [27]. As a result, the hardening h_{II} in Stage II is significantly greater compared to h_I. The hardening rate $\partial h_{II}/\partial \gamma$ however is constant, justifying the fact that Stage II is commonly called the **linear hardening stage**. The dislocation density increases dramatically with deformation in Stage II displaying values up to $10^9/mm^2$. In this state, dislocations are immobilized being unable to glide in the same plane as before, and Stage III commences.

At the onset of Stage III, namely the **dynamic recovery stage**, thermally activated cross slip of screw dislocations is observed [11, 27] allowing dislocations to change slip planes and therefore circumvent obstacles. Cross-slip of screw dislocations ultimately reduces their

---

[12]Recall from Section.2.1 that FCC crystals comprise of 12 slip systems resulting from all possible combinations between their 4 dense planes {111} and 3 dense directions $< 110 >$

density, since dislocations gliding on same planes and opposite directions 'cancel out'. The latter also results into a decreasing hardening rate $(\partial h_{III}/\partial \gamma)$ in Stage III illustrating the 'dynamic recovery'. Figure 3.3 schematically illustrates the three distinct stages of crystal deformation which, when combined, form the $\sigma - \varepsilon$ curve corresponding to uniaxial tension of an FCC metal crystal.

Returning to the mechanics of crystal plasticity, the yield criterion of each slip system α is defined in terms of the resolved shear stresses and is expressed in rate form as:

$$\dot{\Phi}^\alpha = \dot{\tau}^\alpha - \dot{\tau}_{cr}^\alpha \leq 0 \tag{3.18}$$

The consistency condition then takes the following form for every slip system $\alpha \in \mathscr{P}$:

- $\dot{\Phi}^\alpha < 0 \quad \longrightarrow \quad \dot{\gamma}^\alpha = 0$ (3.19)

- $\dot{\Phi}^\alpha = 0 \quad \longrightarrow \quad \dot{\gamma}^\alpha \geq 0$ (3.20)
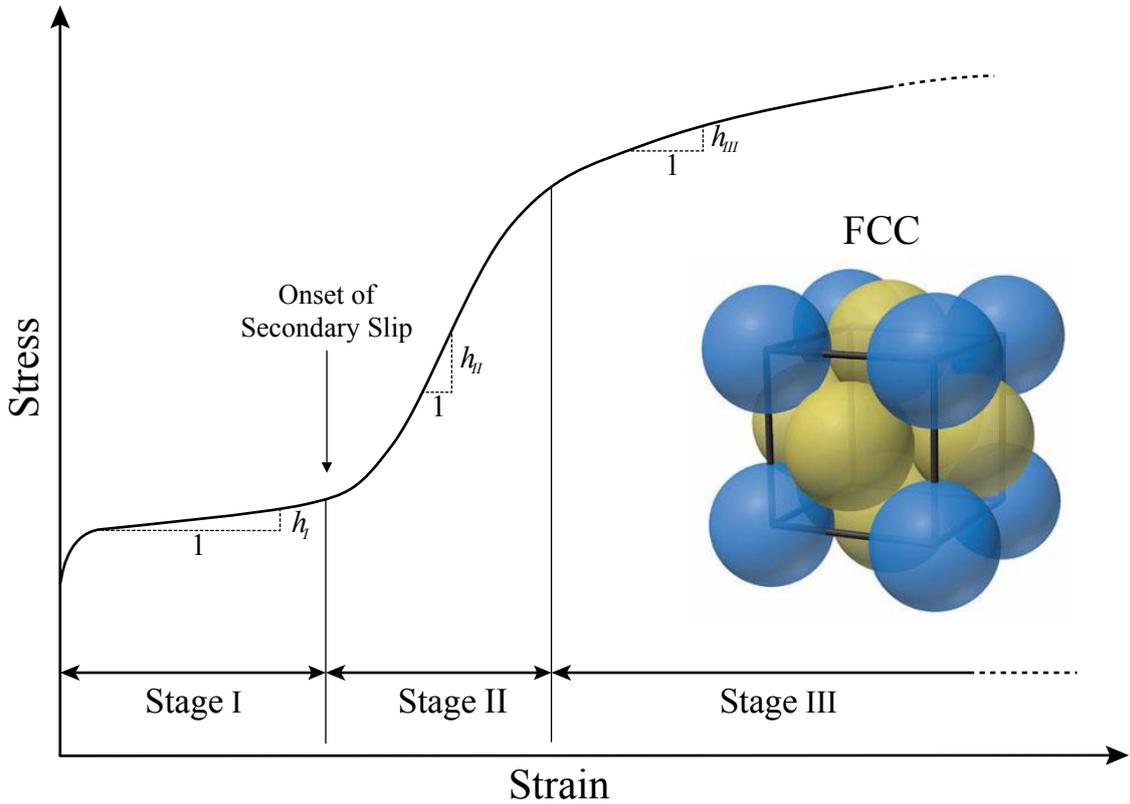
Figure 3.3: The deformation stages of FCC metal single crystals

In the context of developing an analytical expression for the hardening of FCC crystals that is consistent with experiments, Mandel [39] and Hill [28] proposed the following associated flow rule:

$$\dot{\tau}_{cr}^\alpha = \sum_{\beta=1}^{Nas} h^{\alpha\beta} \dot{\gamma}^\beta \qquad \alpha = 1, 2, \ldots, N \tag{3.21}$$

The particular hardening model defines the critical resolved shear stress rate of a slip system α to be linearly dependent to the the slip rates of all active systems $\dot{\gamma}^\beta$. The quantity $h^{\alpha\beta}$ defines the instantaneous hardening moduli which must be able to accurately account for 'active hardening'[13] and 'latent hardening'[14]. The analytical and experimental characterization of $[h^{\alpha\beta}]$ is extensively discussed in the works of Bassani and Wu [11] & [12]. Earlier analytical models have also been proposed by Taylor [50] (isotropic model $h^{\alpha\beta} = h$), Koiter [34] (independent hardening model $h^{\alpha\beta} = h\,\delta_{\alpha\beta}$), Budiansky & Wu [19] (geometrical hardening model $h^{\alpha\beta} = h\mathbf{M}^\alpha : h\mathbf{M}^\beta$ [15]), and Hutchinson [32] & Asaro [9] (latent hardening $h^{\alpha\beta} = q\,h + (1-q)\,h\,\delta_{\alpha\beta}$). In all cases h stands for the active hardening function that monotonically decreases with strain. The following analytical relationship for h was proposed by Asaro [9]:

$$h(\gamma^\alpha) = h_0 \operatorname{sech}^2\left(\frac{h_0\,\gamma^\alpha}{\tau_I - \tau_0}\right) \tag{3.22}$$

where τ_0 stands for the initial critical resolved shear stress on each slip system before any plasticity occurs, τ_I is the saturation stress and h_0 is the hardening modulus at first yield. Then, Asaro [9] suggests a value of $1 \leq q \leq 1.4$ to build the multislip hardening moduli as $h^{\alpha\beta} = q\,h + (1-q)\,h\,\delta_{\alpha\beta}$. However, Bassani & Wu [12] state that this simplified model is inconsistent with the experimental observations. In fact they ([11]-[12]) suggest that the hardening model should be such that the following inequality restrictions are met:

$$\tau_{cr}^\beta\left(\gamma^\alpha | \gamma^\beta = 0\right) < \tau_{cr}^\alpha\left(\gamma^\alpha | \gamma^\beta = 0\right) \tag{3.23a}$$

$$\tau_{cr}^\beta\left(\gamma^\alpha | \gamma^\beta > \gamma_0\right) > \tau_{cr}^\alpha\left(\gamma^\alpha | \gamma^\beta = 0\right) \tag{3.23b}$$

$$h^{\beta\alpha}(\gamma^\alpha, 0) < h^{\alpha\alpha}(\gamma^\alpha, 0) \tag{3.23c}$$

$$h^{\alpha\alpha}(\gamma^\alpha, 0) < h^{\alpha\alpha}(\gamma^\alpha, \gamma^\beta) \tag{3.23d}$$

$$h^{\alpha\alpha}(\gamma^\alpha, \gamma^\beta) \ll h^{\beta\beta}(\gamma^\alpha, \gamma^\beta) \quad \text{if} \quad \gamma^\beta \ll \gamma^\alpha \tag{3.23e}$$

where α stands for the primary slip system and β denotes the secondary system. Now clearly the analytical models for $h^{\alpha\beta}$ presented in previous paragraphs are unable to simultaneously satisfy all these inequality restrictions. Bassani & Wu [12] then suggest that in order to describe complex slip phenomena, the hardening moduli should take into account the accumulated plastic deformation on every slip system and, if possible, the history of plastic slip. Hence, the moduli $h^{\alpha\beta}$ should be introduced as a functional of plastic slip within all systems, ideally as:

$$h^{\alpha\beta} = h^{\alpha\beta}\left(\mathscr{H}(\gamma^\delta) | \delta = 1, 2, \ldots, N\right) \quad \alpha\,,\,\beta = 1, 2, \ldots, N \tag{3.24}$$

and the following form proves to be quite flexible [12]:

$$h^{\alpha\alpha} = F\left(\gamma^\alpha\right) G\left(\gamma^\beta | \beta \neq \alpha\right) \qquad \alpha = 1, 2, \ldots, N \tag{3.25a}$$

$$h^{\beta\alpha} = q\,h_{\alpha\alpha} \qquad \alpha = 1, 2, \ldots, N \tag{3.25b}$$

---

[13]The hardening of system α due to slip activity on system α
[14]The hardening of system α due to slip activity on other systems
[15]$\mathbf{M}^\alpha = \operatorname{symm}\left[\mathbf{s}^\alpha\,\mathbf{m}^\alpha\right]$

where function $F(\gamma^\alpha)$ stands for the instantaneous hardening under single slip whereas $G(\gamma^\beta|\beta \neq \alpha)$ represents the hardening induced from dislocation interactions. The latter should equal unity ($G \equiv 1$) in pure single slip conditions where $\gamma^\alpha > 0$ & $\gamma^\beta = 0$ $\forall$ $\beta \neq \alpha$. The off-diagonal components $h^{\beta\alpha}$ with $\beta \neq \alpha$ represent hardening of system β due to slip on system α and are taken to be a fraction of the active hardening components $h^{\alpha\alpha}$ [16] controlled by parameter q. In the special case where system β is inactive, hardening provided by $h^{\beta\alpha}$ defines the so called **latent hardening**[17]. However, the implementation of latent hardening phenomena as suggested by expression (3.25b), results into a non–symmetric hardening moduli. If required, the symmetric alternative could be easily adopted in the sense $h^{\beta\alpha} = q(h^{\alpha\alpha} + h^{\beta\beta})$. It should be also noted that the particular model defined by equations (3.25a)-(3.25b) is in excellent agreement with experimental results, for a small positive value of q or even $q = 0$ [11],[12].

Functions F and G which are primarily used to build the active hardening components $h^{\alpha\alpha}$ can be physically interpreted as follows. To ease perception let us consider the uniaxial tension of an FCC crystal whose slip system α is optimally oriented for single slip. At the onset of Stage I where only system α is activated and therefore $\gamma^\alpha > 0$ and $\gamma^\beta = 0$ $\forall$ $\beta \neq \alpha$, function $G = 1$ and $h^{\alpha\alpha} = F(\gamma^\alpha)$. Hence, function F represents the hardening phenomena during easy glide, under purely single slip conditions. Subsequently, when secondary slip systems activate[18], function G characterizes the forest hardening effects due to slip interactions in Stage II between the primary α and secondary active systems $\beta \neq \alpha$. Bassani & Wu [12] propose the following simple form for easy glide hardening:

$$F\left(\gamma^\alpha\right) = (h_0 - h_s)\mathrm{sech}^2\left(\frac{h_0 - h_s}{\tau_I - \tau_0}\gamma^\alpha\right) + h_s \tag{3.26}$$

where τ_0 stands for the initial critical resolved shear stress prior to any plastic deformation, τ_I is the Stage I stress where large plastic flow initiates, h_0 is the hardening modulus corresponding to τ_0 and h_s is the easy glide (linear-like) hardening. In the special case of purely single slip conditions, equations (3.21),(3.25a) and (3.26) can be combined and analytically integrated to yield the following expression:

$$\tau_{cr}^\alpha(\gamma^\alpha) = \tau_0 + (\tau_I - \tau_0)\tanh\left(\frac{h_0 - h_s}{\tau_I - \tau_0}\gamma^\alpha\right) + h_s\,\gamma^\alpha \tag{3.27}$$

The particular form of expressions (3.26) and (3.27) facilitates the physical interpretation of the parameters involved but could equivalently written in the following more compact form:

$$F\left(\gamma^\alpha\right) = h^*\mathrm{sech}^2\left(\frac{\gamma^\alpha}{\gamma^*}\right) + h_s \tag{3.28}$$

$$\tau_{cr}^\alpha(\gamma^\alpha) = \tau_0 + \tau^*\tanh\left(\frac{\gamma^\alpha}{\gamma^*}\right) + h_s\,\gamma^\alpha \tag{3.29}$$

---

[16]No sum on α

[17]Latent hardening of an inactive system β is defined as the hardening of that system due to slip on other systems and owes its existence to dislocation interactions

[18]$\exists\beta \neq \alpha : \gamma^\beta > 0$ & $\gamma^\alpha > 0$

where $\tau^* = \tau_I - \tau_0$, $\gamma^* = \tau^*/(h_s - h_0)$ and $h^* = \tau^*/\gamma^*$. In regards to the cross–hardening function (G), the following form proposed by Bassani & Wu [12] equals unity when all arguments are zero (in single slip conditions) and asymptotically approaches finite values in finite multislip conditions:

$$G\left(\gamma^\beta | \beta = 1, 2, \ldots, N : \beta \neq \alpha\right) = 1 + \sum_{\substack{\beta=1 \\ \beta \neq \alpha}}^{N} f_{\alpha\beta} \tanh\frac{\gamma^\beta}{\gamma_0} \qquad (3.30)$$

where γ_0 represents the amount of slip after which the interactions between slip systems α and β reach peak strength. Bassani & Wu [12] propose the same γ_0 for all pairs of systems since the interaction magnitude of various slip interactions solely lies in the choice of the components $f_{\alpha\beta}$, namely the cross–hardening amplitude factors. Table 3.1 [12] presents the rationale for assigning values to the amplitude factors, taking all possible dislocation interactions into account. For instance, coplanar interactions tend to be weaker compared to their anti–planar counterparts and thus the associated amplitude factors must take this into account.

Table 3.1: *Strength amplitude factors $f_{\alpha\beta}$ defining the intensity of cross–hardening interactions on FCC crystals. N=No junction (a_1), H=Hirth lock (a_2), C=Coplanar junction (a_3), G=Glissile junction (a_4), S=Sessile junction (a_5) (Bassani and Wu [11, 12])*

	1	2	3	4	5	6	7	8	9	10	11	12
1	0											
2	C	0										
3	C	C	0									
4	S	G	H	0								
5	G	N	G	C	0							
6	H	G	S	C	C	0						
7	N	G	G	G	S	H	0					
8	G	S	H	N	G	G	C	0				
9	G	H	S	G	H	S	C	C	0			
10	H	S	G	G	G	N	H	S	G	0		
11	S	H	G	S	H	G	G	G	N	C	0	
12	G	G	N	H	S	G	S	H	G	C	C	0

FCC single crystals display five different interaction types, leading to the definition of 5 independent $f_{\alpha\beta}$ components. These distinct slip interactions between systems α and β are subject to the type of dislocation junction formed, which consequently translates into the relative orientation of the systems. This classification of interactions results into the definition of the five distinct constants α_i (where $i = 1, 2, \ldots, 5$) as follows:

- α_1 (No Junction): the Burgers vectors of systems α and β are unaffected by this interaction

- α_2 (Hirth Lock): the Burgers vectors resulting from the interaction between systems α and β is not energetically admissible

- α_3 (Coplanar Junction): the Burgers vector resulting from the interaction between systems α and β is on the same plane as the original ones

- α_4 (Glissile Junction): the Burgers vector resulting from the interaction between systems α and β is energetically admissible and on one of the two slip planes

- α_5 (Sessile Junction): the Burgers vector resulting from the interaction between systems α and β is energetically admissible but not on neither of the two slip planes

where $\alpha_5 > \alpha_4 > \alpha_3 > \alpha_2 > \alpha_1$. The hardening model proposed by Bassani & Wu [12] is then summarized as:

$$
\dot{\tau}_{cr}^{\alpha} = \sum_{\beta=1}^{Nas} h^{\alpha\beta} \dot{\gamma}^{\beta}
$$

$$
h^{\alpha\alpha} = \left[(h_0 - h_s)\mathrm{sech}^2 \left(\frac{h_0 - h_s}{\tau_I - \tau_0} \gamma^{\alpha} \right) + h_s \right] \left[1 + \sum_{\substack{\beta=1 \\ \beta \neq \alpha}}^{N} f_{\alpha\beta} \tanh \frac{\gamma^{\beta}}{\gamma_0} \right]
$$

$$
h^{\beta\alpha} = q \, h^{\alpha\alpha} \quad \alpha \neq \beta
$$

Now note that if the off diagonal ratio parameter q is chosen to be zero, then the hardening moduli is diagonal and the results adequate to reproduce experimental observations according to Bassani & Wu [12]. If the complete hardening moduli is desired however, then only small positive values of q are to be chosen ($q \in [0, 0.3]$). If the symmetric model is chosen instead $h^{\alpha\beta} = q(h^{\alpha\alpha} + h^{\beta\beta})$ then q should be chosen as $q = 0.1$ at most. Assigning greater values to q may violate the uniqueness of the solution (the active systems set cannot be determined).

3.5 Integration of Elastoplastic Equations

Traditionally the constitutive equations of material models accounting for finite elastoplastic deformations[19] are expressed in rate form and their computational implementation[20]

---

[19]The rate form of the constitutive relationships is not limited to finite deformation elastoplasticity. Constitutive equations of nonlinear heat transfer problems, coupled thermal-mechanical problems, coupled electric-mechanical etc, are also expressed in rate form and their development is fundamentally based in the theory of Continuum Mechanics

[20]The Computational implementation involves the numerical approximation of the constitutive model introducing the Finite Element method which is discussed in further detail in Chapter 6

requires numerical integration. The computational solution of all non-linear problems is developed incrementally. Each increment is defined by its time interval $\Delta t = t_{n+1} - t_n$ along which the constitutive equations have to be integrated. All deformation related quantities at $t = t_n$ are passed in from the previous increment[21] and they have to be integrated to t_{n+1}.

In rate–independent crystal plasticity, given $\mathbf{F}_n, \mathbf{F}_n^p, \gamma_n^\alpha, \tau_{cr}^\alpha|_n$ at t_n along with Δt and $\mathbf{F}_{n+1}$ we have to update the plastic part of the deformation gradient $\mathbf{F}_{n+1}^p$, the Cauchy stress tensor $\boldsymbol{\sigma}_{n+1}$, the set of active slip systems $\mathscr{A}_{n+1}$ as well as the plastic strains γ_{n+1}^α and critical stresses $\tau_{cr}^\alpha|_{n+1}$ of every slip system $\alpha \in \mathscr{P}$, at t_{n+1}. However, before being able to proceed with the integration of elastoplastic equations, we first have to restate them in a 'integrable' form. Recalling equation (1.26) we can express the velocity gradient tensor $\mathbf{L}$ in terms of $\dot{\mathbf{F}}$ as:

$$\mathbf{L} = \dot{\mathbf{F}} \cdot \mathbf{F}^{-1} \tag{3.31}$$

Now recall the multiplicative decomposition of $\mathbf{F}$ that we introduced in (3.4). We write:

$$\mathbf{F} = \mathbf{F}^e \cdot \mathbf{F}^p \tag{3.32a} \qquad\qquad \mathbf{F}^{-1} = \mathbf{F}^{p-1} \cdot \mathbf{F}^{e-1} \tag{3.32b}$$

Substituting (3.32a–3.32b) into (3.31) gives:

$$\mathbf{L} = \dot{\mathbf{F}} \cdot \mathbf{F}^{-1} = \overline{\dot{\mathbf{F}^e \cdot \mathbf{F}^p}} \cdot \left(\mathbf{F}^{p-1} \cdot \mathbf{F}^{e-1} \right) =$$

$$= \left(\dot{\mathbf{F}}^e \cdot \mathbf{F}^p + \mathbf{F}^e \cdot \dot{\mathbf{F}}^p \right) \cdot \left(\mathbf{F}^{p-1} \cdot \mathbf{F}^{e-1} \right) =$$

$$= \dot{\mathbf{F}}^e \cdot \mathbf{F}^{e-1} + \mathbf{F}^e \cdot \left(\dot{\mathbf{F}}^p \cdot \mathbf{F}^{p-1} \right) \cdot \mathbf{F}^{e-1} \tag{3.33}$$

The last equation suggests that the velocity gradient is additively decomposed as

$$\boxed{\mathbf{L} = \mathbf{L}^e + \mathbf{L}^p} \tag{3.34}$$

where:

$$\mathbf{L}^e = \dot{\mathbf{F}}^e \cdot \mathbf{F}^{e-1} \tag{3.35a}$$

$$\mathbf{L}^p = \mathbf{F}^e \cdot \left(\mathbf{L}_i^p \right) \cdot \mathbf{F}^{e-1} \tag{3.35b}$$

$$\mathbf{L}_i^p = \dot{\mathbf{F}}^p \cdot \mathbf{F}^{p-1} \tag{3.35c}$$

The quantity $\mathbf{L}_i^p$ is from its definition the velocity gradient corresponding to $\mathbf{F}^p$ in the isoclinic configuration. Hence, in order to contribute to the total velocity gradient $\mathbf{L}$, it needs to be 'pushed–forwards' from the isoclinic to the current configuration via $\mathbf{F}^e$ as equation (3.34) suggests. In Section 3.1 we showed that the velocity gradient associated with dislocation glide on every slip system, $\mathbf{L}_i^p$, has the following form:

$$\mathbf{L}_i^p = \sum_{\alpha=1}^{Nas} \dot{\gamma}^\alpha \mathbf{s}_0^\alpha \, \mathbf{m}_0^\alpha \tag{3.36}$$

---

[21]They are treated as known

Thus, by combining (3.35c) and (3.36) we get:

$$\dot{\mathbf{F}}^p\left(\dot{\gamma}^\alpha\right) = \left(\sum_{\alpha=1}^{Nas} \dot{\gamma}^\alpha \mathbf{s}_0^\alpha \, \mathbf{m}_0^\alpha\right) \cdot \mathbf{F}^p\left(\dot{\gamma}^\alpha\right) \tag{3.37}$$

Equation (3.37) defines an Ordinary Differential Equation with the unknown being the tensor function $\mathbf{F}^p\left(\dot{\gamma}^\alpha\right)$. The solution of a 1st order tensor ODE of the form

$$\dot{\mathbf{Z}}(t) = \mathbf{A} \cdot \mathbf{Z}(t) \quad t \in [t_1, t_2]$$

is the following (Gurtin *et al.*p.669 [26]):

$$\mathbf{Z}(t) = \exp\left[(t_2 - t_1)\,\mathbf{A}\right] \cdot \mathbf{Z}(t_1)$$

Equation (3.37) needs to be integrated over the time increment defined by t_n and t_{n+1}. Therefore, if we assume that $\dot{\gamma}^\alpha$ remains constant during the time interval of the increment under consideration $t \in [t_n, t_{n+1}]$ we can integrate (3.37) to derive:

$$\mathbf{F}_{n+1}^p = \exp\left(\sum_{\alpha=1}^{Nas} \Delta\gamma^\alpha \mathbf{s}_0^\alpha \, \mathbf{m}_0^\alpha\right) \cdot \mathbf{F}_n^p \tag{3.38}$$

while $\mathbf{F}_{n+1}^{p-1}$ can be readily expressed by taking the inverse of the above expression:

$$\mathbf{F}_{n+1}^{p-1} = \mathbf{F}_n^{p-1} \cdot \exp\left(\sum_{\alpha=1}^{Nas} -\Delta\gamma^\alpha \mathbf{s}_0^\alpha \, \mathbf{m}_0^\alpha\right) \tag{3.39}$$

Assuming that $\Delta\gamma^\alpha$'s are known[22] for every slip system $\alpha \in Nas \equiv \mathscr{A}$, we can successfully update $\mathbf{F}_{n+1}^p$. With both $\mathbf{F}_{n+1}, \mathbf{F}_{n+1}^p$ known, we can also update $\mathbf{F}_{n+1}^e$ from (3.32a) as:

$$\mathbf{F}_{n+1}^e = \mathbf{F}_{n+1} \cdot \mathbf{F}_{n+1}^{p-1} = \mathbf{F}_{n+1} \cdot \mathbf{F}_n^{p-1} \cdot \exp\left[\mathbf{B}(\Delta\gamma^\alpha)\right] \Rightarrow$$

$$\mathbf{F}_{n+1}^e(\Delta\gamma^\alpha) = \mathbf{F}_{\text{trial}}^e \cdot \exp[\mathbf{B}(\Delta\gamma^\alpha)] \tag{3.40}$$

$$\mathbf{F}_{\text{trial}}^e = \mathbf{F}_{n+1} \cdot \mathbf{F}_n^{p-1} \tag{3.41a}$$

$$\mathbf{B} = \sum_{\alpha=1}^{Nas} -\Delta\gamma^\alpha \, \mathbf{s}_0^\alpha \, \mathbf{m}_0^\alpha \tag{3.41b}$$

Now that all components of the deformation gradient $\left(\mathbf{F}_{n+1}, \mathbf{F}_{n+1}^e, \mathbf{F}_{n+1}^p\right)$ are known, we can also update the rest of the variables as follows. The right Cauchy-Green deformation tensor corresponding to $\mathbf{F}_{n+1}^e$ is updated as:

$$\mathbf{C}_{n+1}^e(\Delta\gamma^\alpha) = \left(\mathbf{F}_{n+1}^e(\Delta\gamma^\alpha)\right)^T \cdot \mathbf{F}_{n+1}^e(\Delta\gamma^\alpha) \tag{3.42}$$

---

[22]In reality, neither the current set of active systems (which we denote as $\mathscr{A}_{n+1}$) nor $\Delta\gamma^\alpha$'s are known at this point. The algorithms required to determine $\mathscr{A}_{n+1}$ and $\Delta\gamma^\alpha$ are presented in detail in Chapter 5

Leading to the straight forward update of the elastic Green Strain tensor:

$$\mathbf{E}_{n+1}^e(\Delta\gamma^\alpha) = \frac{1}{2}(\mathbf{C}_{n+1}^e(\Delta\gamma^\alpha) - \boldsymbol{\delta}) \tag{3.43}$$

The 2nd Piola-Kirchhoff elastic stress is given in terms of the elasticity matrix $\boldsymbol{\mathcal{L}}^e$ and $\mathbf{E}_{n+1}^e$ as:

$$\mathbf{S}_{n+1}^e(\Delta\gamma^\alpha) = \boldsymbol{\mathcal{L}}^e : (\mathbf{E}_{n+1}^e(\Delta\gamma^\alpha)) \tag{3.44}$$

With $\mathbf{S}_{n+1}^e$ now known, we can update the non-symmetric (in general) Mandel stress $\boldsymbol{\Sigma}$ defined in the intermediate configuration as well as the Kirchhoff stress tensor $\boldsymbol{\tau}$ as:

$$\boldsymbol{\Sigma}_{n+1}(\Delta\gamma^\alpha) = \mathbf{S}_{n+1}^e(\Delta\gamma^\alpha) \cdot \mathbf{C}_{n+1}^e(\Delta\gamma^\alpha) \tag{3.45}$$

$$\boldsymbol{\tau}_{n+1}(\Delta\gamma^\alpha) = \mathbf{F}_{n+1}^e(\Delta\gamma^\alpha) \cdot \mathbf{S}_{n+1}^e(\Delta\gamma^\alpha) \cdot \left(\mathbf{F}_{n+1}^e(\Delta\gamma^\alpha)\right)^T \tag{3.46}$$

The Kirchhoff stress tensor $\boldsymbol{\tau}$ can then be used to update the Cauchy true stress tensor $\boldsymbol{\sigma}$ since from definition the two stress measures are related as:

$$\boldsymbol{\sigma}_{n+1}(\Delta\gamma^\alpha) = J_{n+1}\,\boldsymbol{\tau}_{n+1}(\Delta\gamma^\alpha) \quad , \text{where:} \quad J_{n+1} = \det[\mathbf{F}_{n+1}] \tag{3.47}$$

Stresses are then incrementally updated using equations (3.38–3.47) completing the integration of equations. Note however, that all $\Delta\gamma^\alpha$'s are needed before being able to proceed with stress integration. In fact, stress integration and calculation of $\Delta\gamma^\alpha \;\forall\alpha \in \mathscr{A}_{n+1}$ are treated as a single problem with its computational implementation commonly being referred to as **stress-update algorithms**. A more thorough description of stress update algorithms for finite deformation and rate independent crystal plasticity are presented in Chapter 5.

3.6 Rate Independent Tangent Modulus

3.6.i Elasticity

We postulate that an elastic potential Φ exists (Aravas [6]) in the isoclinic configuration so that:

$$\mathbf{S}^e = \rho_i\frac{\partial\Phi}{\partial\mathbf{E}^e} \quad \text{or equivalently,} \quad \overline{\mathbf{S}^e} = \rho_0\frac{\partial\Phi}{\partial\mathbf{E}^e} \tag{3.48}$$

where $\mathbf{S}^e = J^e\mathbf{F}^{e-1} \cdot \boldsymbol{\sigma} \cdot \mathbf{F}^{e-T}$ is the 2nd Piola-Kirchhoff stress, $\overline{\mathbf{S}^e} = (J/J^e)\mathbf{S}^e$ and ρ_i stands for the mass density in the isoclinic configuration. We can now derive the rate form of the above hyperelastic constitutive equation by taking the derivative with respect to time to find:

$$\dot{\overline{\mathbf{S}^e}} = \overline{\boldsymbol{\mathcal{L}}^e} : \dot{\mathbf{E}}^e \quad \text{where} \quad \overline{\boldsymbol{\mathcal{L}}^e} = \rho_0\frac{\partial^2\Phi}{\partial\mathbf{E}^e\partial\mathbf{E}^e} \tag{3.49}$$

According to the results of Dafalias [22] & Needleman [41], we can "push" the above expression in the current configuration where it takes the following form:

$$\overset{*}{\boldsymbol{\tau}} = \boldsymbol{\mathcal{L}}^{e\tau} : \mathbf{D}^e \tag{3.50}$$

where,

$$\overset{*}{\boldsymbol{\tau}} = \dot{\boldsymbol{\tau}} + \boldsymbol{\tau} \cdot \mathbf{W}^* - \mathbf{W}^* \cdot \boldsymbol{\tau} \tag{3.51}$$

$$\mathbf{W}^* = \mathbf{W} - \mathbf{W}^p \tag{3.52}$$

$$\boldsymbol{\mathcal{L}}^{e\tau} = \boldsymbol{\mathcal{L}}^e + \boldsymbol{\mathcal{T}} \tag{3.53}$$

and:

$$\mathcal{L}^e_{ijkl} = F^e_{im} F^e_{jn} F^e_{kp} F^e_{lq} \overline{\mathcal{L}^e}_{mnpq} \tag{3.54}$$

$$\mathcal{T}_{ijkl} = \frac{1}{2} (\tau_{ik}\, \delta_{jl} + \tau_{il}\, \delta_{jk} + \delta_{ik}\, \tau_{jl} + \delta_{il}\, \tau_{jk}) \tag{3.55}$$

Recall however, that $\overline{\boldsymbol{\mathcal{L}}^e}$ is related to $\boldsymbol{\mathcal{L}}^e$ by (3.17), whereas the moduli $\boldsymbol{\mathcal{L}}^e$ is generated from the elastic constants C_{ij} with respect to the crystal axes as suggested by (3.16)[23]. We next introduce the Jaumann objective rate[24] to write equation (3.50) in the following form:

$$\overset{\nabla}{\boldsymbol{\tau}} = \boldsymbol{\mathcal{L}}^{e\tau} : \mathbf{D}^e + \boldsymbol{\tau} \cdot \mathbf{W}^p - \mathbf{W}^p \cdot \boldsymbol{\tau} \tag{3.56}$$

3.6.ii Plasticity

Taking into consideration the decomposition of the deformation rate as $\mathbf{D} = \mathbf{D}^e + \mathbf{D}^p$, the Constitutive relationship in (3.56) can be rewritten in the form:

$$\overset{\nabla}{\boldsymbol{\tau}} = \boldsymbol{\mathcal{L}}^{e\tau} : (\mathbf{D} - \mathbf{D}^p) + \boldsymbol{\tau} \cdot \mathbf{W}^p - \mathbf{W}^p \cdot \boldsymbol{\tau} \tag{3.57}$$

But the plastic deformation rate $\mathbf{D}^p$ and spin tensor $\mathbf{W}^p$ are both defined in terms of the slip activity within each slip system in the sense:

$$\mathbf{D}^p = \sum_{\alpha=1}^{Nas} \dot{\gamma}^\alpha \mathbf{M}^\alpha \qquad \mathbf{W}^p = \sum_{\alpha=1}^{Nas} \dot{\gamma}^\alpha \boldsymbol{\Omega}^\alpha \tag{3.58}$$

with:

$$\mathbf{M}^\alpha = \frac{1}{2} (\mathbf{s}^\alpha\, \mathbf{m}^\alpha + \mathbf{m}^\alpha\, \mathbf{s}^\alpha) \tag{3.59a}$$

$$\boldsymbol{\Omega}^\alpha = \frac{1}{2} (\mathbf{s}^\alpha\, \mathbf{m}^\alpha - \mathbf{m}^\alpha\, \mathbf{s}^\alpha) \tag{3.59b}$$

At this point recall that $\mathbf{s}^\alpha, \mathbf{m}^\alpha$ represent the slip direction vector and the vector normal to the slip plane of system α. In addition, the slip and normal unit vectors defined in

---

[23]The notation $\boldsymbol{\mathcal{L}}^e$ represents the elasticity matrix with respect to the crystal axes while the notation $\overline{\boldsymbol{\mathcal{L}}^e}$ expresses the elasticity matrix in the global system using the rotation matrix of the transformation $[Q]$

[24]The Jaumann rate is corotational with the plastic spin tensor $\mathbf{W}^p$ and is one of the most commonly implemented objective rates in the constitutive modelling of solids. Objective rates are discussed in greater detail in Chapter 1

the reference configuration $\mathfrak{B}_0$ are denoted as $\mathbf{s}_0^\alpha$ and $\mathbf{m}_0^\alpha$ respectively. Since we already postulated the existence of an isoclinic configuration $\mathfrak{B}_i$ in which the slip and normal vectors are the same as in the reference configuration $\mathfrak{B}_0$, we express the directors $\mathbf{s}^\alpha, \mathbf{m}^\alpha$ in terms of $\mathbf{s}_0^\alpha$ and $\mathbf{m}_0^\alpha$ as:

$$\mathbf{s}^\alpha = \mathbf{F}^e \cdot \mathbf{s}_0^\alpha \qquad\qquad \mathbf{m}^\alpha = \mathbf{m}_0^\alpha \cdot \mathbf{F}^{e-1}$$

and the corresponding rates $\dot{\mathbf{s}}^\alpha$ and $\dot{\mathbf{m}}^\alpha$ can also be expressed as:

$$\dot{\mathbf{s}}^\alpha = \mathbf{L}^e \cdot \mathbf{s}^\alpha \qquad\qquad \dot{\mathbf{m}}^\alpha = -\mathbf{m}^\alpha \cdot \mathbf{L}^e$$

Now lets combine (3.57) and (3.58) to derive:

$$\overset{\nabla}{\boldsymbol{\tau}} = \boldsymbol{\mathcal{L}}^{e\tau} : \left(\mathbf{D} - \sum_{\alpha=1}^{Nas} \dot{\gamma}^\alpha \mathbf{M}^\alpha \right) - \sum_{\alpha=1}^{Nas} \dot{\gamma}^\alpha \left(\boldsymbol{\Omega}^\alpha \cdot \boldsymbol{\tau} - \boldsymbol{\tau} \cdot \boldsymbol{\Omega}^\alpha \right)$$

$$= \boldsymbol{\mathcal{L}}^{e\tau} : \mathbf{D} - \sum_{\alpha=1}^{Nas} \dot{\gamma}^\alpha \left(\boldsymbol{\mathcal{L}}^{e\tau} : \mathbf{M}^\alpha + \boldsymbol{\Omega}^\alpha \cdot \boldsymbol{\tau} - \boldsymbol{\tau} \cdot \boldsymbol{\Omega}^\alpha \right)$$

The above expression leads to the definition of $\mathbf{B}^\alpha$ and $\boldsymbol{\Phi}^\alpha$ as:

$$\mathbf{B}^\alpha = \boldsymbol{\Omega}^\alpha \cdot \boldsymbol{\tau} - \boldsymbol{\tau} \cdot \boldsymbol{\Omega}^\alpha \tag{3.60}$$

$$\boldsymbol{\Phi}^\alpha = \boldsymbol{\mathcal{L}}^{e\tau} : \mathbf{M}^\alpha + \mathbf{B}^\alpha \tag{3.61}$$

And note that:

$$\mathbf{B}^\alpha = \frac{1}{2} \left[(\mathbf{s}^\alpha \mathbf{m}^\alpha - \mathbf{m}^\alpha \mathbf{s}^\alpha) \cdot \boldsymbol{\tau} - \boldsymbol{\tau} \cdot (\mathbf{s}^\alpha \mathbf{m}^\alpha - \mathbf{m}^\alpha \mathbf{s}^\alpha) \right] = \boldsymbol{\tau} \cdot (\mathbf{m}^\alpha \mathbf{s}^\alpha) - (\mathbf{m}^\alpha \mathbf{s}^\alpha) \cdot \boldsymbol{\tau} \tag{3.62}$$

With the above definitions, we can now simplify expression (3.57) to

$$\boxed{ \overset{\nabla}{\boldsymbol{\tau}} = \boldsymbol{\mathcal{L}}^{e\tau} : \mathbf{D} - \sum_{\alpha=1}^{Nas} \dot{\gamma}^\alpha \boldsymbol{\Phi}^\alpha } \tag{3.63}$$

Note that if we are able to express $\dot{\gamma}^\alpha$ in terms of $\mathbf{D}$ then expression (3.63) immediately defines the elastoplastic tangent modulus. To do so, we will make use of the yield and consistency conditions within each slip system,

$$\phi^\alpha = \tau^\alpha - \tau_{cr}^\alpha = 0 \tag{3.64a}$$

$$\dot{\phi}^\alpha = \dot{\tau}^\alpha - \dot{\tau}_{cr}^\alpha = 0 \Rightarrow \dot{\tau}^\alpha - \sum_{\beta=1}^{N} h^{\alpha\beta} \dot{\gamma}^\beta = 0 \tag{3.64b}$$

defined by equations (3.64a) and (3.64b) respectively. The resolved shear stress on slip system α can be expressed in terms of the Kirchhoff stress $\boldsymbol{\tau}$ as:

$$\tau^\alpha = \mathbf{m}_0^\alpha \cdot \boldsymbol{\Sigma} \cdot \mathbf{s}_0^\alpha = \mathbf{m}_0^\alpha \cdot \mathbf{F}^{e-1} \cdot \boldsymbol{\tau} \cdot \mathbf{F}^e \cdot \mathbf{s}_0^\alpha = \mathbf{m}^\alpha \cdot \boldsymbol{\tau} \cdot \mathbf{s}^\alpha \tag{3.65}$$

Then differentiating (3.65) with respect to time t and plugging the result into (3.64b) we get:

$$
\begin{aligned}
\dot{\tau}^\alpha &= \dot{\mathbf{m}}^\alpha \cdot \boldsymbol{\tau} \cdot \mathbf{s}^\alpha + \mathbf{m}^\alpha \cdot \dot{\boldsymbol{\tau}} \cdot \mathbf{s}^\alpha + \mathbf{m}^\alpha \cdot \boldsymbol{\tau} \cdot \dot{\mathbf{s}}^\alpha = \\
&= -\mathbf{m}^\alpha \cdot \mathbf{L}^e \cdot \boldsymbol{\tau} \cdot \mathbf{s}^\alpha + \mathbf{m}^\alpha \cdot \dot{\boldsymbol{\tau}} \cdot \mathbf{s}^\alpha + \mathbf{m}^\alpha \cdot \boldsymbol{\tau} \cdot \mathbf{L}^e \cdot \mathbf{s}^\alpha = \\
&= \mathbf{m}^\alpha \cdot (-\mathbf{L}^e \cdot \boldsymbol{\tau} + \dot{\boldsymbol{\tau}} + \boldsymbol{\tau} \cdot \mathbf{L}^e) \cdot \mathbf{s}^\alpha = \mathbf{m}^\alpha \cdot [-(\mathbf{D}^e + \mathbf{W}^*) \cdot \boldsymbol{\tau} + \dot{\boldsymbol{\tau}} + \boldsymbol{\tau} \cdot (\mathbf{D}^e + \mathbf{W}^*)] \cdot \mathbf{s}^\alpha = \\
&= \mathbf{m}^\alpha \cdot [(\dot{\boldsymbol{\tau}} + \boldsymbol{\tau} \cdot \mathbf{W}^* - \mathbf{W}^* \cdot \boldsymbol{\tau}) - \mathbf{D}^e \cdot \boldsymbol{\tau} + \boldsymbol{\tau} \cdot \mathbf{D}^e] \cdot \mathbf{s}^\alpha = \\
&= \mathbf{m}^\alpha \cdot \overset{*}{\boldsymbol{\tau}} \cdot \mathbf{s}^\alpha + \mathbf{m}^\alpha \cdot (-\mathbf{D}^e \cdot \boldsymbol{\tau} + \boldsymbol{\tau} \cdot \mathbf{D}^e) \cdot \mathbf{s}^\alpha = \\
&= \mathbf{m}^\alpha \cdot (\boldsymbol{\mathcal{L}}^{e\tau} : \mathbf{D}^e) \cdot \mathbf{s}^\alpha + \mathbf{m}^\alpha \cdot (-\mathbf{D}^e \cdot \boldsymbol{\tau} + \boldsymbol{\tau} \cdot \mathbf{D}^e) \cdot \mathbf{s}^\alpha = \\
&= I + J
\end{aligned}
\tag{3.66}
$$

where:

$$
I = \mathbf{m}^\alpha \cdot (\boldsymbol{\mathcal{L}}^{e\tau} : \mathbf{D}^e) \cdot \mathbf{s}^\alpha
\tag{3.67}
$$

$$
J = \mathbf{m}^\alpha \cdot (-\mathbf{D}^e \cdot \boldsymbol{\tau} + \boldsymbol{\tau} \cdot \mathbf{D}^e) \cdot \mathbf{s}^\alpha
\tag{3.68}
$$

But:

$$
I = m_i^\alpha \, \mathcal{L}_{ijkl}^{e\tau} \, D_{kl}^e \, s_j^\alpha = (\mathbf{m}^\alpha \, \mathbf{s}^\alpha)_{ij} \, \mathcal{L}_{ijkl}^{e\tau} \, D_{kl}^e = \mathbf{M}^\alpha : \boldsymbol{\mathcal{L}}^{e\tau} : \mathbf{D}^e
\tag{3.69}
$$

And:

$$
\begin{aligned}
J &= -m_i^\alpha \, D_{ij}^e \, \tau_{jk} \, s_k^\alpha + m_i^\alpha \, \tau_{ij} \, D_{jk}^e \, s_k^\alpha = -\left(-m_i^\alpha \, \tau_{jk} \, s_k^\alpha\right) D_{ij}^e + \left(m_i^\alpha \, \tau_{ij} \, s_k^\alpha\right) D_{jk}^e = \\
&= -(\mathbf{m}^\alpha \, \boldsymbol{\tau} \cdot \mathbf{s}^\alpha)_{ij} \, D_{ij}^e + (\mathbf{m}^\alpha \cdot \boldsymbol{\tau} \, \mathbf{s}^\alpha)_{jk} \, D_{jk}^e = -(\mathbf{m}^\alpha \, \boldsymbol{\tau} \cdot \mathbf{s}^\alpha) : \mathbf{D}^e + (\mathbf{m}^\alpha \cdot \boldsymbol{\tau} \, \mathbf{s}^\alpha) : \mathbf{D}^e = \\
&= (\mathbf{m}^\alpha \cdot \boldsymbol{\tau} \, \mathbf{s}^\alpha - \mathbf{m}^\alpha \, \boldsymbol{\tau} \cdot \boldsymbol{\sigma}^\alpha) : \mathbf{D}^e = (\boldsymbol{\tau} \cdot \mathbf{m}^\alpha \, \mathbf{s}^\alpha - \mathbf{m}^\alpha \, \boldsymbol{\sigma}^\alpha \cdot \boldsymbol{\tau}) : \mathbf{D}^e = \mathbf{B}^\alpha : \mathbf{D}^e
\end{aligned}
\tag{3.70}
$$

Expressions (3.69) and (3.70) allow us to write equation (3.66) as:

$$
\dot{\tau}^\alpha = \mathbf{M}^\alpha : \boldsymbol{\mathcal{L}}^{e\tau} : \mathbf{D}^e + \mathbf{B}^\alpha : \mathbf{D}^e = (\mathbf{M}^\alpha : \boldsymbol{\mathcal{L}}^{e\tau} + \mathbf{B}^\alpha) : \mathbf{D}^e \Rightarrow \dot{\tau}^\alpha = \boldsymbol{\Phi}^\alpha : \mathbf{D}^e
\tag{3.71}
$$

where we used equation (3.61). Recalling that our goal is to express $\dot{\gamma}^\alpha$ in terms of $\mathbf{D}$, we will now replace $\mathbf{D}^e$ with $\mathbf{D} - \mathbf{D}^p$ and also express $\mathbf{D}^p$ as suggested in equation (3.58). Thus,

$$
\dot{\tau}^\alpha = \boldsymbol{\Phi}^\alpha : \mathbf{D} - \boldsymbol{\Phi}^\alpha : \sum_{\beta=1}^{Nas} \dot{\gamma}^\beta \mathbf{M}^\beta
\tag{3.72}
$$

Now lets replace the above expression in the consistency condition (3.64b) to derive:

$$
\boldsymbol{\Phi}^\alpha : \mathbf{D} - \boldsymbol{\Phi}^\alpha : \sum_{\beta=1}^{Nas} \dot{\gamma}^\beta \, \mathbf{M}^\beta - \sum_{\beta=1}^{N} h^{\alpha\beta} \, \dot{\gamma}^\beta = 0 \Rightarrow \sum_{\beta=1}^{Nas} \dot{\gamma}^\beta \left(\boldsymbol{\Phi}^\alpha : \mathbf{M}^\beta + h^{\alpha\beta} \right) = \boldsymbol{\Phi}^\alpha : \mathbf{D} \Rightarrow
$$

$$
\sum_{\beta=1}^{Nas} \dot{\gamma}^\beta \, \Upsilon^{\alpha\beta} = \boldsymbol{\Phi}^\alpha : \mathbf{D}
\tag{3.73}
$$

where we defined matrix $[\Upsilon]$ whose components are given as $\Upsilon^{\alpha\beta} = \Phi^{\alpha} : \mathbf{M}^{\beta} + h^{\alpha\beta}$. Lets also define as $\Psi^{\alpha\beta}$ the inverse components of $\Upsilon^{\alpha\beta}$ ($[\Psi] = [\Upsilon]^{-1}$). As a result of these definitions, expression (3.73) can be written as:

$$\dot{\gamma}^{\alpha} = \sum_{\beta=1}^{Nas} \Psi^{\alpha\beta} \, \mathbf{\Phi}^{\alpha} : \mathbf{D} \tag{3.74}$$

And by defining $\mathbf{\Lambda}^{\alpha}$ as:

$$\mathbf{\Lambda}^{\alpha} = \sum_{\beta=1}^{Nas} \Psi^{\alpha\beta} \, \mathbf{\Phi}^{\beta} \tag{3.75}$$

leads to the desired expression of $\dot{\gamma}^{\alpha}$ in terms of $\mathbf{D}$:

$$\boxed{\dot{\gamma}^{\alpha} = \mathbf{\Lambda}^{\alpha} : \mathbf{D}} \tag{3.76}$$

We will now combine (3.63) and (3.76) to derive an analytic expression for the tangent modulus. Hence,

$$\overset{\triangledown}{\boldsymbol{\tau}} = \boldsymbol{\mathcal{L}}^{e\tau} : \mathbf{D} - \sum_{\alpha=1}^{Nas} \dot{\gamma}^{\alpha} \, \mathbf{\Phi}^{\alpha} = \boldsymbol{\mathcal{L}}^{e\tau} : \mathbf{D} - \sum_{\alpha=1}^{Nas} \mathbf{\Phi}^{\alpha} \, \mathbf{\Lambda}^{\alpha} : \mathbf{D} = \left(\boldsymbol{\mathcal{L}}^{e\tau} - \sum_{\alpha=1}^{Nas} \mathbf{\Phi}^{\alpha} \, \mathbf{\Lambda}^{\alpha} \right) : \mathbf{D}$$

The quantity enclosed in parenthesis above defines the tangent modulus for single crystal plasticity as:

$$\boldsymbol{\mathcal{L}}^{J} = \boldsymbol{\mathcal{L}}^{e\tau} - \sum_{\alpha=1}^{Nas} \mathbf{\Phi}^{\alpha} \, \mathbf{\Lambda}^{\alpha} = \boldsymbol{\mathcal{L}}^{e\tau} - \sum_{\alpha=1}^{Nas} \mathbf{\Phi}^{\alpha} \sum_{\beta=1}^{Nas} \Psi^{\alpha\beta} \, \mathbf{\Phi}^{\beta} = \boldsymbol{\mathcal{L}}^{e\tau} - \sum_{\alpha=1}^{Nas} \sum_{\beta=1}^{Nas} \Psi^{\alpha\beta} \, \mathbf{\Phi}^{\alpha} \, \mathbf{\Phi}^{\beta} \tag{3.77}$$

And finally,

$$\boxed{\boldsymbol{\mathcal{L}}^{J} = \boldsymbol{\mathcal{L}}^{e\tau} - \sum_{\alpha=1}^{Nas} \sum_{\beta=1}^{Nas} \Psi^{\alpha\beta} \, \mathbf{\Phi}^{\alpha} \, \mathbf{\Phi}^{\beta}} \tag{3.78}$$

$$\boxed{\overset{\triangledown}{\boldsymbol{\tau}} = \boldsymbol{\mathcal{L}}^{J} : \mathbf{D}} \tag{3.79}$$

The form (3.78) however, raises two important concerns [10]. First, matrix $\Psi^{\alpha\beta}$ may not always exist, since $\Upsilon^{\alpha\beta}$ is not *a priori* an invertible matrix. In fact, existence of the inverse matrix $\Psi^{\alpha\beta}$ strongly depends on the exact selection of the hardening moduli $h^{\alpha\beta}$. In several cases, the inability to find the inverse of $\Upsilon^{\alpha\beta}$ suggests that a unique solution does not exist[25] and additional information is required. Secondly, in cases where $\Psi^{\alpha\beta}$ exists, it defines a non–symmetric matrix. This immediately declares $\boldsymbol{\mathcal{L}}^{J}$ as non–symmetric as well.

---

[25]i.e. the set of active systems is not unique etc.

Chapter 4

The effect of Hydrogen concentration

The mechanical behavior of structural materials in the presence of Hydrogen has been widely studied by Hirth [29], Birnbaum & Sofronis [15], Birnbaum *et al.*[16] and in the vast majority of studies, the effect of Hydrogen was detrimental causing materials to fail at far lower loads than the ones observed in absence of Hydrogen. This effect is widely known as 'hydrogen embrittlement' and essentially describes a significant reduction in macroscopic ductility and ultimate tensile strength (UTS) and also a change in the type of fracture [29]. Hydrogen related failures are attributed to several mechanisms, with the hydrogen enhanced localized plasticity (HELP) probably being the most viable one according to Beachem [13], Birnbaum & Sofronis [15] and Robertson [43]. The theoretical predictions of Sofronis [45] and Sofronis & Birnbaum [46] as well as the experimental observations of Sirois [44] provide evidence in support of the HELP mechanism, demonstrating that the presence of hydrogen in solid solution reduces the barriers to dislocation motion, increasing the amount of deformation that occurs in a localized region adjacent to the fracture surface.

The strongest incentive in developing a comprehensive constitutive model for single crystal plasticity, is to obtain a deeper understanding of the effect of Hydrogen in the mechanical response and failure of structural materials. A thorough description of the hydrogen-dislocation interactions within single crystals, is considered a prerequisite to the later development of a physically–based polycrystalline model. In the present chapter[1] we will try to derive a concise methodology to implement the effects of hydrogen concentration in the rate–independent constitutive model for single crystal plasticity[2] while taking into consideration the hydrogen solute interactions with the microstructure of metallic materials.

---

[1]This chapter is based on the Master Thesis by Schebler [48]

[2]The rate–independent constitutive model for crystal plasticity in absence of Hydrogen in presented in detail in Chapter 3

Plastic deformation of metal single crystals is fundamentally based on dislocation glide, and thus it is important to obtain a deeper understanding of the hydrogen–dislocation interactions. A series of studies on polycrystalline nickel (Robertson [43]) suggest that the mobility of dislocations tends to increase when hydrogen is present; observations indicate that isolated screw and edge dislocations as well as dislocations involved in forest interactions, are able to glide in greater velocities due to hydrogen. The studies of Robertson [43] also illustrate that the stresses required to move dislocations in hydrogen–charged specimens, are lower than the ones required in absence of hydrogen. As a result of these general observations, it is expected that hydrogen–charged single crystal specimens would exhibit weaker Stage I & II hardening[3].

Despite the fact that the presence of hydrogen facilitates the activity of mobile dislocations, initial activation of immobile dislocations tends to be hindered. Experimental observations showed that the initial macroscopic yield stress for hydrogen–charged FCC polycrystalline specimens was elevated when compared to similar tests in absence of hydrogen. In the works of Abraham & Altstetter [3], the recorded yield stress elevation was attributed to the locking of Frank-Reed dislocation sources due to Hydrogen, a mechanism that may be present in single crystals as well.

Even though similar experimental investigations on single crystal specimens are generally limited, they present even greater interest to our study. Delafosse [23] and Yagodzinskyy [52],[53] performed uniaxial tension experiments on FCC single crystal specimens oriented for easy glide for both hydrogen-free and hydrogen–charged specimens. From these tests we can derive the following interesting ascertainments regarding the effects of Hydrogen on the mechanical behavior of FCC single crystals:

- The initial yield strength in uniaxial tension experiments was considerably elevated in hydrogen charged single crystal specimens, exhibiting up to 25% increase for nickel (Delafosse [23], Yagodzinskyy [53]) and up to 30% (Yagodzinskyy [52]) increase for austenitic stainless steel

- In all experiments Stage I hardening was significantly prolonged, suggesting that the presence of Hydrogen delays the onset of Stage II hardening

- Work hardening during Stage II was significantly greater in Hydrogen charged specimens (Delafosse [23])

At this point we should note that the uniaxial tension experiments of Delafosse [23] were conducted using singificantly higher strain rates ($10^{-2}\,s^{-1}$) than the ones in both Yagodzinskyy's tests [52],[53] ($\leq 10^{-4}\,s^{-1}$).

In the following sections we present a modified formulation to the rate–independent constitutive model for crystal plasticity so as to take into account the effects of Hydrogen concentration.

---

[3]The stages of hardening for FCC crystals are discussed in Section 3.4
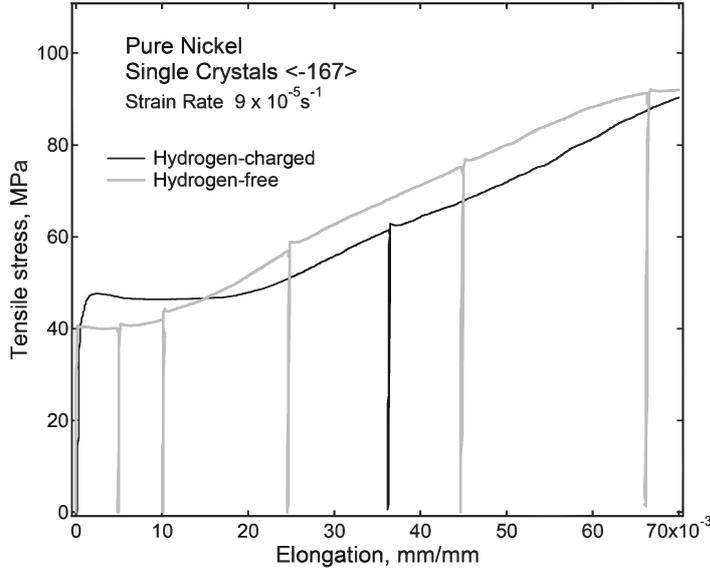
Figure 4.1: The experimental stress–strain curves corresponding to uniaxial tension of hydrogen-free (grey) and hydrogen–charged (black) nickel single crystal specimens in easy glide orientation (Yagodzinskyy et al.[53])

4.1 Modified Formulation

We begin with the multiplicative decomposition of the deformation gradient which is now such to incorporate the effect of Hydrogen concentration in deformation. Hence, the total $\mathbf{F}$ is multiplicatively decomposed in terms of an elastic $\mathbf{F}^e$, a plastic $\mathbf{F}^p$ and a hydrogen associated part $\mathbf{F}^h$ as:

$$\mathbf{F} = \mathbf{F}^e \cdot \mathbf{F}^h \cdot \mathbf{F}^p \tag{4.1}$$

The hydrogen associated part of the deformation gradient $\mathbf{F}^h$ is purely dilatational (Peisl, 1978), thus the hydrogen part of the deformation gradient is expressed as (Sofronis, 1995):

$$\mathbf{F}^h = \left(1 + \frac{e^h}{3}\right)\boldsymbol{\delta} \tag{4.2}$$

with $e^h = \lambda(c - c_0)$. The total current and total initial hydrogen concentrations in the material point under consideration are denoted as c and c_0 respectively and are expressed in hydrogen atoms per lattice atom. Also $\lambda = \Delta v / \Omega$, where Δv is the volume change per hydrogen atom introduced into the solid solution[4] and Ω is the mean atomic volume of the host metal atom. Now using expression (4.1) and the specific form of $\mathbf{F}^h$ in (4.2), we can readily show that the velocity gradient $\mathbf{L}$ corresponding to $\mathbf{F}$ can be additively decomposed as:

$$\mathbf{L} = \mathbf{L}^e + \mathbf{L}^h + \mathbf{L}^p \tag{4.3}$$

---

[4]The volume change per hydrogen atom introduced is related to the partial molar volume of hydrogen via $V_h = \Delta v\, N_A$, where N_A is Avogadro's number

The elastic $\mathbf{L}^e$ and plastic $\mathbf{L}^p$ parts of the total velocity gradient are defined in (3.35a) and (3.35b) respectively. For $\mathbf{L}^h$ we can show that:

$$\mathbf{L}^h = \frac{1}{3}\Lambda(c)\,\dot{c}\,\boldsymbol{\delta} \tag{4.4}$$

where

$$\Lambda(c) = \frac{\lambda}{1 + \lambda(c - c_0)/3} \tag{4.5}$$

Expression (4.4) suggests that $\mathbf{L}^h = \mathbf{D}^h$ and consequently $\mathbf{W}^h = \mathbf{0}$. We should also note that the current formulation to incorporate the deformation effects of hydrogen through $\mathbf{F}^h$, does not alter the lattice orientation.
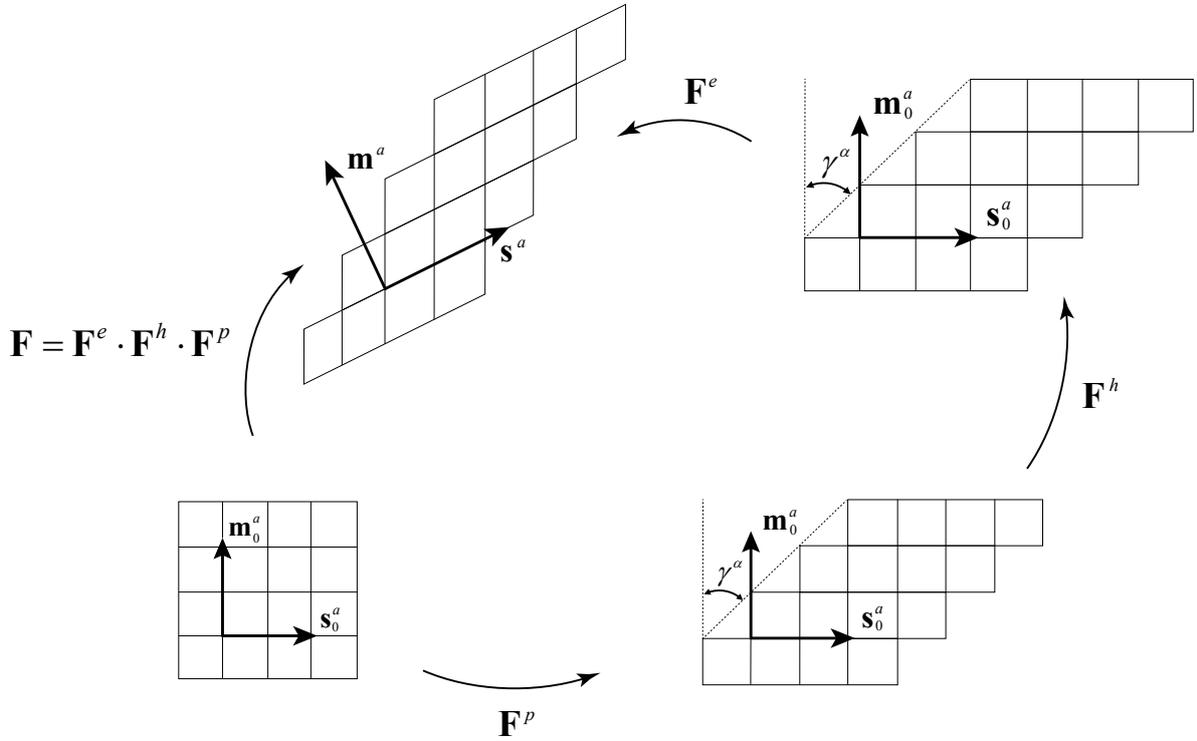
Figure 4.2: A schematic representation of the multiplicative decomposition of $\mathbf{F}$. The purely dilatational effect of $\mathbf{F}^h$ does not alter the lattice orientation

4.2 Hydrogen Equilibrium

In the current model we assume that hydrogen atoms reside in one of two locations within the crystal: normal interstitial lattice sites (NILS) and trapping sites attributed to the plastic deformation. According to the theory of Oriani (1970), the quantities residing in each location are always in equilibrium in the sense:

$$\frac{\theta_T^\alpha}{1 - \theta_T^\alpha} = \frac{\theta_L}{1 - \theta_L}\,K_T \tag{4.6}$$

where θ_L represents the occupancy of lattice sites and θ_T^α the respective occupancy of the trap sites in slip system α. The equilibrium constant K_T is defined as:

$$K_T = \exp\left(\frac{W_B}{RT}\right) \tag{4.7}$$

where W_B is the trap binding energy, R is the gas constant and T the absolute temperature. Next we define the concentrations C_L and C_T^α measured in atoms per unit volume, associated with the occupancy of lattice and trap sites respectively as:

$$C_L = \theta_L \, \zeta \, N_L \tag{4.8a}$$

$$C_T^\alpha = \theta_T^\alpha \, \eta \, N_T^\alpha \tag{4.8b}$$

with ζ and η representing the number of NILS per lattice atom and the number of sites per trap respectively, whereas N_T^α is defined as the number of sites per trap on system α. The number of lattice atoms per unit lattice volume N_L is calculated using Avogadro's number N_A and the molar volume V_M of the lattice as:

$$N_L = N_A / V_M \tag{4.9}$$

The normalized lattice and trapped concentrations are also introduced as:

$$c_L = C_L / N_L \tag{4.10a}$$

$$c_T^\alpha = C_T^\alpha / N_L \tag{4.10b}$$

In the current model, we assume that trap sites in each slip system are associated with dislocations and that only one trap site may exist in every atomic plane threaded by a dislocation (Thomas [51]). Based on this assumption, the trap density on slip system α is directly related to the dislocation density on that system by an expression of the form:

$$\rho^\alpha = N_T^\alpha \, b \tag{4.11}$$

where b stands for the dislocation Burgers vector. Equation (4.11) provides an immediate correlation between the trapped hydrogen concentration and the crystal's mechanical response. The dislocation density on every slip system directly depends on the slip activity of that system, in the sense that increasing deformation introduces new dislocations on every atomic plane of the crystal's microstructure[5]. The relationship that couples the dislocation density on slip system α with the critical resolved shear stress on that system was initially proposed by Taylor [49] and has the following form:

$$\tau_{cr}^\alpha = \tilde{\alpha}\mu b \sqrt{\rho^\alpha} \tag{4.12}$$

where μ is the shear modulus[6] and $\tilde{\alpha}$ is a proportionality constant. Combining equations (4.11) and (4.12) we can derive:

$$N_T^\alpha = \left(\frac{\tau_{cr}^\alpha}{\tilde{\alpha}\mu}\right)^2 \frac{1}{b^3} \tag{4.13}$$

---

[5]In FCC single crystals, the dislocation density dramatically increases during Stage II hardening
[6]The shear modulus is defined in isotropic polycrystals in terms of the Young's modulus of elasticity

which illustrates that the trap density is proportional to the square of the the critical shear stress on a given slip system.

4.3 Hydrogen Diffusion

At this point, it is necessary to address the diffusion of hydrogen in the microstructure of a single crystal specimen. The major 'driving forces' for the diffusion of hydrogen atoms residing in lattice sites, are the gradient of the hydrostatic stress along with the gradient of the chemical potential in every material point. NILS hydrogen concentration has to be in equilibrium with the local hydrostatic stress [36] in the material point under consideration, in the sense that they tend to accumulate in regions of increased hydrostatic stress. In a uniaxial tension experiment however, the hydrostatic stress is uniform throughout the specimen[7], and thus no significant hydrogen accumulation can occur as a result of hydrostatic stress peaks. In the present study, we only consider uniaxial tension experiments of hydrogen–charged single crystal specimens, and therefore we focus on the slow diffusion process driven from the gradient of chemical potential.

In order to get a sense for the diffusion speed of hydrogen in FCC crystals, we consider the hydrogen charging process of a nickel single crystal specimen and assume that the diffusion phenomena can be described by the solution of 2nd Fick's law for uni–dimensional diffusion within a semi–infinite medium:

$$\frac{c(x,t)}{c_0} = \text{erfc}\left(\frac{x}{2\sqrt{D_h\,t}}\right) \tag{4.14}$$

where $c(x,t)$ represents the hydrogen concentration $x[m]$ away from the boundary and $t[sec]$ after the charging process initiation. Also, erfc is the complementary error function, c_0 is the fixed boundary hydrogen concentration, and $D_h = 6.6 \cdot 10^{-14}\, m^2/sec$ is the diffusivity of hydrogen in nickel (Sirois and Birnbaum [44]). The average duration of the uniaxial tension experiments performed by Yagodzinskyy *et al.*[53] on pure nickel single crystals was about $13\,min$ and the smallest dimension of the dogbone[8] specimens used was $0.3mm$. Given these values, we can make use of (4.14) to show that after $13min$ of charging in room temperature, hydrogen atoms are unable to travel distances greater than $33\mu m$[9] based on a 0.1% criterion. Clearly, such diffusion distances are negligible when compared to the smallest dimension of the single crystal specimens, suggesting that hydrogen diffusion in room temperature during a uniaxial tension experiment is not significant.

Hydrogen diffusion was also considered insignificant in the works of Somerday *et al.*[47] on austenitic stainless steel welds, when the hydrogen concentration after the test was found to be relatively equal to the initial concentration before the test. Hence, in the context of the theoretical prediction and numerical simulation of the hydrogen effect in single crystal

---

[7]Away from the grip locations

[8]Specimens (*see* Section 7.2) commonly used in uniaxial tension experiments of single crystals

[9]$c(x, 13min) = 0.1\%\, c_0 \Rightarrow x = 33\mu m$

specimens subjected to uniaxial tension, we can ignore the diffusion phenomena and assume that the total hydrogen concentration remains fixed during a uniaxial tension experiment. Under this assumption, we postulate that the NILS and trapped hydrogen concentrations on every slip system are such that equation:

$$c_L + \sum_\alpha c_T^\alpha = c_0 \tag{4.15}$$

is satisfied at all times and in every material point of the continuum body. Furthermore, assuming that $c(\mathbf{x}, t) = c_0 \ \ \forall \ \mathbf{x} \in \mathfrak{B_t}$ and $\forall t$, we can simplify 4.2 to:

$$\mathbf{F}^h = \left(1 + \lambda\frac{(c - c_0)}{3}\right)\boldsymbol{\delta} = \left(1 + \lambda\frac{0}{3}\right)\boldsymbol{\delta} = \boldsymbol{\delta} \tag{4.16}$$

Now using (4.16) we can readily show that $\mathbf{L}^h = \mathbf{D}^h = \mathbf{W}^h = \mathbf{0}$, and therefore we do not have to take into account the dilatational effect of hydrogen concentration to deformation. In complete contrast to the diffusion phenomena however, the interchange of hydrogen atoms between NILS and trap sites is highly significant in such experiments, due to the finite plasticity of the specimen and the associated trap (dislocation) generation.

4.4 The Modified Hardening Model

Back to the constitutive modelling of hydrogen charged single crystals, we seek to formulate a modified hardening model, based on the model presented in Section 3.4, taking into account the experimental observations on the uniaxial tension of hydrogen–charged single crystal specimens. In particular, the hardening model accounting for hydrogen effects, must be introduced so that the extension of the easy glide stage (Stage I) as well as the reduction of the corresponding work hardening are both captured by the model and also defined as functions of the hydrogen concentration. In addition, the fact that hydrogen charged crystal specimens exhibit up to a 25% increase (see Figure 4.1) of the initial yield strength suggests that special treatment is also required for the initial critical shear stresses.

Taking into consideration that only the hydrogen atoms residing in trapped sites interfere with the mechanical behavior of the single crystal, we restate the hardening model of Bassani & Wu [11, 12] in the following modified form:

$$\dot{\tau}_{cr}^\alpha = \sum_{\beta=1}^{Nas} h_H^{\alpha\beta}\,\dot{\gamma}^\beta \tag{4.17}$$

The new instantaneous hardening moduli $h_H^{\alpha\beta}$ is now such to incorporate the effects of the trapped hydrogen concentration within each slip system, using the following linear model:

$$h_H^{\alpha\beta} = (1 + H_c\,c_T^\alpha)h^{\alpha\beta} \tag{4.18}$$

where H_c is the parameter controlling the linear effect of c_T^α on $h_H^{\alpha\beta}$ and $h^{\alpha\beta}$ is the hardening moduli defined by equations (3.25a,3.25b) which are restated below

$$h^{\alpha\alpha} = \left[(h_0 - h_s)\mathrm{sech}^2\left(\frac{h_0 - h_s}{\tau_I - \tau_0}\gamma^\alpha\right) + h_s\right]\left[1 + \sum_{\substack{\beta=1 \\ \beta\neq\alpha}}^{N} f_{\alpha\beta}\tanh\frac{\gamma^\beta}{\gamma_0}\right]$$

$$h^{\beta\alpha} = q\,h^{\alpha\alpha}\quad,\quad \alpha\neq\beta$$

The initial critical shear stresses are also introduced as linear functions of c_T^α in the sense:

$$(\tau_0^\alpha)_H = (1 + T_c\,c_T^\alpha)\tau_0 \tag{4.19}$$

with T_c representing the parameter controlling the linear effect of c_T^α on $(\tau_0)_H$. The parameters H_c and T_c should be chosen so that the current model be in agreement with the experimental observations of Delafosse [23] and Yagodzinskyy *et al.*[52, 53]. In particular, the parameter H_c controlling the effect of c_T^α on hardening, should be negative in order to capture the 'softening' effect attributed to the presence of hydrogen delaying the onset of Stage II. In contrary, T_c must be positive, so that higher hydrogen concentrations would translate to a corresponding increase in the initial yield strength in uniaxial tension.

To conclude the discussion on the modified hardening model, we should note that since hydrogen concentration is explicitly involved in τ_{cr}^α, special treatment is necessary for the computational–incremental implementation of the new model. The algorithm to predict the active systems set and integrate the constitutive equations should also impose the hydrogen equilibrium taking into account the interdependency of critical stresses and trapped hydrogen concentration. These computational issues are discussed in further detail in Section 5.1.i.

Chapter 5

Computational Issues I - Stress Update Algorithms

The numerical integration of the constitutive equations as well as the calculation of the linearization moduli $\mathcal{L}^J$ presented in previous chapters, implicitly assume that the set of active slip systems $\mathscr{A}$ is known. However, the process of determining the set of active systems $\mathscr{A}$ at a given time, requires information regarding the Mandel stress tensor $\boldsymbol{\Sigma}$ and the critical shear stresses of each system τ_{cr}^{α}. The integration of equations is therefore prerequisite to update the active set $\mathscr{A}$ while simultaneously the numerical integration itself is not possible without providing the set of active systems. The latter illustrates the inherent interdependency of integrating the constitutive equations and identifying the set of active systems. From now on we treat the integration of equations and the problem of determining the active set as a single problem. The algorithms developed to solve the aforementioned problem are commonly referred to as stress-update algorithms.

The stress update algorithms proposed by Cuitiño & Ortiz [21] and by Anand & Kothari [4] are among the most popular ones, while Borja and Wren [18] propose a so-called *ultimate algorithm* for rate-independent crystal plasticity. In the following section we will present the algorithm by Miehe and Schröder [40] which is a modified version of the one proposed by Cuitiño and Ortiz [21].

5.1 The Heuristic Algorithm

At first, let us denote with $\mathscr{P}$ the set containing all available slip systems in the sense $\mathscr{P} := \{1, ..., N\}$[1]. Loading a single crystal in an incremental manner, eventually violates the

---

[1]Recall that in the case of an FCC cubic crystal there is a total of 12 slip systems with two slip possibilities (*positive slip-negative slip*) for each system, leading to a total of $N = 2 \times 12 = 24$ slip possibilities

yield functions for some systems $\alpha \in \mathscr{P}$ in the sense $\phi^\alpha > 0$. The set of active systems $\mathscr{A}$, is then defined as follows:

$$\mathscr{A} := \{\alpha \in \mathscr{P} | \gamma^\alpha > 0 \;\; \text{and} \;\; \phi^\alpha = 0 \;\; \forall \alpha \in \mathscr{A}\} \tag{5.1}$$

As aforementioned however, we are unable to determine 'a priori' the set of active systems and we therefore introduce an heuristic algorithm to populate the set with potentially active systems in an iterative manner. The heuristic algorithm is initiated by postulating (as a first estimate) that the set at time $t = t_{n+1} \rightarrow \mathscr{A}_{n+1}$ coincides with the converged set of the previous increment at $t = t_n \rightarrow \mathscr{A}_n$. Hence:

$$\mathscr{A}_{n+1} = \mathscr{A}_n \tag{5.2}$$

If this assumption (5.2) proves to be wrong, we clear the active set and restart the iteration with the condition:

$$\mathscr{A}_{n+1} = \emptyset \tag{5.3}$$

Having estimated the active set from either (5.2) or (5.3) we next try to determine the plastic strains $\gamma_{n+1}^\alpha \;\; \forall \alpha \in \mathscr{A}_{n+1}$, given $\gamma_n^\alpha, \mathbf{F}_{n+1}$ and $\mathbf{F}_n^p$. Systems are then added to or removed from the active set successively one after the other. Calculation of $\gamma_{n+1}^\alpha = \gamma_n^\alpha + \Delta\gamma^\alpha$ immediately allows us to remove all slip systems that violate the constraint $\Delta\gamma^\alpha \geq 0$ and update the active set as:

$$\mathscr{A}_{n+1} \Leftarrow \{\mathscr{A} - (\alpha : \Delta\gamma^\alpha \leq 0 \in \mathscr{P})\} \tag{5.4}$$

If slip systems had to be removed, then the local iterative procedure is restarted with the new updated active set. If however the constraint $\Delta\gamma^\alpha \geq 0$ was not violated and no systems were removed, we have to check for violation of the yield conditions for systems that are currently assumed inactive. The active systems set is then updated by adding the ones that violate the yield condition the most in the sense:

$$\mathscr{A}_{n+1} \Leftarrow \{\mathscr{A} + (\alpha : \arg[\max \phi^\alpha] : \phi^\alpha \geq 0 \in \mathscr{P})\} \tag{5.5}$$

At this point it is important to note that only the most loaded system is added to the active set, which translates to the system that violates the yield condition the most. If multiple systems violate their respective yield conditions in an equivalent manner then all such systems are added to the active set list. If new systems were added to the set we need to restart the iterative procedure with the updated set. If no systems were added nor removed from the set then we assume that the current active set $\mathscr{A}_{n+1}$ has converged and we can successfully continue to update the solution dependent variables, proceed with the integration of equations and the calculation of the linearization moduli.

The convergence criteria of the stress–update algorithm (5.4–5.5) are fundamentally based in the assumption that the plastic slips $\Delta\gamma^\alpha$ are known $\forall \alpha \in \mathscr{A}$. Up until to this point we treated $\Delta\gamma^\alpha$'s as known quantities, but in reality their calculation is necessary every increment, so that the yield and consistency conditions[2] are satisfied for every slip

---

[2]In the case of crystal plasticity, the yield and consistency conditions are both expressed in terms of the resolved shear stresses within each system, τ^α

system. Now recalling the Mandel stress measure defined in the intermediate configuration and expressed by (3.45), the resolved shear stress τ^α within slip system α can be calculated as:

$$\tau_{n+1}^\alpha(\Delta\gamma^\beta) = \mathbf{m}_0^\alpha \cdot \boldsymbol{\Sigma}_{n+1}(\Delta\gamma^\beta) \cdot \mathbf{s}_0^\alpha \tag{5.6}$$

where $\mathbf{s}_0^\alpha$ and $\mathbf{m}_0^\alpha$ are the unit vectors defining the slip direction and normal to slip plane of system α respectively. The hardening of each system is then expressed as:

$$\tau_{cr}^\alpha(\Delta\gamma^\beta)|_{n+1} = \tau_{cr}^\alpha|_n + \sum_{\beta=1}^N \left[(1-\delta)h^{\alpha\beta}|_n + \delta h^{\alpha\beta}|_{n+1}\right]\Delta\gamma^\beta \qquad \delta \in [0,1] \tag{5.7}$$

which essentially represents an integrated form of (3.21). The instantaneous hardening moduli (*hm*) $h^{\alpha\beta}$ is in this case defined as an adjusted combination of the moduli referring to the last converged increment ($h^{\alpha\beta}|_n$) and of the one calculated using information from the current increment ($h^{\alpha\beta}|_{n+1}$). The yield conditions of all slip systems are then introduced in terms of (5.6) and (5.7) as

$$\phi^\alpha(\Delta\gamma^\beta) = \tau_{n+1}^\alpha(\Delta\gamma^\beta) - \tau_{cr}^\alpha(\Delta\gamma^\beta)|_{n+1} \le 0 \tag{5.8}$$

The condition $\phi^\alpha < 0$ indicates that system α behaves elastically in the current increment, whereas the case of $\phi^\alpha = 0$ suggests that the system currently undergoes plasticity. Elasticity on α[3] corresponds to $\Delta\gamma^\alpha = 0$, while $\Delta\gamma^\alpha > 0$ when accounting for plasticity. Therefore, the unknowns $\Delta\gamma^\beta$ are determined as the solution of the following system:

$$\phi^\alpha(\Delta\gamma^\beta) = 0 \tag{5.9}$$

Only numerical solutions are applicable to (5.9) since both τ^α and τ_{cr}^α are highly non–linear functions of the unknowns $\Delta\gamma^\beta$. Implementing the Newton Raphson method, we iteratively solve for the unknowns $\Delta\gamma^\alpha$ until convergence is achieved. Newton iterations for multivariate systems however, require the Jacobian matrix of the system, which in this case is defined as $\left(\partial\phi^\alpha/\partial\Delta\gamma^\beta\right)$. Next, we calculate the derivatives[4] necessary to build the Jacobian matrix, starting from the derivative of the deformation gradient. Recalling (3.40), the variation of $\mathbf{F}^e$ with respect to $\Delta\gamma^\alpha$ is:

$$\frac{\partial\mathbf{F}_{n+1}^e}{\partial\Delta\gamma^\alpha} = -\mathbf{F}_{\text{trial}}^e \cdot \mathbf{s}_0^\alpha \mathbf{m}_0^\alpha + O(\Delta\gamma^\alpha)^2 \tag{5.10a}$$

The corresponding variation of the right Cauchy–Green elastic tensor defined as $\mathbf{C}^e = \mathbf{F}^{eT} \cdot \mathbf{F}^e$ is then calculated using (5.10a) as:

$$\frac{\partial\mathbf{C}_{n+1}^e}{\partial\Delta\gamma^\alpha} = \frac{\left(\partial\mathbf{F}_{n+1}^e\right)^T}{\partial\Delta\gamma^\alpha} \cdot \mathbf{F}_{n+1}^e + \left(\mathbf{F}_{n+1}^e\right)^T \cdot \frac{\partial\mathbf{F}_{n+1}^e}{\partial\Delta\gamma^\alpha} \tag{5.10b}$$

Expression (5.10b) enables the calculation of the Green strain[5] variation:

$$\frac{\partial\mathbf{E}_{n+1}^e}{\partial\Delta\gamma^\alpha} = \frac{1}{2}\frac{\partial\mathbf{C}_{n+1}^e}{\partial\Delta\gamma^\alpha} \tag{5.10c}$$

---

[3] Elastic response of a system equivalently declares the same system as inactive
[4] In the current discussion all derivatives are with respect to $\Delta\gamma^\alpha$
[5] The Green strain is defined in Table 1.1

and also the calculation of the 2nd Piola–Kirchhoff's variation:

$$\frac{\partial \mathbf{S}_{n+1}^e}{\partial \Delta \gamma^\alpha} = \boldsymbol{\mathcal{L}}^e : \frac{\partial \mathbf{E}_{n+1}^e}{\partial \Delta \gamma^\alpha} \tag{5.10d}$$

Now by calculating the derivative $\partial \boldsymbol{\Sigma} / \partial \Delta \gamma^\alpha$ as:

$$\frac{\partial \boldsymbol{\Sigma}_{n+1}}{\partial \Delta \gamma^\alpha} = \frac{\partial \mathbf{S}_{n+1}^e}{\partial \Delta \gamma^\alpha} \cdot \mathbf{C}_{n+1}^e + \frac{\partial \mathbf{C}_{n+1}^e}{\partial \Delta \gamma^\alpha} \cdot \mathbf{S}_{n+1}^e \tag{5.10e}$$

we can successfully define the first component needed for the Jacobian matrix, namely the variation of the resolved shear stress on system α with respect to all slips $\Delta \gamma^\beta$ as

$$\frac{\partial \tau_{n+1}^\alpha}{\partial \Delta \gamma^\beta} = \mathbf{s}_0^\alpha \cdot \frac{\partial \boldsymbol{\Sigma}_{n+1}}{\partial \Delta \gamma^\alpha} \cdot \mathbf{m}_0^\alpha \tag{5.10f}$$

Finally, the critical shear stress variation can be directly calculated by derivatizing (5.7):

$$\frac{\partial \tau_{cr}^\alpha|_{n+1}}{\partial \Delta \gamma^\beta} = \left[(1 - \delta) h^{\alpha\beta}|_n + \delta h^{\alpha\beta}|_{n+1} \right] + \delta \sum_{\gamma=1}^{N} \frac{h^{\alpha\gamma}|_{n+1}}{\partial \Delta \gamma^\beta} \Delta \gamma^\gamma \tag{5.10g}$$

The expression for the Jacobian matrix of the system in (5.9) is found by combining (5.10f) and (5.10g):

$$\frac{\partial \phi_{cr}^\alpha|_{n+1}}{\partial \Delta \gamma^\beta} = \frac{\partial \tau_{n+1}^\alpha}{\partial \Delta \gamma^\beta} - \frac{\partial \tau_{cr}^\alpha|_{n+1}}{\partial \Delta \gamma^\beta} \tag{5.11}$$

The Jacobian matrix has dimensions $N \times N$, where N stands for the Number of total slip systems in the crystal. Returning to the implementation of NR method to solve for the unknowns $\Delta \gamma$, we begin by providing an initial estimate for the plastic slips $\Delta \gamma_0^\alpha$ for all systems currently in the active set. Recalling equations (3.61),(3.75) and (3.76) a reasonable first estimate for $\Delta \gamma^\alpha$'s can be found as follows:

$$\dot{\gamma}^\alpha = \boldsymbol{\Lambda}^\alpha : \mathbf{D} \Rightarrow \boxed{\Delta \gamma_0^\alpha = \boldsymbol{\Lambda}^\alpha : \Delta \mathbf{E}} \tag{5.12}$$

where

$$\boldsymbol{\Lambda}^\alpha = \sum_{\beta=1}^{Nas} \Psi^{\alpha\beta} \boldsymbol{\Phi}^\beta$$

$$\Psi^{\alpha\beta} = \left(\boldsymbol{\Phi}^\alpha : \mathbf{M}^\beta + h^{\alpha\beta} \right)^{-1}$$

$$\boldsymbol{\Phi}^\alpha = \boldsymbol{\mathcal{L}}^{e\tau} : \mathbf{M}^\alpha + \mathbf{B}^\alpha$$

$$\mathbf{B}^\alpha = \boldsymbol{\tau} \cdot (\mathbf{m}^\alpha \mathbf{s}^\alpha) - (\mathbf{m}^\alpha \mathbf{s}^\alpha) \cdot \boldsymbol{\tau}$$

$$\mathbf{M}^\alpha = \mathrm{symm} \left(\mathbf{s}^\alpha \mathbf{m}^\alpha \right)$$

With the Jacobian matrix now known and the first estimate given by (5.12), we can successfully initiate the Newton iterations for $\Delta \gamma^\alpha$. A schematic flowchart of the Newton iterations is illustrated in Figure 5.1 below. After solving for the unknowns, we need to check for convergence and continue with the stress–update algorithm.

The heuristic algorithm, is outlined in Table 5.1 and also schematically illustrated in Figure 5.2 as part of the elastic prediction–plastic correction scheme.
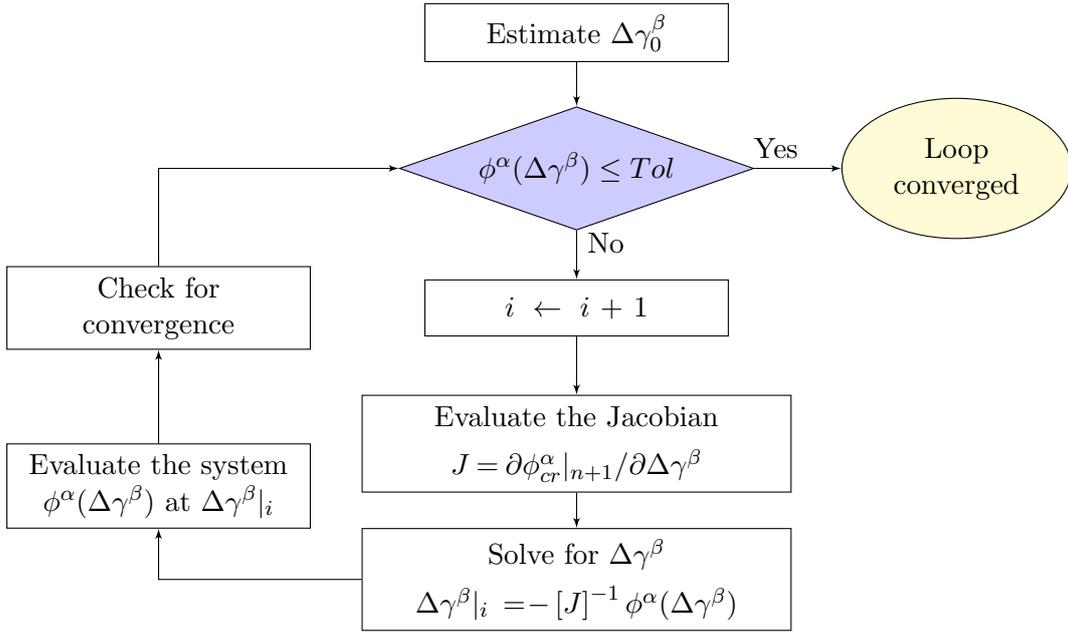
Figure 5.1: A flowchart of the Newton iterations for $\Delta\gamma^\alpha$

Table 5.1: A summary of the heuristic stress–update algorithm for rate–independent crystal plasticity

1. Initiate slip system iteration loop. Set $i_{set} = 0$

2. Estimate active set as $\mathscr{A}_{n+1} = \mathscr{A}_n$

3. Set $i_{set} \Leftarrow i_{set} + 1$. If $i_{set} = 2$ and $\mathscr{A} \neq \emptyset$ then set $\mathscr{A}_{n+1} = \emptyset$

4. Having estimated the active set, initiate Newton iterations to find $\Delta\gamma^\alpha$, $\forall \alpha \in \mathscr{P}$

5. Drop from $\mathscr{A}_{n+1}$ all systems for which $\Delta\gamma^\alpha \leq 0$

6. If systems were removed, update $\mathscr{A}_{n+1}$ and GOTO **3.**

7. Check for violation of the yield function $\forall$ system α assumed inactive. If $\phi^\alpha > 0$ for any $\alpha \notin \mathscr{A}$, then add to active set $\mathscr{A}_{n+1}$ the most loaded inactive systems with $\phi^\alpha > 0$

8. If systems were added to the set update $\mathscr{A}_{n+1}$ and GOTO **3.**

9. If no systems were added or removed from the active set then convergence is achieved
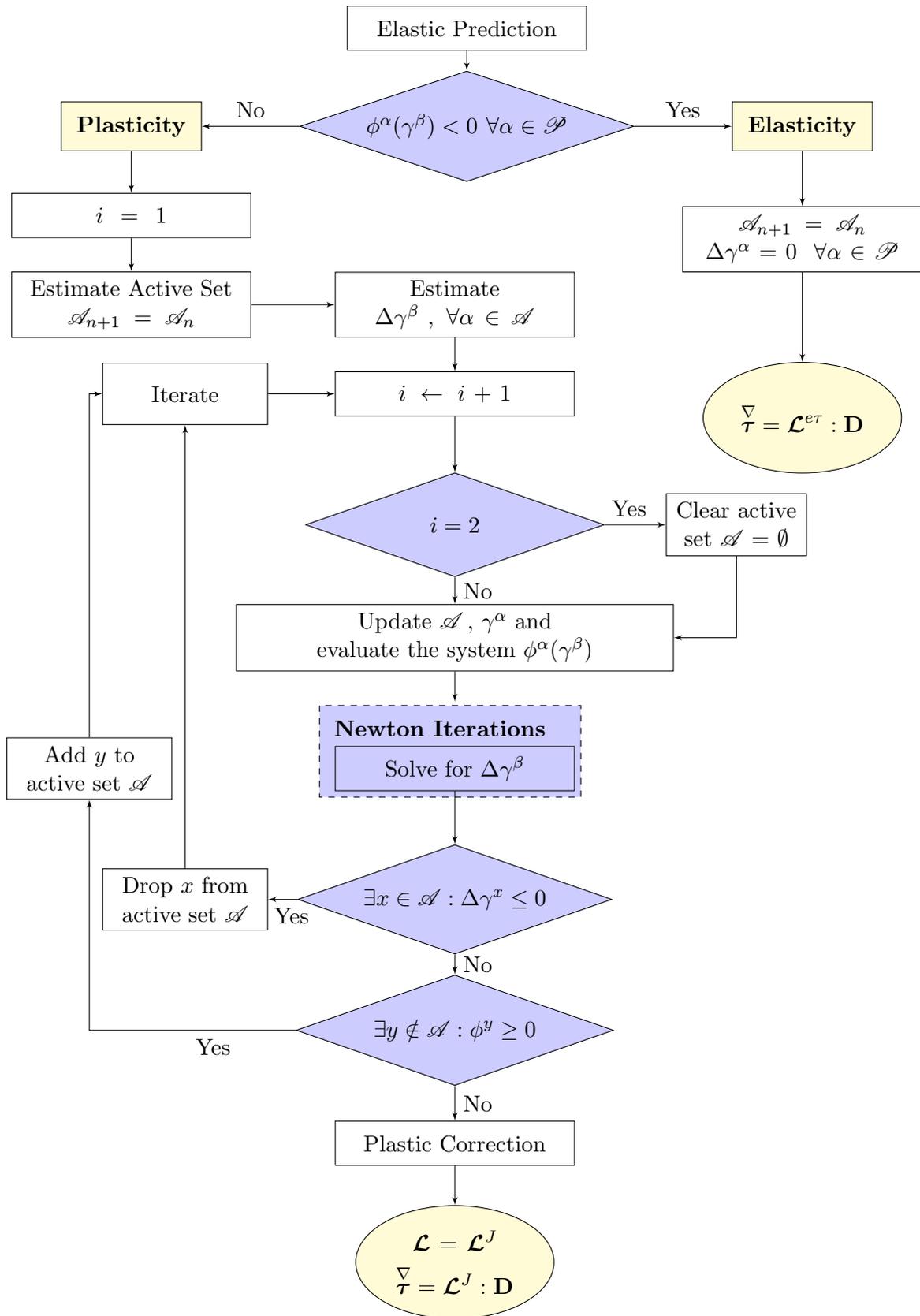
Figure 5.2: A flowchart of the Elastic Prediction - Plastic Correction implementing the heuristic stress update algorithm algorithm for crystal plasticity

5.1.i Special Treatment for Hydrogen Charged Crystals

The current subsection serves as a supplement to the heuristic stress update algorithm just presented, to take into account the effects of hydrogen concentration. Let us restate the modified hardening model (4.16,4.17) we proposed in Chapter 4:

$$\dot{\tau}_{cr}^{\alpha} = \sum_{\beta=1}^{Nas} h_H^{\alpha\beta}\, \dot{\gamma}^{\beta}$$

$$h_H^{\alpha\beta} = (1 + H_c\, c_T^{\alpha})h^{\alpha\beta}$$

Recall the incremental setting, in which we have to update all variables at t_{n+1} given their values at t_n. Based on the integrated form of the hydrogen–free hardening model (5.7), we introduce the corresponding integrated[6] form of (4.16,4.17) accounting for the presence of hydrogen as:

$$\tau_{cr}^{\alpha}|_{n+1} = \tau_{cr}^{\alpha}|_n + \sum_{\beta=1}^{N} \left[(1-\delta)(1 + H_c\, c_T^{\alpha}|_n)h^{\alpha\beta}|_n + \delta(1 + H_c\, c_T^{\alpha}|_{n+1})h^{\alpha\beta}|_{n+1}\right] \Delta\gamma^{\beta} \qquad (5.13)$$

The concentration of hydrogen atoms residing in the trap sites of each slip system must always be in equilibrium with the lattice hydrogen concentration. Therefore combining equations (4.6,4.8a,4.8b,4.10a,4.10b) we can restate equilibrium at t_{n+1} in the form:

$$c_T^{\alpha}|_{n+1} = \frac{K_T\, \zeta\, c_L|_{n+1}}{\eta\, N_L + (K_T - 1)\, N_L\, c_L|_{n+1}} \left(N_T^{\alpha}|_{n+1}\right) \qquad (5.14)$$

Also, the trap density at t_{n+1} is expressed in terms of the burgers vector b, the proportionality constant $\tilde{\alpha}$, the polycrystal shear modulus μ and the critical stress at that time as:

$$N_T^{\alpha}|_{n+1} = \left(\frac{\tau_{cr}^{\alpha}|_{n+1}}{\tilde{\alpha}\mu}\right)^2 \frac{1}{b^3} \qquad (5.15)$$

Equations (5.13–5.15) define a non–linear system that needs to be solved every increment with respect to $\tau_{cr}^{\alpha}|_{n+1}$, $c_T^{\alpha}|_{n+1}$ and $N_T^{\alpha}|_{n+1}$ and for every slip system $\alpha \in \mathscr{P}$. Alternatively, we can reduce the number of equations forming the system by substituting equation (5.15) to (5.14), so that:

$$c_T^{\alpha}|_{n+1} = \frac{K_T\, \zeta\, c_L|_{n+1}}{\tilde{\alpha}^2\, \mu^2\, b^3\, [\eta\, N_L + (K_T - 1)\, N_L\, c_L|_{n+1}]} \left(\tau_{cr}^{\alpha}|_{n+1}\right)^2 \qquad (5.16)$$

Now the non–linear system is defined using only equations (5.13) and (5.16) which we need to solve for the critical shear stress $\tau_{cr}^{\alpha}|_{n+1}$ and the trapped hydrogen concentration $c_T^{\alpha}|_{n+1}$ on slip system α at t_{n+1}.

Recall the heuristic stress update algorithm for hydrogen–free single crystals, where we introduced two iterative schemes, namely the slip system iterations and the Newton iterations

---

[6]Integration is carried out in the time interval $[t_n, t_{n+1}]$

for $\Delta\gamma$. The slip system iterations are initiated by making an estimate for the active systems set $\mathscr{A}_{n+1}$ at t_{n+1}, whereas the Newton loop for $\Delta\gamma$ solves the system of equations (5.9) for the plastic slips $\Delta\gamma^\alpha$, $\forall\ \alpha \in \mathscr{P}$ given the active set estimate. Then, at the end of every iteration, given the active systems set $\mathscr{A}_{n+1}$ and the plastic slips $\Delta\gamma^\alpha$, it is necessary to evaluate the system $\phi^\alpha(\Delta\gamma^\beta)$ and check for convergence. The latter, involves the calculation of the critical shear stress on each slip system τ_{cr}^α at t_{n+1}, which in the hydrogen–free formulation is readily possible with a straightforward evaluation of (5.7).

In the current formulation however, immediate calculation of τ_{cr}^α's given $\Delta\gamma^\alpha$'s is not possible, since the lattice and trapped hydrogen concentrations involved in (5.13) and (5.16) are unknowns at t_{n+1}. For this reason, we introduce two additional nested procedures[7], one to impose the conservation of total hydrogen concentration and a second to solve the system of equations (5.13 & 5.16) for $\tau_{cr}^\alpha|_{n+1}$ and $c_T^\alpha|_{n+1}$.

At all times and within every material point of the continuum, the lattice c_L and trapped c_T^α hydrogen concentrations should be in equilibrium but also such to satisfy the conservation of hydrogen in the solid solution. In an incremental setting, the conservation of hydrogen can be expressed in terms of the concentration values $c_L|_{n+1}$ and $c_T^\alpha|_{n+1}$ at t_{n+1} along with the initial concentration c_0 as:

$$H(c_L|_{n+1}, c_T^\alpha|_{n+1}|\alpha \in \mathscr{P}) \leq \text{htol} \qquad (5.17)$$

where htol is an appropriately selected tolerance and the H function is defined as:

$$H(c_L|_{n+1}, c_T^\alpha|_{n+1}|\alpha \in \mathscr{P}) = c_0 - c_L|_{n+1} - \sum_{\alpha=1}^{Nsp/2} c_T^\alpha|_{n+1} \qquad (5.18)$$

Note that the summation in the above expression is carried over half of the defined slip systems, since the notations (α) and $(\alpha + \frac{NSP}{2})$[8] for $\alpha \in [1, \frac{NSP}{2}]$ represent the same slip system.

The conservation of hydrogen is formulated in the form of an iterative scheme within the Newton iterations for $\Delta\gamma^\alpha$. We begin by assuming[9] that the lattice hydrogen concentration in the material point under consideration $c_L|_{n+1}$ at t_{n+1} coincides with the last converged value $c_L|_n$ at t_n. We continue with solving[10] the system of equations (5.13,5.16) for $\tau_{cr}^\alpha|_{n+1}$ and $c_T^\alpha|_{n+1}$ for all systems $\alpha \in \mathscr{P}$ using the estimated value for $c_L|_{n+1}$. If the calculated values for $c_T^\alpha|_{n+1}$ do not satisfy the hydrogen conservation in (5.17), we then calculate a new value for $c_L|_{n+1}$ as:

$$c_L|_{n+1} = c_0 - \sum_\alpha c_T^\alpha|_{n+1} \qquad (5.19)$$

---

[7]The Newton iterations for $\Delta\gamma^\alpha$ are already nested inside the heuristic algorithm. The hydrogen equilibrium iteration, is introduced inside the Newton iterations, since it is now a prerequisite to obtain the critical stresses τ_{cr}^α on each slip system

[8]Positive and negative slip is accounted separately in the current constitutive model for FCC crystals, and therefore systems α and $\alpha + NSP/2$ essentially represent the same system

[9]As a reasonable first estimate

[10]The solution techniques used to solve this system are discussed in detail in Appendix C

and solve again for $\tau_{cr}^\alpha|_{n+1}$ and $c_T^\alpha|_{n+1}$ $\forall \alpha \in \mathscr{P}$ as many times as necessary to satisfy equation (5.17). Figure 5.3 schematically illustrates these modifications to the heuristic algorithm to further facilitate supervision.
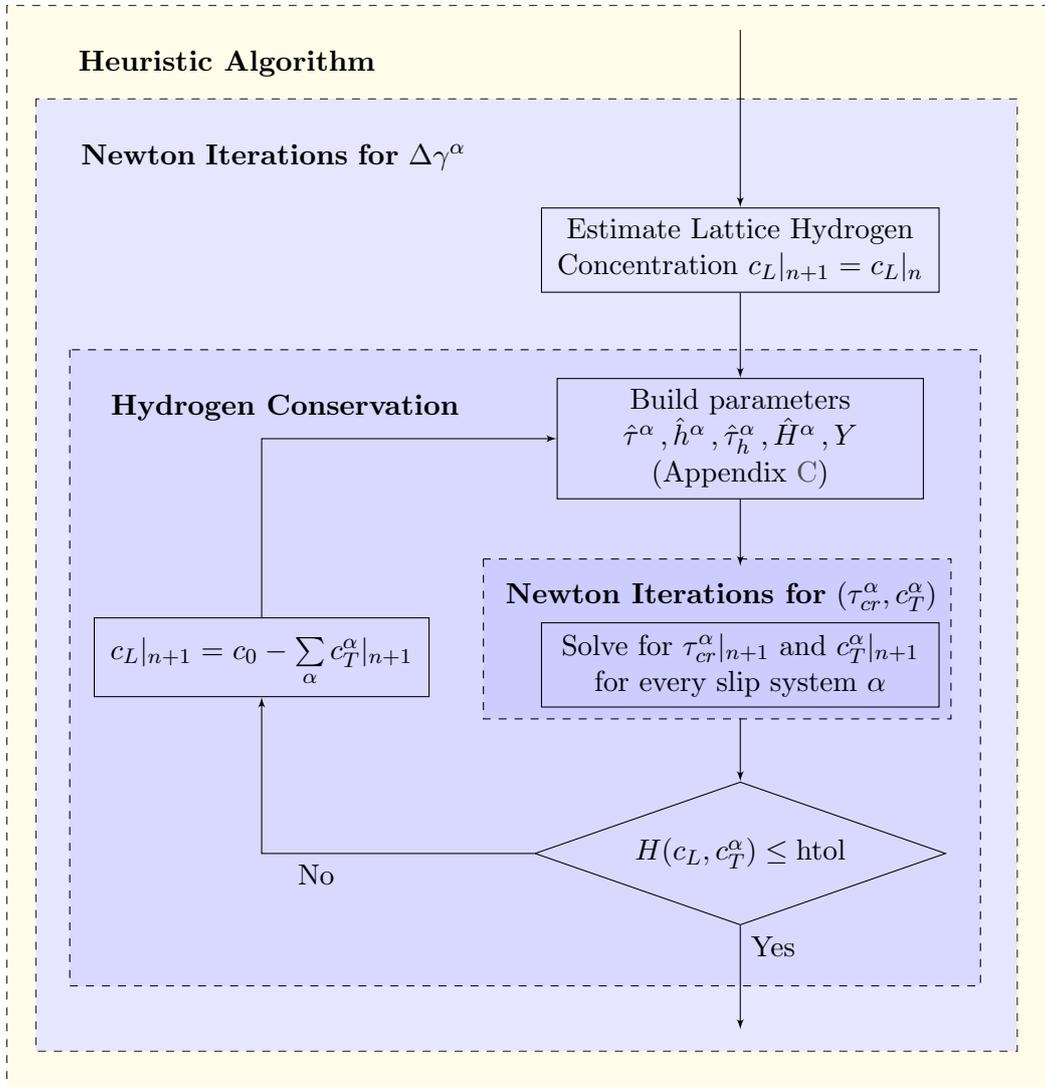

Figure 5.3: A flowchart of the heuristic stress update algorithm including the special treatment required to account for the presence of hydrogen

5.2 A Nonlinear Optimization Formulation

As aforementioned, the principal obstacle in rate-independent crystal plasticity, is to determine the set of active slip systems $\mathscr{A} \subseteq \mathscr{P}$ at any given time so as to integrate the constitutive equations and build the linearization moduli. A crystal system α is assumed to be active whenever its corresponding yield condition is satisfied in the sense $\phi^\alpha = 0$ resulting to a non–negative plastic slip $\Delta\gamma^\alpha \geq 0$. Inverting this definition, we can define a system β as inactive whenever the current stress state for this system is located inside the yield surface in the sense $\phi^\beta < 0$ and therefore $\Delta\gamma^\beta = 0$. In math form, we write:

$$\phi^\alpha \leq 0 \tag{5.20a}$$

$$-\Delta\gamma^\alpha \leq 0 \tag{5.20b}$$

Next, we demonstrate that the set of active systems $\mathscr{A}$ along with the corresponding plastic slips $\Delta\gamma^\alpha$ can be introduced as the optimal solution of a nonlinear optimization problem. First, recall that the yield function ϕ^α of each slip system α implicitly depends on the slip activity $\Delta\gamma^\beta$ of all active systems $\beta \in \mathscr{A}$. In a dimensionless form we write:

$$\hat{\phi}^\alpha(\Delta\gamma^\beta) = \frac{1}{\tau_0} \left[\tau^\alpha(\Delta\gamma^\beta) - \tau_{cr}^\alpha(\Delta\gamma^\beta) \right] = \frac{1}{\tau_0} \left[\mathbf{m}_0^\alpha \cdot \boldsymbol{\Sigma}(\Delta\gamma^\beta) \cdot \mathbf{s}_0^\alpha - \tau_{cr}^\alpha(\Delta\gamma^\beta) \right] \tag{5.21}$$

Now let us multiply equations (5.20a) and (5.20b) and also use (5.21) to derive:

$$-\phi^\alpha(\Delta\gamma^\beta)\,\Delta\gamma^\alpha \geq 0 \Rightarrow \frac{1}{\tau_0} \left[\mathbf{m}_0^\alpha \cdot \boldsymbol{\Sigma}(\Delta\gamma^\beta) \cdot \mathbf{s}_0^\alpha - \tau_{cr}^\alpha(\Delta\gamma^\beta) \right] \Delta\gamma^\alpha \geq 0 \quad \forall \alpha \in \mathscr{P} \tag{5.22}$$

We next define the following convex function:

$$F\left(\Delta\gamma^\beta\right) = \sum_{\alpha=1}^{N} \left[\hat{\phi}^\alpha(\Delta\gamma^\beta)\,\Delta\gamma^\alpha \right]^2 \tag{5.23}$$

Note that the summation in the above equation is carried over all the slip systems available and not only on those assumed active. Equation (5.22) clearly suggests that the minimum value for $F\left(\Delta\gamma^\beta\right)$ is zero. In addition, nonzero values for F would indicate that the criteria for ϕ^α and $\Delta\gamma^\alpha$ (5.20a–5.20b) are violated for at least one system $\alpha \in \mathscr{P}$. We can therefore introduce the following optimization problem:

$$\textbf{Minimize} \quad F\left(\Delta\gamma^\beta\right) = \sum_{\alpha=1}^{N} \left[\hat{\phi}^\alpha(\Delta\gamma^\beta)\,\Delta\gamma^\alpha \right]^2 \tag{5.24a}$$

$$\textbf{s.t.} \quad G^\alpha\left(\Delta\gamma^\beta\right) = \phi^\alpha(\Delta\gamma^\beta) \leq 0 \qquad (\alpha = 1, 2, \ldots, 24) \tag{5.24b}$$

$$H^\alpha(\Delta\gamma^\alpha) = -\Delta\gamma^\alpha \leq 0 \qquad (\alpha = 1, 2, \ldots, 24) \tag{5.24c}$$

the solution of which, is guaranteed to satisfy the necessary constraints for ϕ^α and $\Delta\gamma^\alpha$. Clearly, due to (5.21), the above formulation defines a nonlinear optimization problem,

whose decision variables are taken to be the plastic slips for all slip systems $\alpha \in \mathscr{P}$. Then, the values of $\Delta\gamma^\alpha$ that minimize (5.24a) can be used to determine the set of active systems in the following sense:

$$\Delta\gamma^\alpha \leq 0 \rightarrow \text{System } \alpha \text{ inactive. Elastic response}$$

$$\Delta\gamma^\alpha > 0 \rightarrow \text{System } \alpha \text{ is active. Plasticity}$$

Subsequently we calculate the derivatives with respect to $\Delta\gamma^\beta$ for the objective function and the constraints as they are necessary to determine the optimal solution:

$$\frac{\partial F}{\partial \Delta\gamma^\beta} = 2 \sum_{\alpha=1}^{N} \left(2\hat{\phi}^\alpha(\Delta\gamma^\beta) \, \Delta\gamma^\alpha \right) \left(\frac{\partial \hat{\phi}^\alpha}{\partial(\Delta\gamma^\beta)} \, \Delta\gamma^\alpha + \delta_{\alpha\beta} \right)$$

$$\frac{\partial G^\alpha}{\partial \Delta\gamma^\beta} = \frac{\partial \hat{\phi}^\alpha}{\partial(\Delta\gamma^\beta)} \qquad (\beta = 1, 2, \ldots, 24)$$

$$\frac{\partial H^\alpha}{\partial \Delta\gamma^\beta} = -\delta_{\alpha\beta} \qquad (\beta = 1, 2, \ldots, 24)$$

where δ above stands for the Kronecker delta.

The particular optimization formulation presents a direct alternative to the heuristic algorithm we discussed in a previous section. As a general rule however, nonlinear optimization problems are very 'expensive' in terms of the computation time necessary to find the global optimum. In fact, in some extreme cases that involve highly non–linear constraints and many decision variables, determining a globally optimum solution may even be impossible. Motivated by the need to reduce nonlinear constraints, we also consider the following 'alternative' formulation:

$$\textbf{Minimize} \quad F\left(\Delta\gamma^\beta\right) = \sum_{\alpha=1}^{N} \left\{ \left[\phi^\alpha - \tau^\alpha(\Delta\gamma^\beta) + \tau_{cr}^\alpha(\Delta\gamma^\beta) \right]^2 + (\phi^\alpha \, \Delta\gamma^\alpha)^2 \right\} \qquad (5.25\text{a})$$

$$\textbf{s.t.} \quad G^\alpha = \phi^\alpha \leq 0 \qquad (\alpha = 1, 2, \ldots, 24) \qquad (5.25\text{b})$$

$$H^\alpha = -\Delta\gamma^\alpha \leq 0 \qquad (\alpha = 1, 2, \ldots, 24) \qquad (5.25\text{c})$$

In this case, the decision variables are take to be the yield functions ϕ^α and plastic slips $\Delta\gamma^\alpha$ of all slip systems available. Even though the particular formulation doubles the number of the decision variables for which we have to solve, it only involves **linear constraints**[11].

5.3 A Linear Optimization Approach

In an effort to minimize the computational cost necessary to determine the set of active systems and plastic slips as the solution of an optimization problem we next consider a linearized approach to the optimization formulation. Let us restate the problem of determining

---

[11]Previously, half of those constraints were nonlinear

the active systems $\alpha \in \mathscr{A} \subseteq \mathscr{P}$ and their corresponding plastic slips $\Delta\gamma^\alpha$:

$$\phi^\alpha(\Delta\gamma^\beta)\Delta\gamma^\alpha = 0 \tag{5.26}$$

$$\Delta\gamma^\alpha \geq 0 \tag{5.27}$$

$$\phi^\alpha(\Delta\gamma^\beta) \leq 0 \tag{5.28}$$

We next introduce a linear Taylor series approximation for all the yield functions $\phi^\alpha(\Delta\gamma^\beta)$ around for $\Delta\gamma^\beta = 0$ as:

$$\phi^\alpha(\Delta\gamma^\beta) \cong \phi^\alpha|_{\Delta\gamma^\beta=0} + \sum_{\beta=1}^{Nas} \frac{\partial\phi^\alpha}{\partial\Delta\gamma^\beta}\Delta\gamma^\beta = 0 \qquad \alpha = 1, 2, \ldots, N \tag{5.29}$$

In an incremental setting, the quantities evaluated at $\Delta\gamma^\beta = 0$ essentially correspond to the previous increment at t_n and their values are known. Furthermore, the quantity $\partial\phi^\alpha/\partial\Delta\gamma^\beta$ is from definition the Jacobian that we calculate in the Newton's loop for $\Delta\gamma^\alpha$ in the heuristic algorithm. Thus, we can rewrite expression (5.29) in the form:

$$\phi^\alpha|_{n+1} = \phi^\alpha|_n + \sum_{\beta=1}^{Nas} J_{\alpha\beta}\Delta\gamma^\beta = 0 \qquad \alpha = 1, 2, \ldots, N \tag{5.30}$$

Using (5.30) we can alternatively determine the plastic slips of all available systems as the solution of the following linear optimization problem:

$$\textbf{Minimize} \quad \phi^\alpha|_n + \sum_{\beta=1}^{Nas} J_{\alpha\beta}\Delta\gamma^\beta = 0$$

$$\textbf{s.t.} \quad \Delta\gamma^\alpha \geq 0$$

$$\phi^\alpha \leq 0$$

Then again, the optimal values for $\Delta\gamma^\alpha$'s are used to populate the set of active systems $\mathscr{A}_{n+1}$ at t_{n+1} as:

$$\Delta\gamma^\alpha \leq 0 \rightarrow \text{System } \alpha \text{ inactive. Elastic response}$$

$$\Delta\gamma^\alpha > 0 \rightarrow \text{System } \alpha \text{ is active. Plasticity}$$

Computationally, finding the optimal solution for the linear optimization problem stated above, is considerably easier than solving the corresponding nonlinear optimization problem. Furthermore, the linear formulation guarantees that a unique optimal solution will always exist. However, implementing the above linear optimization problem instead of the heuristic algorithm or the nonlinear optimization formulation, should be accompanied with a significantly smaller time step Δt for convergence[12] within a reasonable amount of iterations. In addition, special treatment is required in general before solving the aforementioned minimization problem, since the Jacobian matrix is not always symmetric.

---

[12]Convergence here refers to the non–linear finite element equations that approximate the actual problem. The finite element implementation and the system of equations that needs to be solved incrementally are both addressed in detail in Chapter 6

Chapter 6

Computational Issues II - FEM Implementation

Let us consider the spatial configuration of a general continuum body, which in it's reference state at $t = 0$ occupies volume V_0 with a mass density ρ_0. The body is then loaded by body forces $\mathbf{b}$ per unit mass and traction forces $\hat{\mathbf{t}}$ acting on a part of its surrounding surface S_t, while a portion of it's surface S_u[1] is subjected to known displacements $\hat{\mathbf{u}}$. As a result, after a time period Δt the body is deformed and occupies volume V with a mass density ρ, surrounded by surface S. The equilibrium equations[2] are expressed in terms of the Cauchy stress tensor as:

$$\frac{\partial \sigma_{ij}}{\partial x_j} + \rho b_i = 0 \tag{6.1}$$

The kinematic relationships are also introduced as:

$$D_{ij} = \frac{1}{2}\left(\frac{\partial v_i}{\partial x_j} + \frac{\partial v_j}{\partial x_i}\right) \tag{6.2}$$

defining the deformation rate tensor $\mathbf{D}$ that corresponds to the velocity field $\boldsymbol{v}$. The deformable material is governed by a general constitutive law of the form:

$$\overset{\triangledown}{\boldsymbol{\sigma}} = \overset{\triangledown}{\boldsymbol{\sigma}}(\mathbf{L}) \tag{6.3}$$

where $\overset{\triangledown}{\boldsymbol{\sigma}}$ represents the Jaumann rate of $\boldsymbol{\sigma}$ commonly used to describe the constitutive behavior of solids and $\mathbf{L}$ is the velocity gradient tensor defined in Section 1.5. We also introduce the conditions defining the applied forces and displacements in the boundary ∂S:

$$\mathbf{u} = \hat{\mathbf{u}} = \text{known} \quad \text{on } S_u \tag{6.4}$$

---

[1]Note that $S_u \cap S_t = \emptyset$ and $S_u \cup S_t = S$

[2]Assuming that dynamic phenomena are not involved and therefore the acceleration field $\mathbf{a}$ vanishes

$$\hat{\mathbf{t}} = \boldsymbol{\sigma} \cdot \mathbf{n} = \text{known} \quad \text{on } S_t \tag{6.5}$$

Equations (6.1–6.5) constitute the **Strong Formulation** of the Boundary Value problem. An alternative formulation can also be introduced as follows. We begin by replacing the three equilibrium equations in (6.1) by a unique scalar equation[3] over the entire body. This equation is obtained by multiplying the differential equations in (6.1) by a virtual (arbitrary but continuous and differentiable) velocity field $\delta\boldsymbol{v}^*$ and then integrating over the entire volume of the continuum body (Papatriantafyllou [42]). Hence:

$$\int_{V(t)} \left[\boldsymbol{\nabla} \cdot \boldsymbol{\sigma} + \rho\mathbf{b} \right] \cdot \delta\boldsymbol{v}^* \, dV = 0 \tag{6.6}$$

The chain rule permits us to write:

$$\boldsymbol{\nabla} \cdot (\boldsymbol{\sigma} \cdot \delta\boldsymbol{v}^*) = (\boldsymbol{\nabla} \cdot \boldsymbol{\sigma}) \cdot \delta\boldsymbol{v}^* + \boldsymbol{\sigma} : (\boldsymbol{\nabla} \, \delta\boldsymbol{v}^*)$$

and making use of Gauss's theorem[4] we can also write:

$$\int_{V(t)} \left[\boldsymbol{\nabla} \cdot \boldsymbol{\sigma} \right] \cdot \delta\boldsymbol{v}^* \, dV = \int_{V} \left[\boldsymbol{\nabla} \cdot (\boldsymbol{\sigma} \cdot \delta\boldsymbol{v}^*) - \boldsymbol{\sigma} : (\boldsymbol{\nabla} \, \delta\boldsymbol{v}^*) \right] dV$$

$$= \int_{S(t)} \mathbf{n} \cdot \boldsymbol{\sigma} \cdot \delta\boldsymbol{v}^* \, dS - \int_{V(t)} \boldsymbol{\sigma} : (\boldsymbol{\nabla} \, \delta\boldsymbol{v}^*) \, dV$$

$$= \int_{S(t)} \hat{\mathbf{t}} \cdot \delta\boldsymbol{v}^* \, dS - \int_{V} \boldsymbol{\sigma} : \delta\mathbf{L}^* \, dV \tag{6.7}$$

where $\delta\mathbf{L}^*$ is the velocity gradient tensor corresponding to the virtual velocity field $\delta\boldsymbol{v}^*$. Let us also decompose $\delta\mathbf{L}^*$ into its symmetric $\delta\mathbf{D}^*$ and antisymmetric part $\delta\mathbf{W}^*$ and take advantage of the symmetry of $\boldsymbol{\sigma}$ to write[5]:

$$\boldsymbol{\sigma} : \delta\mathbf{L}^* = \boldsymbol{\sigma} : (\delta\mathbf{D}^* + \delta\mathbf{W}^*) = \boldsymbol{\sigma} : \delta\mathbf{D}^* + \boldsymbol{\sigma} : \delta\mathbf{W}^* = \boldsymbol{\sigma} : \delta\mathbf{D}^* \tag{6.8}$$

Now combining equations (6.6),(6.7) and (6.8) we can express the alternative formulation of the BVP as:

$$\boxed{G(\Delta\mathbf{u}) = \int_{V(t)} \boldsymbol{\sigma} : \delta\mathbf{D}^* \, dV - \int_{S(t)} \hat{\mathbf{t}} \cdot \delta\boldsymbol{v}^* \, dS - \int_{V(t)} \rho\mathbf{b} \cdot \delta\boldsymbol{v}^* \, dV = 0} \tag{6.9}$$

The above formulation is also called the **Weak Formulation** of the BVP and provides the basis for the **Finite Element approximation** introduced in the following section.

---

[3]Note that this replacement does not violate the generality
[4]Also known as the divergence theorem
[5]Recall that the double dot product of a symmetric and an antisymmetric tensor equals to zero

6.1 Finite Element Approximation

In a finite element setting, the solution is developed incrementally with the displacement variation denoted as $\Delta\mathbf{u}(\mathbf{x})$ being the primary unknown of the problem. Once $\Delta\mathbf{u}$ is determined, the displacement field at the end of the current increment at $t = t_{n+1}$ is calculated as [42]:

$$\mathbf{u}_{n+1}(\mathbf{x}) = \mathbf{u}_n(\mathbf{x}) + \Delta\mathbf{u}(\mathbf{x}) \tag{6.10}$$

and consequently the current position of any material point within the continuum body can be directly updated as:

$$\mathbf{x}_{n+1} = \mathbf{X} + \mathbf{u}_{n+1}(\mathbf{x}) \tag{6.11}$$

Discretizing the continuum body into finite elements, we express the unknown displacement increment $\Delta\mathbf{u}$ as a function interpolation[6] within each element as:

$$\underset{3\times 1}{\{\Delta u(\mathbf{x})\}} = \underset{3\times n}{[N(\mathbf{x})]} \underset{n\times 1}{\{\Delta u^N\}} \tag{6.12}$$

where $[N(\mathbf{x})]$ is the interpolation matrix that consists of user–defined "shape" functions, whereas $\{\Delta u^N\}$ is the vector of nodal unknowns. Now recall that the virtual velocity field, $\delta\boldsymbol{v}^*$, must be compatible with all kinematic constraints. The interpolation introduced in (6.12) however, constrains the displacement to have a certain spatial variation and therefore $\delta\boldsymbol{v}^*$ must also be defined using the same function interpolation [2]. Hence,

$$\underset{3\times 1}{\{\delta v^*\}} = \underset{3\times n}{[N(\mathbf{x})]} \underset{n\times 1}{\{\Delta v^{*N}\}} \tag{6.13}$$

The virtual strain rate tensor $\delta\mathbf{D}^*$ is also expressed in array form as:

$$\underset{6\times 1}{\{\delta D^*\}} = \underset{6\times n}{[B(\mathbf{x})]} \underset{n\times 1}{\{\Delta v^{*N}\}} \tag{6.14}$$

where $[B(\mathbf{x})]$ is the matrix containing the spatial derivatives of the shape functions $N^\alpha(\mathbf{x})$ in the sense $B_{\alpha\beta} = 1/2(N_{\alpha,\beta} + N_{\beta,\alpha})$. Finally we introduce the array notations of the rest quantities in the Weak form (6.9) as:

$$\boldsymbol{\sigma} \longrightarrow \underset{6\times 1}{\{\sigma\}} \qquad \hat{\mathbf{t}} \longrightarrow \underset{3\times 1}{\{t\}} \qquad \mathbf{b} \longrightarrow \underset{3\times 1}{\{b\}}$$

Substituting each term in (6.9) we derive:

$$\lfloor \Delta v_e^{*N} \rfloor \underset{e}{\mathbf{A}} \left[\int_{V_{n+1}^e} \left([B]_{n+1}^T \{\sigma\}_{n+1} - [N]_{n+1}^T \{b\}_{n+1} \right) dV^e - \int_{S_{n+1}^e} [N]_{n+1}^T \{t\}_{n+1} \, dS^e \right] = 0$$

where $\mathbf{A}_e$ represents the Assembly operation. Note however, that since the above expression must hold $\forall \lfloor \Delta v_e^{*N} \rfloor$, we can derive:

---

[6]The specific interpolation was first introduced by Galerkin

$$\mathop{\mathbf{A}}_{e} \left[\int_{V_{n+1}^e} [B]_{n+1}^T \{\sigma\}_{n+1} \, dV^e - \int_{S_{n+1}^e} [N]_{n+1}^T \{t\}_{n+1} \, dS^e - \int_{V_{n+1}^e} [N]_{n+1}^T \{b\}_{n+1} \, dV^e \right] = 0$$

Now let's define the external load vector comprising of the traction and body forces as:

$$\{F\}_{n+1}^{\text{ext}} = \mathop{\mathbf{A}}_{e} \left[\int_{S_{n+1}^e} [N]_{n+1}^T \{t\}_{n+1} \, dS^e + \int_{V_{n+1}^e} [N]_{n+1}^T \{b\}_{n+1} \, dV^e \right]$$

At this point recall that $\{\sigma\}_{n+1}$ is a non–linear (in general) function of the unknowns $\{\Delta u^N\}$, so that we write:

$$\boxed{\left\{ R(\Delta u^N) \right\}_{n+1} \equiv \mathop{\mathbf{A}}_{e} \int_{V_{n+1}^e} [B]_{n+1}^T \{\sigma\}_{n+1} \, dV^e - \{F\}_{n+1}^{\text{ext}} = \{0\}} \tag{6.15}$$

where $\{R(\Delta u^N)\}_{n+1}$ is the residual forces vector expressing the difference between the internal σ_{n+1} and external t_{n+1}, b_{n+1} forces. The solution of the 'weak' problem is the displacement field $\{\Delta u^N\}$ that satisfies the system of equations in (6.15), or equivalently, the displacement field that at $t = t_{n+1}$ equates the applied loads $\{F\}_{n+1}^{\text{ext}}$ to the internal forces $\{\sigma\}_{n+1}$.

The non–linear system of equations is solved numerically implementing Newton's method. Thus, we need to derive an expression for the Jacobian matrix and then iteratively solve for the unknowns Δu^N each increment. From definition, the Jacobian matrix, which we denote as $[K]$, is:

$$[K] = \left[\frac{\partial \{R(\Delta u^N)\}_{n+1}}{\partial \{\Delta u^N\}} \right] \tag{6.16}$$

6.2 Calculation of the Jacobian

Instead of trying to derive an expression for the Jacobian $[K]$ from the approximated form in (6.15) we will alternatively begin with the continuum form in (6.9), calculate dG and then introduce the finite element approximation. First, let us express all integrals involved in (6.9) with respect to the reference configuration. Doing so, we avoid having to take into account variations of the form $V = V(t)$ and $S = S(t)$, involved in the limits of integration, when taking the derivative dG[7].

$$G(\Delta \mathbf{u}) = \int_V \text{tr}\left(\boldsymbol{\sigma} \cdot \delta \mathbf{L}^*\right) dV - \int_{V_0} \rho_0 \mathbf{b} \cdot \delta \boldsymbol{v}^* dV_0 - \int_{S_0} \hat{\mathbf{t}}_0 \cdot \delta \boldsymbol{v}^* dS_0 \tag{6.17}$$

---

[7]Here we also take into account expression (6.8) to replace $\boldsymbol{\sigma} : \delta \mathbf{D}^*$ with $\boldsymbol{\sigma} : \delta \mathbf{L}^*$.

where ρ_0 and $\hat{\mathbf{t}}_0$ stand for the mass density and nominal traction vector at $t = 0$ respectively. Recalling equations (6.10) and (6.11) we note that:

$$d\mathbf{x}_{n+1} = d(\mathbf{X} + \mathbf{u}_{n+1}) = d(\mathbf{x}_n + \Delta\mathbf{u}) = d(\Delta\mathbf{u}) \tag{6.18}$$

Next, we 'push–back' the first integral in (6.17) from the current to the reference state.

$$\int_V \operatorname{tr}\left(\boldsymbol{\sigma} \cdot \delta\mathbf{L}^*\right) dV = \int_{V_0} \operatorname{tr}\left(\boldsymbol{\sigma} \cdot \frac{\partial\delta\boldsymbol{v}^*}{\partial\mathbf{X}} \cdot \frac{\partial\mathbf{X}}{\partial\mathbf{x}}\right) J \, dV_0 = \int_{V_0} \operatorname{tr}\left(\boldsymbol{\sigma} \cdot \frac{\partial\delta\boldsymbol{v}^*}{\partial\mathbf{X}} \cdot \mathbf{F}^{-1}\right) J \, dV_0$$

and by substituting into (6.17), the Weak formulation of the BVP can be written with respect to the reference state as:

$$G(\Delta\mathbf{u}) = \int_{V_0} \operatorname{tr}\left(\frac{\partial\delta\boldsymbol{v}^*}{\partial\mathbf{X}} \cdot \mathbf{F}^{-1} \cdot \boldsymbol{\sigma}\right) J \, dV_0 - \int_{V_0} \rho\mathbf{b} \cdot \delta\boldsymbol{v}^* dV_0 - \int_{S_0} \hat{\mathbf{t}}_0 \cdot \delta\boldsymbol{v}^* dS_0 \tag{6.19}$$

Now assuming that all initially applied forces are independent of the body's motion, we can derive:

$$dG = \int_{V_0} \operatorname{tr}\left[\frac{\partial\delta\boldsymbol{v}^*}{\partial\mathbf{X}} \cdot \left(d(\mathbf{F}^{-1}) \cdot \boldsymbol{\sigma} + \mathbf{F}^{-1} \cdot d\boldsymbol{\sigma} + \mathbf{F}^{-1} \cdot \boldsymbol{\sigma}\frac{dJ}{J}\right)\right] J \, dV_0$$

but:

$$\frac{\partial\delta\boldsymbol{v}^*}{\partial\mathbf{X}} = \frac{\partial\delta\boldsymbol{v}^*}{\partial\mathbf{x}} \cdot \frac{\partial\mathbf{x}}{\partial\mathbf{X}} = \delta\mathbf{L}^* \cdot \mathbf{F}$$

so that the last expression for dG becomes:

$$dG = \int_{V_0} \operatorname{tr}\left[\delta\mathbf{L}^* \cdot \left(\mathbf{F} \cdot d(\mathbf{F}^{-1}) \cdot \boldsymbol{\sigma} + d\boldsymbol{\sigma} + \boldsymbol{\sigma}\frac{dJ}{J}\right)\right] J \, dV_0 \tag{6.20}$$

and therefore we only need to evaluate the expressions $\mathbf{F} \cdot d(\mathbf{F}^{-1})$, $d\boldsymbol{\sigma}$ and dJ/J.

Evaluation of $\mathbf{F} \cdot d(\mathbf{F}^{-1})$:

$$\mathbf{F} \cdot \mathbf{F}^{-1} = \boldsymbol{\delta} \Rightarrow d\mathbf{F} \cdot \mathbf{F}^{-1} + \mathbf{F} \cdot d(\mathbf{F}^{-1}) = 0 \Rightarrow \mathbf{F} \cdot d(\mathbf{F}^{-1}) = -d\mathbf{F} \cdot \mathbf{F}^{-1}$$

but note that:

$$d\mathbf{F} = d\left(\frac{\partial\mathbf{x}}{\partial\mathbf{X}}\right) = \frac{\partial(d\mathbf{x})}{\partial\mathbf{X}} = \frac{\partial(d(\Delta\mathbf{u}))}{\partial\mathbf{X}}$$

where we made use of the result in (6.18). Now combining the above two expressions we have:

$$\mathbf{F} \cdot d(\mathbf{F}^{-1}) = -\frac{\partial(d(\Delta\mathbf{u}))}{\partial\mathbf{X}} \cdot \frac{\partial\mathbf{X}}{\partial\mathbf{x}} = -\frac{\partial d(\Delta\mathbf{u})}{\partial\mathbf{x}} \Rightarrow$$

$$\mathbf{F} \cdot d(\mathbf{F}^{-1}) = -d\mathbf{L} \tag{6.21}$$

Evaluation of dJ/J:

Recalling the definition of J as the determinant of the deformation gradient $\mathbf{F}$ we write:

$$J = \det\mathbf{F}$$

Using Jacobi's formula, we can express the quantity dJ (the derrivative of the determinant of $\mathbf{F}$) in terms of the adjugate matrix of $\mathbf{F}$ and $d\mathbf{F}$ as follows:

$$dJ = \text{tr}\left[\text{adj}(\mathbf{F}) \cdot d\mathbf{F}\right]$$

but since the inverse $\mathbf{F}^{-1}$ exists from definition, the adjugate of $\mathbf{F}$ is given by:

$$\text{adj}(\mathbf{F}) = J\,\mathbf{F}^{-1}$$

and thus:

$$dJ = J\,\text{tr}\left[\mathbf{F}^{-1} \cdot d\mathbf{F}\right]$$

but we have already shown that:

$$d\mathbf{F} \cdot \mathbf{F}^{-1} = d\mathbf{L}$$

Therefore, combining the last two expressions, the quantity dJ/J can be expressed as:

$$\frac{dJ}{J} = dL_{kk} \tag{6.22}$$

Before continuing with the evaluation of $d\mathbf{S}$ let us substitute expressions (6.21) and (6.22) to (6.20) while taking into account that $\text{tr}[\mathbf{A} \cdot \mathbf{B}] = \mathbf{A} : \mathbf{B}^T$ to derive:

$$dG = \int\limits_{V(t)} \delta\mathbf{L}^* : \left[d\boldsymbol{\sigma} - \boldsymbol{\sigma} \cdot d\mathbf{L}^T + \boldsymbol{\sigma}\, dL_{kk}\right] dV \tag{6.23}$$

Evaluation of $d\boldsymbol{\sigma}$:

At this point we note that $d\boldsymbol{\sigma}$ expresses the stress variation with respect to the displacement increment $\Delta\mathbf{u}$. Analytical expressions for $d\boldsymbol{\sigma}$ depend on both the constitutive model under consideration and the algorithm used for the numerical integration[8] of the constitutive equations. Furthermore, expressions for $d\boldsymbol{\sigma}$ are widely based on approximate techniques since it's exact evaluation is a very involved process when accounting for finite strains and rotations.

First, let us express the time variation of the deformation gradient F during the time increment $[t_n, t_{n+1}]$ as:

$$\mathbf{F}(t) = \Delta\mathbf{F}(t) \cdot \mathbf{F}_n \tag{6.24}$$

and the corresponding deformation rate tensor $\mathbf{D}$ can be expressed as:

$$\mathbf{D}(t) = \left[\dot{\mathbf{F}}(t) \cdot \mathbf{F}^{-1}\right]_{\text{s}} = \left[\overline{\dot{\Delta\mathbf{F}(t)}} \cdot \Delta\mathbf{F}^{-1}\right]_{\text{s}} \tag{6.25}$$

---

[8]i.e. Forward Euler, Backward Euler etc.

Recalling the Polar Decomposition theorem, we can write $\Delta \mathbf{F}(t) = \mathbf{R}(t) \cdot \mathbf{U}(t)$. Assuming that the Lagrangian triad associated with $\Delta \mathbf{F}(t)$ remains fixed over the period of one increment we can substitute the polar decomposition of $\Delta \mathbf{F}(t)$ to (6.25) and write $\mathbf{D}$ in the form:

$$\mathbf{D}(t) = \mathbf{R}(t) \cdot \dot{\mathbf{E}}(t) \cdot \mathbf{R}^T(t) \tag{6.26}$$

where $\mathbf{E}$ stands for the logarithmic strain[9]. It can also be shown that the spin tensor $\mathbf{W}(t)$ is in this case given by:

$$\mathbf{W}(t) = \dot{\mathbf{R}}(t) \cdot \mathbf{R}^T(t) \tag{6.27}$$

The Jaumman rate of Cauchy stress is then expressed as:

$$\overset{\nabla}{\boldsymbol{\sigma}}(t) = \mathbf{R}(t) \cdot \frac{d}{dt}\left[\hat{\boldsymbol{\sigma}}(t)\right] \cdot \mathbf{R}^T(t) \tag{6.28}$$

where:

$$\hat{\boldsymbol{\sigma}}(t) = \mathbf{R}^T(t) \cdot \boldsymbol{\sigma}(t) \cdot \mathbf{R}(t) \tag{6.29}$$

We also note that:

$$\dot{\hat{\boldsymbol{\sigma}}}(t) = \frac{\partial \hat{\boldsymbol{\sigma}}(t)}{\partial \mathbf{E}(t)} : \dot{\mathbf{E}}(t) = \hat{\boldsymbol{\mathcal{C}}}(t) : \dot{\mathbf{E}}(t) = \hat{\boldsymbol{\mathcal{C}}}(t) : \left(\mathbf{R}^T(t) \cdot \mathbf{D}(t) \cdot \mathbf{R}(t)\right) \tag{6.30}$$

Substituting the last result into expression (6.29) we derive:

$$\overset{\nabla}{\boldsymbol{\sigma}}(t) = \mathbf{R}(t) \cdot \left[\hat{\boldsymbol{\mathcal{C}}}(t) : \left(\mathbf{R}^T(t) \cdot \mathbf{D}(t) \cdot \mathbf{R}(t)\right)\right] \cdot \mathbf{R}^T(t) =$$

$$= \boldsymbol{\mathcal{C}}(t) : \mathbf{D}(t) = \boldsymbol{\mathcal{C}}(t) : \mathbf{L}(t) \tag{6.31}$$

where $\boldsymbol{\mathcal{C}}$ and $\hat{\boldsymbol{\mathcal{C}}}$ are related by:

$$\mathcal{C}_{ijkl} = R_{im} R_{jn} R_{kp} R_{lq} \hat{\mathcal{C}}_{mnpq} \tag{6.32}$$

Next, recalling the definition of Jaumann stress rate as:

$$\overset{\nabla}{\boldsymbol{\sigma}} = \dot{\boldsymbol{\sigma}} + \boldsymbol{\sigma} \cdot \mathbf{W} - \mathbf{W} \cdot \boldsymbol{\sigma}$$

we can replace $\mathbf{W}$ as $\mathbf{L}_\mathrm{s}$ and then express $\dot{\boldsymbol{\sigma}}$ as:

$$\dot{\boldsymbol{\sigma}} = \overset{\nabla}{\boldsymbol{\sigma}} - \frac{1}{2}\boldsymbol{\sigma} \cdot \left(\mathbf{L} - \mathbf{L}^T\right) + \frac{1}{2}\left(\mathbf{L} - \mathbf{L}^T\right) \cdot \boldsymbol{\sigma} \Rightarrow$$

$$\dot{\boldsymbol{\sigma}} = \boldsymbol{\mathcal{C}} : \mathbf{L} - \frac{1}{2}\boldsymbol{\sigma} \cdot \left(\mathbf{L} - \mathbf{L}^T\right) + \frac{1}{2}\left(\mathbf{L} - \mathbf{L}^T\right) \cdot \boldsymbol{\sigma} \tag{6.33}$$

Expression (6.33) can now be used to approximate $d\boldsymbol{\sigma}$ as:

$$\boxed{d\boldsymbol{\sigma} \cong \boldsymbol{\mathcal{C}} : d\mathbf{L} - \frac{1}{2}\boldsymbol{\sigma} \cdot \left(d\mathbf{L} - d\mathbf{L}^T\right) + \frac{1}{2}\left(d\mathbf{L} - d\mathbf{L}^T\right) \cdot \boldsymbol{\sigma}} \tag{6.34}$$

---

[9]In the special case where the principal directions of $\mathbf{U}(t)$ remain constant, the logarithmic strain rate is associated with the stretch tensor $\mathbf{U}(t)$ as $\dot{\mathbf{E}} = \dot{\mathbf{U}} \cdot \mathbf{U}^{-1}$

Let us know substitute the above approximation for $d\boldsymbol{\sigma}$ into (6.23) to derive:

$$dG = \int\limits_{V(t)} \delta\mathbf{L}^* : \left[\boldsymbol{\mathcal{C}} : d\mathbf{L} - \frac{1}{2}\boldsymbol{\sigma} \cdot \left(d\mathbf{L} - d\mathbf{L}^T\right) + \frac{1}{2}\left(d\mathbf{L} - d\mathbf{L}^T\right) \cdot \boldsymbol{\sigma} + dL_{kk}\boldsymbol{\sigma} \right] dV$$

or equivalently and in a more compact form:

$$\boxed{dG = \int\limits_{V(t)} \delta\mathbf{L}^* : [\boldsymbol{\mathcal{C}} + \boldsymbol{\mathcal{S}} + \boldsymbol{\sigma}\,\boldsymbol{\delta}] : d\mathbf{L}\, dV} \tag{6.35}$$

where $\boldsymbol{\mathcal{S}}$ is given by:

$$\mathcal{S}_{ijkl} = \frac{1}{2}\left(\delta_{ik}\sigma_{jl} - \delta_{il}\sigma_{jk} - \sigma_{ik}\delta_{jl} + \sigma_{il}\delta_{jk}\right)$$

Since we successfully derived an epxression for the Jacobian (6.35), we can now introduce the finite element approximation summarized by expressions (6.12–6.13). Let us also approximate $\delta\mathbf{L}^*$ and $d\mathbf{L}$ as:

$$\left\{\delta L^*\right\}_{6\times1} = [B_L(\mathbf{x})]_{6\times n} \left\{\Delta v^{*N}\right\}_{n\times1} \tag{6.36}$$

$$\left\{dL\right\}_{6\times1} = [B_L(\mathbf{x})]_{6\times n} \left\{\Delta v^N\right\}_{n\times1} \tag{6.37}$$

where the matrix $[B_L(\mathbf{x})]$ contains the shape function derrivatives in the sense $B_{L_{\alpha\beta}} = N_{\alpha,\beta}$ and therefore differs from matrix $[B(\mathbf{x})]$ used to approximate $\delta\mathbf{D}^*$ in (6.14). Now if we substitute (6.12), (6.13) along with (6.36) and (6.37) to (6.35) we will eventually derive:

$$dG = \lfloor\Delta v^{*N}\rfloor \left[\boldsymbol{\mathsf{A}}_e \int\limits_{V_e} [B_L]^T \left([\mathcal{C}] + [\mathcal{S}] + \{\sigma\}\lfloor\delta\rfloor\right) [B_L]\, dV^e \right] \left\{\Delta v^N\right\}$$

and since the global Jacobian[10] is made up by assembling the Jacobians defined within each element as:

$$[K] = \boldsymbol{\mathsf{A}}_e [k^e]$$

we can express the Local Jacobian of every element as:

$$\boxed{[k^e] = \int\limits_{V_e} [B_L]^T \left([\mathcal{C}] + [\mathcal{S}] + \{\sigma\}\lfloor\delta\rfloor\right)[B_L]\, dV^e} \tag{6.38}$$

It should be noted that the expression for the Local Jacobian given by (6.38) is approximate, not only because we introduced the Finite Element approximation for the basic quantities involved, but mainly because of the approximation for $d\boldsymbol{\sigma}$ expressed in (6.34). This approximation however, only affects the rate of convergence to the solution but not the

---

[10]Also referred to as the global Stiffness Matrix

solution itself. We should also note that while $[\mathcal{S}]$ defines a symmetric matrix, the product $\{\sigma\}\lfloor\delta\rfloor$ is a non–symetric matrix causing the local jacobian $[k^e]$ to be non–symetric as well. Furthermore, in our single crystal model, $[\mathcal{C}]$ is non–symmetric as well.

Abaqus/Standard [2] module of the Abaqus general purpose finite element software is based on the formulation presented above and uses expression (6.38) to build the local stiffness matrix of every finite element. The Abaqus [2] software supports the computational implementation of user–defined, enabling users to introduce complex constitutive material models in the form of a **U**ser **MAT**erial subroutine.

6.3 **User MATerial Subroutines**

User **MAT**erial subroutines (UMAT) are used in conjuction with the ABAQUS [1] general purpose finite element software and enable the finite element analysis of complex non–linear materials. Abaqus provides a general user interface so that a particular constitutive model can be introduces as a 'user–subroutine' in a programming language such as FORTRAN.

Recalling the finite element approximation that we introduced in (6.12), the unknown displacement field is approximated by a function interpolation defined within each element. The nodal displacements are the main unknowns of the discretized problem, whereas stresses and strains are being calculated at the integration points of each element[11]. UMAT subroutines can be used with any ABAQUS procedure that includes mechanical behavior and are called by ABAQUS at every integration point of all elements for which the material definition includes a user-defined material behavior. Primarily, a UMAT subroutine must update stresses at the end of the increment for which it is called, and also provide the material (Local) Jacobian matrix $\partial(\Delta\boldsymbol{\sigma})/\partial(\Delta\boldsymbol{\epsilon})$ corresponding to the mechanical constitutive model under consideration. When developing a UMAT subroutine the user is also free to define solution–dependent state variables (STATEV)[12] and ABAQUS will store their values at the end of every increment, making them available for future calculations on subsequent increments. Solution dependent variables however, also need to be updated to their values at the end of every increment.

A typical iterface of a UMAT subroutine [2] is demonstrated below.

---

[11]The number of integration points of a finite element as well as their position within the element both depend on the type of element being used (i.e. Full Integration, Reduced Integration, Shell Elements, Continuum Elements, Membrane Elements etc.)

[12]A Solution Dependent variable could be any variable whose value is necessary to conduct material calculations at a given time, or even a variable whose values are needed to be stored for post–processing usage.

```
1           SUBROUTINE UMAT(STRESS,STATEV,DDSDDE,SSE,SPD,SCD,
2      + RPL,DDSDDT,DRPLDE,DRPLDT,
3      + STRAN,DSTRAN,TIME,DTIME,TEMP,DTEMP,PREDEF,DPRED,CMNAME,
4      + NDI,NSHR,NTENS,NSTATV,PROPS,NPROPS,COORDS,DROT,PNEWDT,
5      + CELENT,DFGRD0,DFGRD1,NOEL,NPT,LAYER,KSPT,KSTEP,KINC)
6  C
7        INCLUDE 'ABA_PARAM.INC'
8  C
9        CHARACTER*80 CMNAME
10       DIMENSION STRESS(NTENS),STATEV(NSTATV),
11     + DDSDDE(NTENS,NTENS),DDSDDT(NTENS),DRPLDE(NTENS),
12     + STRAN(NTENS),DSTRAN(NTENS),TIME(2),PREDEF(1),DPRED(1),
13     + PROPS(NPROPS),COORDS(3),DROT(3,3),DFGRD0(3,3),DFGRD1(3,3)
14
15       user coding to define DDSDDE, STRESS, STATEV, SSE, SPD, SCD
16       and, if necessary, RPL, DDSDDT, DRPLDE, DRPLDT, PNEWDT
17
18       RETURN
19       END
```

As aforementioned the user coding must update all state variables (STATEV) and stresses (STRESS) to their values at the end of the increment and also build the local Jacobian matrix (DDSDDE). The user is also free to define auxiliary subroutines to perform lengthy and repeating calculations required in the UMAT subroutine (i.e. matrix inversion, matrix multiplication, polar decomposition of a tensor etc.). The coding can also take advantage of the ulility subroutines that are already implemented into ABAQUS[13].

---

[13]ABAQUS Utility routines are able to find principal directions of tensors, calculate their invariants etc.

Chapter 7

Finite Element Results

In the current chapter, we present the results from the finite element simulations on single crystal specimens subjected to a series of uniaxial tension experiments. All finite element analyses were performed using the Abaqus [1] general purpose finite element software and the rate independent crystal plasticity model was computationally implemented in the form of a UMAT (User Material) subroutine. The UMAT subroutine uses the heuristic stress update algorithm (*see* Section 5.1) to iteratively predict the set of active systems and perform the numerical integration of the constitutive equations[1]. All uniaxial tension simulations were performed using the Static/General step option within the Abaqus/Standard [1] module of the Abaqus software.

The elastoplastic material constants used in all the finite element simulations, are taken by the experimental results of Delafosse [24] for nickel single crystals and are summarized in Table 7.1 that follows.

Table 7.1: Elastoplastic material constants for nickel single crystals (Delafosse 2012)

	Material Constant	**Value**
Elastic Constants	C_{11}	246.5 [GPa]
	C_{12}	147.3 [GPa]
	C_{44}	124.7 [GPa]
Initial flow stress	τ_0	8.5 [MPa]

Continues on next page

---

[1]Section 7.3 is the only exception, where two additional user material subroutines were developed to implement the Nonlinear Optimization (*see* Section 5.2) formulation and the Linear Optimization (*see* Section 5.3) formulation respectively, for comparison purposes

Table 7.1 – Continued

	Material Constant	Value
Saturation stress	τ_I	12 [MPa]
Hardening	h_0	500 [MPa]
	h_s	26 [MPa]
Strain to cause 1st yield	γ_0	0.001
Ratio Active/Cross Hardening	q	[0,0.1]

7.1 One Element Test of a Single Crystal

In order to validate the computational implementation of the crystal plasticity model we first conducted a series of finite element simulations using a mesh consisting of a single finite element[2]. The specimen's shape is assumed to be a cube with sides of 1 [mm] and is discretized using one C3D8H[3] finite element from the Abaqus [1] element library. A prescribed concentrated force field along the $\mathbf{e}_2$ direction is then applied to the vertices of the cube, subjecting the single crystal specimen to uniaxial tension. Boundary conditions are also added to constraint the bare minimum[4] of 6 displacement degrees of freedom, in order to enable the single crystal specimen to deform freely and simultaneously eliminate rigid body modes. The concentrated force field and boundary conditions are illustrated in Figure 7.1 that follows.
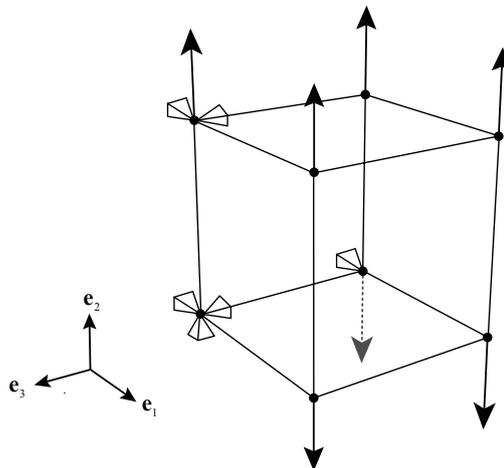

Figure 7.1: An illustration of the prescribed force field and boundary conditions applied on the single finite element subjected to unconstrained uniaxial tension

---

[2]Abaqus [2] strongly recommends that User MATerial subroutines have to be initially tested on a single-element model with prescribed traction loading

[3]C3D8H: A hybrid 3D continuum brick with linear shape functions and costant pressure

[4]It can be mathematically proven that a minimum of 6 displacement d.o.f. need to be constrained to eliminate rigid body motions and rotations in 3D analyses

Before subjecting the single crystal specimen to uniaxial tension, we have to decide an initial relative orientation of the local crystal system with respect to the global cartesian system shown in Figure 7.1. Recalling our discussion on the relative orientation in Section 3.2, we can successfully position the crystal in space once we define two vectors[5] with respect to the global and crystal systems. Hence, we choose:

$$\mathbf{p} = \mathbf{e}_2 = \frac{1}{\sqrt{35}} \left(1\,\mathbf{n}^{(1)} + 3\,\mathbf{n}^{(2)} + 5\,\mathbf{n}^{(3)} \right) = [1\,3\,5] \tag{7.1a}$$

$$\mathbf{q} = \mathbf{e}_3 = \frac{1}{\sqrt{1190}} \left(29\,\mathbf{n}^{(1)} - 18\,\mathbf{n}^{(2)} + 5\,\mathbf{n}^{(3)} \right) = [29\,\overline{18}\,5] \tag{7.1b}$$

The transformation matrix requires the definition of a third vector, which can be readily obtained from $\mathbf{p}$ and $\mathbf{q}$ as $\mathbf{r} = \mathbf{q} \times \mathbf{p}$. The above selections for $\mathbf{p}$ and $\mathbf{q}$ are such that the crystal is initially oriented for easy glide[6] and also the slip direction will initially be 45° relative to the $\mathbf{e}_3$ axis. In order to identify the primary slip systems for the specific easy glide orientation, we calculate the Schmid factors that correspond to each system (Table 7.2).

Table 7.2: The Schmid factors of the 12 slip systems of FCC crystals for uniaxial tension in the [1 3 5] crystal direction

| Slip System	Schmid Factor
5	**0.489897949**
2	0.419912527
6	−0.326598632
7	−0.279941685
1,3	−0.209956264
4	−0.163299316
8,9	0.139970842
10	−0.093313895
11	0.069985421
12	0.023328474

The resulting Schmid factors justify that aligning the tension direction with the crystal direction $[1\,3\,5]$, positions the crystal for easy glide, since slip system 5 exhibits the greatest factor and will be the only system to yield first. In addition, slip system 2 will be the second slip system to activate, probably soon after the activation of system 5. The Schmid factors[7] for all other slip systems are quite smaller, and thus we do not expect those systems to add significantly to the crystal's deformation during the uniaxial tension experiment.

---

[5]The vectors must not be parallel with each other

[6]Aligning the loading direction in uniaxial tension with the crystal direction $[1\,3\,5]$ guarantees that only one system will be initially activated. This can be easily shown by calculating the Schmid factors for the specific orientation to show that slip system no.5 is the only optimally oriented system

[7]Negative Schmid factors indicate that the corresponding slip system will activate in the opposite direction

Figures 7.2a and 7.2b illustrate the anisotropic and non–uniform deformation of the single crystal specimen, presenting the actual undeformed and deformed shapes before and after the uniaxial tension analysis.
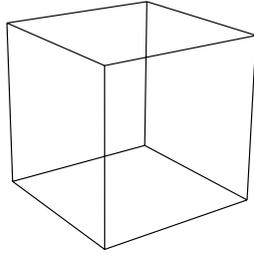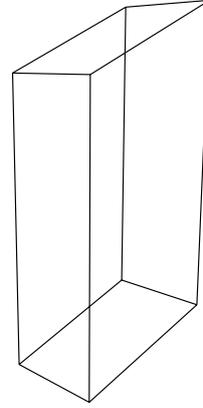
(a) Undeformed Shape   (b) Deformed Shape

Figure 7.2: The deformed and undeformed shapes of a single crystal finite element subjected to uniaxial tension

Next we present the finite element results for the aforementioned uniaxial tension setting. The first analyses correspond to a selection of the cross–hardening parameter as $q = 0$ (Bassani & Wu [11, 12]) and therefore a diagonal[8] hardening moduli $h^{\alpha\beta}$. Figure 7.3 illustrates the macroscopic true stress–logarithmic strain curve for the specific uniaxial tension setting. Coloured points indicate the corresponding slip system currently activating and added to the active systems set $\mathscr{A}$.
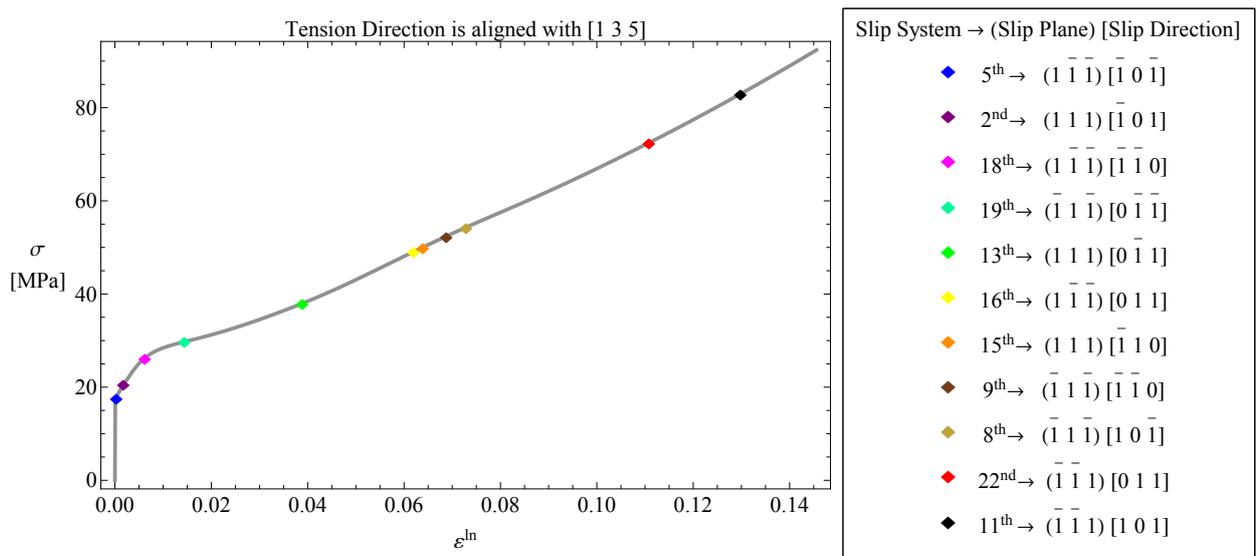

Figure 7.3: True stress–logarithmic strain curve for uniaxial tension of a single crystal finite element with $q = 0$

---

[8]Latent hardening effects are ignored as a result of $q = 0$

In total, 11 slip systems activate during the uniaxial tension test, and the order of activation is in complete agreement with the one predicted using the Schmid factors in Table 7.2. Figures 7.4a and 7.4b present the resolved shear plastic strains and critical shear stresses respectively, for all slip systems that were found to be active during the analysis. Critical shear stresses are normalized using the initial flow stress τ_0.

(a) Resolved shear strains γ^α

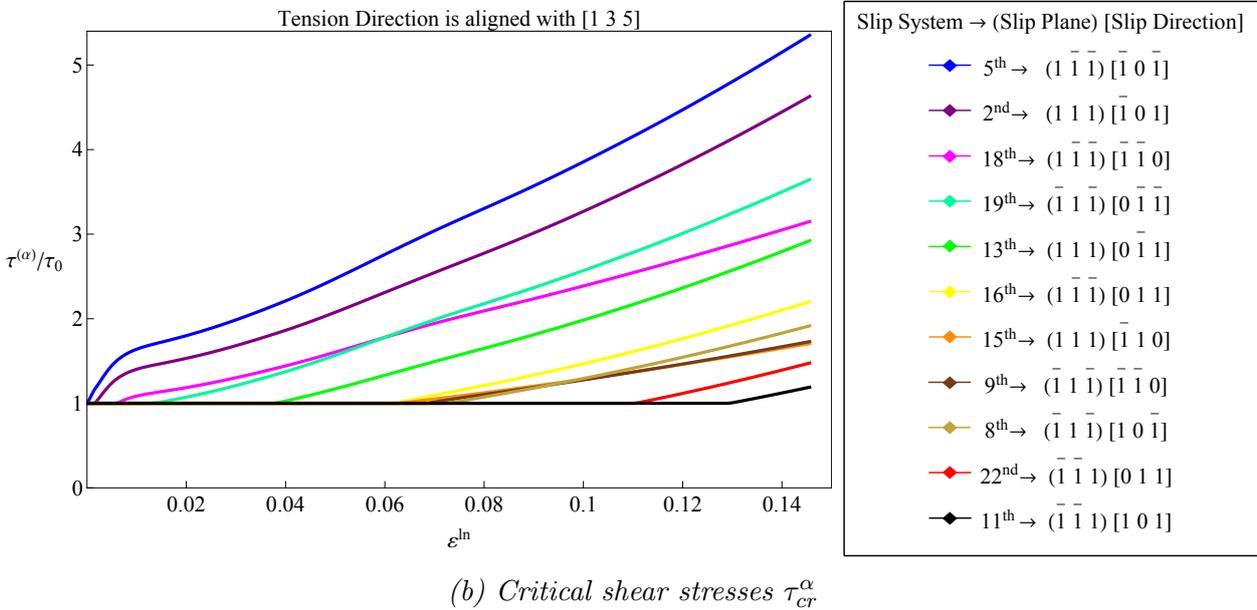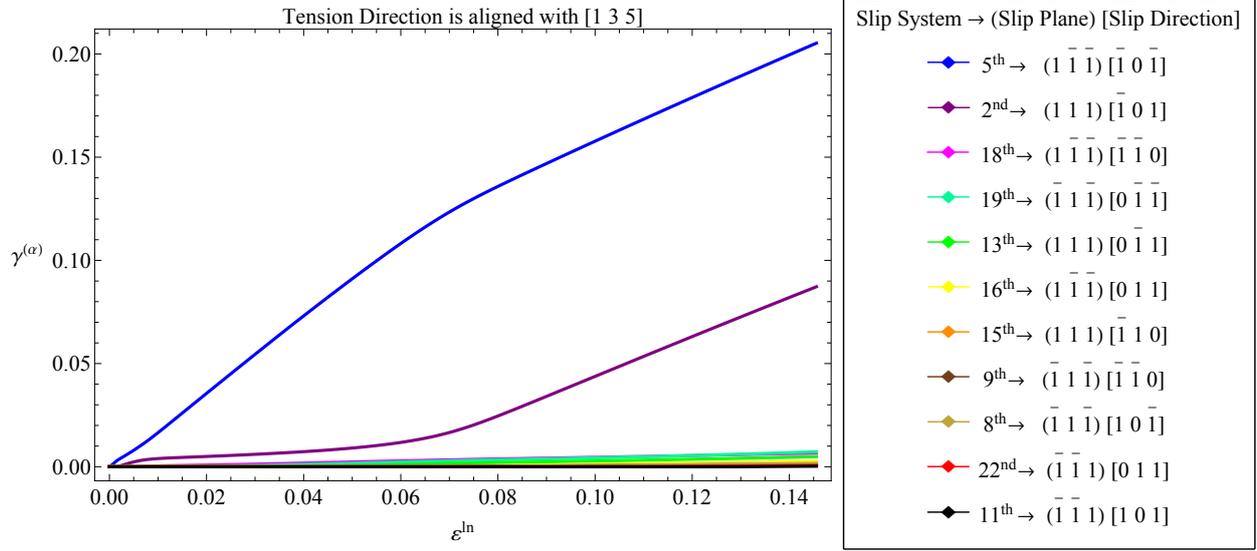*(b) Critical shear stresses τ_{cr}^α*

Figure 7.4: The evolution of resolved shear strains and critical stresses of all active systems with respect to the logarithmic strain in tension direction for uniaxial tension of a single crystal finite element with $q = 0$

Figure 7.4a, demonstrates that the macroscopic deformation $\varepsilon^{\ln}$ during the test is mainly[9]

---

[9]All other systems undergo insignificant plastic deformation compared to slip system no.5

the result of plastic slip on slip systems 5 & 2. The latter may be suggesting that the use of a diagonal hardening moduli ($q = 0$) eventually populates the set $\mathscr{A}$ with 'pseudo–active' systems, that do not undergo significant plastic slip. To identify if including the latent hardening phenomena indeed affects the number of slip systems activated, we performed the same uniaxial tension simulation with a parameter q equal to 0.1. The σ–$\varepsilon^{\ln}$ curve for $q = 0.1$ is presented in Figure 7.5 along with the curve (Figure 7.3) for $q = 0$ to ease comparison.

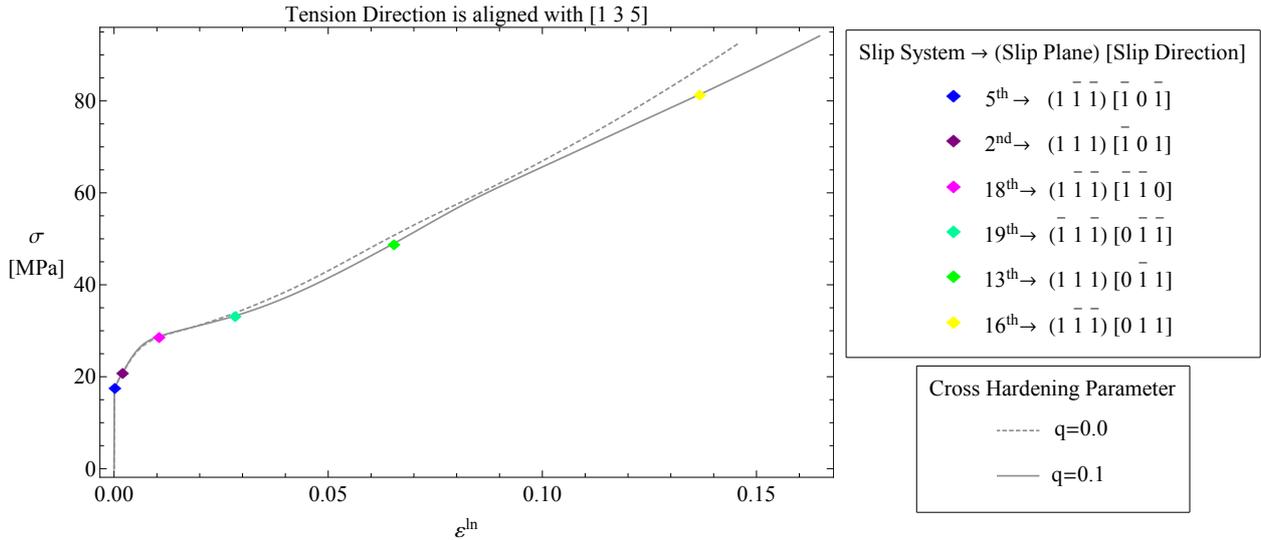*Figure 7.5: True stress–logarithmic strain curve for uniaxial tension of a single crystal finite element with $q = 0.1$. The dashed σ–$\varepsilon^{\ln}$ curve corresponds to $q = 0$. Coloured points indicate the activation of the corresponding slip system*

Evidently, accounting for latent hardening with $q = 0.1$ is sufficient to populate the set $\mathscr{A}$ with fewer systems. According to the coloured points in Figure 7.5, 6 slip systems were activated in total during the analysis, which is nearly half the number of systems activated if no latent hardening is present ($q = 0$). When Latent hardening phenomena are included, the critical shear stress τ_{cr}^{α} of a system α increases with deformation even if the system is not active. The latter, is sufficient to suppress the activation of minor loaded systems, which would undergo insignificant slip even if they activated.

Subsequently, we present the plots for the evolution of γ^{α} and τ_{cr}^{α} with respect to the logarithmic strain in tension direction $\varepsilon^{\ln}$, for the dominantly active systems 5 and 2. The plots are drawn for both the hardening cases ($q = 0, q = 0.1$) and presented in Figures 7.6a and 7.6b. A comparison for the different hardening cases, illustrates that the curves for the dominant slip systems are not dramatically affected by including the latent hardening phenomena.

Finally, we address the issue of the crystal's rotation during the uniaxial tension analyses for both hardening cases ($q = 0, q = 0.1$). Recalling the concept of stereographic projection that we introduced in section 2.3, we can demonstrate the evolution of the crystal's orientation by making use of the inverse pole figure diagrams. Taking into consideration that in both analyses the crystal was initially oriented for tension along the [135] direction, we save
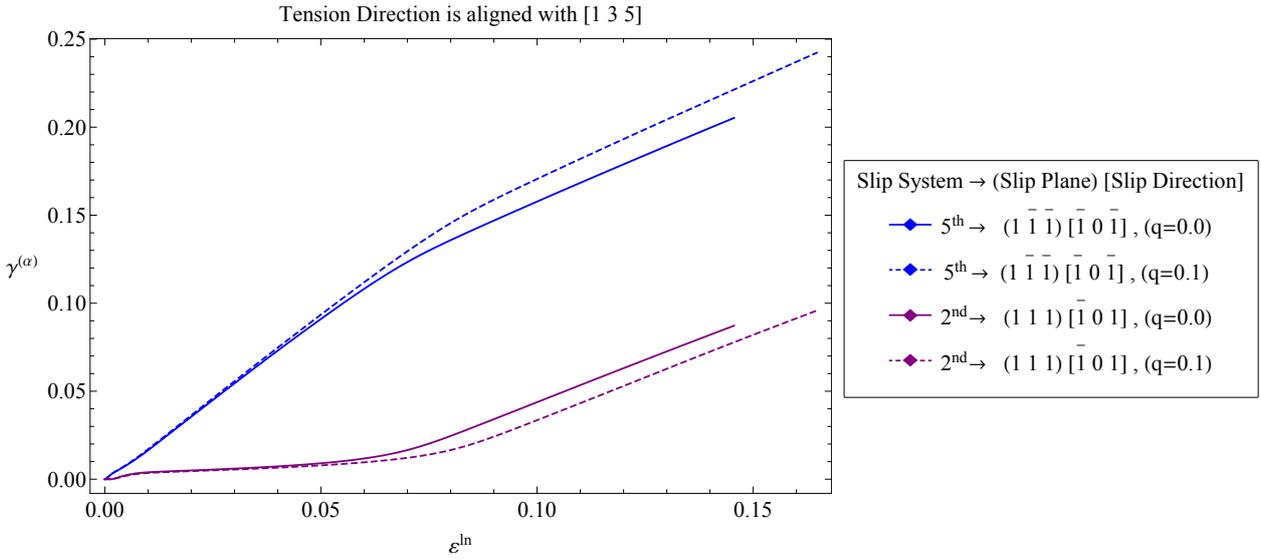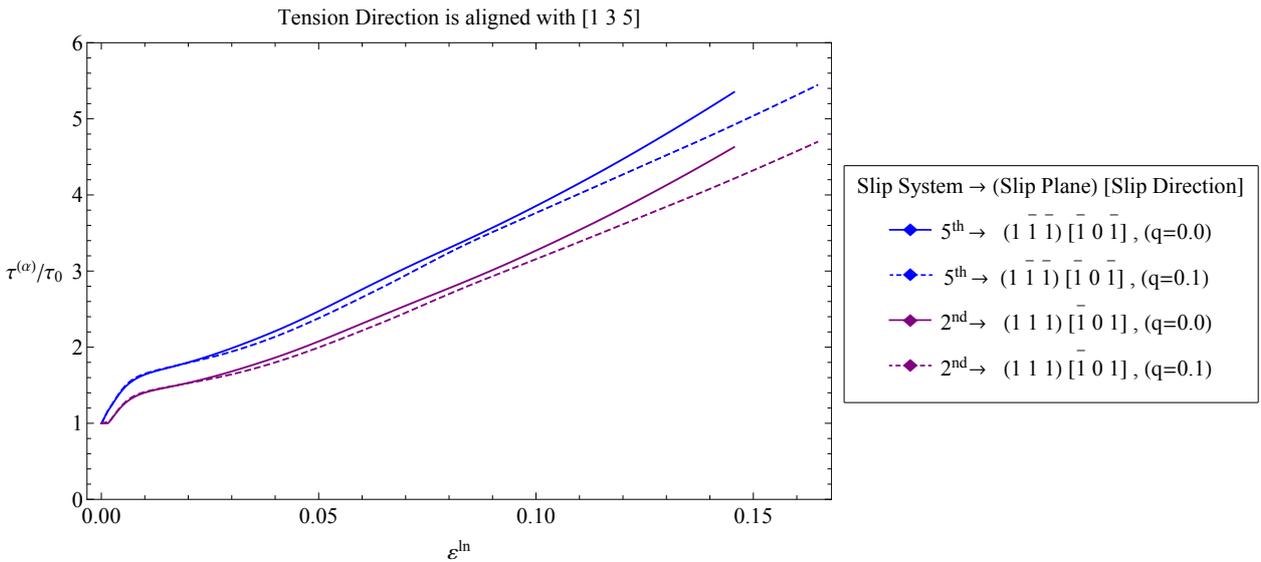
Tension Direction is aligned with [1 3 5]

(a) *Resolved shear strains γ^α of primary active systems No.5 & 2*

Tension Direction is aligned with [1 3 5]

(b) *Critical shear stresses τ_{cr}^α of primary active systems No.5 & 2*

Figure 7.6: A comparison of the the γ^α–ε^{ln} and τ_{cr}^α/τ_0–ε^{ln} curves for $q = 0$ (no cross–hardening) and $q = 0.1$

the current direction which is incrementally rotated (*see* 3.14) by $\mathbf{F}^p$, and plot the loading direction route in an inverse pole figure[10] diagram in the standard triangle. The results for the uniaxial tension analyses for $q = 0$ and $q = 0.1$ are displayed in Figure 7.7.

---

[10]To produce the inverse pole diagrams we implemented an auxiliary subroutine within the UMAT for crystal plasticity to incrementally rotate the crystal direction with $\mathbf{F}^p$
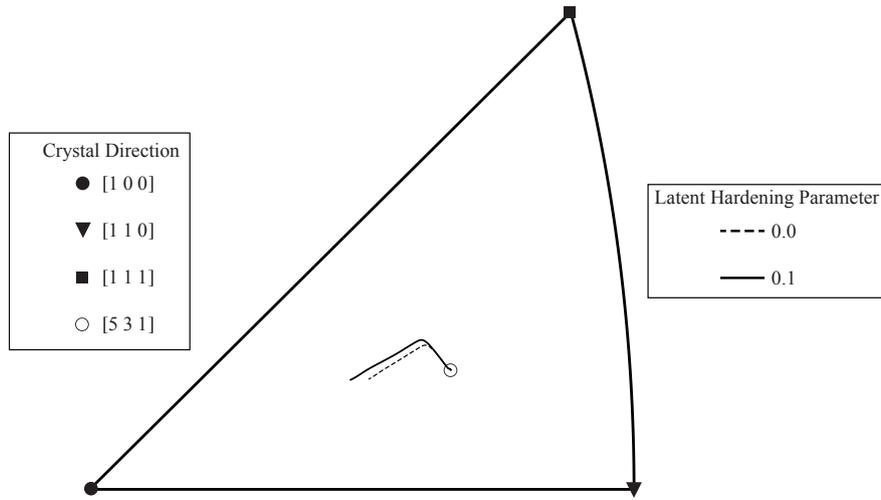
Figure 7.7: The loading direction route in the standard triangle, during the uniaxial tension for $q = 0$ and $q = 0.1$. Initially, the loading direction is aligned with $[1\,3\,5]$.

7.2 Uniaxial Tension of Single Crystal Specimens

Upon completing the initial testing of the computational model as well as the calibration of the hardening parameter[11] q, we conducted a series of finite element analyses to multi–element models, representing actual specimens used for single crystal testing. Three specimens designs are considered in total, and their engineering designs are shown in Figures 7.8a, 7.8b and 7.8c below.

(a) Specimen 1

(b) Specimen 2

---
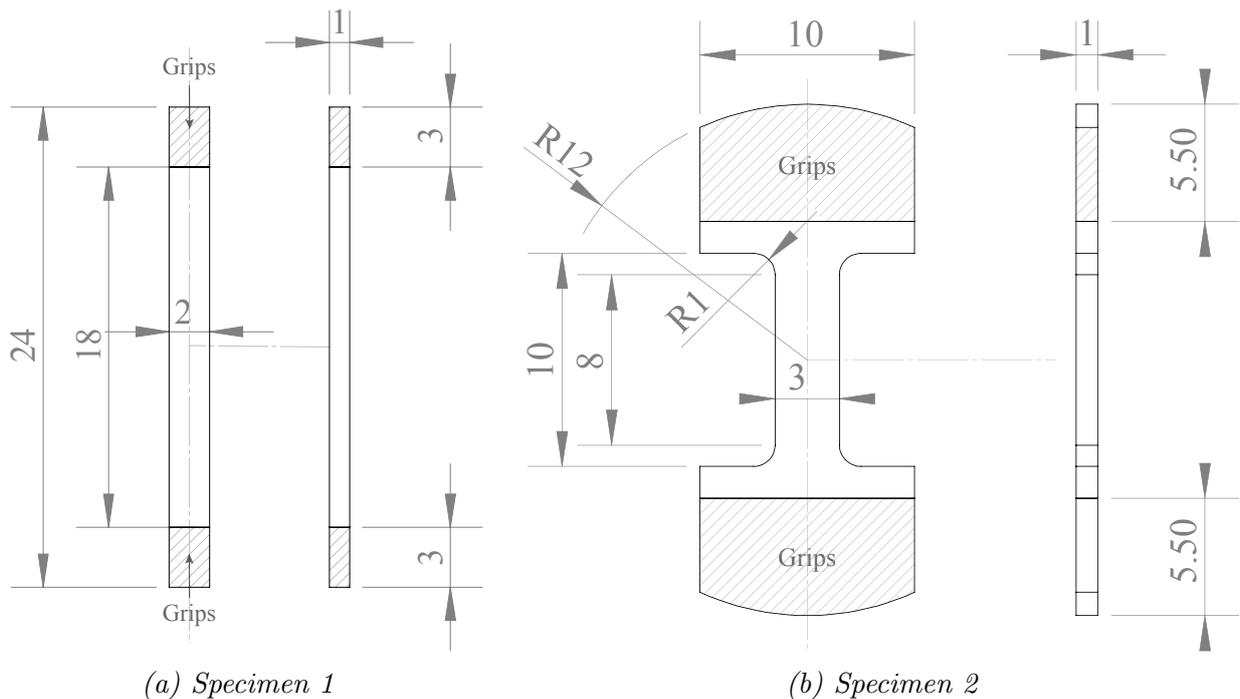
[11]From now on we proceed by assuming $q = 0.1$

From now on, we will refer to these specimens as *Specimen 1,2* and *3* respectively. The uniform specimen (Specimen 1) is computationally tested only for comparison and validation purposes and cannot be used in a real–world experiment; it's uniform shape may result into unpredictable fracture, anywhere in the region between the grips. Specimen 2, is a commonly used specimen for the uniaxial tension experiments on single crystals, and is also referred to as *dogbone* specimen, a naming convention that justifies its shape.

The specimen models where then discretized using continuum hybrid C3D8H elements from the Abaqus [1] library. Table 7.3 presents the number of elements,nodes and degrees of freedom for the mesh of each specimen model and Figures 7.9a–7.9c illustrate an isometric 3D view of the discretized specimens in the undeformed state.
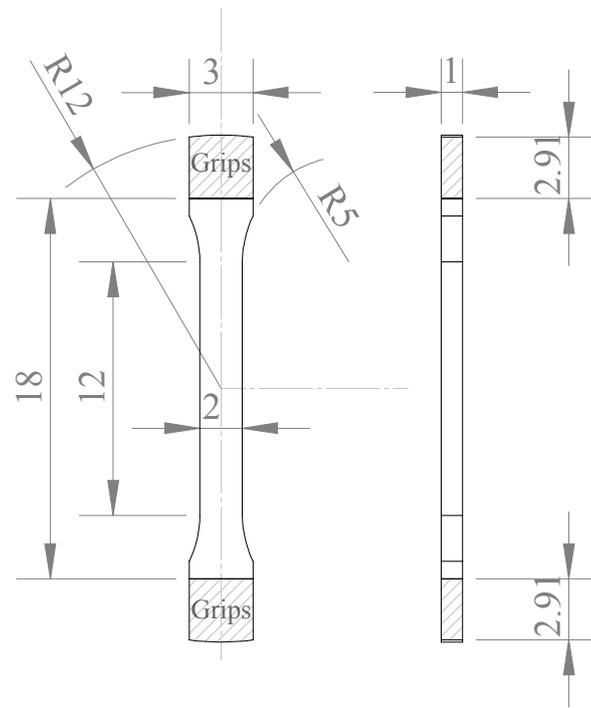
(c) Specimen 3

Figure 7.8: Engineering Sketches of the uniaxial tension specimens (dimensions are in mm)

Table 7.3: The finite element meshes used to discretize the specimens for the uniaxial tension

#	Specimen 1	Specimen 1	Specimen 3
Elements	1242	3840	1782
Nodes	3203	9425	4463
d.o.f.	7123	20593	9823

The specimens are then subjected to uniaxial deformation in the following sense. In contrast to the **uniform force field** applied to the single–element test, a real–world tensile
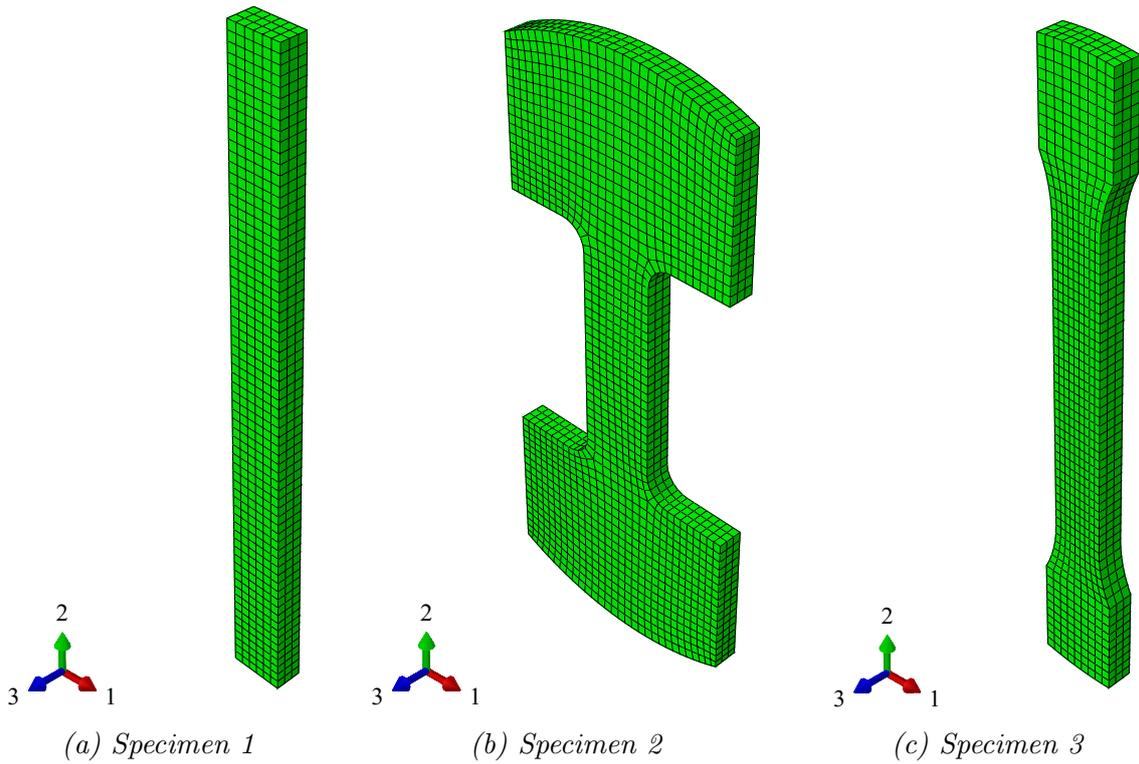
(a) Specimen 1   *(b) Specimen 2*   *(c) Specimen 3*

Figure 7.9: The finite element meshes used for the uniaxial tension simulations of the single crystal specimens. The meshes consist of C3D8H continuum hybrid elements from the Abaqus library

machine[12] is only able to impose a **uniform displacement field**, subjecting the crystal to constrained uniaxial deformation. We assume that the bottom grip remains fixed during the experiment and thus constraints all displacement degrees of freedom, namely 1,2 and 3. The top grip applies a uniform displacement field along direction 2 and also constraints the specimen from moving along directions 1 and 3.

In the analyses performed, the uniform force field was set equal to 1.8mm for all specimens, even though it clearly subjects the specimens to different nominal deformations, taking into consideration the respective grip distances prescribed by the designs in Figure 7.8. Subsequently, we present the comparative results for all 3 analyses, in the form of contour plots of the variables that exhibit the greatest interest to our study.

Figures 7.10a–7.10c display the contour plots of the logarithmic strain in tension direction, while figures 7.11a–7.11c the contours of total accumulated plastic strain on the primary active slip system no.5. A comparison between figures 7.10a–7.11b,7.10b–7.11b and 7.10c–7.11c suggests that the macroscopic deformation $\varepsilon_{22}^{\ln}$ is mainly the result of plastic deformation occurring on slip system 5. Figures 7.12a–7.12c present the contours of the critical stress on slip system 5, whereas the activation region of the same system is displayed

---

[12]In fact, engineers are in the process of developing a new class of special tensile machines, that would facilitate experimentation on single crystals. These machines are designed to constraint as few degrees of freedom as possible, enabling the specimen to rotate or even move transversely to the tension direction during the experiment. Such machines, try to simulate the uniform force field we applied to the single–element test in the previous section
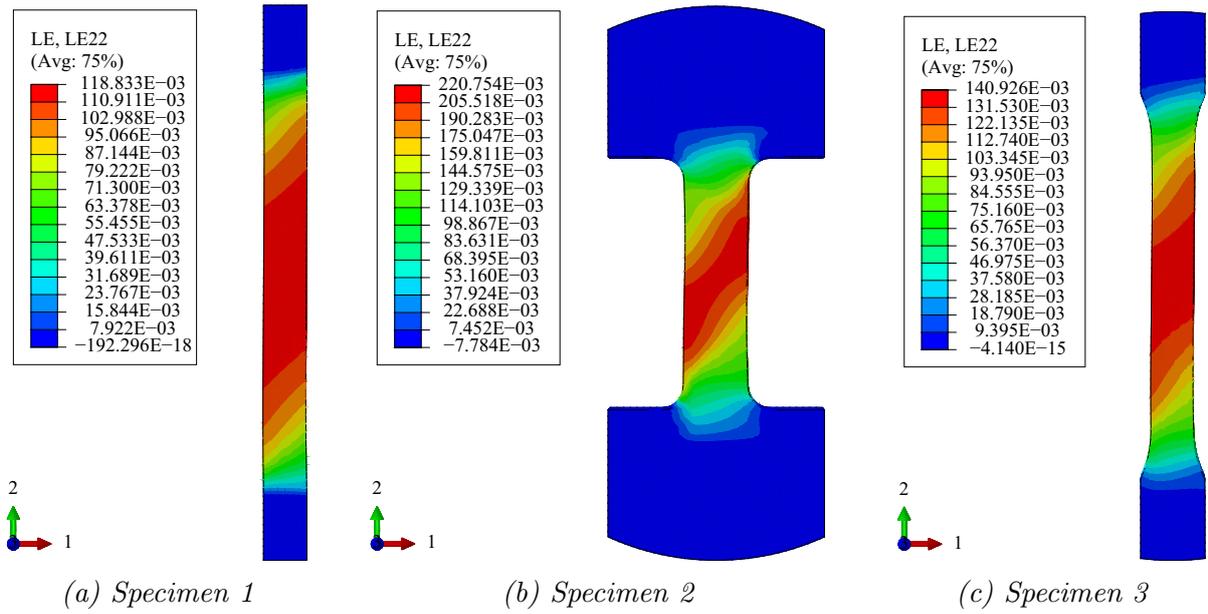
(a) Specimen 1   (b) Specimen 2   (c) Specimen 3

Figure 7.10: Contour plots of the logarithmic strain in tension direction ε_{22}^{ln}

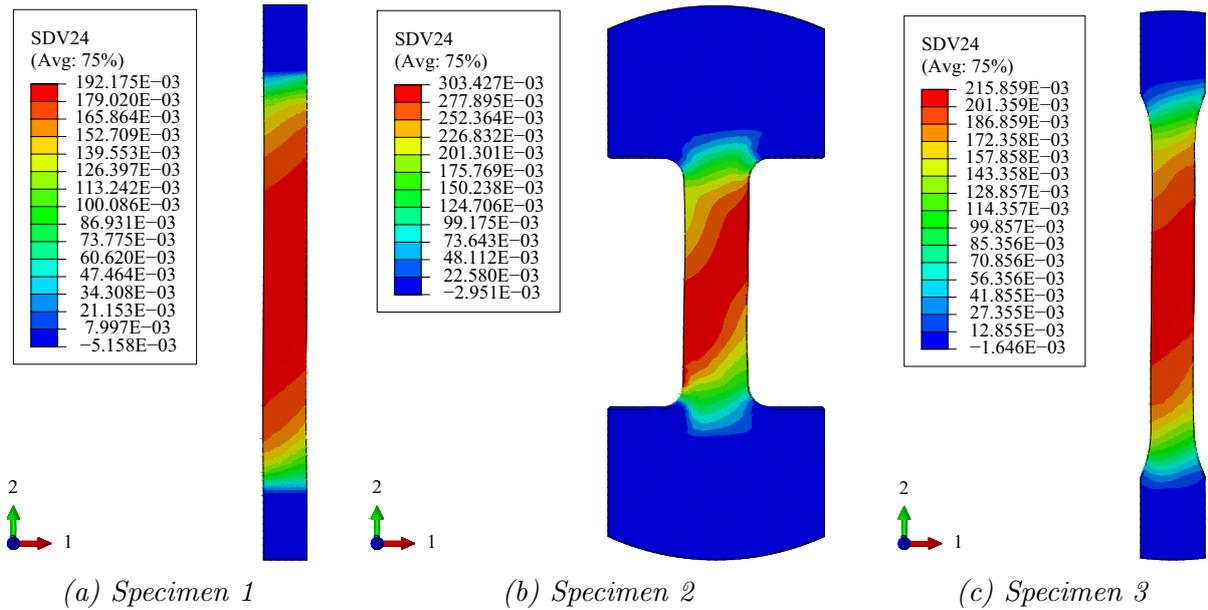(a) Specimen 1   (b) Specimen 2   (c) Specimen 3

Figure 7.11: Contour plots of the accumulated plastic strain γ^5 on slip system 5

in figures 7.13a–7.13c. Clearly the activation region of slip system 5 for Specimens 1 & 3 is uniform along the complete length between the specimens's grips. In contrast, the contours for Specimen 2, illustrate that plasticity on system mainly occurs in the narrow tensile region, but system 5 is also locally active near the grip location.

Finally, figures 7.14a–7.14c illustrate the contours of the Von Misses equivalent stress and figures 7.15a–7.15c display the contour plots of the number of active systems at the end of the uniaxial tension experiment. Ideally, the specimen used for the tension experiment should result in a uniform number of active systems somewhere in the region between the
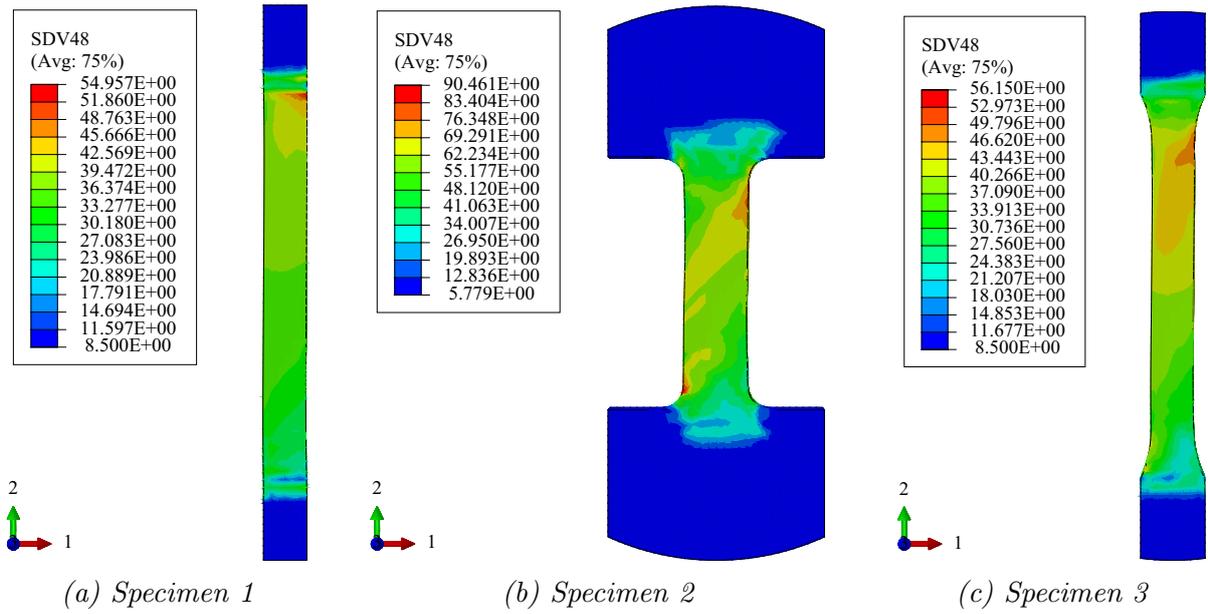
(a) Specimen 1   (b) Specimen 2   (c) Specimen 3

Figure 7.12: Contour plots of the critical shear stress τ_{cr}^5 of slip system 5

(a) Specimen 1   (b) Specimen 2   (c) Specimen 3
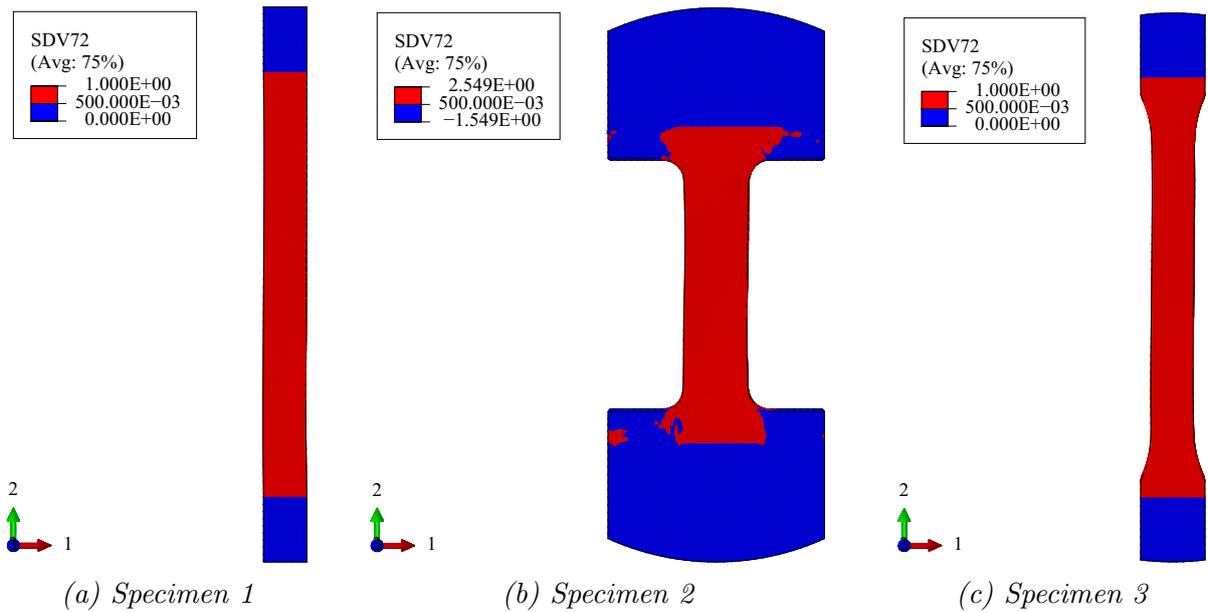
Figure 7.13: The activation region of slip system 5

grips. In contrast to Specimens 1 and 3, specimen 2 fails to facilitate the activation of a uniform number of slip systems. This particular observation raises concerns regarding the adequacy of Specimen 2 for use in uniaxial tension experiments of single crystals. From the analyses we conducted, Specimen 3 seems to embody the ideal shape, behaving remarkably similar to Specimen 1. The latter, even though it presents the simplest possible geometry for a uniaxial tension specimen, cannot be used in a real world experiment.

The force–displacement data were also extracted for each specimen by incrementally saving the upper grips' reaction force for a given displacement. Using the initial tensile

(a) Specimen 1   *(b) Specimen 2*   *(c) Specimen 3*
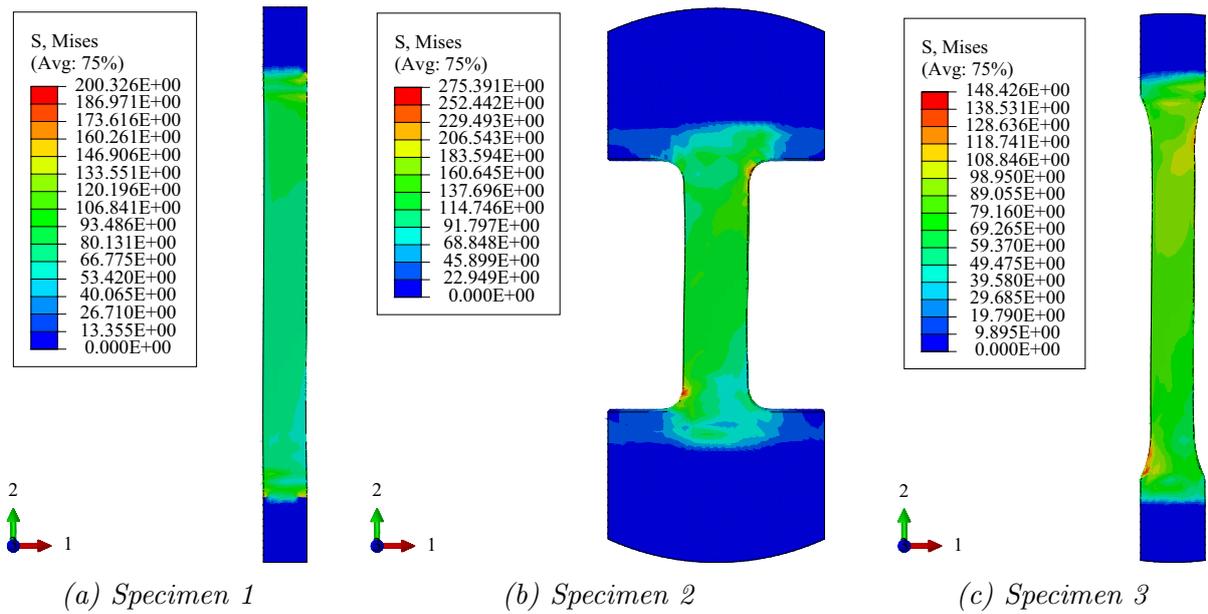
Figure 7.14: Contours of the Misses equivalent stress $\sigma|_e$

(a) Specimen 1   *(b) Specimen 2*   *(c) Specimen 3*
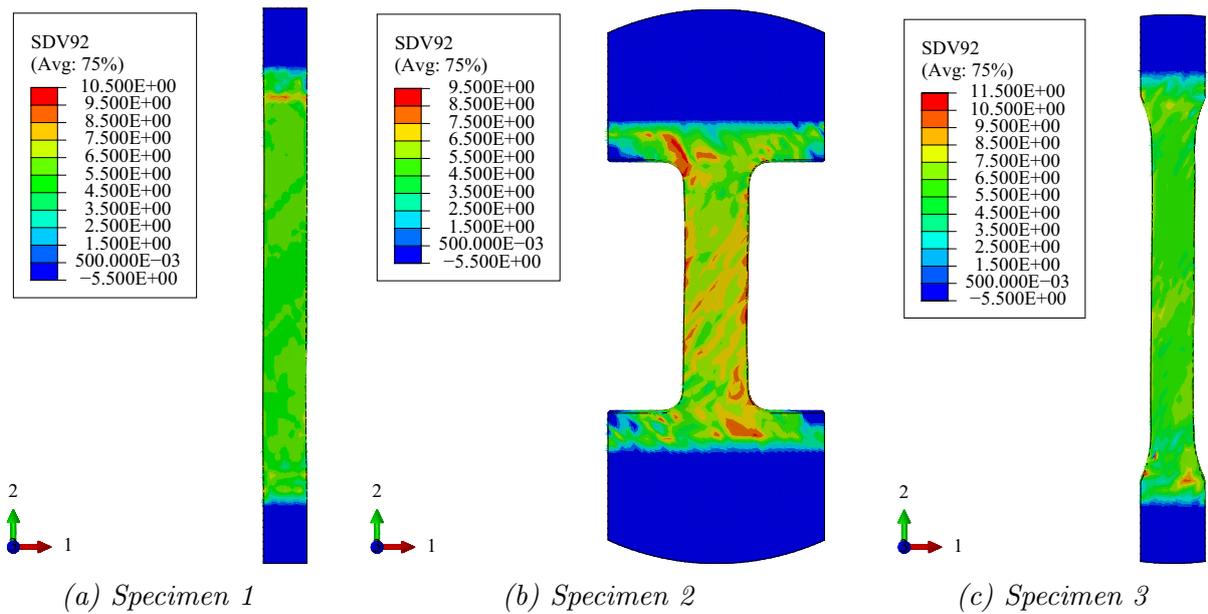
Figure 7.15: Contours plots showing the total number of active systems after imposing the uniform displacement field

lengths and cross sections for each specimen, the f–δ curves were converted to nominal stress ($\mathbf{T}$)–nominal strain (e) curves. Figure 7.16 presents the comparative results after the application of a $1.8mm$ displacement for each specimen. The curves are in almost complete agreement with each other and the minor discrepancies can be attributed to the inability for an accurate estimate of the 'actual' tensile lengths of Specimens 2 and 3.

Figure 7.16: The nominal strain e–nominal stress T curves for the uniaxial tension of Specimens 1,2 and 3 after a uniform elongation of 1.8mm

7.3 Stress Update Algorithms

In the present section we address the issue of determining the set of active systems $\mathscr{A}$ by implementing the three different stress–update algorithms presented in Chapter 5. I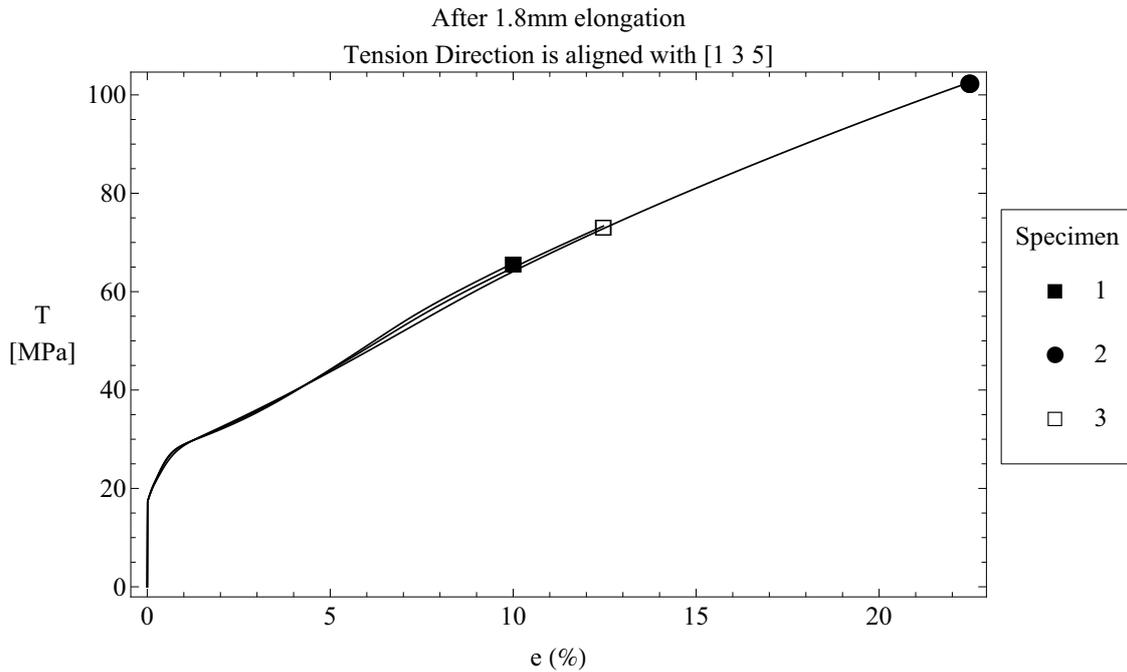n particular, we investigate the effect of the stress–update algorithm being used in the accuracy of the active systems set prediction, during the uniaxial tension of a single finite element (*see* Section 7.1). We are also interested in comparing the 'computational requirements' of each algorithm, to determine which (if any) is the most suitable for use in the finite element analysis of models with many degrees of freedom.

At first, we conducted three uniaxial tension analyses on the single–element model, using a diagonal hardening moduli $h^{\alpha\beta}$, $(q = 0)$ to ensure that the Jacobian matrix $(\partial\phi^{\alpha}/\partial\Delta\gamma^{\beta})$ is symmetric[13]. The single–element was subjected to unconstrained uniaxial deformation as described in Section 7.1 and for every analysis the incremental active set prediction was accomplished using the heuristic algorithm, a non–linear optimization subroutine and a linear optimization algorithm respectively. The nonlinear optimization was executed by the CON-MAX [33] subroutine, that is able to solve a class of nonlinearly constrained optimization problems. To compare the algorithms, we extracted the true stress–logarithmic strain points for each analysis and the results are comparatively displayed in Figure 7.17.

Clearly, the curves are in complete agreement, suggesting that the three stress–update

---

[13]The symmetry of the Jacobian matrix is a prerequisite for the implementation of the linear optimization algorithm. Including the latent hardening phenomena in the form $h^{\beta\alpha} = q\,h^{\alpha\alpha}$ leads to a non–symmetric hardening moduli and therefore, a non–symmetric Jacobian matrix

algorithms incrementally converge to the same active set $\mathscr{A}$ and plastic slips $\Delta\gamma^\alpha$. This not only corroborates the proper formulation of the optimization algorithms and their implementation as a direct alternative to the heuristic algorithm, but also validates the predictions made by the latter.
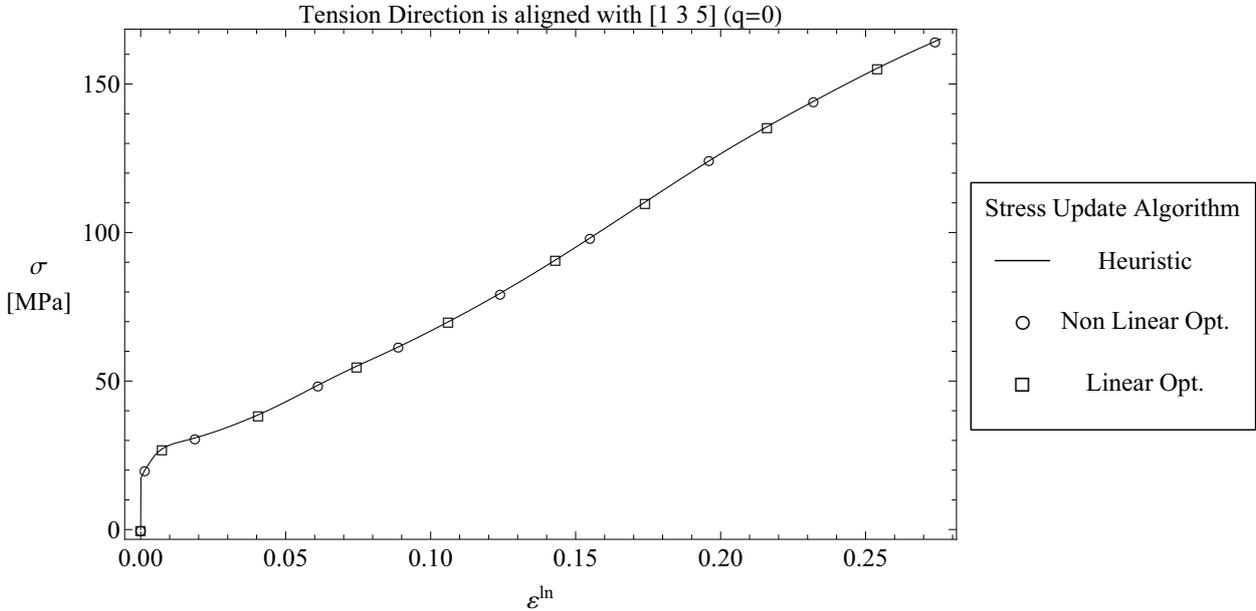

Figure 7.17: A comparison of the heuristic and optimization based stress update algorithms in the form of a true stress–logarithmic strain curve for the uniaxial tension of a single element. Latent hardening is ignored $(q = 0)$

The heuristic algorithm, which is summarized in Table 5.1 and Figure 5.2, is able to perform robust predictions for the set of active systems $\mathscr{A}$ and is fairly stable even for large time increments. Assigning $\mathscr{A}_{n+1} = \mathscr{A}_n$ as a fist estimate is not a bad estimate of the actual set for monotonous loading cases. In addition, even when the first estimate fails to meet the convergence criteria, emptying the set $\mathscr{A}_{n+1} = \emptyset$ guarantees that it will populate with the correct systems within a few iterations.

Concerning the optimization algorithms, the linear optimization option performs almost identical predictions with the heuristic algorithm, while consuming practically the same computational resources per increment and integration point. On the other hand, the nonlinear optimization approach requires dramatically greater time to predict the set of active systems in the form of the solution of the nonlinear minimization problem. Table 7.4 illustrates the average times[14] required by each algorithm per increment and integration point for the finite element analysis of a single C3D8H finite element.

---

[14]Even though in general those times depend on the available computational resources, the cpu–time required for single–element analyses using the Abaqus [1] FEA software is relatively the same on every machine

Table 7.4: Actual time required (sec) per integration point for the successful completion of one increment using the heuristic, the nonlinear optimization and the linear optimization algorithms respectively

	Heuristic	Nonlinear Opt.	Linear Opt.
sec/inc,ipt	0.017995	8.1527	0.018366

The nonlinear optimization algorithm, requires on average 453 times greater processing time per increment and integration point than the other two options. Clearly then, the nonlinear optimization approach does not present a realizable alternative to neither the heuristic, nor the linear optimization algorithm for multi finite element analyses. However, the fact that the nonlinear optimization is so time consuming is not a surprise. Recall that CONMAX incrementally solves an optimization problem with respect to 48 decision variables (*see* Section 5.2) for every integration point of every finite element in the model. If for instance we tried to perform an analysis on Specimen 1 using CONMAX to predict the active set, for every increment the program would have to solve 9936 optimization problems with 48 decision variables and 48 constraints each!

Subsequently, we subjected Specimen no.3 (*see* Figure 7.8c) to uniaxial tension imposing a uniform displacement field along the tension direction. The heuristic and linear optimization algorithms were then tested successively. The latent hardening phenomena were taken into account by the hardening model in both cases in the following sense,

$$h^{\beta\alpha} = q(h^{\alpha\alpha} + h^{\beta\beta}) \quad \alpha \neq \beta$$

with $q = 0.001$, building a symmetric hardening moduli $h^{\alpha\beta}$. Figure 7.18 illustrates the nominal stress–nominal strain curves corresponding to each algorithm predicting the set of active systems. The T–e curves were created using the output data points for the reaction force and displacement for the upper grip respectively.

The curves are again in perfect agreement, and the time required for both analysis was roughly the same suggesting that the linear optimization formulation constitutes a realizable alternative to the heuristic algorithm. However, we are forced to use a hardening model that would result into a symmetric $h^{\alpha\beta}$ moduli, whereas the heuristic algorithm do not poses such constraints.

7.4 Crystal Orientation Sensitivity Analysis

The relative orientation of the crystal lattice with respect to the loading direction in a uniaxial tension experiment is a very important issue for both computational and experimental crystal plasticity. The initial crystal orientation prior to uniaxial tension, ultimately defines the slip systems that are going to activate during the experiment, their order of activation, the existence of the easy glide stage, the 'amount' of the crystal system's rotation and so
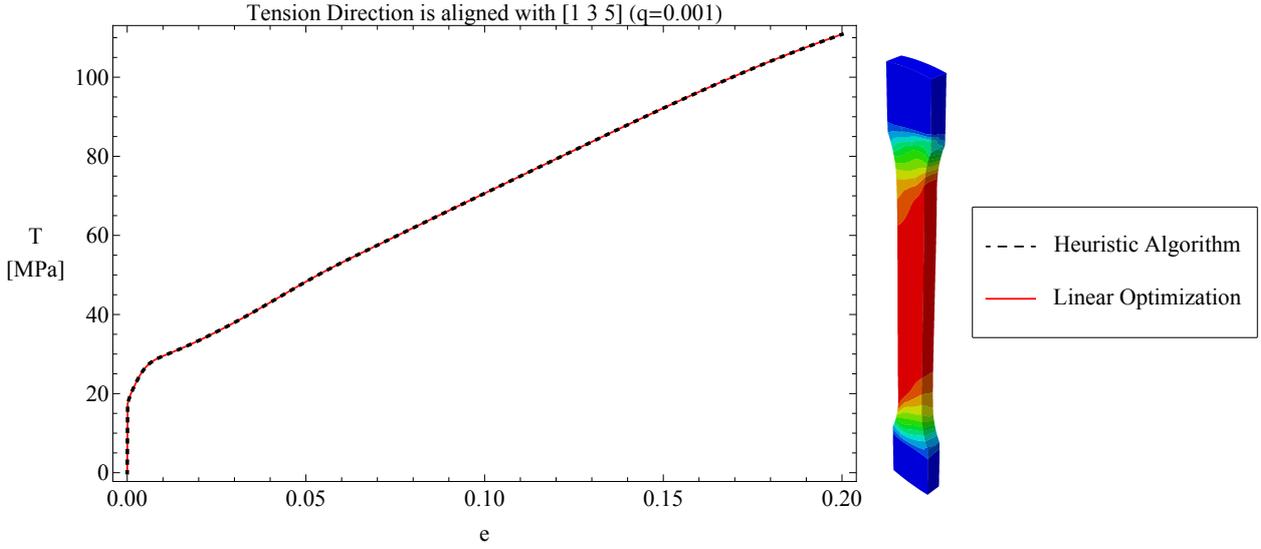
Figure 7.18: True stress–logarithmic strain curves for the uniaxial tension of a single crystal specimen. The two curves where extracted using the heuristic stress–update algorithm and the linear optimization formulation to determine active systems respectively

on. In the following section we investigate the effect of the crystal's initial orientation to deformation in uniaxial tension, in the form of a sensitivity analysis, quantifying the results in comparative graphs and contour plots.

Motivated by the experimental investigations of Diehl [25] presented in the works of Honeycombe [31], we subjected the single finite element to a series of uniaxial tension analyses. The tension direction was successively aligned with a different crystal direction for every finite element analysis, through the definition of the transformation matrix between the crystal and global axes. The stereographic projections of all the crystal directions under consideration are assumed to lie on the standard triangle[15]. To facilitate the description of points within the triangle, we introduce the auxiliary coordinates (r, Θ) in the following sense.

Any crystal direction $\mathbf{p}$ can be written with respect to the crystal axes $\mathbf{n}^{(i)}$ in terms of it's spherical components as:

$$\mathbf{p} = \sin\theta(\cos\phi\,\mathbf{n}^{(1)} + \sin\phi\,\mathbf{n}^{(2)}) + \cos\theta\,\mathbf{n}^{(3)}$$

The corresponding stereographic projection vector can then be written in the form:

$$\boldsymbol{\rho} = r(\cos\Theta\mathbf{n}^{(2)} + \sin\Theta\mathbf{n}^{(3)})$$

where

$$\tan\Theta = (\tan\theta\,\sin\phi)^{-1} \qquad \text{and} \qquad r = \sqrt{\frac{(\sin\theta\,\sin\phi)^2 + \cos^2\theta}{(1 + \sin\theta\,\cos\phi)^2}}$$

Then, the region inside the standard triangle can be defined as the collection of points for

---

[15]without any loss of generality

which $\Theta \in [0, \pi/4]$ and $r \in [0, R_{max}(\Theta)]$, with:

$$R_{max}(\Theta) = \sqrt{1 + \cos^2 \Theta} - \cos \Theta$$

The new set of coordinates (r, Θ) is schematically illustrated within the standard triangle in Figure 7.19 that follows. In order to 'scan' a representative area of the standard triangle, we consider the points that correspond to $\Theta = 0^o, 9^o, 18^o, 27^o, 36^o, 45^o$ and $r/R_{max} = 0, 0.2, 0.4, 0.6, 0.8, 1$ which are displayed in Figure 7.20.
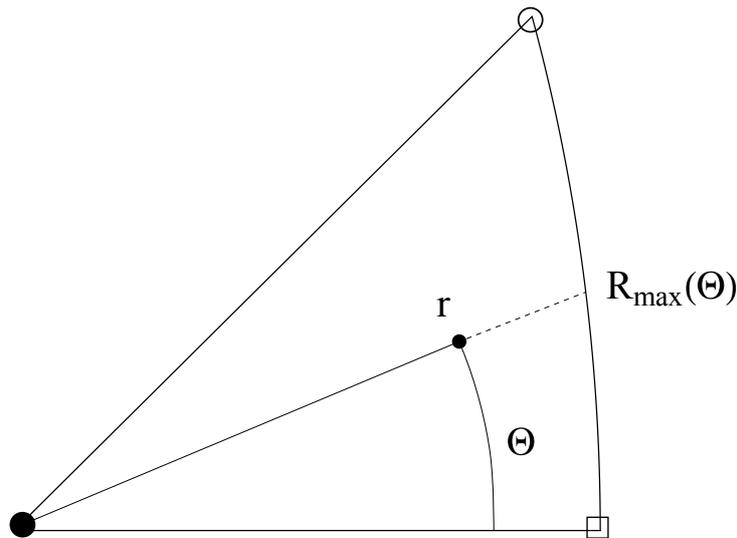

Figure 7.19: A schematic representation of the auxiliary coordinates (r, Θ) that facilitate the description of projections inside the standard triangle

Assuming that the tension direction is successively aligned with the crystal direction implied by the point under consideration, every coloured marker in Figure 7.20 essentially represents a different crystal orientation. In this sense then, every coloured marker corresponds to a finite element analysis and 31 finite element analyses were required in total to extract the comparative results. In all finite element simulations, the finite element was subjected to the **same–uniform force field** and the active systems were determined by making use of the heuristic stress–update algorithm. Also, all analyses were performed using the same time incrementation.

Figures 7.21a–7.21f illustrate the true stress–logarithmic strain curves that correspond to each finite element analysis. The results were grouped so that each figure demonstrates the σ–$\varepsilon^{\ln}$ curves for constant Θ and varying r/R_{max}.

The qualitative 'variaty' of the resulting σ–$\varepsilon^{\ln}$ curves, validates the preliminary hypothesis that the plastic behavior of single crystals strongly depends on the initial crystal's orientation with respect to the loading direction. Even though the same force field was applied in all cases, the overall behavior varies substantially for different orientations. For orientations corresponding to $\Theta = 0^o$ for instance (Figure 7.21a), the crystal exhibits logarithmic strains that vary from 2% up to 50% for r/R_{max} equal to 0 and 0.6 respectively. In fact, the σ–$\varepsilon^{\ln}$
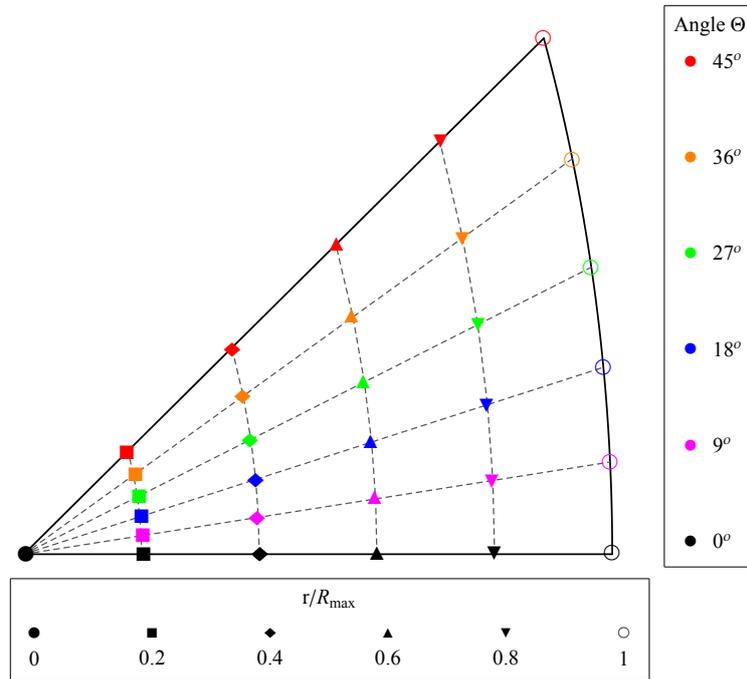
Figure 7.20: Each coloured point in the standard triangle corresponds to a crystal direction. The crystal is initially oriented so that the tension direction is parallel to the crystal direction implied by every point and finite element analyses are conducted successively

curve for $(0.6R_{max}, 0^o)$, is almost identical to the hardening curve in Figure 3.3 which was drawn qualitatively, based only on the 'physics' of dislocation motion and their interactions. In particular, the σ–$\varepsilon^{\ln}$ curve exhibits a prolonged Stage I[16], while also clearly displaying the linear hardening and dynamic recovery stages.

Finally, the resulting curves all together, are very close to the experimental results of Diehl [25], although the comparison has only qualitative sense since Diehl conducted experiments on copper single crystals.

Subsequently, we conducted a second series of similar analyses in an effort to obtain a comprehensive supervision of the crystal's orientation 'sensitivity'. Particularly, representing the orientation dependance of a macroscopic or internal variable in the form of a contour plot, would facilitate perception regarding 'how' the variable being plotted is affected by the crystal's orientation. A typical macroscopic variable of interest would be the logarithmic strain in tension direction and the respective contours at the end of the tension experiment. The contours of $\varepsilon^{\ln}$ in the standard triangle for instance, would facilitate the division of the standard triangle into 'softer' and 'harder' regions[17]. On the other hand, we could also draw the contours of internal variables such as the critical stress or plastic strain on a given slip system. These plots, would inform us about which 'orientations' facilitate the activation of a given slip system, but also facilitate the perception of latent hardening phenomena[18].

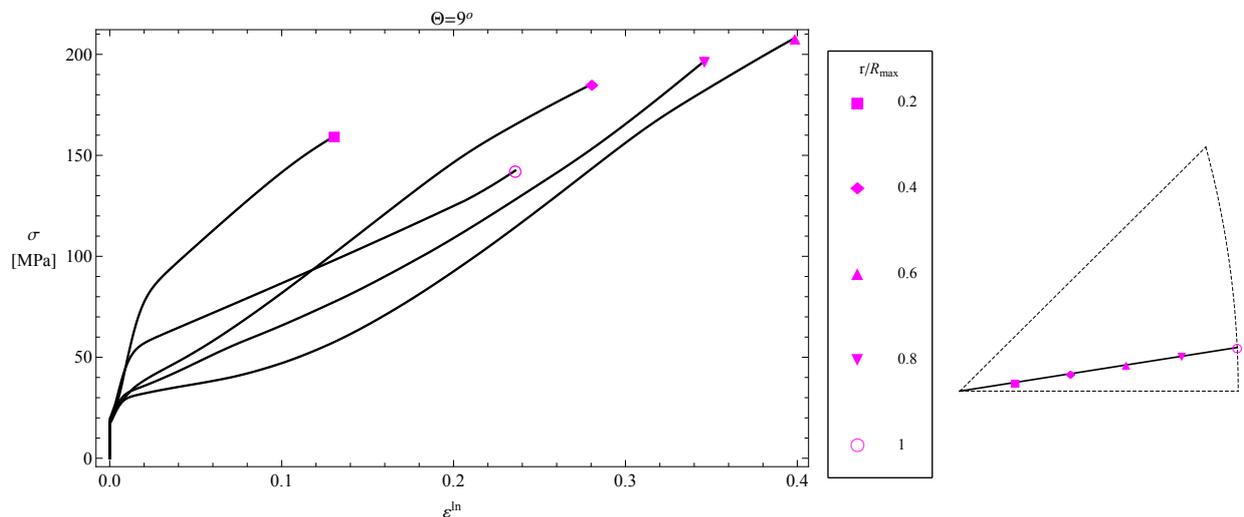[16]implying that that the point $(0.6R_{max}, 0^o)$ corresponds to an easy glide orientation

[17]Recall that we apply a fixed uniform force field

[18]It is not clear how at this point. We will focus on how the aforementioned contour plots can be used to
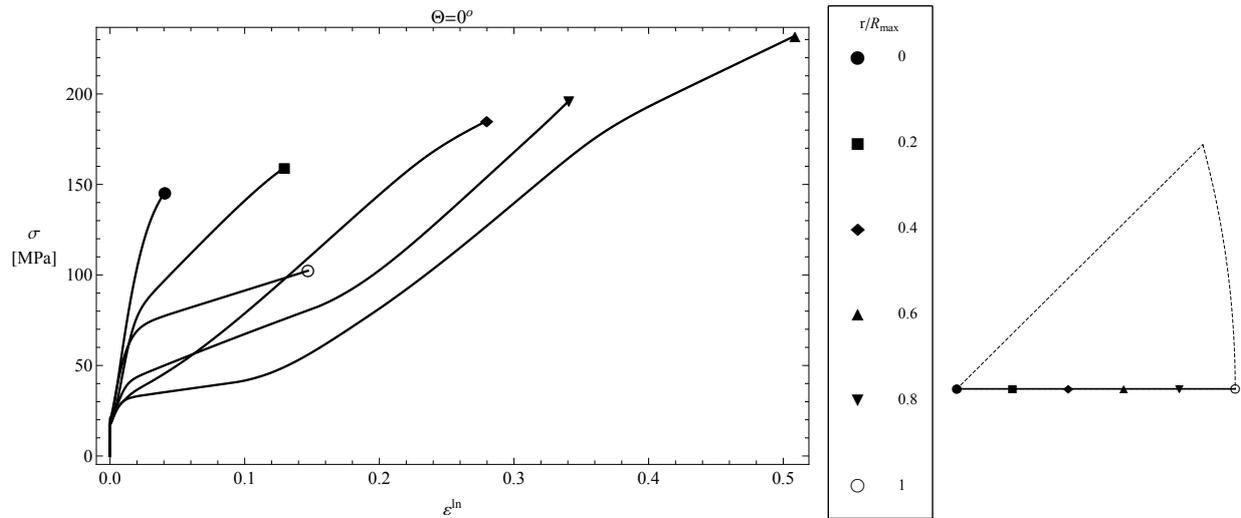
(a) Curves for $\Theta = 0^o$ and varying r/R_{max}

(b) Curves for $\Theta = 9^o$ and varying r/R_{max}

Based on Figure 7.20, we conducted uniaxial tension analyses aligning different crystal directions with the tension direction. However, the 31 analysis points used to extract the σ–ε^{ln} curves do not suffice for the construction of a high quality contour plot. To make sure that the output information would be sufficient to draw the contours for each variable, we considered the analyses points indicated by the coloured markers in Figure 7.22.

The coloured markers imply that a total of 111 finite element analyses was necessary. In an effort to minimize the post–processing time required to extract the results for every analysis, we developed a URDFIL[19] Abaqus [1] subroutine, to work in conjunction with the UMAT subroutine.

Figures 7.23 and 7.24a–7.24m that follow demonstrate the contour plots for ε^{ln} as well as

---

get a sense of latent hardening intensity, later on when we present the contour plots themselves

[19]URDFIL subroutines are capable of accessing the .fil results file of the desired Abaqus job, to automatically extract and save any results requested
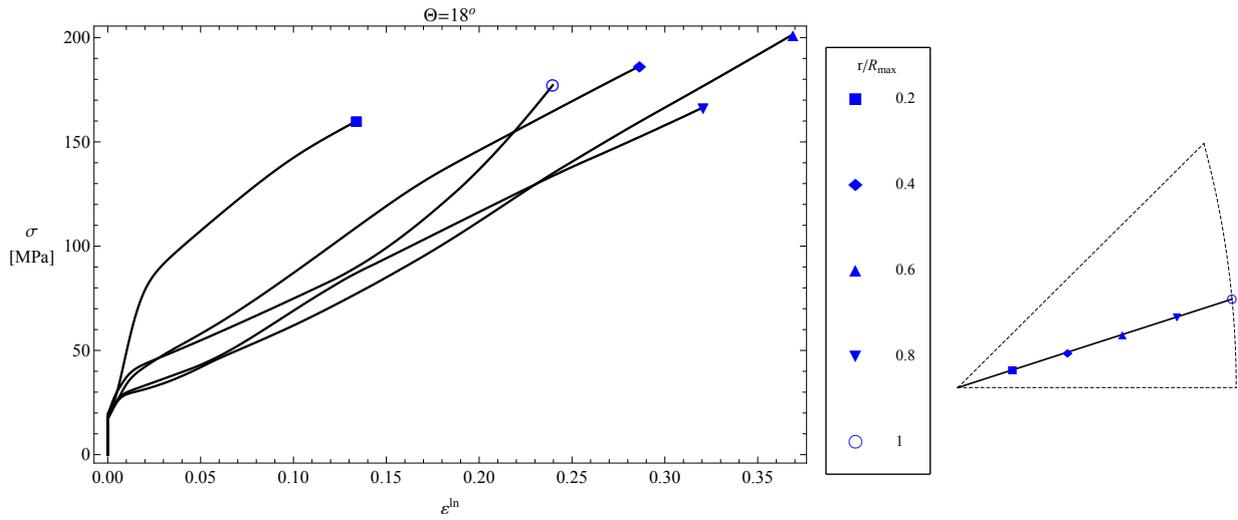
(c) Curves for $\Theta = 18^o$ and varying r/R_{max}
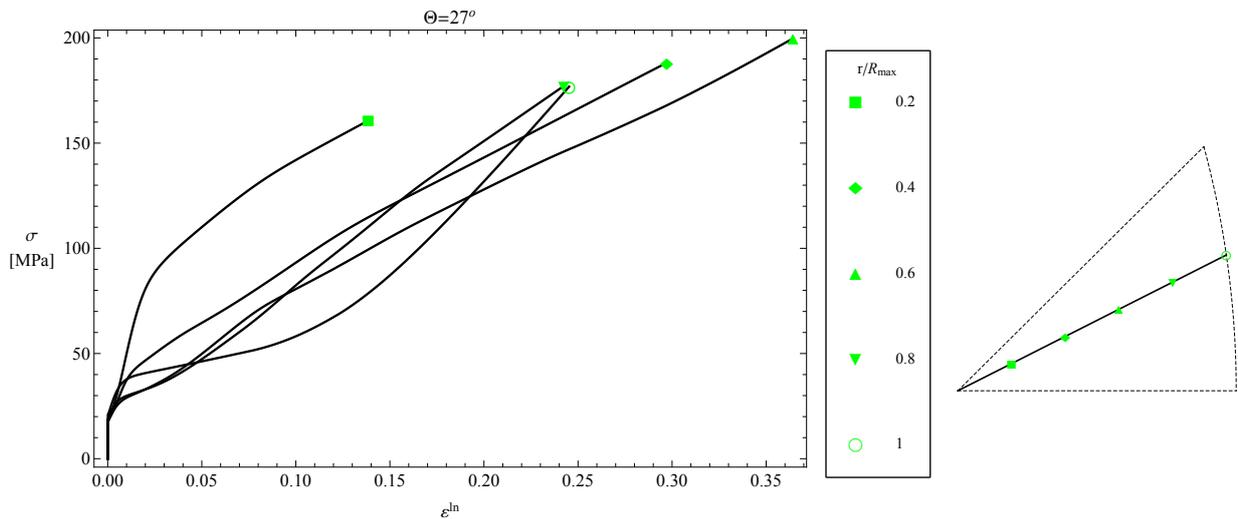
(d) Curves for $\Theta = 27^o$ and varying r/R_{max}

for the critical stresses and plastic strains for all slip systems that were activated in at least one of the 111 analyses. The contours are drawn in the standard triangle to illustrate their dependence on the chosen crystal orientation.

The contour plot of $\varepsilon^{\ln}$ shown in Figure 7.23, can be interpreted as follows. Red tinted areas correspond to crystal orientations for which the macroscopic logarithmic strain is greater, for a fixed force field, and therefore constitute the triangle's 'softer' regions. In contrast, blue tinted regions, constitute the 'harder' regions, since they correspond to smaller $\varepsilon^{\ln}$ for a given F. It is also worth mentioning that the region classification implied by Figure 7.23, is almost identical to the classification presented in the works of Honeycombe [31] based on the experiments by Diehl [25].

The plots illustrated in Figures 7.24a–7.24m display the contours of $\tau_{cr}^{\alpha}/\tau_0$ and γ^{α}/γ_0 side by side to ease comparison. The contours drawn, are based on the respective values at the
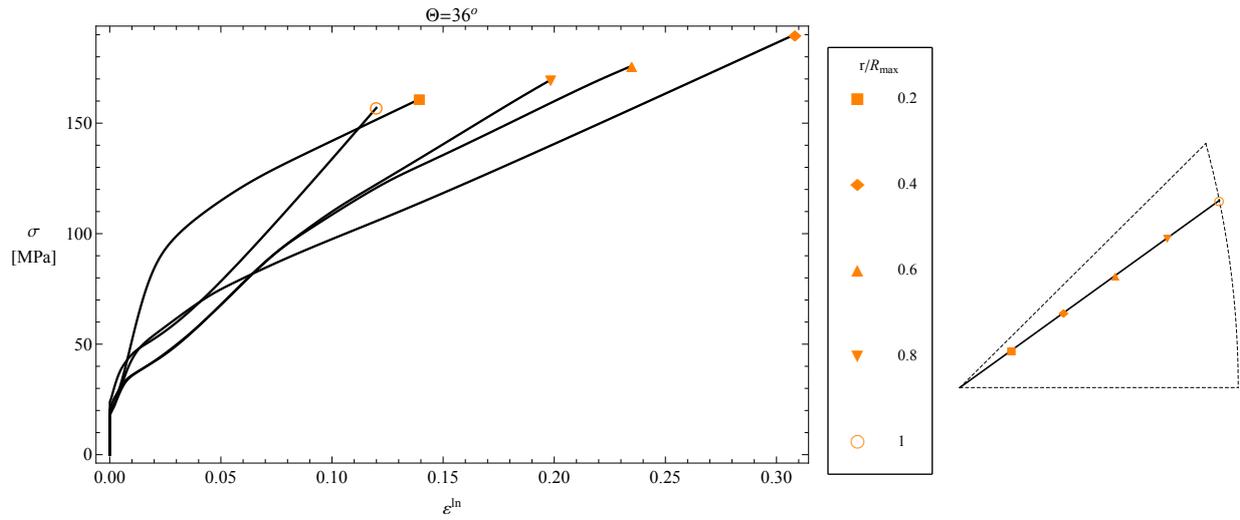
(e) Curves for $\Theta = 36^o$ and varying r/R_{max}
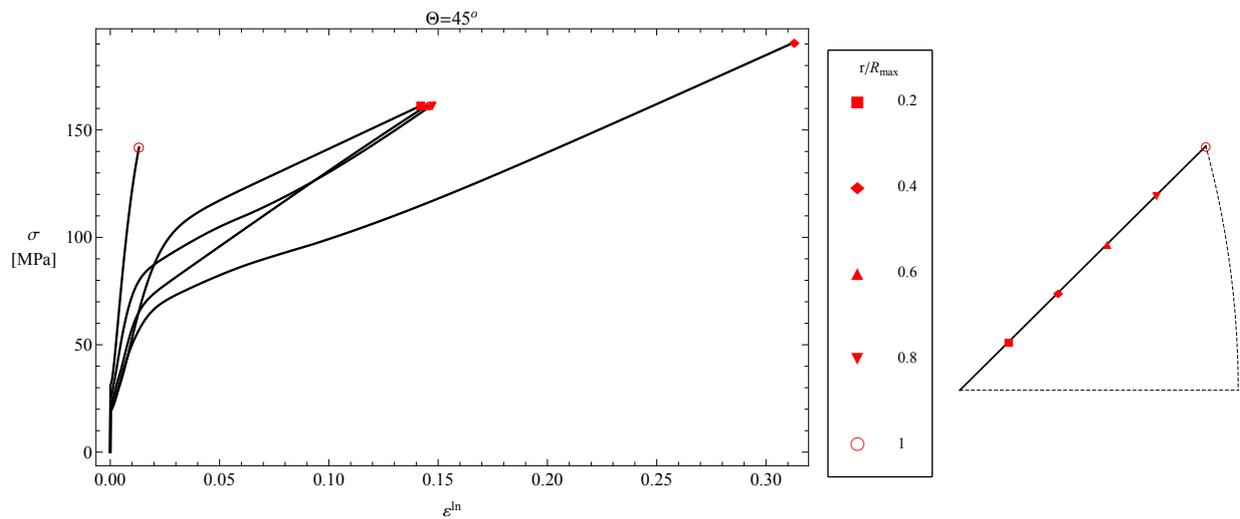
(f) Curves for $\Theta = 45^o$ and varying r/R_{max}

Figure 7.21: Comparison of true stress–logarithmic strain curves for various loading direction cases

end of each finite element analysis and are only presented for systems that were activated for at least 1 orientation case. The specific plots can be interpreted in more than one ways, two of which are discussed thereafter.

At first, the contour plots of γ^{α}/γ_0 straightforwardly illustrate which orientations promote the activation of slip system α in the form of 'regions' within the standard triangle. For instance, blue tinted regions represent orientations that do not facilitate the activation of the slip system under consideration. On the other hand, red tinted regions, indicate orientations for which the corresponding system is probably one of the primary active slip systems. The contour plots of $\tau_{cr}^{\alpha}/\tau_0$ on the other hand, cannot be used to determine a slip system's preferable orientations. If they are presented without being accompanied by the corresponding plot for γ^{α}/γ_0, their interpretation is limited to the supervision of the hardening model.
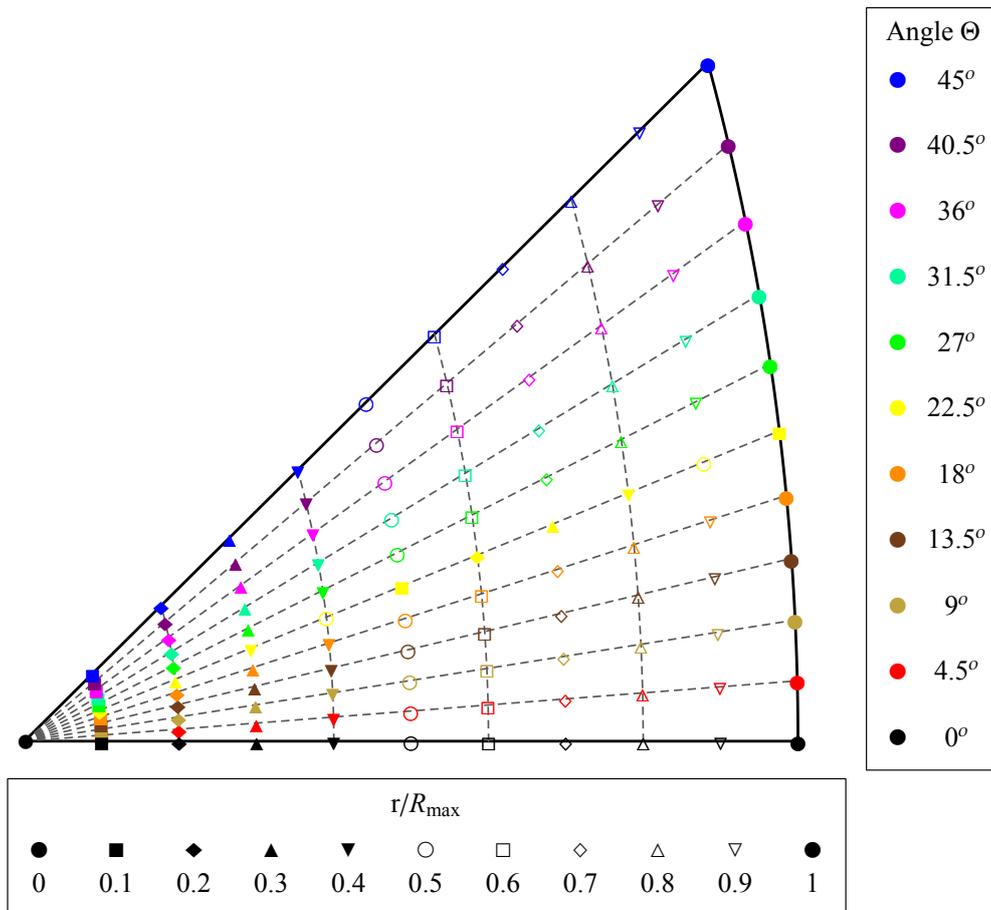
Figure 7.22: A finite element analysis is preformed for every coloured point in the standard triangle, assuming that the tension direction is aligned with the crystal direction implied by the point

If however both contours for $\tau_{cr}^{\alpha}/\tau_0$ and γ^{α}/γ_0 are to be interpreted together, they present perhaps one of the most perceivable illustrations for latent hardening. In particular, coloured –other than blue– regions of the $\tau_{cr}^{\alpha}/\tau_0$ contours, that correspond to a blue region in the γ^{α}/γ_0 contours are the result of latent hardening on system α. The latter is true, since the only way for a system to harden without being active, is through latent hardening. Alternatively, it is impossible to determine a blue area in the plot for $\tau_{cr}^{\alpha}/\tau_0$ if the same region in the respective plot for γ^{α}/γ_0 is not blue.

Finally, as shown below, we present a total of 13 plot pairs displaying the contours for $\tau_{cr}^{\alpha}/\tau_0$ and γ^{α}/γ_0, which means that, in total, 13 slip systems were activated in all the analyses performed. This is not unexpected, as it illustrates that each one of the 12 available slip systems for FCC crystals, will activate for at least one relative orientation implied by the standard triangle. In fact, the activation of 13 systems, indicates that one slip system did undergo both positive and negative slip, but not necessarily in the same analysis.

ε^{ln}

ε^{ln}
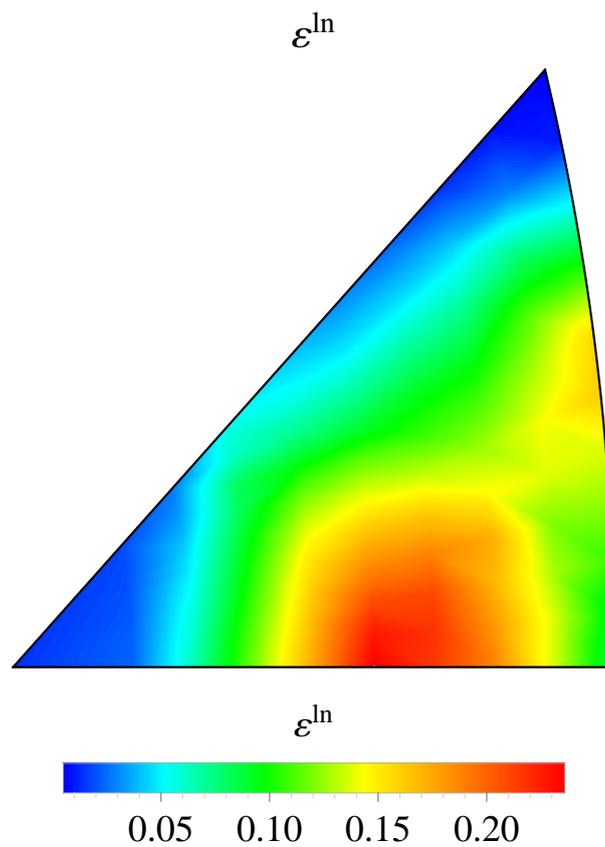
Figure 7.23: Contour plot of the macroscopic logarithmic strain in tension direction for the uni-axial tension of a single finite element. The contours illustrate the dependance of the resulting deformation from the crystal's initial orientation with respect to the loading direction
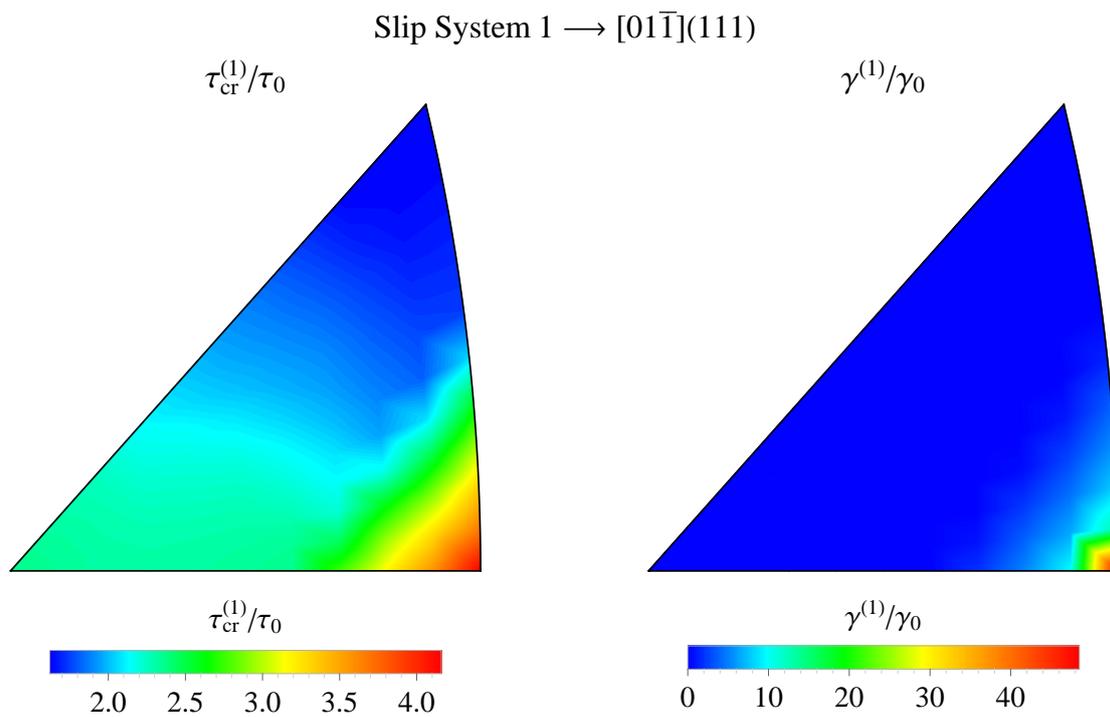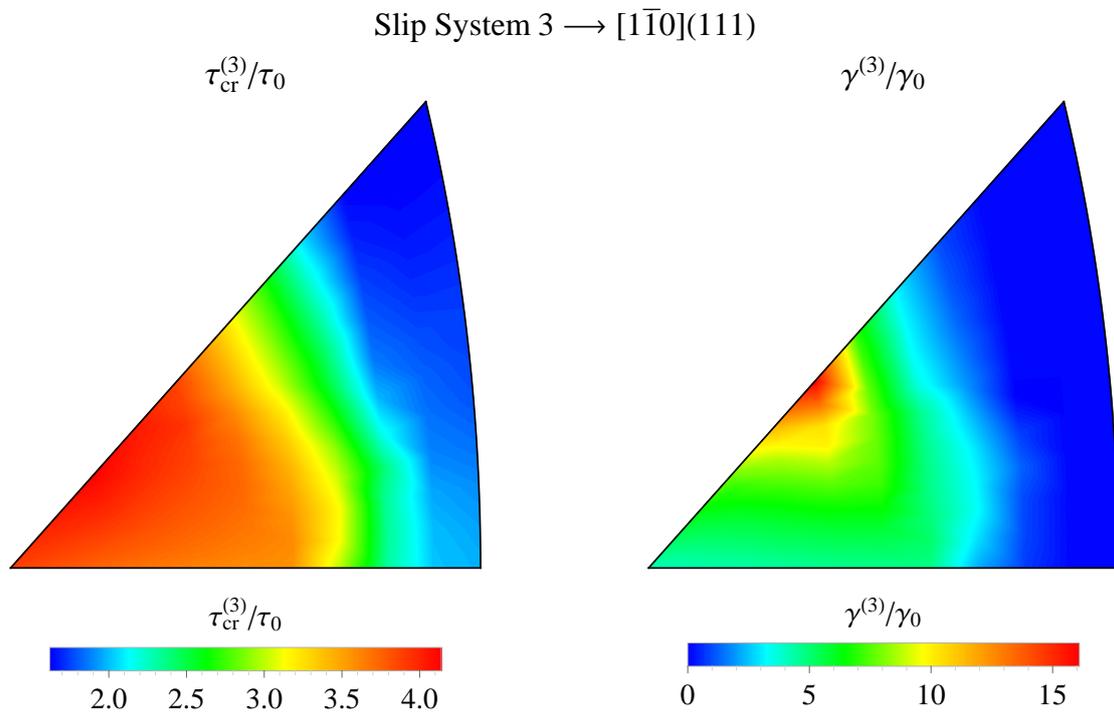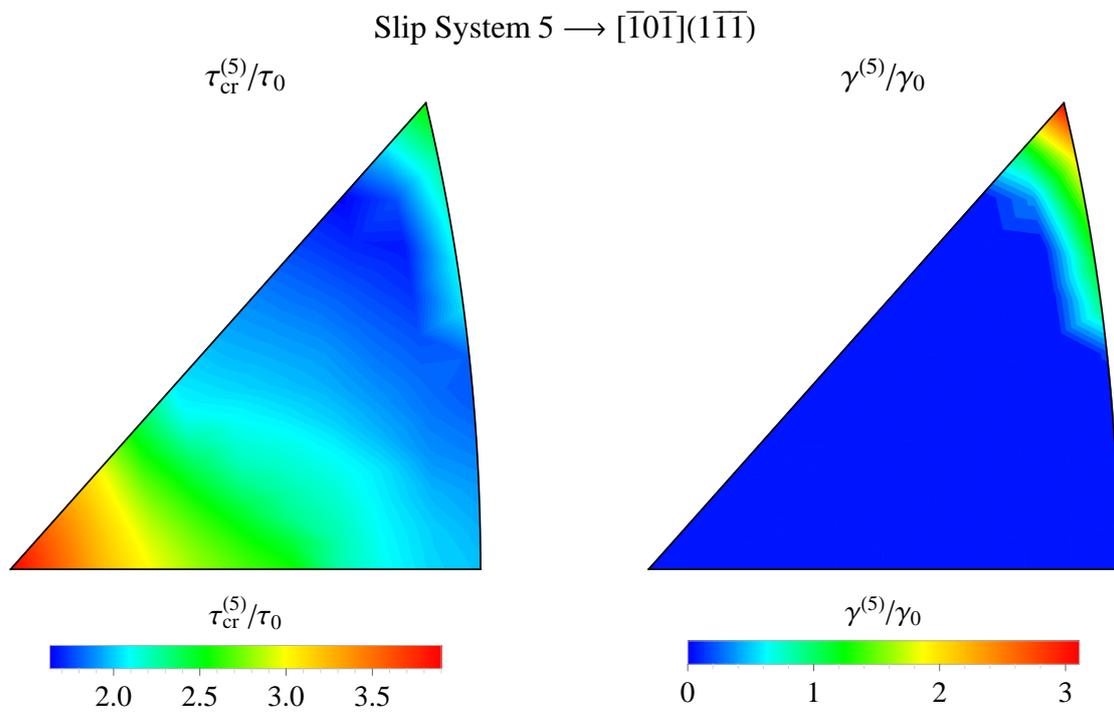
Slip System 1 $\longrightarrow$ $[01\bar{1}](111)$

$\tau_{\text{cr}}^{(1)}/\tau_0$ $\gamma^{(1)}/\gamma_0$

$\tau_{\text{cr}}^{(1)}/\tau_0$ $\gamma^{(1)}/\gamma_0$

(a) Slip System no.1

Slip System 3 $\longrightarrow$ [1$\bar{1}$0](111)

$\tau_{\mathrm{cr}}^{(3)}/\tau_0$

$\gamma^{(3)}/\gamma_0$

$\tau_{\mathrm{cr}}^{(3)}/\tau_0$

$\gamma^{(3)}/\gamma_0$

(b) Slip System no.3

Slip System 5 $\longrightarrow$ [$\bar{1}$0$\bar{1}$](1$\bar{1}\bar{1}$)

$\tau_{\mathrm{cr}}^{(5)}/\tau_0$

$\gamma^{(5)}/\gamma_0$

$\tau_{\mathrm{cr}}^{(5)}/\tau_0$

$\gamma^{(5)}/\gamma_0$

(c) Slip System no.5

Slip System 6 $\longrightarrow$ [110]($1\overline{1}\overline{1}$)

$\tau_{\mathrm{cr}}^{(6)}/\tau_0$

$\gamma^{(6)}/\gamma_0$

$\tau_{\mathrm{cr}}^{(6)}/\tau_0$

$\gamma^{(6)}/\gamma_0$

(d) Slip System no.6

Slip System 9 $\longrightarrow$ [$\overline{1}\overline{1}0$]($\overline{1}1\overline{1}$)

$\tau_{\mathrm{cr}}^{(9)}/\tau_0$

$\gamma^{(9)}/\gamma_0$

$\tau_{\mathrm{cr}}^{(9)}/\tau_0$

$\gamma^{(9)}/\gamma_0$

(e) Slip System no.9

Slip System 10 $\longrightarrow$ $[0\overline{1}\overline{1}](\overline{1}\overline{1}1)$

$\tau_{cr}^{(10)}/\tau_0$

$\gamma^{(10)}/\gamma_0$

$\tau_{cr}^{(10)}/\tau_0$

$\gamma^{(10)}/\gamma_0$

(f) Slip System no.10

Slip System 12 $\longrightarrow$ $[\overline{1}10](\overline{1}\overline{1}1)$

$\tau_{cr}^{(12)}/\tau_0$

$\gamma^{(12)}/\gamma_0$

$\tau_{cr}^{(12)}/\tau_0$

$\gamma^{(12)}/\gamma_0$

(g) Slip System no.12

Slip System 14 $\longrightarrow$ [10$\overline{1}$](111)

$\tau_{\mathrm{cr}}^{(14)}/\tau_0$

$\gamma^{(14)}/\gamma_0$

$\tau_{\mathrm{cr}}^{(14)}/\tau_0$

$\gamma^{(14)}/\gamma_0$

(h) Slip System no.14

Slip System 17 $\longrightarrow$ [101](1$\overline{1}\overline{1}$)

$\tau_{\mathrm{cr}}^{(17)}/\tau_0$

$\gamma^{(17)}/\gamma_0$

$\tau_{\mathrm{cr}}^{(17)}/\tau_0$

$\gamma^{(17)}/\gamma_0$

(i) Slip System no.17

Slip System 18 $\longrightarrow$ $[\overline{1}\overline{1}0](1\overline{1}\overline{1})$

$\tau_{\text{cr}}^{(18)}/\tau_0$

$\gamma^{(18)}/\gamma_0$

$\tau_{\text{cr}}^{(18)}/\tau_0$

$\gamma^{(18)}/\gamma_0$

(j) Slip System no.18

Slip System 19 $\longrightarrow$ $[0\overline{1}\overline{1}](\overline{1}1\overline{1})$

$\tau_{\text{cr}}^{(19)}/\tau_0$

$\gamma^{(19)}/\gamma_0$

$\tau_{\text{cr}}^{(19)}/\tau_0$

$\gamma^{(19)}/\gamma_0$

(k) Slip System no.19

Slip System 20 $\longrightarrow$ $[\bar{1}01](\bar{1}1\bar{1})$

$\tau_{\mathrm{cr}}^{(20)}/\tau_0$ $\gamma^{(20)}/\gamma_0$

$\tau_{\mathrm{cr}}^{(20)}/\tau_0$ $\gamma^{(20)}/\gamma_0$

2.0   2.5   3.0   3.5   0   1   2   3   4

(l) Slip System no.20

Slip System 23 $\longrightarrow$ $[\bar{1}0\bar{1}](\bar{1}\bar{1}1)$

$\tau_{\mathrm{cr}}^{(23)}/\tau_0$ $\gamma^{(23)}/\gamma_0$

$\tau_{\mathrm{cr}}^{(23)}/\tau_0$ $\gamma^{(23)}/\gamma_0$

3   4   5   50   100 150 200 250
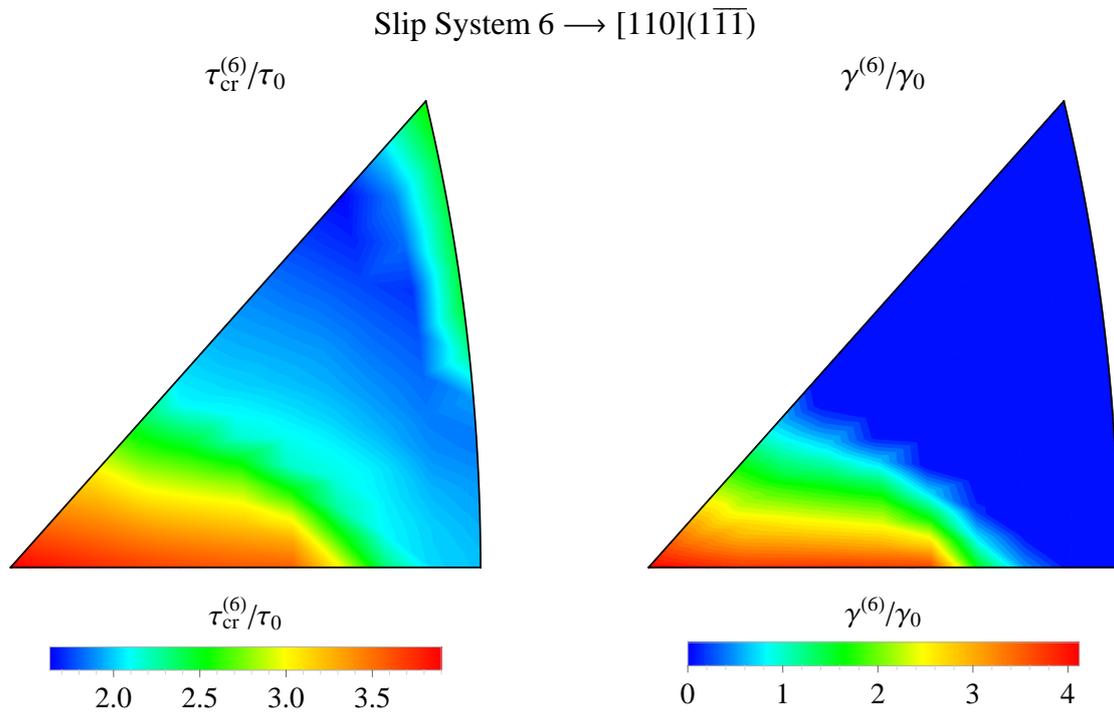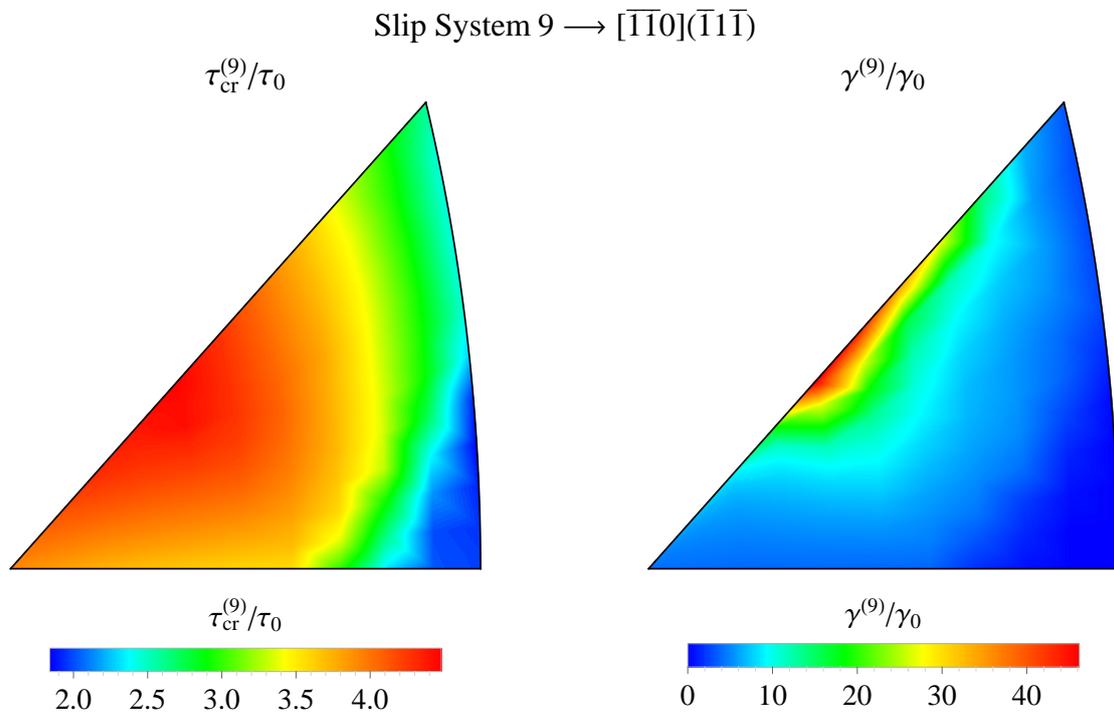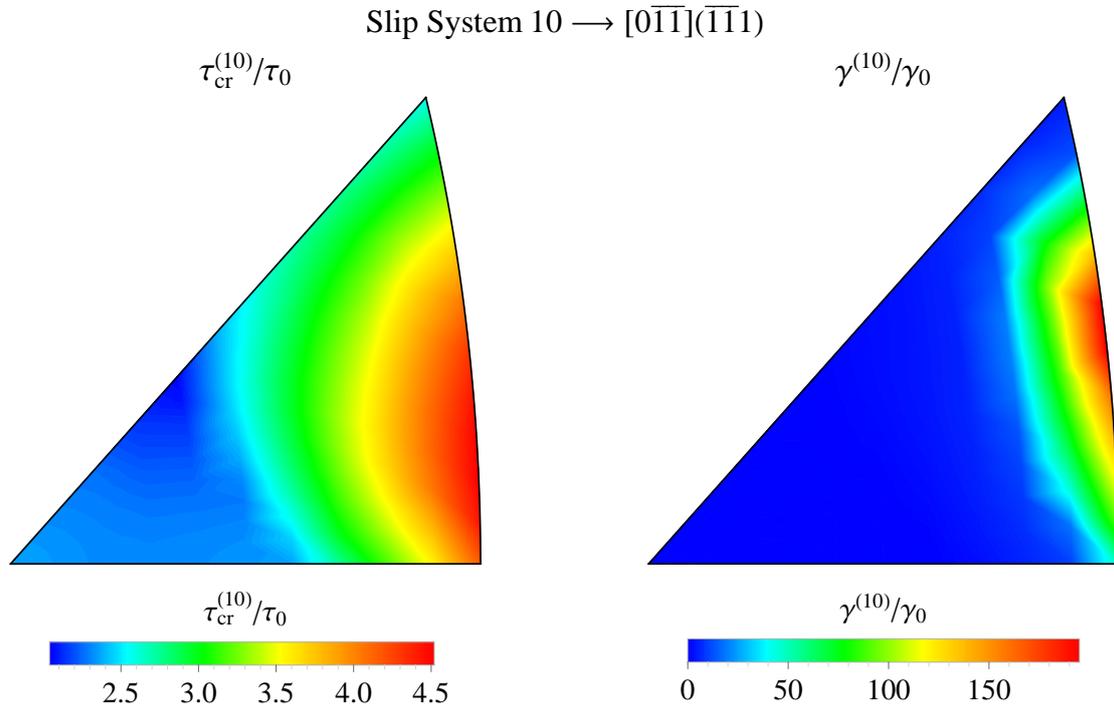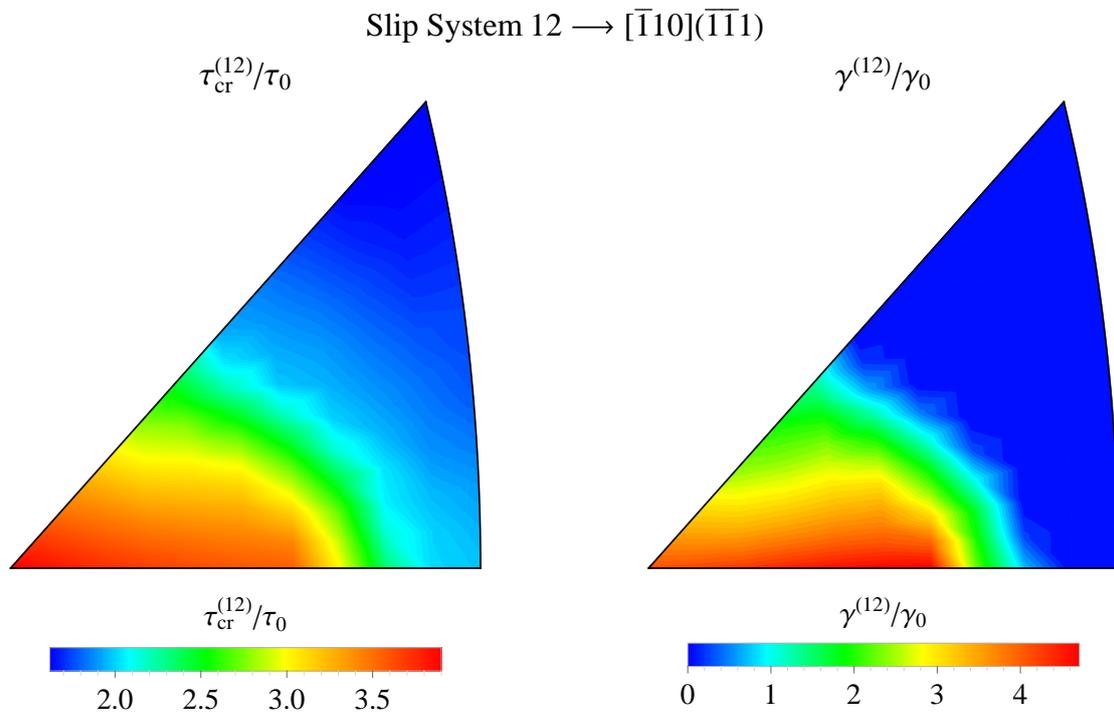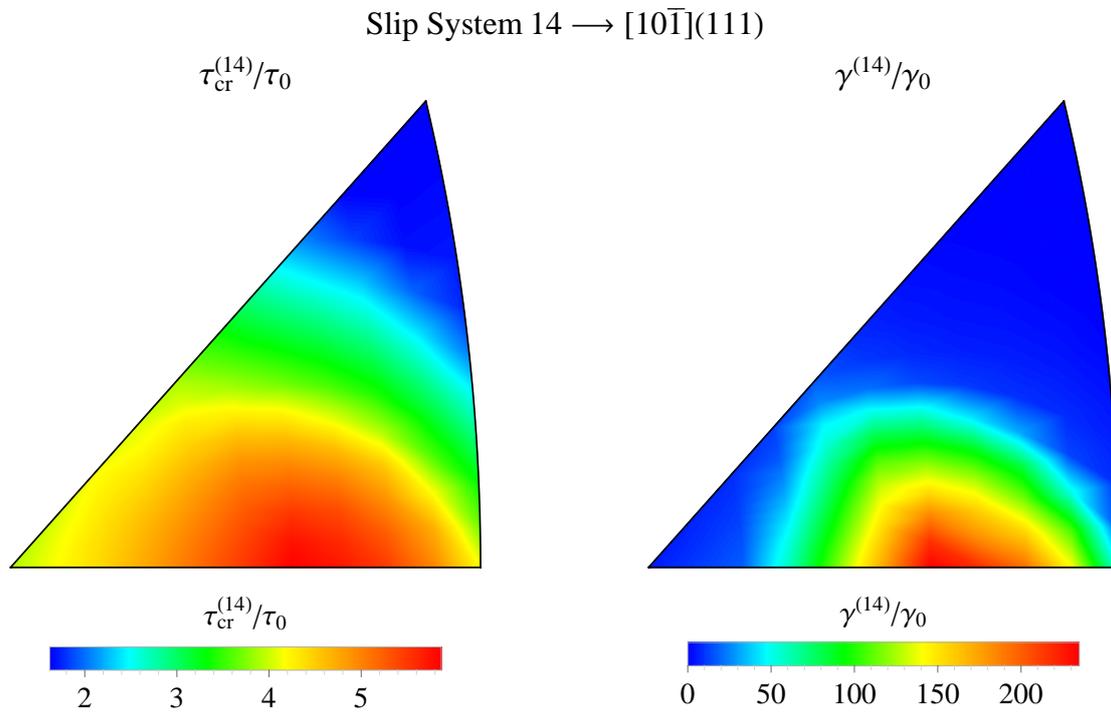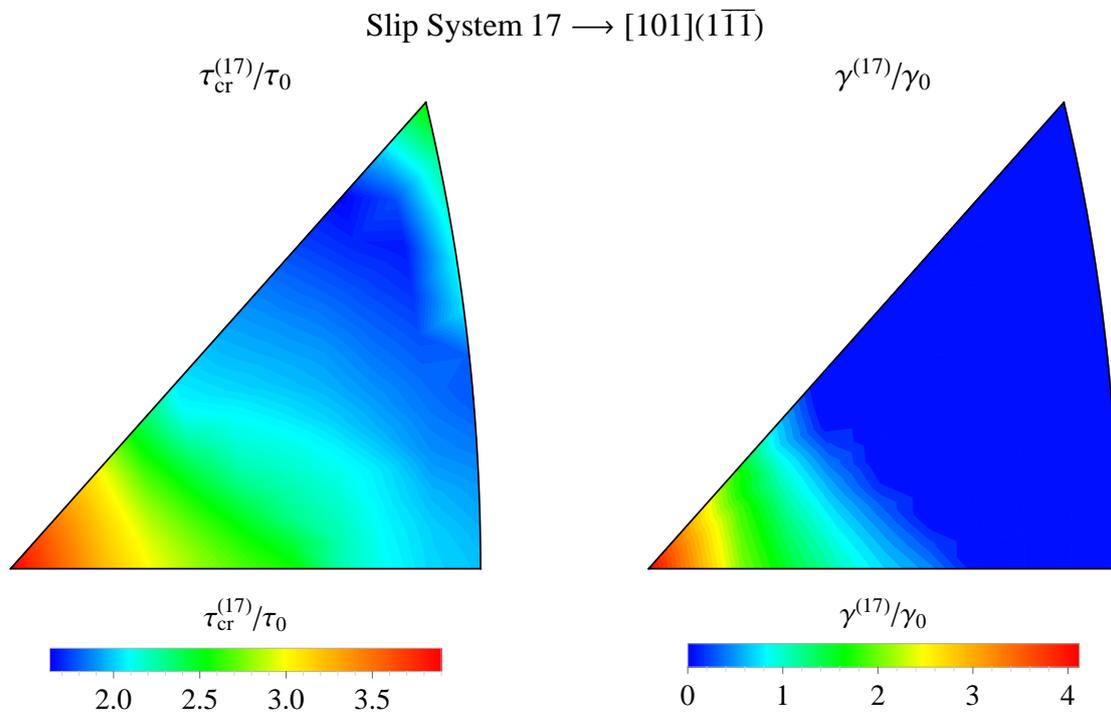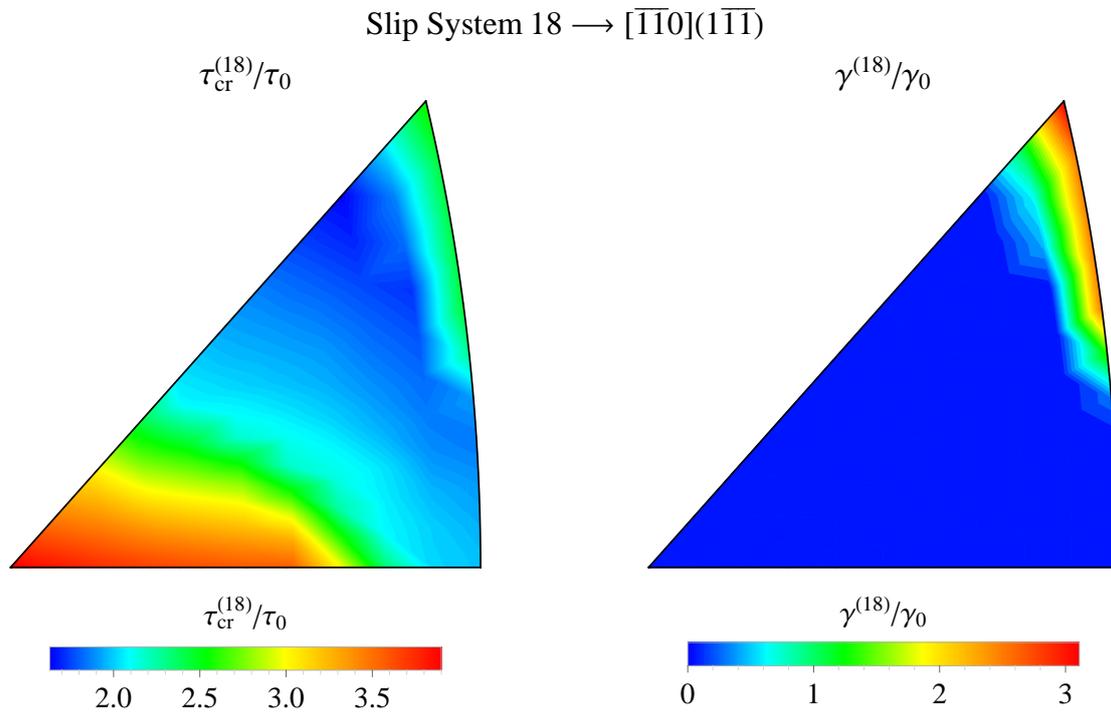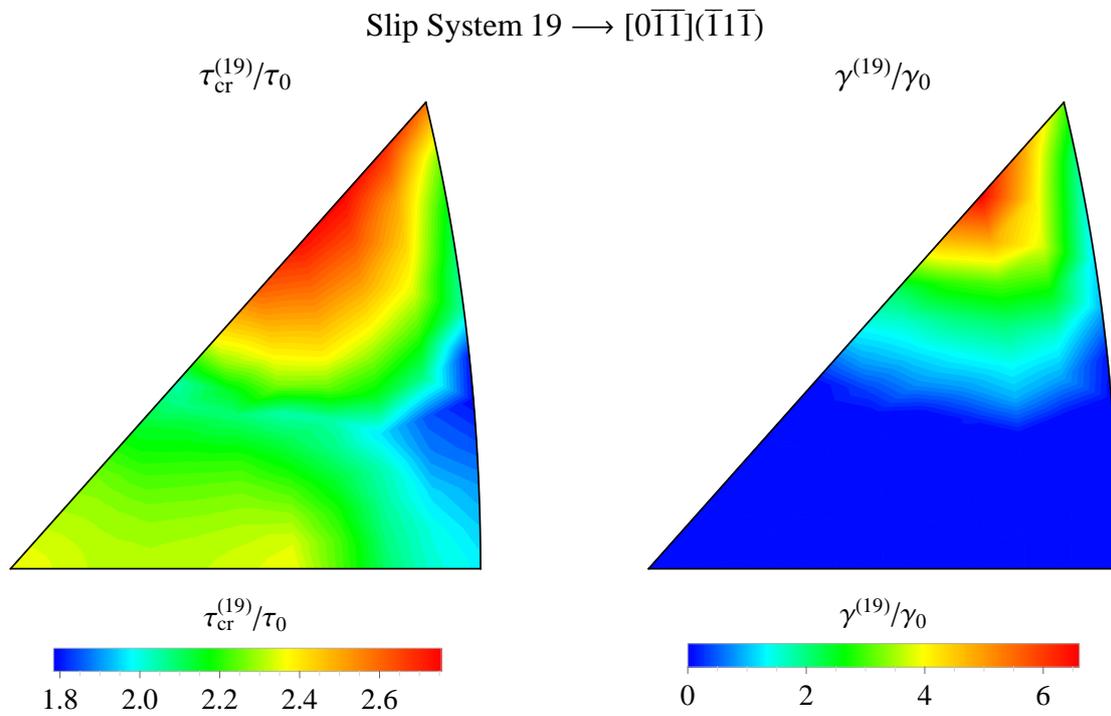
(m) Slip System no.23
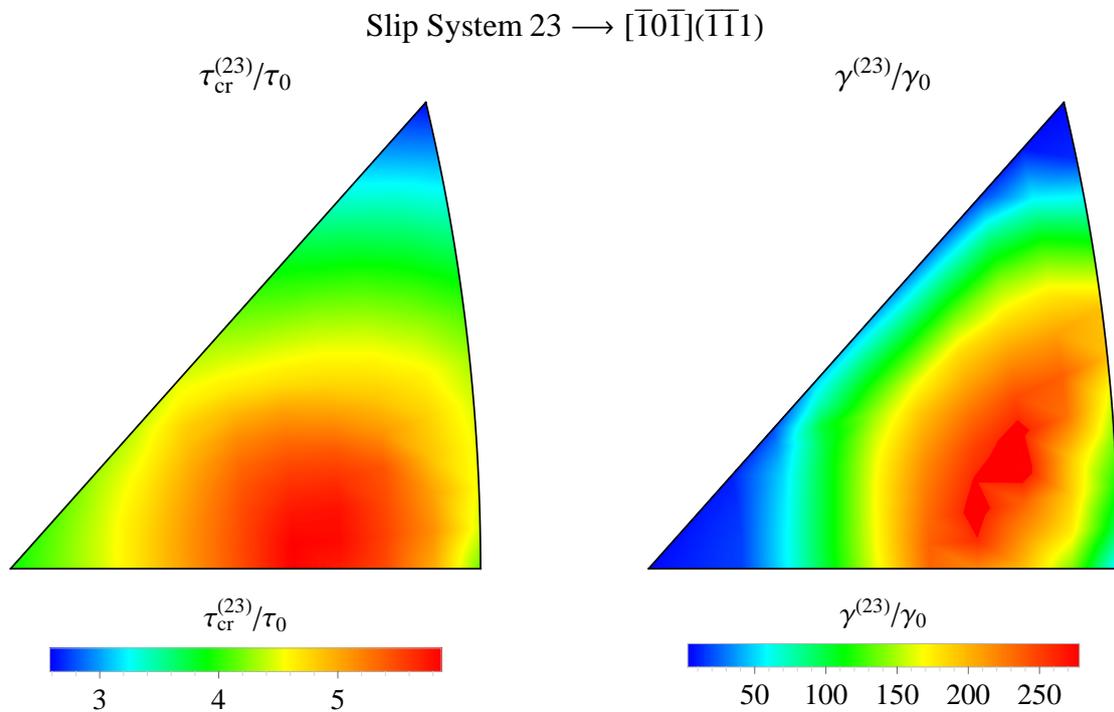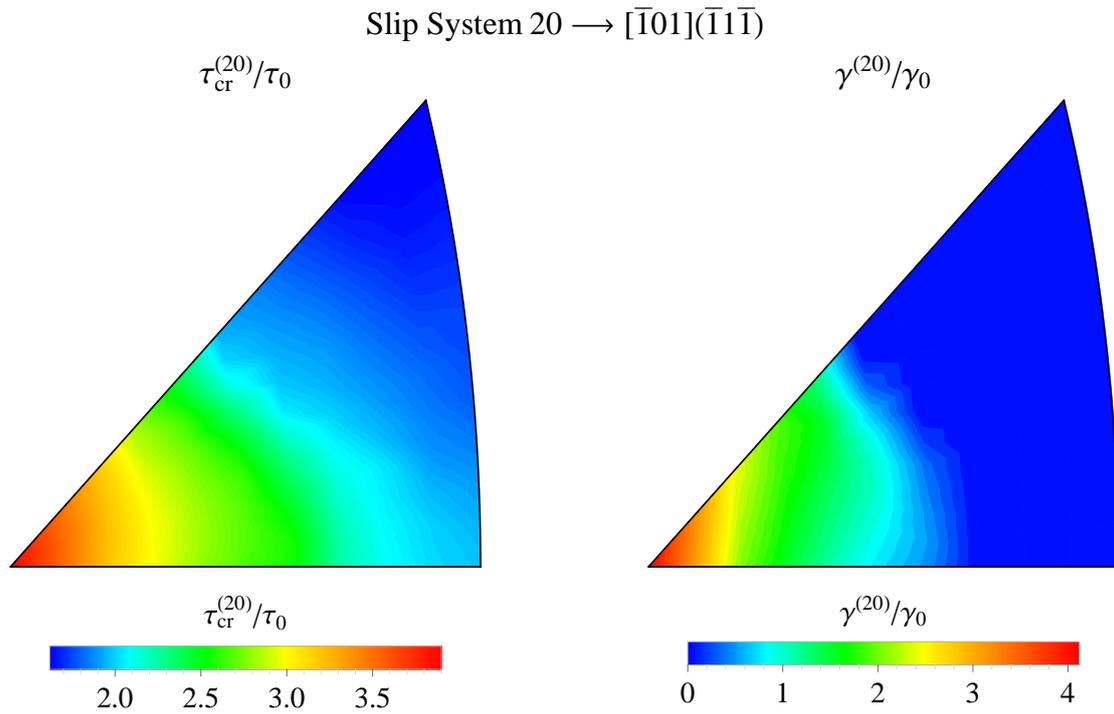
Figure 7.24: Contour Plots of normalized critical stresses τ_{cr}/τ_0 (left) and plastic shear strains γ/γ_0 (right) for all slip systems. The contour plots illustrate the dependance of τ_{cr}^{α} and γ^{α} from the imposed loading direction

7.5 Analysis of Hydrogen Charged Specimens

In the present section we investigate the behavior of hydrogen–charged crystals subjected to unconstrained uniaxial tension. The hydrogen concentration affects both the initial critical shear stress τ_0 of every slip system and also the hardening model as described in Section 4.4 of Chapter 4. The results are compared with the respective ones for hydrogen–free crystals in an effort to reproduce the experimental observations of Delafosse *et al.* and Yagodzinskyy *et al.* [23, 52, 53].

For the analysis of a hydrogen charged finite element subjected to uniaxial tension, we consider the following values for the parameters $W_B, R, T, K_T, G, b, V_M, N_L, \zeta, \eta, \tilde{\alpha}, T_c, H_c, c_0$:

Table 7.5: The parameters used in the computational implementation of the crystal plasticity model accounting for hydrogen-dislocation interactions

	Parameter	Value
Trap Binding Energy	W_B	9.56 [kJ/mol]
Gas Constant	R	8.314 [J/mol K]
Absolute Temperature	T	300 [K]
Equilibrium Constant	K_T	46.28
Shear Modulus[20]	G	86 [GPa]
Burgers vector	b	0.249 [nm]
Molar Volume of Nickel	V_M	$6.59 \cdot 10^{-6}$ [m^3/mol]
Lattice atoms per unit volume	N_L	$9.14 \cdot 10^{28}$
Sites per trap	η	1
NILS sites per lattice atom	ζ	1
Proportionality constant	$\tilde{\alpha}$	0.3
Coefficient of hydrogen effect on τ_0	T_c	$6 \cdot 10^6$
Coefficient of hydrogen effect on $h^{\alpha\beta}$	H_c	$-1.2 \cdot 10^5$
Initial Hydrogen Concentration	c_0	0.015

In the analysis performed, the tension direction is aligned with the crystal direction [135] and latent hardening is take into account via $q = 0.1$. Also, active systems are determined using the heuristic stress–update algorithm.

Figure 7.25 displays the true stress–logarithmic strain curve for the uniaxial tension of a hydrogen–charged single element with $c_0 = 0.015$. The dotted line represents the corresponding curve for a hydrogen–free crystal, whereas the markers along with the vertical lines indicate the onset of Stage II hardening. The σ–$\varepsilon^{\ln}$ curves suggest that the particular implementation of the effect of Hydrogen to the crystal plasticity model, does indeed capture

---

[20]The Shear modulus for a Nickel polycrystal

the following experimental ascertainments (Delafosse [23], Yagodzinskyy [52, 53]):

- A 25% elevation of the initial yield stress

- Delayed onset of Stage II hardening $\equiv$ extension of Stage I hardening

The extension of Stage I hardening suggests that the presence of Hydrogen ultimately reduces the amount of crystal rotation during single slip, responsible for the activation of secondary slip systems. However, a comparison between the curves in Figure 7.25 and the experimental ones by Yagodzinskyy [52, 53] in Figure 4.1, indicates that the particular model accounting for hydrogen presence may not be sufficient for a perfect agreement with experimental observations. This can be attributed to our simplistic approach for the modified hardening model, where we postulated a linear dependence of $h^{\alpha\beta}$ from c_T^α.
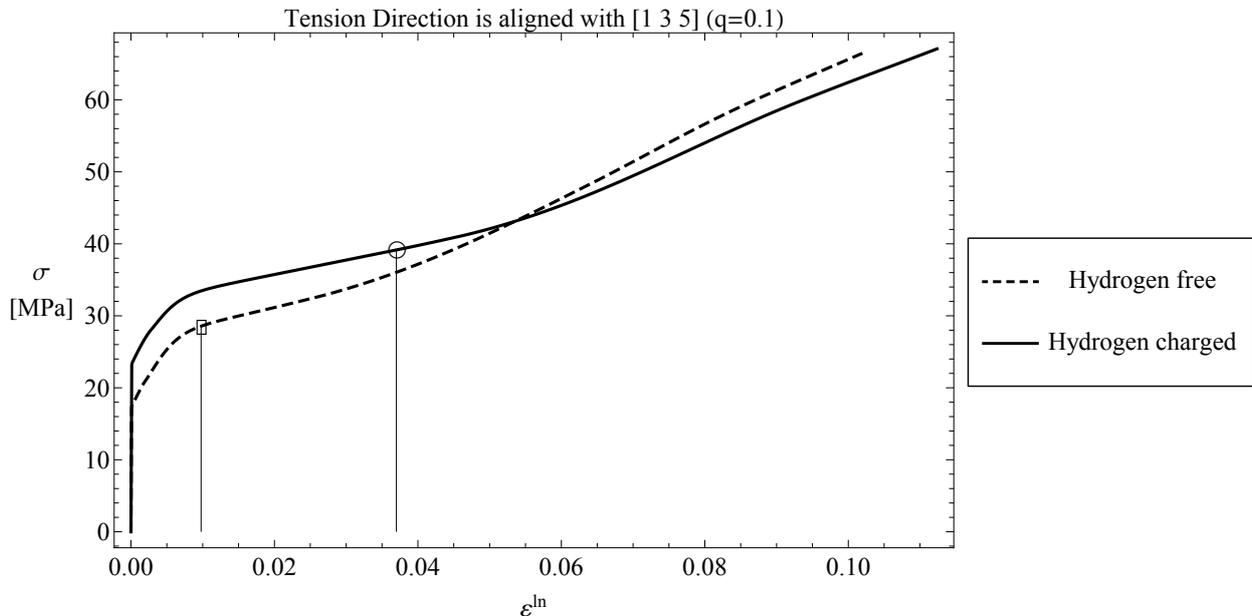

Figure 7.25: The true stress logarithmic strain curves for that correspond to the uniaxial tension of a hydrogen free and a hydrogen charged single crystal with $c_0 = 1.5\%$. The vertical lines indicate the onset of Stage II, or equivalently the extent of Stage I

Finally, figure 7.26 illustrates the evolution of the normalized concentrations c_T^α/c_0, with respect to the logarithmic strain in tension direction. The absence of discontinuities in the curves for c_T^α corroborates the fact that hydrogen equilibrium as well as the conservation of total hydrogen concentration were properly implemented in the computational model.
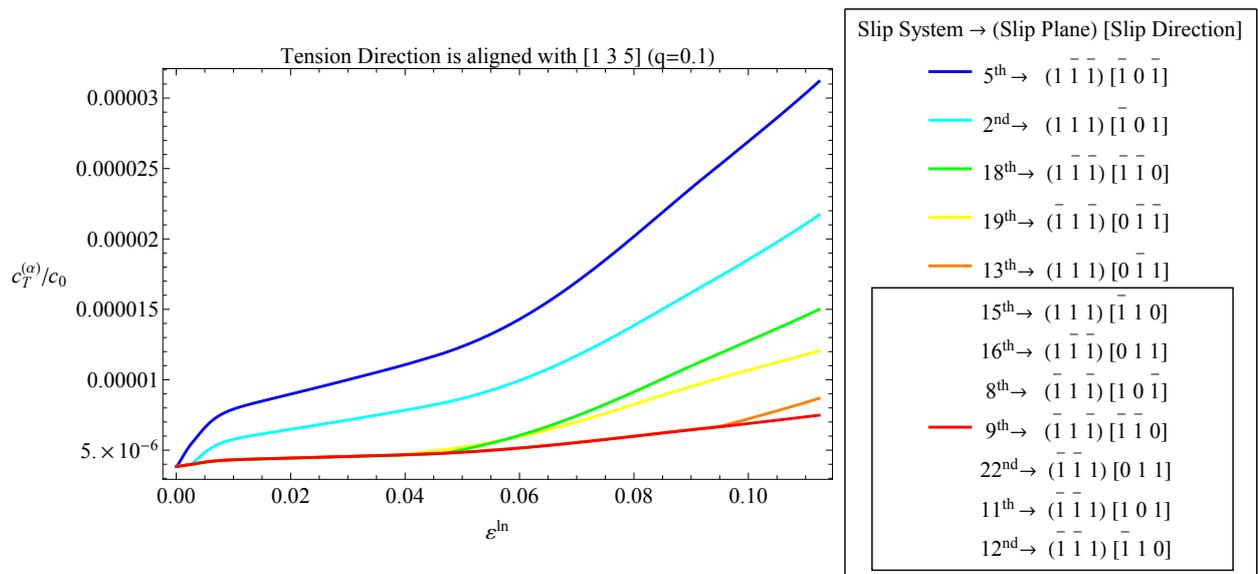
Figure 7.26: The evolution of the normalized trapped hydrogen concentration in the trap sites of the primarily active slip system no. 5, with respect to the logarithmic strain in tension direction

Closure

The constitutive description and computational implementation of a rate independent constitutive model for single crystal plasticity is not only an intriguing problem but also a challenging one. The main obstacle encountered in the computational implementation of the crystal plasticity model, is to incrementally determine the set of active slip systems. The latter is made possible through the formulation of stress–update algorithms which in general use iterative methods to determine which systems are active every increment and populate the active set.

In this work we were concerned with the formulation of a rate independent constitutive model for single crystal plasticity, combining elementary concepts from material's science and continuum mechanics. We presented a heuristic stress–update algorithm but also introduced the problem using two optimization based formulations. A modified hardening model was also introduced to incorporate the effects of hydrogen concentration to the plastic behavior of metal single crystals. A series of finite element simulations were conducted on both single and multi finite element models, in an effort to investigate the effects of latent hardening, specimen shape, crystal orientation and hydrogen concentration to the plastic behavior of FCC metal single crystals. Computationally, we also performed a comparison between the heuristic and optimization based stress–update algorithms.

Several research directions may be proposed for future work, all of which aim to the development of a robust, comprehensive and computationally implementable crystal plasticity model. A problem of particular interest would be to introduce alternative formulations to incorporate the hardening effects of hydrogen concentration in an effort to capture experimental observations. Another interesting project would be to computationally investigate the behavior of single crystal materials that are subjected into complex loading conditions. To this end, an intriguing project would be the fracture analysis of single crystal specimens.

Another proposition would be the development of a rate–dependent constitutive model for crystal plasticity and its comparison with the rate–independent one in several cases.

Ultimately, all aforementioned research directions are motivated by the need for a robust crystal plasticity model that would be able to perform realistic predictions, be in agreement with the experimental observations and also simulate the effect of various parameters (i.e. strain rate, hydrogen concentration, geometric discontinuities, complex loading conditions) to the plastic behavior of single crystals.

Bibliography

[1] ABAQUS/Standard, Version 6.12 © Dassault Systèmes', (2012)

[2] ABAQUS, 'Abaqus Theory Manual, Version 6.12 © Dassault Systèmes', (2012)

[3] Abraham D.P., Altstetter C.J., 'The effect of hydrogen on the yield and flow stress of an austenitic stainless steel', *Metallurgical and Materials Transactions A*, **26**, (1995): 2849–2858

[4] Anand L. and Kothari M., 'A computational procedure for rate-independent crystal plasticity', *J. Mech. Phys. Solids*, **44**(4), (1996): 525–558

[5] Aravas N. and Aifantis E.C., 'On the Geometry of Slip and Spin in Finite Plastic Deformation', *Int. J. Plast.*, **7**, (1991): 141–160

[6] Aravas N., 'Finite Elastoplastic Transformations of Trasversely Isotropic Metals', *Int. J. Solids Struct.*, **29**, (1992): 2137–2157

[7] Aravas N. (2005), 'Cartesian Tensors',University of Thessaly Publications

[8] Aravas N. (2014), 'Mechanics of Materials Volume I: *An Introduction to the Mechanics of Deformable bodies and Linear Elasticity*' Tziolas Publications

[9] Asaro, R.J., 'Micromechanics of crystals and polycrystals', *Adv. appl. Mech.*, **23**, (1983):1–115

[10] Asaro R.J. and Lubarda V.A. (2006), 'Mechanics of Solids and Materials',Cambridge University Press

[11] Bassani J.L., Wu T.Y., 'Latent hardening in single crystals I.Theory and experiments', *Proc. Roy. Soc. Lond. A*, **435**, (1991): 1–19

[12] Bassani J.L., Wu T.Y., 'Latent hardening in single crystals II.Analytical Characterization and Predictions', *Proc. Roy. Soc. Lond. A*, **435**, (1991): 21–41

[13] Beachem C.D., 'A new model for hydrogen-assisted cracking (hydrogen 'embritttlement')', *Metallurgical and Materials Transactions B*, **3**, (1972): 437–451

[14] Bigoni D. (2012), 'Nonlinear Solid Mechanics', Cambridge University Press

[15] Birnbaum H.K., Sofronis P., 'Hydrogen–enhanced localized plasticity - a mechanism for hydrogen-related fracture')', *Materials Science & Engineering A*, **176**, (1994): 191–202

[16] Birnbaum H.K., Robertson I.M., Sofronis P., Teter D., 'Hydrogen–enhanced localized plasticity - a mechanism for hydrogen-related fracture')', *Corrosion Deformation Interactions CDI'96, Second International Conference, Nice France, 1996*, The Institute of Materials, Great Britain, (1997): 172–195

[17] Bonet J. and Wood R.D. (2008), 'Nonlinear Continuum Mechanics for Finite Element Analysis',Cambridge University Press

[18] Borja R.I., Wren J.R., 'Discrete micromechanics of elastoplastic crystals', *Int. J. Numer. Methods Eng.*, **36**, (1993): 3815–3840

[19] Budiansky B., Wu T.T., 'Theoretical Prediction of Plastic Strains of Polycrystals', *Proc. 4th U.S. Nat. Cong. Appl. Mech. (ASME)*, (1962): 1175–1185

[20] Clayton J.D., (2011), 'Nonlinear Mechanics of Crystals',Springer Dordrecht Heidelberg

[21] Cuitiño A.M., Ortiz M., 'Computational modelling of single crystals', *Modelling and Simulation in Materials Science and Engineering*, **129**, (1996): 235–254

[22] Dafalias.Y.F., 'A missing link in the macroscopic constitutive formulation of large plastic deformations', Elsevier.Chichester.U.K., Int. Symp.,*Recent Trends and results in Plasticity. Plasticity Today*,(Edited by A.Ewczuk and G.Bianchi), (1985): 135–151

[23] Delafosse D., Feaugas X., Aubert I., Saintier N., Olive J.M., 'Hydrogen Effects on the Plasticity of FCC Nickel and Austenitic Alloys', *Proceedings of the 2008 International Hydrogen Conference*, B. Somerday, P. Sofronis, and R. Jones, eds, (2009): 78–87

[24] Delafosse D., 'Hydrogen effects on the plasticity of face centred cubic (fcc) crystals', *Gaseous hydrogen embrittlement of materials in energy technologies*, Gangloff R.P., Somerday. B.P. (eds), (2012): 247–285

[25] Diehl J.V., 'Zugverformung von Kupfer Einkristallen', *Z.Metallk.*, **47**, (1956): 331–343

[26] Gurtin M.E.,Fried E. and Annand L., (2009) 'The Mechanics and Thermodynamics of Continua',Cambridge University Press

[27] Haidemenopoulos G.N., (2007), 'Physical Metallurgy', Tziolas Publications

[28] Hill R., 'Generalized constitutive relations for incremental deformation of metal crystals by multislip', *J. Mech. Phys. Solids*, **14**, (1966) : 95–102.

[29] Hirth J.P., 'Effects of hydrogen on the properties of iron and steel', *Metallurgical and Materials Transactions A*, **11**, (1980): 861–890

[30] Hjelmstad K.D. (2005), 'Fundamentals of Structural Mechanics',2nd edition Springer, Academic Press

[31] Honeycombe R.W.K., Bhadeshia H.K.D.H., (1995), 'Steels: Microstructure and Properties', 2nd edition, Butterworth–Heinemann

[32] Hutchinson J.W., 'Elastic-plastic behaviour of polycrystalline metals and composites', *Proc. Roy. Soc. Lond. A*, **319**, (1970): 274–272

[33] Kaufman E.H., Leeming D.J., Taylor G.D., 'CONMAX subroutine package for general nonlinearly constrained function minimization', *Numerical Algorithms*, **9**, (1995): 25–37

[34] Koiter W.T., 'Stress-strain relations, uniqueness and variational theorems for elastic-plastic materials with a singular yield surface', *Q. Appl. Math.*, **11**, (1953): 350–354

[35] Lee E.H., 'Elastic–Plastic Deformation at Finite Strains', *J. Appl. Mech.*,**36(1)**, (1969): 1–6

[36] Liang Y., Sofronis P., Aravas N., 'On the effect of hydrogen on plastic instabilities in metals', *Acta Mater.*,**51**, (2003): 2717–2730

[37] Lubarda V.A., 'Constitutive theories based on the multiplicative decomposition of deformation gradient: Thermoelasticity, elastoplasticity, and biomechanics', *Appl. Mech. Rev.*,**57(2)**,(2004):95–108

[38] Malvern L.E. (1969), 'Introduction to the Mechanics of a Continuous Medium', Prentice Hall

[39] Mandel J., 'Une gènèralisation de la theoriè de la plasticitè de W.T.Koiter', *Int. J. Solids Struct.*, **1**, (1965) : 273–295.

[40] Miehe C. and Schröder J., 'A comparative study of stress update algorithms for rate-independent and rate-dependent crystal plasticity', *Int. J. Numer. Methods Eng.*, **50**, (2001) : 273–298.

[41] Needleman.A., 'On the finite element formulations for large elastic-plastic deformations', *Comput. and Struct.*,**20**, (1985): 247–257

[42] Papatriantafyllou I.C., 'Trip Steels: Constitutive Modeling and Computational Issues', *University of Thessaly, School of Engineering, Department of Mechanical Engineering*, Ph.D. Thesis, (2005)

[43] Robertson I.M., 'The effect of hydrogen on dislocation dynamics', *Engng Fract. Mech.*,**68**, (2001): 671–692

[44] Sirois E., Birnbaum H.K., 'Effects of hydrogen and carbon on thermally activated deformation in nickel', *Acta Metall. Mater.*,**40**, (1992): 1377–1385

[45] Sofronis P., 'The influence of mobility of dissolved hydrogen on the elastic response of a metal', *J. Mech. Phys. Solids*,**43**, (1995): 1385–1407

[46] Sofronis P., Birnbaum H.K., 'Mechanics of the hydrogen dislocation impurity interactions I. Increasing shear modulus', *J. Mech. Phys. Solids*,**43**, (1995): 49–90

[47] Somerday B.P., Dadfarnia M., Balch D.K., Nibur K.A., Cadden C.H., Sofronis P., 'Hydrogen-Assisted Crack Propagation in Austenitic Stainless Steel Fusion Welds', *Metallurgical and Materials Transactions A*,**40**, (2009): 2350–2362

[48] Schebler G., 'On the mechanics of hydrogen interaction with single crystal plasticity', *University of Illinois at Urbana–Champaign*, Master Thesis, (2010)

[49] Taylor G.I., 'The Mechanism of Plastic Deformation of Crystals. Part I. Theoretical', *Proc. Roy. Soc. Lond. A*,**145**, (1934): 362–387

[50] Taylor G.I., 'Plastic Strain in Metals', *J. Inst. Metals*,**62**, (1938): 307–324

[51] Thomas G.J., 'Hydrogen trapping in FCC metals', *Hydrogen Effects in Metals*, Bernstein and A.W. Thompson, eds. pp. 77–84

[52] Yagodzinskyy Y., Tarasenko O., Hnninen H., 'Effect of hydrogen on plastic deformation of stable 18Cr-16Ni-10Mn austenitic stainless steel single crystals', *Hydrogen Effects on Material Behavior and Corrosion Deformation Interactions*, N.R. Moody, A.W. Thompson, R.E. Ricker, G.W. Was, and R.H. Jones, eds. pp. (2003): 201–210

[53] Yagodzinskyy Y., Saukkonen T., Hnninen H., Tuomisto F., Barannikova S., Zuev L., 'Effect of Hydrogen on Plastic Strain Localization in Single Crystals of Nickel and Austenitic Stainless Steel', *Proceedings of the 2008 International Hydrogen Conference*, B. Somerday, P. Sofronis, and R. Jones, eds, (2009): 97–104

Appendices

Appendix A

Deformation Analysis of Simple Shear

The mapping of a simple shear motion with a slip direction $\mathbf{s}$ and upon a slip plane $\mathbf{m}$ is of the form:

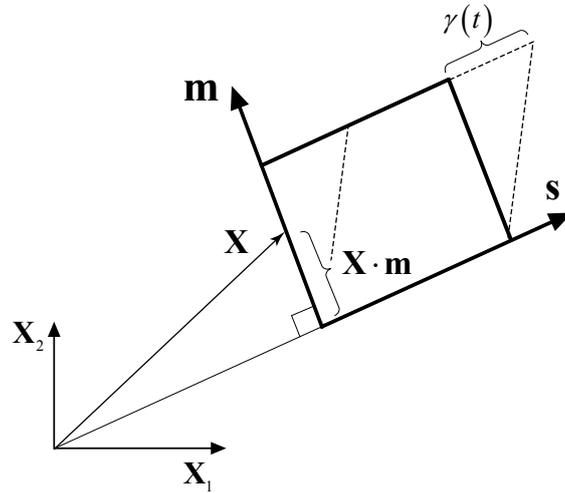$$\mathbf{x} = \mathbf{X} + \gamma(t)(\mathbf{X} \cdot \mathbf{m})\mathbf{s} \tag{A.1}$$

Figure A.1: A schematic representation of simple shear where $\mathbf{s}$ is the slip direction and $\mathbf{m}$ is the normal to the slip direction

The deformation gradient $\mathbf{F}$ that corresponds to this motion is:

$$x_i = X_i + \gamma(t)X_k m_k s_i \Rightarrow F_{ij} = \frac{\partial x_i}{\partial X_j} = \delta_{ij} + \gamma(t)\delta_{kj}m_k s_i = \delta_{ij} + \gamma(t)s_i m_j \Rightarrow$$

$$\boxed{\mathbf{F} = \boldsymbol{\delta} + \gamma(t)\mathbf{sm}} \tag{A.2}$$

The velocity gradient $\mathbf{L}$, the deformation rate $\mathbf{D}$ as well as the spin tensor $\mathbf{W}$ can also be calculated for the simple shear motion as:

$$\mathbf{L} = \dot{\mathbf{F}} \cdot \mathbf{F}^{-1} \Rightarrow \mathbf{L} = \dot{\gamma}(t)\mathbf{sm} \tag{A.3}$$

$$\mathbf{D} = \mathrm{symm}(\mathbf{L}) \Rightarrow \mathbf{D} = \frac{\dot{\gamma}(t)}{2}(\mathbf{sm} + \mathbf{ms}) \tag{A.4}$$

$$\mathbf{W} = \mathrm{skew}(\mathbf{L}) \Rightarrow \mathbf{W} = \frac{\dot{\gamma}(t)}{2}(\mathbf{sm} - \mathbf{ms}) \tag{A.5}$$

Now imagine that a body experiences n simultaneous simple shears. In general, each α simple shear, where $\alpha = 1, 2, ...n$, takes place at a different slip direction $\mathbf{s}^\alpha$ and slip plane $\mathbf{m}^\alpha$. The corresponding deformation gradient is:

$$\mathbf{F} = \boldsymbol{\delta} + \sum_{\alpha=1}^{n} \gamma^\alpha(t)\mathbf{s}^\alpha\mathbf{m}^\alpha \tag{A.6}$$

Note however that the deformation gradient in (A.6) does not represent in general a simple shear, although we derived that expression by postulating n simultaneous simple shears. Only in the special cases of $\mathbf{s}^1 = \mathbf{s}^2 = ...\mathbf{s}^n$ (simultaneous shears along the same slip direction but on different slip planes) , or $\mathbf{m}^1 = \mathbf{m}^2 = ...\mathbf{m}^n$ (simultaneous shears upon the same slip plane but on different slip directions) equation (A.6) does indeed represent a generalized simple-shear.

Appendix B

Uniaxial Tension of a Single Crystal in Single Slip

Herein we present an analytical constitutive description of a single crystal subjected to uniaxial tension. In general, it is not possible to derive analytical expressions for the constitutive behavior of a single crystal, even for the simplest of cases. The simplistic approach of a single crystal that can only undergo plastic deformation in terms of single slip[1,2] is one of the few exceptions for which analytical solutions exist.

In single slip conditions, where the total plastic deformation is the result of plastic slip in only one system, the motion can be thought as a simple shear motion. Recalling equation (A.2), the intermediate 'isoclinic' configuration, defined by $\mathbf{F}^p = \boldsymbol{\delta} + \gamma\mathbf{sm}$ is such that the 'directors' $\mathbf{s}$ and $\mathbf{m}$ have the same directions as those of the undeformed configuration. Let $\mathbf{p}$ be the unit vector along the tension direction. Then the stress tensor $\boldsymbol{\sigma}$ is of the form:

$$\boldsymbol{\sigma} = \sigma\mathbf{pp} \tag{B.1}$$

The testing machine however constraints the specimen in the sense that material fibers that are parallel to $\mathbf{p}$ are allowed to stretch but not to rotate. In math form this constraint takes the form:

$$\mathbf{p}' = \mathbf{F} \cdot \mathbf{p} = \lambda\mathbf{p} \quad (\lambda = |\mathbf{p}'|) \tag{B.2}$$

Since in metal plasticity the elastic strains are always small we can write that $\mathbf{U}^e \approx \boldsymbol{\delta}$ and the total deformation gradient can be decomposed[3] as:

$$\mathbf{F} = \mathbf{F}^e \cdot \mathbf{F}^p = (\mathbf{R}^e \cdot \mathbf{U}^e) \cdot \mathbf{F}^p = \mathbf{R}^e \cdot (\boldsymbol{\delta} + \gamma\mathbf{sm}) \tag{B.3}$$

---

[1]Equivalent to Stage I deformation in Figure 3.3

[2]Such an imaginary crystal would have to comprise of 1 slip system in total

[3]The Polar Decomposition of a 2nd order tensor as well as it's physical interpretation are discussed in Section 1.3
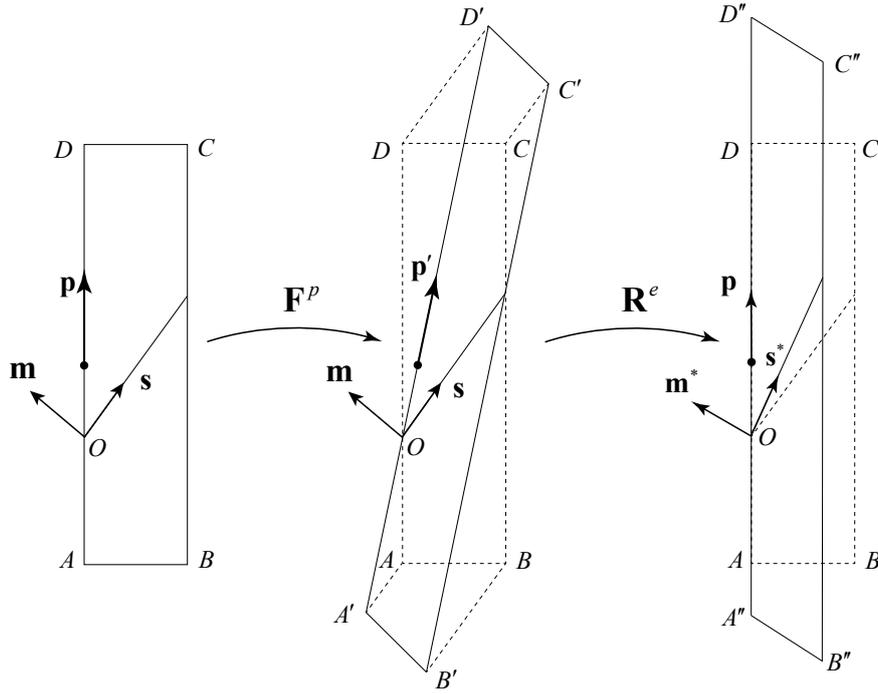
Figure B.1: A single crystal in single slip under uniaxial tension

with $\mathbf{R}^e \cdot \mathbf{R}^{eT} = \boldsymbol{\delta}$. Now combining equations (B.2) and (B.3) we get:

$$\mathbf{R}^e \cdot (\boldsymbol{\delta} + \gamma \mathbf{sm}) \cdot \mathbf{p} = \lambda \mathbf{p} \Rightarrow (\boldsymbol{\delta} + \gamma \mathbf{sm}) \cdot \mathbf{p} = \lambda \mathbf{R}^{eT} \cdot \mathbf{p} \Rightarrow \mathbf{p} + \gamma (\mathbf{m} \cdot \mathbf{p}) \mathbf{s} = \mathbf{R}^{eT} \cdot (\lambda \mathbf{p}) \quad \text{(B.4)}$$

Equation (B.4) enables the definition of both λ and $\mathbf{R}^e$. For λ:

$$\lambda(\gamma) = |\mathbf{p} + \gamma (\mathbf{m} \cdot \mathbf{p}) \mathbf{s}| = \sqrt{[\mathbf{p} + \gamma (\mathbf{m} \cdot \mathbf{p}) \mathbf{s}] \cdot [\mathbf{p} + \gamma (\mathbf{m} \cdot \mathbf{p}) \mathbf{s}]} \quad \text{(B.5)}$$

$$\boxed{\lambda(\gamma) = \sqrt{1 + 2\gamma(\mathbf{m} \cdot \mathbf{p})(\mathbf{s} \cdot \mathbf{p}) + \gamma^2(\mathbf{m} \cdot \mathbf{p})^2}} \quad \text{(B.6)}$$

In order to proceed and determine the rotation tensor $\mathbf{R}^e$ we have to interpret equation (B.4). Equation (B.4) suggests that vector $\gamma (\mathbf{m} \cdot \mathbf{p}) \mathbf{s}$ is added to the original vector $\mathbf{p}$ to produce the new vector $\mathbf{R}^{eT} \cdot (\lambda \mathbf{p})$ which is the original vector stretched by λ and rotated by $\mathbf{R}^{eT}$. This means that the axis of rotation due to $\mathbf{R}^{eT}$ must be perpendicular to the plane defined by $\mathbf{p}$ and $\mathbf{s}$. Therefore, the unit vector $\mathbf{n}$ that defines the axis of rotation due to $\mathbf{R}^{eT}$ is given by:

$$\mathbf{n} = \frac{\mathbf{p} \times \mathbf{s}}{|\mathbf{p} \times \mathbf{s}|} \quad \text{(B.7)}$$

Then, the elastic rotation $\mathbf{R}^e$ can be written as:

$$\mathbf{R}^{eT} = \cos \theta \boldsymbol{\delta} + (1 - \cos \theta)\mathbf{nn} + \sin \theta(\mathbf{n}\times) \Rightarrow \mathbf{R}^e = \cos \theta \boldsymbol{\delta} + (1 - \cos \theta)\mathbf{nn} - \sin \theta(\mathbf{n}\times) \quad \text{(B.8)}$$

Next, we have to determine the angle of rotation θ and thus we dot the last equation with $\mathbf{p}$

$$\mathbf{R}^e \cdot \mathbf{p} = \cos \theta \mathbf{p} + (1 - \cos \theta)\mathbf{n} \underbrace{(\mathbf{n} \cdot \mathbf{p})}_{0} - \sin \theta(\mathbf{n} \times \mathbf{p}) = \cos \theta \mathbf{p} - \sin \theta(\mathbf{n} \times \mathbf{p}) \quad \text{(B.9)}$$

Now combining equations (B.9) and (B.4) we get:

$$\mathbf{p} + \gamma(\mathbf{m} \cdot \mathbf{p})\mathbf{s} = \lambda \cos\theta \mathbf{p} - \lambda \sin\theta(\mathbf{n} \times \mathbf{p}) \tag{B.10}$$

Now let us dot again (B.10) with $\mathbf{p}$ to get:

$$\underbrace{\mathbf{p} \cdot \mathbf{p}}_{1} + \gamma(\mathbf{m} \cdot \mathbf{p})(\mathbf{s} \cdot \mathbf{p}) = \lambda \cos\theta \underbrace{\mathbf{p} \cdot \mathbf{p}}_{1} - \lambda \sin\theta \underbrace{(\mathbf{n} \times \mathbf{p}) \cdot \mathbf{p}}_{0} \Rightarrow 1 + \gamma(\mathbf{m} \cdot \mathbf{p})(\mathbf{s} \cdot \mathbf{p}) = \lambda \cos\theta \Rightarrow$$

$$\boxed{\cos\theta(\gamma) = \frac{1 + \gamma(\mathbf{m} \cdot \mathbf{p})\mathbf{s} \cdot \mathbf{p}}{\lambda(\gamma)}} \tag{B.11}$$

To fully define the angle θ however we also need to determine the $\sin\theta$, so we dot expression (B.10) with $\mathbf{s}$ to get:

$$\mathbf{p} \cdot \mathbf{s} + \gamma(\mathbf{m} \cdot \mathbf{p})\underbrace{\mathbf{s} \cdot \mathbf{s}}_{1} = \lambda \cos\theta \mathbf{p} \cdot \mathbf{s} - \lambda \sin\theta(\mathbf{m} \times \mathbf{p}) \cdot \mathbf{s} \overset{(B.11)}{\Rightarrow}$$

$$\mathbf{p} \cdot \mathbf{s} + \gamma(\mathbf{m} \cdot \mathbf{p}) = \mathbf{p} \cdot \mathbf{s} + \gamma(\mathbf{m} \cdot \mathbf{p})(\mathbf{s} \cdot \mathbf{p})^2 - \lambda \sin\theta(\mathbf{m} \times \mathbf{p}) \cdot \mathbf{s} \Rightarrow$$

$$\sin\theta(\gamma) = -\frac{\gamma(\mathbf{m} \cdot \mathbf{p})\left[1 - (\mathbf{s} \cdot \mathbf{p}\right]^2}{\lambda(\gamma)(\mathbf{m} \times \mathbf{p}) \cdot \mathbf{s}} \tag{B.12}$$

But,

$$|\mathbf{p} \times \mathbf{s}| = \sqrt{(\mathbf{p} \times \mathbf{s})_i(\mathbf{p} \times \mathbf{s})_i} = \sqrt{(e_{ijk} p_j s_k)(e_{imn} p_m s_n)} = \sqrt{(\delta_{jm}\delta_{kn} - \delta_{jn}\delta_{km})p_j s_k p_m s_n}$$
$$= \sqrt{p_j s_k p_j s_k - p_j s_k p_k s_j} = \sqrt{1 - (\mathbf{s} \cdot \mathbf{p})^2}$$

and

$$(\mathbf{n} \times \mathbf{p}) \cdot \mathbf{s} = \left(\frac{\mathbf{p} \times \mathbf{s}}{|\mathbf{p} \times \mathbf{s}|} \times \mathbf{p}\right) \cdot \mathbf{s} = \frac{(e_{ijk} p_j s_k \mathbf{e}_i) \times (p_l \mathbf{e}_l)}{\sqrt{1 - (\mathbf{s} \cdot \mathbf{p})^2}} \cdot \mathbf{s} = \frac{e_{ijk} e_{ilm} p_j s_k p_l \mathbf{e}_m}{\sqrt{1 - (\mathbf{s} \cdot \mathbf{p})^2}} \cdot \mathbf{s} =$$

$$= \frac{(\delta_{jl}\delta_{km} - \delta_{jm}\delta_{kl})p_j s_k p_l \mathbf{e}_m}{\sqrt{1 - (\mathbf{s} \cdot \mathbf{p})^2}} \cdot \mathbf{s} = \frac{p_j s_k p_j \mathbf{e}_k - p_j s_k p_k \mathbf{e}_j}{\sqrt{1 - (\mathbf{s} \cdot \mathbf{p})^2}} \cdot \mathbf{s} =$$

$$= \frac{\mathbf{s} - (\mathbf{s} \cdot \mathbf{p})\mathbf{p}}{\sqrt{1 - (\mathbf{s} \cdot \mathbf{p})^2}} \cdot \mathbf{s} = \frac{1 - (\mathbf{s} \cdot \mathbf{p})^2}{\sqrt{1 - (\mathbf{s} \cdot \mathbf{p})^2}} \tag{B.13}$$

Now using equation (B.13) we can express the $\sin\theta$ in (B.12) as:

$$\boxed{\sin\theta(\gamma) = -\frac{\gamma(\mathbf{m} \cdot \mathbf{p})\sqrt{1 - (\mathbf{s} \cdot \mathbf{p})^2}}{\lambda(\gamma)}} \tag{B.14}$$

and recall that:

$$\boxed{\mathbf{R}^e(\gamma) = \cos\theta(\gamma)\boldsymbol{\delta} + (1 - \cos\theta(\gamma))\mathbf{nn} - \sin\theta(\gamma)(\mathbf{n}\times)} \tag{B.15}$$

Uniaxial tension of a single crystal in single slip is perhaps the only case for which we can derive analytical expressions to describe the $\sigma - \varepsilon$ curve. Recall that in purely single slip conditions, the flow rule is described by expression (3.27) which we restate below:

$$\tau_{cr}^{\alpha}(\gamma^{\alpha}) = \tau_0 + (\tau_I - \tau_0) \tanh \left(\frac{h_0 - h_s}{\tau_I - \tau_0} \gamma^{\alpha} \right) + h_s \, \gamma^{\alpha} \tag{B.16}$$

The resolved shear stress τ can be expressed with respect to the applied tensile stress $\boldsymbol{\sigma}$ by Schmid's law:

$$\tau = \mathbf{s}^* \cdot \boldsymbol{\sigma} \cdot \mathbf{m}^* \tag{B.17}$$

where $\mathbf{s}^*$ is the vector along the slip direction and $\mathbf{m}^*$ is the normal to the slip plane, in the current (deformed) state respectively. Now recall that the slip direction vector transforms during deformation according to $\mathbf{s}^* = \mathbf{F} \cdot \mathbf{s}$, whereas the normal to the slip plane as $\mathbf{m}^* = \mathbf{m} \cdot \mathbf{F}^{-1}$. The multiplicative decomposition of the deformation gradient however ($\mathbf{F} = \mathbf{F}^e \cdot \mathbf{F}^p$) is such that the intermediate configuration defined by $\mathbf{F}^p$ is "isoclinic" suggesting that $\mathbf{F}^p$ does not contribute to vector rotation. Furthermore, the polar decomposition of $\mathbf{F}$ combined with the fact that $\mathbf{U}^e \approx \boldsymbol{\delta}$ enable us to rewrite the slip and normal transformations as:
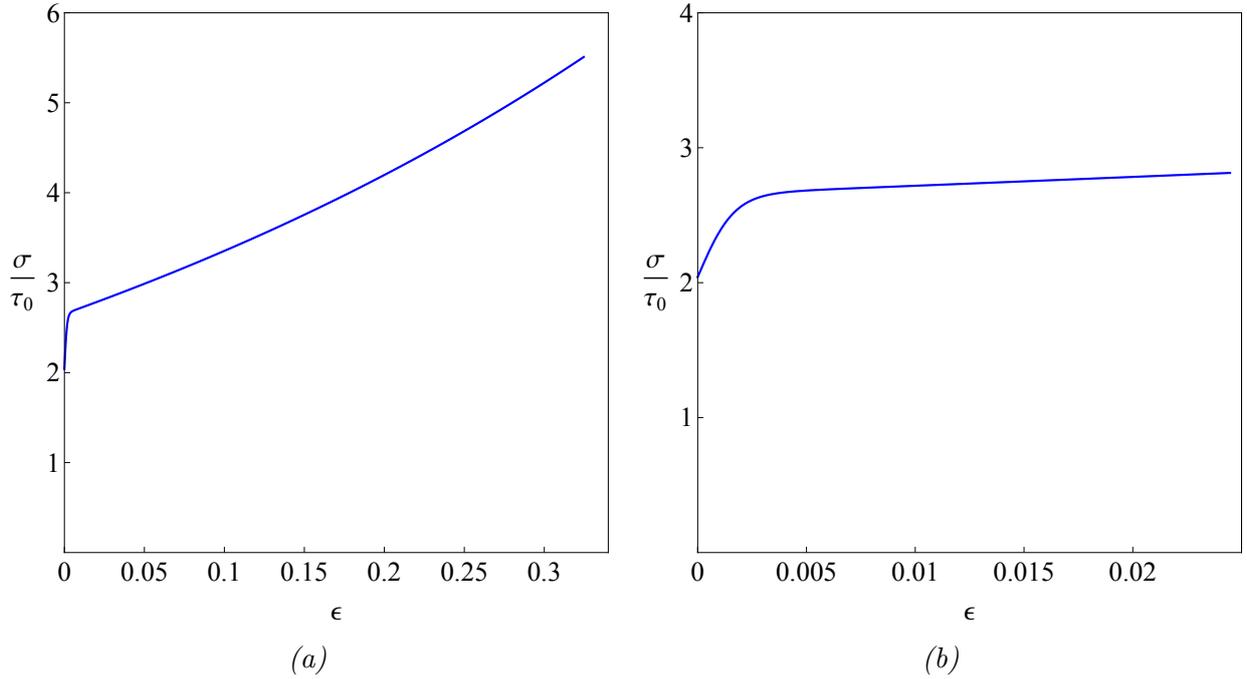

Figure B.2: The true stress–logarithmic strain curves for the uniaxial tension of a single crystal in single slip for finite (a) and small strains (b) respectively

$$\mathbf{s}^* = \mathbf{R}^e \cdot \mathbf{s} \quad \text{and} \quad \mathbf{m}^* = \mathbf{m} \cdot \mathbf{R}^{eT} \tag{B.18}$$

Now let us combine expressions (B.1),(B.16),(B.17) and (B.18) all together to get:

$$\tau = (\mathbf{s} \cdot \mathbf{R}^e) \cdot (\sigma \mathbf{n}\mathbf{n}) \, (\mathbf{R}^e \cdot \mathbf{m}) = \sigma \, [\mathbf{p} \cdot \mathbf{R}^e(\gamma)\mathbf{s}] \, [\mathbf{p} \cdot \mathbf{R}^e(\gamma)\mathbf{m}] \Rightarrow$$

$$\sigma(\gamma) = \frac{\tau(\gamma)}{[\mathbf{p} \cdot \mathbf{R}^e(\gamma)\mathbf{s}]\,[\mathbf{p} \cdot \mathbf{R}^e(\gamma)\mathbf{m}]} \tag{B.19}$$

The macroscopic strain in the loading direction ε is related to the resolved shear strain γ by:

$$\varepsilon = \ln \lambda(\gamma) \tag{B.20}$$

Equations (B.19) and (B.20) define a parametric description of the $\sigma - \varepsilon$ curve.

Appendix C

Solving the Nonlinear System of $\tau^a_{cr} - c^a_T$

The interdependency of the critical shear stresses and trapped hydrogen concentration on every slip system, requires the implementation of a numerical method to solve the system of equations (5.13) & (5.16) which we restate herein:

$$\tau^\alpha_{cr}|_{n+1} = \tau^\alpha_{cr}|_n + \sum_{\beta=1}^{N} \left[(1-\delta)(1+H_c\,c^\alpha_T|_n)h^{\alpha\beta}|_n + \delta(1+H_c\,c^\alpha_T|_{n+1})h^{\alpha\beta}|_{n+1}\right]\Delta\gamma^\beta$$

$$c^\alpha_T|_{n+1} = \frac{K_T\,\zeta\,c_L|_{n+1}}{\tilde{\alpha}^2\,\mu^2\,b^3\left[\eta\,N_L + (K_T-1)\,N_L\,c_L|_{n+1}\right]}\,(\tau^\alpha_{cr}|_{n+1})^2$$

Note that this system of equations needs to be solved for every slip system $\alpha \in \mathscr{P}$. Before we proceed by implementing the Newton method, let us simplify the above equations taking into consideration that all quantities referring to t_n along with $\Delta\gamma^\alpha$, $\mathscr{A}_{n+1}$, $h^{\alpha\beta}|_{n+1}$ and $c_L|_{n+1}$[1] are known. The quantities $\hat{\tau}^\alpha$, $\hat{h}^\alpha$, $\hat{\tau}^\alpha_h$ and $\hat{H}^\alpha$ are introduced in terms of known parameters within every iteration as:

$$\hat{\tau}^\alpha = \tau^\alpha_{cr}|_n + (1-\delta)(1+H_c\,c^\alpha_T|_n)\sum_{\beta=1}^{Nsp} h^{\alpha\beta}|_n\,\Delta\gamma^\beta \tag{C.1a}$$

$$\hat{h}^\alpha = \delta\sum_{\beta=1}^{Nsp} h^{\alpha\beta}|_{n+1}\,\Delta\gamma^\beta \tag{C.1b}$$

$$\hat{\tau}^\alpha_h = \hat{\tau}^\alpha + \hat{h}^\alpha \tag{C.1c}$$

$$\hat{H}^\alpha = H_c\,\hat{h}^\alpha \tag{C.1d}$$

---

[1]The lattice hydrogen concentration at t_{n+1} is iteratively passed in from the hydrogen equilibrium

We also define Y as:

$$Y = \frac{K_T \, \zeta \, c_L|_{n+1}}{\tilde{\alpha}^2 \, \mu^2 \, b^3 \, [\eta \, N_L + (K_T - 1) \, N_L \, c_L|_{n+1}]} \tag{C.1e}$$

As a result of the definitions (C.1a–C.1e), we can restate the system of (5.13) and (5.16) in the following simplified form:

$$\tau_{cr}^\alpha|_{n+1} = \hat{\tau}_h^\alpha + \hat{H}^\alpha \, c_T^\alpha|_{n+1} \tag{C.2}$$

$$c_T^\alpha|_{n+1} = Y \, (\tau_{cr}^\alpha|_{n+1})^2 \tag{C.3}$$

At this point we note that we could either solve the above system numerically, or alternatively substitute equation (C.3) to (C.2) to derive a quadratic equation for $\tau_{cr}^\alpha|_{n+1}$. However, it is wiser to proceed with a numerical solution, mainly for two reasons. First, a nested algorithm to solve the system numerically can fairly easily be modified to account for a more complex hardening model with hydrogen effects. Secondly, the quadratic equation for $\tau_{cr}^\alpha|_{n+1}$ would in general produce two possible solutions from which we would have to determine the correct one. The latter is not always straightforward however, and also introduces the problem of developing a solution selection criterion.

To implement the Newton Raphson method and solve the system of (C.2–C.3) we rewrite the equations in the form $\mathbf{F}(\tau_{cr}^\alpha, c_T^\alpha|_{n+1}) = \mathbf{0}$ as:

$$\mathbf{F}^\alpha(\tau_{cr}^\alpha, c_T^\alpha|_{n+1}) = \left\{ \begin{array}{c} F_1^\alpha \\ F_2^\alpha \end{array} \right\} = \left\{ \begin{array}{c} \tau_{cr}^\alpha|_{n+1} - \hat{\tau}_h^\alpha - \hat{H}^\alpha \, c_T^\alpha|_{n+1} \\ c_T^\alpha|_{n+1} - Y \, (\tau_{cr}^\alpha|_{n+1})^2 \end{array} \right\} = \left\{ \begin{array}{c} 0 \\ 0 \end{array} \right\} = \mathbf{0} \tag{C.4}$$

The Jacobian matrix of the above system can be readily calculated as:

$$[J^\alpha] = \left[\begin{array}{cc} \partial F_1^\alpha/\partial \tau_{cr}^\alpha & \partial F_1^\alpha/\partial c_T^\alpha \\ \partial F_2^\alpha/\partial \tau_{cr}^\alpha & \partial F_2^\alpha/\partial c_T^\alpha \end{array} \right] = \left[\begin{array}{cc} 1 & -\hat{H}^\alpha \\ -2Y\tau_{cr}^\alpha|_{n+1} & 1 \end{array} \right] \tag{C.5}$$

and is used to calculate the iterative corrections $\Delta\tau_{cr}^\alpha|_{n+1}$ and $\Delta c_T^\alpha|_{n+1}$ for $\tau_{cr}^\alpha|_{n+1}$ and $c_T^\alpha|_{n+1}$ respectively as:

$$\left\{ \begin{array}{c} \Delta\tau_{cr}^\alpha|_{n+1} \\ \Delta c_T^\alpha|_{n+1} \end{array} \right\} = -[J^\alpha]^{-1} \cdot \{F^\alpha\} \tag{C.6}$$

The Newton method is initiated by passing in the set $(\tau_{cr}^\alpha|_n, c_T^\alpha|_n)$ and also assigning both variations equal to zero[2]. In general, this assumption will violate[3] the system in (C.4), and iterative correction of $\tau_{cr}^\alpha|_{n+1}$ and $c_T^\alpha|_{n+1}$ will be necessary. The variables are updated to their values at $i+1$ using their previous values at i and the iterative corrections[4] in (C.6) as:

$$\tau_{cr}^\alpha|_{n+1}^{(i+1)} = \tau_{cr}^\alpha|_{n+1}^{(i)} + \Delta\tau_{cr}^\alpha|_{n+1} \tag{C.7a}$$

---

[2] $\Delta\tau_{cr}^\alpha|_{n+1} = \Delta c_T^\alpha|_{n+1} = 0$

[3] The plastic slips $\Delta\gamma^\alpha$ that are passed in by the Newton iteration nested in the heuristic algorithm guarantee that at least for some systems α expression (C.4) will be violated. The effect of $\Delta\gamma^\alpha$ is included in the constants defined in (C.1a–C.1e)

[4] $[J]$ and $\{F\}$ are evaluated at i to calculate the corrections and update the solution at $i+1$

$$c_T^\alpha|_{n+1}^{(i+1)} = c_T^\alpha|_{n+1}^{(i)} + \Delta c_T^\alpha|_{n+1} \tag{C.7b}$$

After updating $\tau_{cr}^\alpha|_{n+1}$ and $c_T^\alpha|_{n+1}$ to their values in the current iteration, we check for convergence in (C.4), and if necessary we iterate again. The algorithm is also summarized in the following table:

Table C.1: A summary of the Newton iterations required to solve the nonlinear system of $\tau_{cr}|_{n+1}$ and $c_T|_{n+1}$

1. Set $\tau_{cr}^\alpha|_{n+1} = \tau_{cr}^\alpha|_n$ and $c_T^\alpha|_{n+1} = c_T^\alpha|_n$

2. Evaluate the system of equations (C.4) at $(\tau_{cr}^\alpha|_{n+1}, c_T^\alpha|_{n+1})$

3. If $||\mathbf{F}^\alpha(\tau_{cr}^\alpha|_{n+1}, c_T^\alpha|_{n+1})|| \leq$ tol then GOTO **5.** Else continue with **4.**

4. Reset counter $i = 0$ and set $\tau_{cr}^\alpha|_{n+1}^{(i)} = \tau_{cr}^\alpha|_n$ and $c_T^\alpha|_{n+1}^{(i)} = c_T^\alpha|_n$.

   i. Update Counter $i \leftarrow i + 1$

   ii. Calculate the solution corrections $(\Delta\tau_{cr}^\alpha|_{n+1}, \Delta c_T^\alpha|_{n+1})$ from (C.6)

   iii. Update solution using (C.7a–C.7b) and evaluate the system (C.4)

   iv. If $||\mathbf{F}^\alpha(\tau_{cr}^\alpha|_{n+1}^{(i+1)}, c_T^\alpha|_{n+1}^{(i+1)})|| \leq$ tol then GOTO **5.** Else GOTO **i.**

5. Solution $(\tau_{cr}^\alpha|_{n+1}, c_T^\alpha|_{n+1})$ has converged for slip system α. Restart calculations for a different system $\beta \neq \alpha$

Finally, we need to address the issue of initial hydrogen allocation in the single crystal specimen. Before subjecting the hydrogen–charged crystal to uniaxial tension, we have to determine the concentration of atoms residing in trapped and lattice sites. Usually, for hydrogen charged single crystal specimens, we determine the 'amount' of charging in terms of the total and constant hydrogen concentration c_0 which is the same for every material point within the continuum body. This introduces the additional problem of determining how this initial concentration c_0 is allocated to c_L and c_T^α.

Recall the conservation of hydrogen that is expressed in (4.15) and is restated below:

$$c_L + \sum_\alpha c_T^\alpha = c_0 \tag{C.8}$$

Now recall that the trapped hydrogen concentration, depends on the critical shear stress τ_{cr}^α of the slip system under consideration. Before subjecting the specimen to uniaxial tension, all slip systems are assumed to have equal flow stresses ($\tau_{cr}^\alpha = (\tau_0)_H \ \forall\alpha$) and therefore equal trapped hydrogen concentrations ($c_T^\alpha = c_T|_0 \ \forall\alpha$). Assuming that c_0 is given and therefore

known, we can restate the conservation of hydrogen as:

$$c_L|_0 = c_0 - \frac{Nsp}{2}c_T|_0 \tag{C.9}$$

Besides the hydrogen conservation, the lattice and trapped concentrations must also satisfy the hydrogen equilibrium which is expressed using equation (5.16) as:

$$c_T|_0 = \frac{K_T \, \zeta \, c_L|_0}{\tilde{\alpha}^2 \, \mu^2 \, b^3 \left[\eta \, N_L + (K_T - 1) \, N_L \, c_L|_0 \right]} \, (\tau_0)^2_H \tag{C.10}$$

Substituting (C.9) to (C.10) we get:

$$c_T|_0 - \frac{K_T \, \zeta \left(c_0 - \frac{Nsp}{2}c_T|_0 \right)}{\tilde{\alpha}^2 \, \mu^2 \, b^3 \left[\eta \, N_L + (K_T - 1) \, N_L \left(c_0 - \frac{Nsp}{2}c_T|_0 \right) \right]} \, (\tau_0)^2_H = 0 \tag{C.11}$$

Finally, recall that trapped hydrogen concentration also affects the initial flow stresses as we suggested in (4.19):

$$(\tau_0)_H = (1 + T_c \, c_T|_0)\tau_0 \tag{C.12}$$

Equation (C.12) can be used to write (C.11) in the form:

$$c_T|_0 - \frac{K_T \, \zeta \left(c_0 - \frac{Nsp}{2}c_T|_0 \right)}{\tilde{\alpha}^2 \, \mu^2 \, b^3 \left[\eta \, N_L + (K_T - 1) \, N_L \left(c_0 - \frac{Nsp}{2}c_T|_0 \right) \right]} \, (1 + T_c \, c_T|_0)^2 \, \tau_0^2 = 0 \tag{C.13}$$

which is a nonlinear equation that needs to be solved for $c_T|_0$. Once we solve for $c_T|_0$, we can use equation (C.9) to also calculate $c_L|_0$ and completely determine the way hydrogen is allocated at $t = 0$.